Behaviour of Multilayer External Walls with an Exterior Layer of Glazed Ceramic Tiles. Vol. 1

Björk, Bo; Björklund, Kjell; Leander, Karl; Magnusson, Sven Erik; Näslund, Ivan; Pettersson, Ove

1977

LUND INSTITUTE OF TECHNOLOGY · LUND · SWEDEN · 1977
DIVISION OF STRUCTURAL MECHANICS AND CONCRETE CONSTRUCTION · BULLETIN 57

BO BJÖRK — KJELL BJÖRKLUND — KARL LEANDER —
SVEN ERIK MAGNUSSON — IVAN NÄSLUND —
OVE PETTERSSON

BEHAVIOUR OF MULTILAYER EXTERNAL WALLS WITH AN EXTERIOR LAYER OF GLAZED CERAMIC TILES

Volume 1

With contributions also by JAN ALEMO, GÖRAN FAGERLUND, TOMMY LOVÉN and GÖSTA E. SCHERLING

LUND INSTITUTE OF TECHNOLOGY · LUND · SWEDEN · 1977
DIVISION OF STRUCTURAL MECHANICS AND CONCRETE CONSTRUCTION · BULLETIN 57

BO BJÖRK - KJELL BJÖRKLUND - KARL LEANDER - SVEN ERIK MAGNUSSON - IVAN NÄSLUND - OVE PETTERSSON

BEHAVIOUR OF MULTILAYER EXTERNAL WALLS WITH AN EXTERIOR LAYER OF GLAZED CERAMIC TILES

Volume 1

With contributions also by JAN ALEMO, GÖRAN FAGERLUND, TOMMY LOVÉN and GÖSTA E. SCHERLING

Offsettryck: Elegant-tryck, Växjö 1977

PREFACE

This bulletin constitutes the first volume of three, reporting a combined experimental and theoretical investigation of the functional behaviour of a multilayer, external wall with an outer layer of ceramic tiles with regard to heat and moisture transfer and frost formation as well as stresses and deformations, when exposed to a long-term loading and a fluctuating exterior climate.

The present volume deals with the background and purpose of the investigation, the planning and general outlines of the experimental study, the characteristics and data of the test houses, the observation and measuring technique, and the relevant initial properties of the materials comprised experimentally. In volume 2 the results will be reported from the long-term test house registrations and observations, from some special test house investigations of more instantaneous character and from some parallel experiments on single panel elements. Volume 3, finally, will be devoted to a supplementary theoretical analysis and to a drawing of some conclusions with respect to the application of the results of the investigation in practice.

The investigation was carried out as a joint research project between Höganäs AB and the division of Structural Mechanics and Concrete Construction, Civil Engineering Department, Lund University. The project was sponsored by the Swedish Council of Building Research, Siporex AB, Dalby, as concerns the delivery of the aerated concrete for the test houses, and Höganäs AB.

The main responsibility of the investigation, as reported in the present volume, rests with us, the undersigned. Important support then has been given by

Dr. Jan Alemo, Division of Structural Mechanics and Concrete Construction, Lund University, as concerns the initial physical properties of concrete - section 1.5.5,

Dr. Göran Fagerlund, Swedish Cement and Concrete Research Institute, Stockholm, in carrying through a determination of the critical moisture contents at freezing of the ceramic tiles - appendix 1.5.1c,

Prof. Dr. Hellmuth Hertz, Division of Electrical Measurements, Lund University - as concerns fundamental problems of measuring technique,

Tommy Lovén, Aeronautical Research Institute of Sweden, FFA, Stockholm, in performing the small and full scale studies of the local flow around the test houses - appendix 1.3.1a,

Bertil Rodhe and Roger Taesler, Swedish Meteorological and Hydrological Institute, Norrköping, in giving points of view and advice with regard to the meteorological observations, the personnel at the lighthouse at Kullen in supplying with weather observations, and

Gösta E. Scherling, Aeronautical Research Institute of Sweden, FFA, Stockholm, in developing the application technique of the strain-gauges for long-term measurements in outdoor environment - appendix 1.4.6a.

Important practical assistance further has been given by

Kjell Andersson, Lars Berg, Carl E. Fredricsson, Sven-Ingvar Granemark, Gunnar Holgersson, Arne Holm, Ture Jansson, Lise-Lotte Johansson, Bertil Nilsson and Uno Nilsson in the performance of the tests,

Ann Schollin and Bo Zadig in making the drawings, and

Tarja Aunola, Lisbeth Henning and Ann-Britt Thagesson in typing the manuscript.

Our best thanks to the Swedish Council of Building Research for its financial support and to all persons listed above for their skilful contributions to the investigation.

Höganäs and Lund, December, 1976

Bo Björk	Kjell Björklund	Karl Leander
Sven Erik Magnusson	Ivan Näslund	Ove Pettersson

CONTENTS

6th - 10th April, 1970, Paper 40, Institution of Mechanical Engineers, London, 1971.

By GÖSTA E. SCHERLING

Introduction

Purpose and scope of measurements

The environment

Choice of strain-gauges

Application technique and cement

Lead wires and connections

Protection of gauge installations

Installation procedure

Investigation of the strain-gauge bond under various conditions

The main tests

Some observations from the measurements on the test houses

Concluding remarks

Appendix 1.5.1a. Determination of ultimate compressive strength of ceramic tiles at balanced deformation

Appendix 1.5.1b. Tensile strength of ceramic tiles, determined by splitting tension test

A1. Theoretical background

A2. Testing procedure

A3. Test results

A4. Discussion of test results

Appendix 1.5.1c. Determination of critical moisture contents at freezing of two types of glazed ceramic tiles

By GÖRAN FAGERLUND

A1. Aim of the investigation

A2. Materials tested

A3. Specimens

A4. Scope

A5. Determination of critical moisture contents - method and results

A6. Determination of water uptake - method and results

A7. Summary

1.1. BACKGROUND, PURPOSE, AND GENERAL OUTLINES

During the 1960th, mainly in the beginning of the period, damages have been observed on glazed ceramic tiles applied on the outside of different types of external walls. The damages are related to tiles with a certain porosity, identical or similar to the tiles named "N" in this report. Mostly, the damages are characterized by a partial scaling off of the glazing and portions of the underlying body of the tiles. The damages, usually arising one year or more after the fixing of the tiles, generally are initiated by the appearance of cracks.

As a rule, the damages are related to tiles which have been fixed manually on load-bearing external walls of varying material. The highest frequency of damage applies to wall material of aerated concrete, ordinary concrete with external insulation of aerated concrete, and brick masonry. Damages of the described type also have occured in small extent on ceramic tiles, forming the facade layer of prefabricated curtain wall elements.

The summarily related circumstances constitute one primary reason for the combined experimental and theoretical investigation, reported in this volume and in two subsequent volumes. The investigation consists in a functional analysis of the behaviour of a multilayer, external wall with an outer layer of ceramic tiles with regard to heat and moisture transfer as well as stresses and deformations due to creep, shrinkage, temperature and moisture variations, and frost formation, when the wall is exposed simultaneously to a long-term loading and a fluctuating exterior climate.

In a long-range perspective, the most essential reason for the investigation is to get a better understanding of the integrated function of a multilayer, external wall in practice with the final aim to develop a differentiated design system, comprising a mechanical-physical model for the behaviour of the wall and systematically determined relevant material properties, required as entrance quantities in the model. With such a design system available,

(1) the results of experimental studies, carried through for specific types of multilayer, external walls, could be generalized for an application also to wall types, considerably diverse from the type investigated,

(2) it should be possible to draw up elaborate instructions for the use and fixing technique of the present types of ceramic tiles within different fields of application, and

(3) the detailed functional requirements to be made upon the glazing and body of the ceramic tiles could be stated with reference to different types of external walls, giving an essential basis for a future choice and development of the material properties and the production and application technique for the ceramic tiles as well as for the joint and fixing mortars.

It is the humble hope of the authors that the investigation presented below may be seen as some step of development in the direction of a differentiated design system of the type touched upon.

The investigation contains four main parts, viz:

(1) A registration of macro and micro climate data of relevance to an integrated design of external walls - quantity and height of clouds, air temperature, air humidity, atmospheric pressure, direction and velocity of wind, solar radiation, quantity of precipitation (rain, snow, hail etc), and direction and quantity of pelting rain

(2) An accurate and detailed determination of the mechanical and physical properties of the materials, used in the experimental part of the investigation, viz ceramic tiles, fixing mortar, joint mortar, concrete, and aerated concrete - density, porosity, stress-strain relation, modulus of elasticity, creep, strength in compression, tension and flexure, specific heat capacity, thermal

conductivity, thermal dilatation, moisture fixation and transport, shrinkage and moisture dilatation, and freezing properties

(3) An experimental, full scale study of the integrated behaviour of some different types of multilayer, external walls and columns with an outer layer of ceramic tiles, simultaneously exposed to a long-term loading and exterior climate variations - measurements of the time-fields of temperature and moisture distribution, and of the time variation of strains and deformations in various points of the walls, due to creep, shrinkage, heat and moisture transfer, and frost formation

(4) A comprehensive, theoretical analysis of the results of the experimental, full scale study, including a development of some simplified, mechanical-physical models - on the basis of the available, advanced knowledge - for the integrated behaviour, or for single components of this behaviour, of a multilayer, external wall under combined long-term loading and exterior climate variations.

As previously touched on, the investigation is planned to be reported in three volumes. The present volume 1 deals with

the background and purpose of the investigation,

the general and detailed planning of the experimental, full scale study,

the characteristics and data of the two test houses, constructed for the experimental study,

the observation and measuring technique for the registration of weather-climate data and of strain, deformation, temperature and moisture for the test house wall elements, and

the relevant, initial, material properties of the ceramic tiles, fixing mortar, joint mortars, concrete, and aerated concrete.

In volume 2 the results will be reported from

the general test house registrations and observations,

some parallel experiments on single panel elements, used partly as reference panels, partly as test specimens for heat, moisture and load studies after the main test period,

some special investigations, comprising temporary unloading and loading of the test house elements, artificial heat tests, moisture tests, freezing studies, shear studies on brick-mortar-aerated concrete, and dismounting of test house element tiles, and

a determination of the change of the initial material properties, mainly for the ceramic tiles, due to the influence of time and environment conditions.

Finally, volume 3 will be devoted to the theoretical analysis of the results of the experimental studies and to a drawing of some conclusions with respect to the application of the results in practice.

1.2. PLANNING OF EXPERIMENTS

1.2.1. MAIN INFLUENCES ON THE BEHAVIOUR OF A MULTILAYER EXTERNAL WALL

The problem, comprised of this investigation - the functional behaviour of a multilayer external wall with regard to heat and moisture transfer as well as stresses and deformations due to creep, shrinkage, temperature and moisture variations, and frost formation, when exposed to a long-term loading and a fluctuating exterior climate - is a problem of extremely high complexity. Summarized, the behaviour and the connected causes of any damages that may occur can be described according to the flow diagram in Fig. 1.2.1a.

Thermodynamically, the processes of heat and moisture transfer are following the law of conservation and transformation of energy and the law of conservation of mass, and the principle of the increase of entropy (second law of classical thermodynamics). In modern form, the thermodynamics of the transient state includes the phenomenological theories of the molecular transfer of heat, mass and momentum of fluids, and the hydrodynamics of viscous fluids with linked phase and chemical transformations. The axiomatics of the potential of transfer are fundamental, implying, among other things, that the transfers of energy and mass proceed in the direction from the higher potential to the lower.

In the general case, the heat transfer takes place in the three modes - heat conduction, heat convection and heat radiation - and is combined with a storage of heat energy. Heat conduction occurs in solid bodies and in very thin, stationary layers of liquid or gas and consists of a heat propagation as a result of the thermal motion of the elementary particles of the material. Convective heat transfer occurs in moving liquids and gases and in porous materials and implies a transportation and exchange of heat due to conduction and a direct mixing motion of different macroscopic parts of the fluid. Heat radiation is the energy transfer, caused by temperature, from one body to another by an electromagnetic wave motion through a transparent medium or the empty space.

In application to the present investigation, the heat exchange between

the wall elements of the test houses and the surrounding medium - the surface heat transfer - consists in convection and radiation while the heat conduction mode is practically negligible. Ordinarily, the heat transfer part connected to the air flow in front of the wall surface is caused by free or natural convection due to the temperature difference between the wall surface and the fluid as well as by the forced convection due to wind as an extraneous stimulus. Within the wall elements, built up of porous materials as ceramic tiles, mortar, ordinary concrete and aerated concrete, the heat transfer process is strongly dominated by conduction but comprises also, in minor extent, a convection contribution, provided that the real behaviour is dealt with under the simplifying assumption of disconnected heat and moisture transfer. To these heat transfer mechanisms, the influence of phase transformations - evaporation and freezing of water, condensation of water vapour and melting of ice - must be added.

In capillary-porous bodies, the following forms of the bond between the moisture and the material are distinguished:

(1) Chemically combined water, with a distinction between water in the form of hydroxyl ions and water in molecular compounds
(2) Adsorptionally bound water, mainly represented by a monomolecular layer on the internal and external surfaces of the porous body, distinguished with respect to the bond energy between adsorption isotherms for hydrophilic, intermediate and hydrophobic surfaces
(3) Capillary-bound water, consisting of a very thin layer of water, adsorptionally bound to the walls of the capillary and of free water contained in the capillaries and bounded by free menisci
(4) Osmotically bound water, determined by the measure of the entropy and most clearly expressed in dilute solutions, and
(5) Free water, occuring in larger cavities of the material and having no defined border to the capillary-bound water.

In a state of equilibrium with moist air, a capillary-porous body has the same temperature as the air temperature and the same pressure of the water vapour in the material as the partial pressure of water vapour in the air. The body then attains the equilibrium moisture content or the equilibrium humidity, which depends on the temperature, the humidity of the surrounding air and the method of reaching the hygrothermic equilibrium state - by sorption or desorption.

The moisture transfer within a body, for instance a wall element, and between the surface of a body and the surrounding medium, for instance air, ordinarily is the result of a number of different transfer mechanisms, simultaneously active and interrelated to each other. The main moisture transfer comprises water vapour and liquid but also a transfer of ice through a material is a possible mode. The moisture transfer depends on the temperature and moisture distribution of the body, the temperature, pressure and humidity of the environment, the form of bond between the moisture and the material, and the basic structural properties of the material.

The mass transfer between a wall surface and the adjacent air flow occurs usually in the presence of a heat transfer. The mass transfer potential is the relative partial pressure of the transferred component and the moisture transport mechanisms are a molecular mass transfer, diffusion, and a molar mass transfer, convection. The convective transfer is defined above. The diffusion process in a stream of a gas mixture is forced by a non-uniform concentration and comprises a mixing by means of a molecular motion. A larger number of molecules then is passing in the direction of the diffusion current than in the opposite direction.

The diffusion and convection processes also are the decisive modes for the vapour transfer in a capillary-porous body.

The diffusion takes place in the macro-capillaries provided that the capillaries mainly are filled up with air and the moisture ratio of the material is within the hygroscopic region. At a temperature gradient in the length direction of a macro-capillary, the vapour diffusion transfer is affected by a thermal slip which is a macroscopic movement of the vapour layer along the capillary wall. This thermal slip movement takes place in a direction opposite to the heat flow. In micro-capillaries, neither any laminar nor turbulent aerodynamic flow can be formed and consequently no diffusion transfer arise. In micro-capillaries, the movement of the gas molecules is not determined by collisions with adjacent molecules but by collisions with the capillary walls. Due to repeated collisions with the capillary walls, the vapour molecules attain thermal equilibrium with the molecules of the material. Such a molecular motion is called effusion.

The convection transfer mechanism is characterized by water vapour following an air flow which is pressed through a capillary-porous body under the influence of a total pressure gradient. Such a difference in total pressure can be obtained by a wind exposure, a thermal driving force or an effect of a ventilation system. The vapour diffusion is, as a rule, a slow process and the diffused moisture quantities are most often small. The moisture quantities, transferred by the vapour convection, are ordinarily considerably larger, particularly in the presence of cracks, fissures or other types of leakages.

The transfer of moisture in the form of water in a capillary-porous body can occur as a water transportation due to the wind force and gravity (molar or convective transfer), as a capillary absorption and as a water transportation due to an osmotic pressure gradient.

The convective water transfer occurs for an external wall, for instance, at a pelting rain when a wind pressure squeezes the water into the wall. The water convection due to gravity depends on the size of the pores, i.e. on the magnitude of the forces binding the water to the material. Ordinarily, then the influence of the gravity is negligible at a pore size less than 0.01 mm.

The water transfer in the form of a capillary absorption can be described by the gradient of a potential which consists of the capillary potential, given by the differences in the capillary pressure within the porous material, and the gravity potential.

In materials with constituents, which are soluble in water, there can exist differences in concentration between different parts of the body. The osmotic pressure difference arisen in this way then causes a molecular water transfer equalizing the concentration differences.

With the different modes of heat and mass transfer defined, the behaviour of a multilayer external wall now will be summarily described as exposed to a long-term loading and a fluctuating exterior climate. The behaviour then may be assumed to start in a state of temperature and moisture equilibrium with - in the general case - free water and water bound chemically, adsorptionally, capillarily and osmotically, Fig. 1.2.1a.

Under the influence of a fluctuating exterior climate, a simultaneous transfer of heat, liquid, and a vapour-gas mixture gets started. In a region of the wall of negative temperatures, the substance bound with the capillary-porous field can be in the form of ice, sub-cooled liquid or vapour or gas. Depending on the form of bond of the moisture within the wall, the freezing temperature of a liquid varies not inconsiderably. Consequently, there is always a certain amount of sub-cooled liquid at negative temperatures in a capillary-porous body with different kinds of moisture bond. Another characteristic feature of the mass and heat transfer is the partial filling of the pores and capillaries with moisture, i.e. some of the pores and capillaries of the wall are filled with liquid or ice and the rest are filled with a vapour-gas mixture. The amount of moisture in one state or another varies perpetually in the mass and heat transfer process.

A calculation of the transient temperature and moisture states requires heat and moisture dynamical models of analysis to be available. In the general case, these models are interdependent and comprise the different modes of heat transfer (conduction, convection and radiation) and the different modes of moisture transfer (diffusion, moisture convection, capillary absorption and osmosis) as well as the phase transformations (evaporation and freezing of water, condensation of water vapour and melting of ice). Input information is the climatic data and the appurtenant thermal and moisture material properties. At certain conditions, the analysis can be facilitated by separating the heat transfer and moisture transfer processes. This will be further dealt with in volume 3.

The moisture, transported to the external wall in different ways or transferred within or through the wall can give rise to troubles or damages of different types. The influence of the moisture on the durability of the materials then is a serious problem, requiring a thorough investigation. In certain cases, the material destruction occurs at a specific, critical moisture content in the material. This applies to the freezing of porous and brittle materials, cf. appendix 1.5.1c. In other cases, the material properties and the material function are changed gradually, for instance, a successive deterioration of the heat insulating capacity with an increased moisture content.

Regarding the durability of the materials, moisture can cause a material degradation in the actual case of application by acting as

(1) a medium at chemical reactions between the material and substances dissolved in the water
(2) a transfer medium for salts, giving rise to bursting forces in the material, e.g. salt decomposition
(3) a medium for dissolving components of a material, e.g. calcium hydrate leaching in concrete
(4) an electrolyte at corrosion of metals, e.g. the reinforcement of concrete and aerated concrete, and
(5) an expanding pore filling at freezing of the material.

The deformation of the external wall due to a fluctuating exterior climate and a simultaneous long-term loading comprises the following modes - Fig. 1.2.1a:

(1) Instantaneous, stress related deformation, based on the stress-strain curves of the material, obtained at a stabilized state of temperature and of moisture content
(2) Thermal deformation, defined in this connection as related to the thermal dilatation and having the same time function as the temperature
(3) Moisture deformation, analogously defined as related to the short-term moisture dilatation
(4) Creep deformation, being a function of stress and time. For tile materials, this mode of deformation is practically negligible at ordinary stress levels. For cement-bound materials, e.g. concrete, aerated concrete, cement-mortar, lime-cement-mortar, the creep depends on parameters as composition, properties and amount of materials component included, temperature and pore humidity before as well as during the loading process, maturity at loading, and state and magnitude of loading. The creep can be split up into basic creep, occuring at an equilibrium state of humidity and temperature, sorption creep, occuring at changing humidity, and creep that occurs at changing temperature. Basic creep can be further split up into an irrecoverable, viscous component and a recoverable, delayed elastic component. Sorption creep occurs both at drying and wetting of the material. A special kind of creep occurs at the first temperature increase of a cyclic temperature variation. This mode of deformation is here - in accordance to recent suggestions in the literature - named

(5) Transient deformation. It is considered to have the same time function as the temperature increase of the material and to be proportional to this. The transient deformation is insignificant at temperature decreases and also at temperature increases after the first one. The deformation mode occurs for cement-bound materials but does not come up for, for instance, ceramic materials.
(6) Shrinkage, being a function of time and independent of stress. For cement-bound materials, the shrinkage depends on composition, properties and amount of materials included, and environmental characteristics. The cause of shrinkage can be divided into drying and carbonization. The drying shrinkage, which usually predominates, is due to the fact that the calcium silicate gel contracts when the moisture content decreases. The carbonization means that the carbon dioxide of the air reacts with certain constituents of the cement.

Depending on the conditions of the application, the different modes of deformation are to be dealt with as interrelated in varying extent. Some modes, for instance, moisture deformation and drying shrinkage are not to be separated in reality.

For a calculation of the transient stress-strain state of the multilayer wall elements of the test houses, a stress-strain mechanics model of analysis must be developed with the different modes of deformation as components. Input information is the load data, the appurtenant mechanical material properties and the transient temperature and moisture states, determined earlier in the computation procedure, including the adherent history. If the stress-strain state attains defined limit states, mechanical damages are caused, e.g. in the form of cracking, crushing or bond failure. An interaction with moisture damage and frost damage then may occur.

REFERENCES

[1] JAKOB, M., Heat Transfer, Vol.I. New York - London - Sydney, 1949. Ditto, Vol. II, 1963.

[2] GRÖBER, H. - ERK, S. - GRIGULL, U., Die Grundgesetze der Wärmeübertragung. Berlin - Göttingen - Heidelberg, 1963.

[3] LYKOV, A.V. - MIKHAILOV, Y.A., Theory of Heat and Mass Transfer. Israel Program for Scientific Translations, Jerusalem, 1965.

[4] LUIKOV, A.V., Heat and Mass Transfer in Capillary-porous Bodies. Oxford - London - Edinburgh - New York - Paris - Frankfurt, 1966.

[5] CRAWFORD, F.H. - VAN HORST, W. D., Thermodynamics for Engineers. New York - Chicago - San Francisco - Atlanta, 1968.

[6] ADAMSON, B. - AHLGREN, L. - BERGSTRÖM, S.G. - NEVANDER, L.E., Fukt (Moisture). Programskrift 12, Statens råd för byggnadsforskning, Stockholm, 1970.

[7] ECKERT, E.R.G. - DRAKE, R.M., Analysis of Heat and Mass Transfer. McGraw Hill Series in Mechanical Engineering, New York, 1972.

[8] HANSEN, T.C. - ERIKSSON, L., Temperature Change Effect on Behaviour of Cement Paste, Mortar and Concrete Under Load. ACI Journal, Proc. 63, 1966, pp. 489-504.

[9] ILLSTON, J.M., Components of Creep in Mature Concrete. ACI Journal, Proc. 65, 1968, pp. 219-227.

[10] BAZANT, Z.P., Thermoviscoelasticity of Aging Concrete. Journal of the Engineering Mechanics Division, ASCE, Vol.100, No. EM3, Proc. Paper 10621, June, 1974, pp. 575-597.

[11] THELANDERSSON, S., Mechanical Behaviour of Concrete Under Torsional Loading at Transient, Hightemperature Conditions. Bulletin 46, Division of Structural Mechanics and Concrete Construction, Lund Institute of Technology, Lund, 1974.

[12] ALEMO, J., The Effects of Imposed Deformations on the Behaviour of Loaded Concrete Structures. Bulletin 53, Division of Structural Mechanics and Concrete Construction, Lund Institute of Technology, Lund, 1976.

1.2.2. MAIN CHARACTERISTICS OF THE EXPERIMENTAL FULL SCALE INVESTIGATION

The definition of the purpose and the description of the general outlines of the combined experimental and theoretical study according to section 1.1, and a summary analysis of the functional behaviour of a multilayer external wall, when exposed to a simultaneous long-term loading and a fluctuating exterior climate, according to section 1.2.1 constitute the primary basis for the planning of the experimental full scale investigation within the project.

For the experimental full scale investigation, two test houses were planned and constructed on the roof of the Central Laboratory building of Höganäs AB - Fig. 1.3.1a-j. The detailed design of the test houses is described in section 1.3.2 and the characteristics of the local wind flow around the test houses, determined in the building aerodynamics-tunnel at the Aeronautical Research Institute of Sweden (FFA) and by complementary observations at a full scale smoke test at Höganäs, are reported in appendix 1.3.1a.

In test house I, the external walls were made by, from within, 150 mm concrete, centrically reinforced - 125 mm aerated concrete - 20 mm fixing and splash mortar, with a reinforcement net, anchored to the concrete with wires - ceramic tiles. In the south front of the test house, the wall was divided into vertical elements, having the possibilities to deform independently of each other. Cf. further Fig. 1.3.2c, d, and q.

In test house II, the external walls of the east, north and west fronts were made by, from within, 250 mm aerated concrete - 20 mm fixing and splash mortar, with a reinforcement net, anchored to the aerated concrete with nails - ceramic tiles. In the south front of the test house, the wall was made alternately by vertical wall elements with characteristics according to the other fronts and by reinforced concrete columns with a cross section of 197 x 150 mm^2, internally insulated by 100 mm styrofoam and externally covered by ceramic tiles, fixed to the concrete columns as for the other wall sections. The connections between the wall elements and the concrete columns in the south front were designed in such a way that the members could deform independently of each other. Cf. further Fig. 1.3.2g-i, u, and v.

As regards the ceramic tile facings, the wall of the two test houses were divided into rectangular panels, comprising 5 x 5 tiles and representing different combinations of type of tiles and type of joints between the tiles.

Two tile types then were selected, viz. tile type N with to some extent a porous body with a glazed non-porous outside layer, and tile type F with a low porosity and a more or less transparent glaze. The way of the tile material selection is described in section 1.2.3 and the initial technical properties of the tiles are specified in section 1.5.1.

The types of joints applied to the different panels were joints of cement mortar C 100/300, joints of cement mortar C 100/600 and unfilled joints. The characteristics of the different panels are reported in Fig. 1.3.2ℓ with notations according to p. 1.3.2-2 and in section 1.4.7. The initial technical properties of the fixing mortar, which generally was a lime-cement-mortar of the type KC 35/65/550, and of the joint mortars are specified in section 1.5.2 and 1.5.3, respectively.

The corresponding properties of the concrete and aerated concrete used for the walls and columns of the test houses are collected in sections 1.5.4 and 1.5.5.

The choice of wall types for the experimental full scale investigation was guided by the frequency of observed tile damages for tiles fixed on varying wall materials. The observed tile damage situation also was the main reason for including ceramic tiles of type N in the investigation in spite of the fact that this type of tile now almost entirely has been replaced by ceramic tiles of type F, as concerns outdoors applications. As the study also comprises a development of simplified, mechanical-physical models for a theoretical determination of the integrated behaviour of a multilayer, external wall under combined long-term loading and exterior climate variations, the choice of wall types for the experimental investigation was not considered as a decisive problem otherwise.

In the experimental investigation, the east, north and west walls of the test houses were exposed only to the exterior climate variations.

The additional influence of a simultaneous long-term loading was examined parallelly for the wall and column elements of the south fronts of the test houses. The way of applying this load by a hydraulic system is described on page 1.3.2-2 - cf. Fig. 1.3.2j to ℓ and x and section 1.4.7 - where also the load and stress levels for the different wall and column elements are specified.

As already pointed out in section 1.1, the purpose of the experimental full scale investigation is to get a better understanding of the functional behaviour of a multilayer, external wall under combined long-term loading and exterior climate variations, to form a background for a development of mechanical-physical models, enabling a theoretical prediction of this behaviour, and to check the validity of such models. This purpose decided the general observations technique at the test houses, as concerns the registration of weather-climate data - section 1.4.1 - and of temperature, moisture, strain, change of length and curvature of the wall and column elements - sections 1.4.2 to 1.4.6. A survey of the complete system of measuring points for temperature and strain is given - with further references - in section 1.4.7, specifying for the two test houses the wall and column elements numbers, the type of tiles, the type of joints, and positions and numbering of the temperature sensors and the strain-gauges. Measurements, which could facilitate a detailed interpretation of the test results with regard to different influences, were aimed at. Thus, the strain-gauge measurements were arranged in a way to give explicit information on the effect on the state of strain of the ceramic tiles from instantaneous and time dependent deformations of the structure behind the tiles, from temperature variations of the tiles, and from moisture variations of the tiles - cf. further section 1.4.6.

In order to improve the understanding of the functional behaviour of the wall and column elements and in order to simplify the theoretical analysis of the test results - particularly in a preparatory phase of the analysis - the long-term observations were supplemented with special investigations of short duration, e.g. temporary unloading and reloading of wall and column elements, artificial tests with alternating sun radiation and sun shield of the elements, high frequency observations of walls and columns during a 24 hours period, and dismounting of test house tiles.

1.2.3. TILE MATERIAL SELECTION

The two tile types selected for the investigation are denominated N and F.

Tile type N (440 creamwhite - GL 511) has been in production in the Höganäs AB plant in Skromberga from about 1950 and has a more porous body than

tile type F (440 smooth F - GL 511 TT), which has been produced in the same plant from 1961-1962 on.

The tiles (split tiles) are manufactured as wet-extruded in attached pairs, back to back, each unit after splitting giving two separate tiles, cf. Fig. 1.2.3a.

Initial technical properties of the tiles are reported in section 1.5.1.

Below is described the way of selection for the tiles from the production and the technique used to get information of the variation of the general elastic properties of the tiles within the lots.

For those wall and column elements of the test houses, intended for accurate measurements, about 600 tiles of ordinary thickness 15 mm of each type N and F and about 50 thin tiles of thickness 10 mm of type F were required.

For the remaining elements of the test houses, approximately another 600 tiles of each type N and F together with some 60 thin tiles of both type N and F were required.

From running production in the year 1967 were taken 2500 units (pairs, giving 5000 tiles) of each type N and F. Each unit was marked with consecutive numbers and the tiles of each pair were with respect to manufacturing markings marked A and B according to Fig. 1.2.3a.

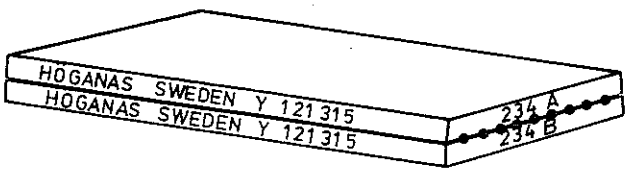

Figure 1.2.3a. A pair of two split tiles with applied marking technique

Of the selected population, 2000 units of each tile type N and F were in the usual way split with a special chisel into 2000 tiles marked A and 2000 tiles marked B. Both A and B tiles should alternatively be used on the test elements. The not used twin tiles were stored for possible future investigations.

The following two non-destructive tests were used to get information of the variations in the general elastic properties:

(1) Measurements of ultrasonic velocity (sine wave) along the tile by use of a pulse generator - transmitter - receiver - oscilloscope combination (Fig. 1.2.3b), and

(2) Measurements of flexural resonance of the tile by use of an oscillator - vibrator - pick-up - oscilloscope - counter combination (Fig. 1.2.3c).

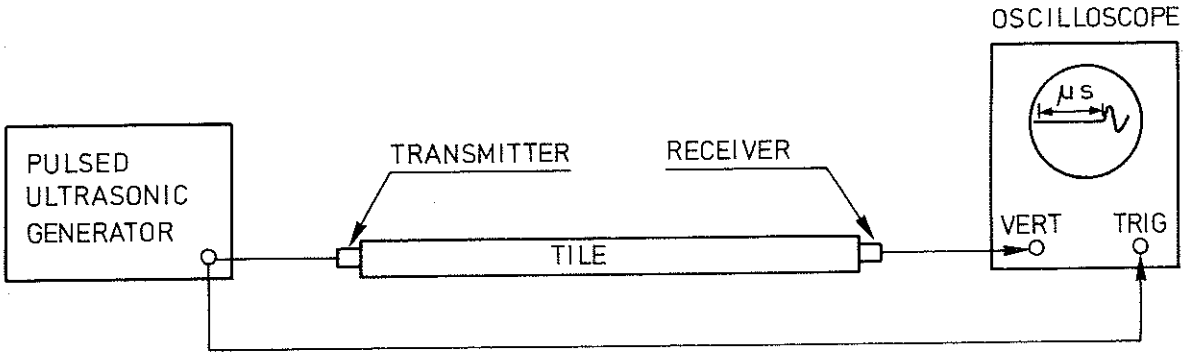

Figure 1.2.3b. Equipment, used for a determination of the ultrasonic velocity along the tiles

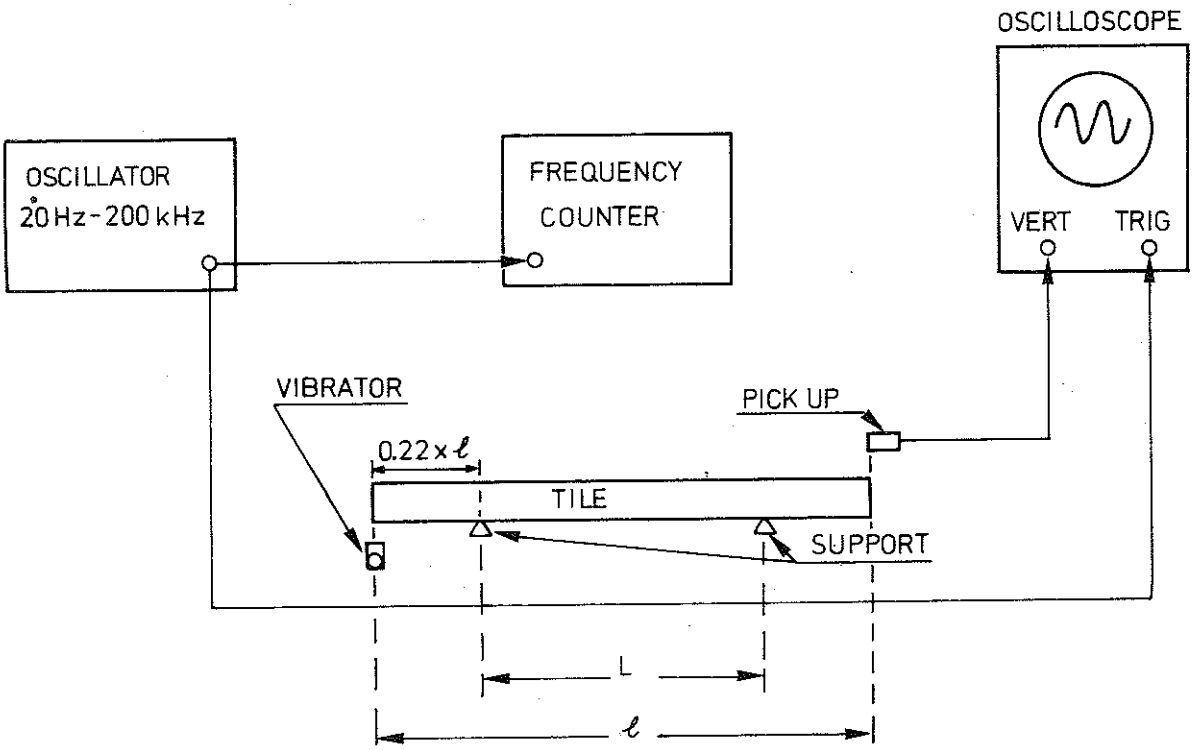

Figure 1.2.3c. Equipment, used for a determination of the natural, flexural vibration frequency of the tiles

The ultrasonic velocity observations were used to remove tiles with possible hidden structural defects, e.g. cracks.

The flexural resonance measurements then were used to classify the tiles with regard to general elastic properties. The strain ε constitutes the main experimental and numerical variable of this study. For this reason, it was found functionally suitable for choose either the strain ε or the inverted strain $1/\varepsilon$, referred to a centrical, uniformly distributed, axial, compressive unit force P = 1, as decisive quantity in the classification procedure. For this case, the following formula applies

$$\varepsilon = \frac{P}{EA} = \frac{1}{EA} = \frac{1}{Ebt} \qquad (1.2.3a)$$

or

$$\frac{1}{\varepsilon} = Ebt \qquad (1.2.3b)$$

where

E = the modulus of elasticity,
b = the width of the tile, and
t = the thickness of the tile.

Connected to the flexural resonance test, the modulus of elasticity E is given by the formula

$$E = k \frac{f^2 m L^4}{I} = 12k \frac{f^2 m L^4}{bt^3} \qquad (1.2.3c)$$

where

k = a dimensionless coefficient, depending on the support conditions,
f = the natural vibration frequency,
m = the mass per unit length of the tile,
I = the bending moment of inertia of the cross section of the tile, and
L = the span length of the tile in the test.

From the formulas (1.2.3b) and (1.2.3c) it follows that

$$\frac{1}{\varepsilon} = 12k \frac{f^2 m L^4}{t^2} = 12k \frac{f^2 \rho b L^4}{t} = 12k \frac{f^2 \rho^2 b^2 L^4}{m} \qquad (1.2.3d)$$

where

ρ = the density of the tile material.

From existing experience of production technique, it has been verified that the probabilistic scatter of the quantities entering into Eq. (1.2.3d) with sufficient accuracy is limited to the natural vibration frequency f and the thickness of the tiles t. As a consequence, the probabilistic scatter of $1/\varepsilon$ will be proportional to the variance of f^2/t or f^2/m, i.e.

$$\mathrm{Var}\left(\frac{1}{\varepsilon}\right) \sim \mathrm{Var}\left(\frac{f^2}{m}\right) \qquad (1.2.3e)$$

and of that reason the quotient f^2/m was used for the classification of the tiles with respect to the general elastic properties.

Of additional interest is the corresponding probabilistic scatter of the modulus of elasticity E. For this scatter, it follows from Eq. (1.2.3c) and from what has been stated above concerning the existing experience of production technique, that

$$\mathrm{Var}(E) \sim \mathrm{Var}\left(\frac{f^2 m}{t^3}\right) \sim \mathrm{Var}\left(\frac{f^2}{t^2}\right) \sim \mathrm{Var}\left(\frac{f^2}{m^2}\right) \qquad (1.2.3f)$$

Hence, the quotient f^2/m^2 has been calculated and given in this report, too.

1.2.3.1. N-tiles

The ultrasonic observations, evaluated as time in µs of the sine wave propagation along the tile, could only be measured in undivided µs.

The probabilistic scatter of the test results is given in the histogram of Fig. 1.2.3.1a, characterized by the following figures of the mean value $\bar{x}$, standard deviation s, and number of observations n

$\bar{x}$ = 42.5 µs
s = 0.74 µs
n = 1982

Of the 2000 tiles tested, 18 had visual defects or gave a propagation time > 45 µs. These tiles were discarded and, as consequence, not included in the histogram of Fig. 1.2.3.1a.

The flexural resonance frequency observations, expressed in f^2/m and f^2/m^2, are given in the histograms of Fig. 1.2.3.1b and c, respectively. As concerns the quantity f^2/m, the probabilistic characteristics are

Figure 1.2.3.1a. Histogram of the time of the ultrasonic sine wave propagation along the N-tiles

$\bar{x} = 5.30 \cdot 10^6$ Hz^2/kg
$s = 0.16 \cdot 10^6$ Hz^2/kg
$n = 1982$

Due to differences in mass m between A- and B-tiles, a division of the complete population is of interest, too. This gives for the A-tiles the following sample statistics

$\bar{x} = 5.19 \cdot 10^6$ Hz^2/kg
$s = 0.14 \cdot 10^6$ Hz^2/kg
$n = 994$

and for the B-tiles

$\bar{x} = 5.40 \cdot 10^6$ Hz^2/kg
$s = 0.14 \cdot 10^6$ Hz^2/kg
$n = 988$

The N-tiles, finally selected for the test house elements, were taken from the shadowed classes in Fig. 1.2.3.1b.

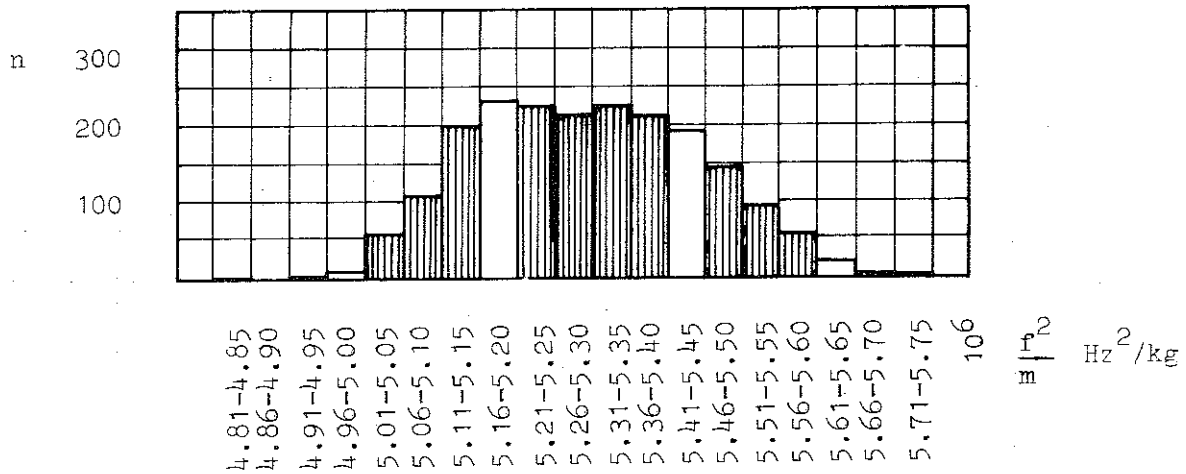

Figure 1.2.3.1b. Histogram of the flexural resonance frequency quantity f^2/m of the N-tiles

For the quantity f^2/m^2, the corresponding probabilistic characteristics are

$\bar{x} = 9.07 \cdot 10^6$ Hz^2/kg^2

$s = 0.20 \cdot 10^6$ Hz^2/kg^2

$n = 1982$

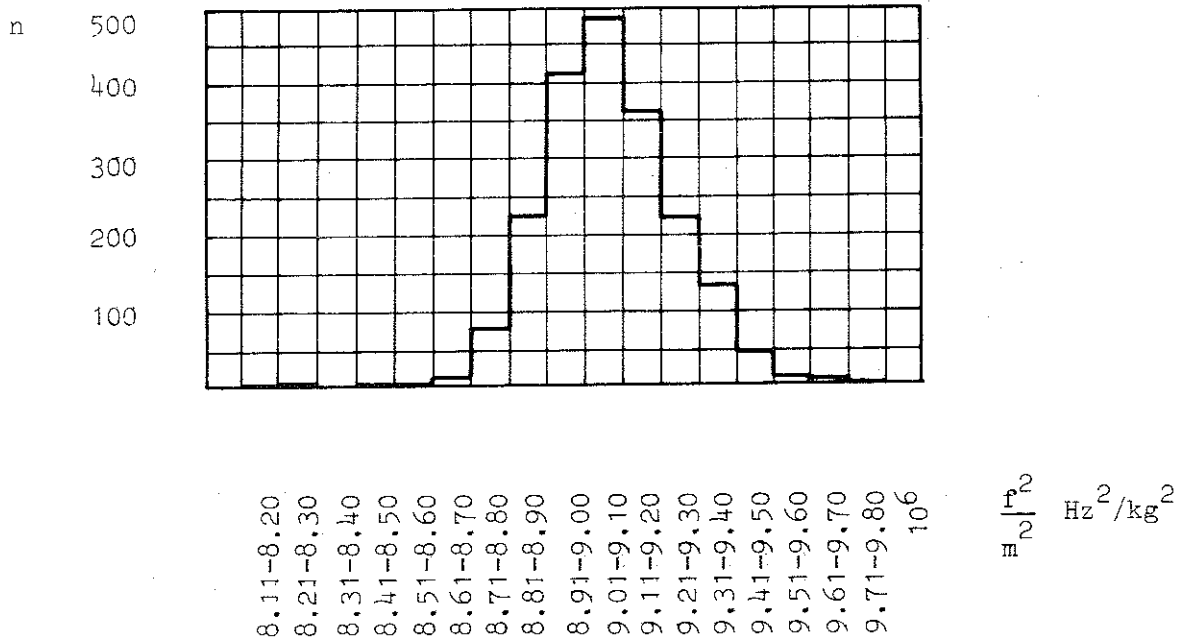

Figure 1.2.3.1c. Histogram of the flexural resonance frequency quantity f^2/m^2 of the N-tiles

The probabilistic characteristics of the geometrical measures in mm and of the mass m in kg of the N-tiles are summarized in the following table[1].

	length		width		thickness		mass (m)	
	A	B	A	B	A	B	A	B
$\bar{x}$	196.1	195.9	96.0	96.0	12.6	13.1	0.576	0.592
s	0.3	0.4	0.2	0.2	0.1	0.1	0.004	0.004
n	80	79	79	79	80	79	180	180

The values show a good uniformity for length and width but a clear difference between A- and B-tiles in thickness with a corresponding difference in mass.

The densities, measured according to the mercury method, of tiles A and B are near the same: 2230 $\pm$ 20 and 2220 $\pm$ 25 kg/m^3 (n=9), respectively.

1.2.3.2. F-tiles

The ultrasonic observations, evaluated as time in µs of the sine wave propagation along the tile, could be observed for the F-tiles in classes of 0.5 µs.

The test results are reported in the histogram of Fig. 1.2.3.2a for the whole population of the tiles without any defects, comprising 1997 tiles. Of totally 2000 tiles, 10 had visual defects or indicated time propagation values > 39 µs. These 3 tiles are excluded from the histogram in Fig. 1.2.3.2a.

The histogram indicates two distributions, one around 37.1 µs and one around 38.1 µs. For use on the test house elements, only tiles from the left population were selected. These tiles are characterized by the following population statistics

$\bar{x}$ = 37.1 µs
s = 0.26 µs
n = 700

---

1. Further information of measures is reported in section 1.5.1.

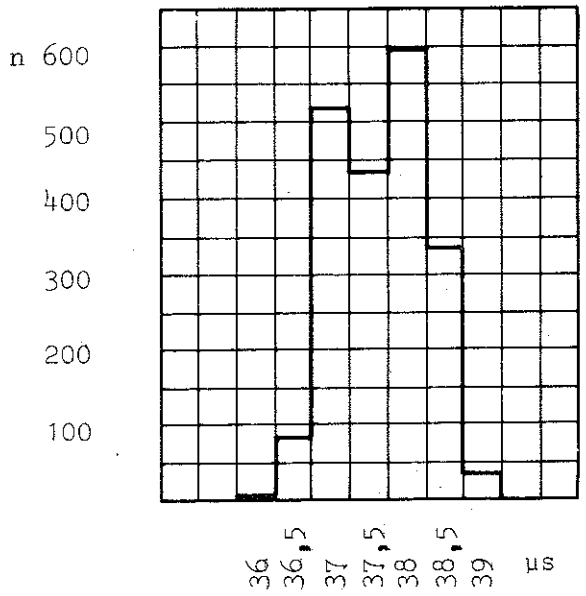

Figure 1.2.3.2a. Histogram of the time of the ultrasonic sine wave propagation along those F-tiles, selected for the test house elements

The flexural resonance frequency observations, expressed in f^2/m and f^2/m^2 histograms of Fig. 1.2.3.2b and c, respectively, show clearly marked two distributions.

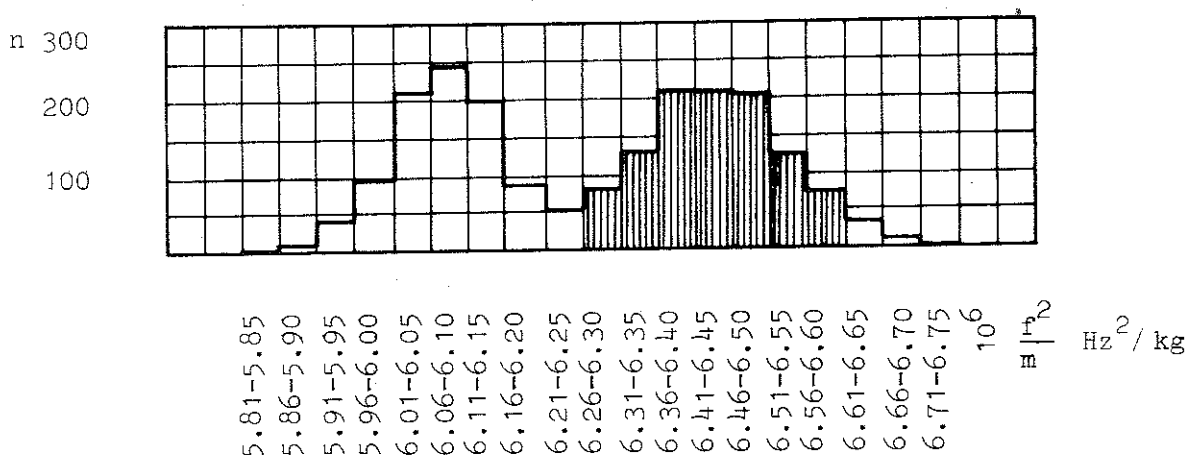

Figure 1.2.3.2b. Histogram of the flexural resonance frequency quantity f^2/m of the F-tiles

The tiles to be used on the test house elements were taken from the right distribution of f^2/m - selected classes shadowed - giving the sample statistics

$\bar{x} = 6.43 \cdot 10^6$ Hz^2/kg
$s = 0.10 \cdot 10^6$ Hz^2/kg
$n = 1117$

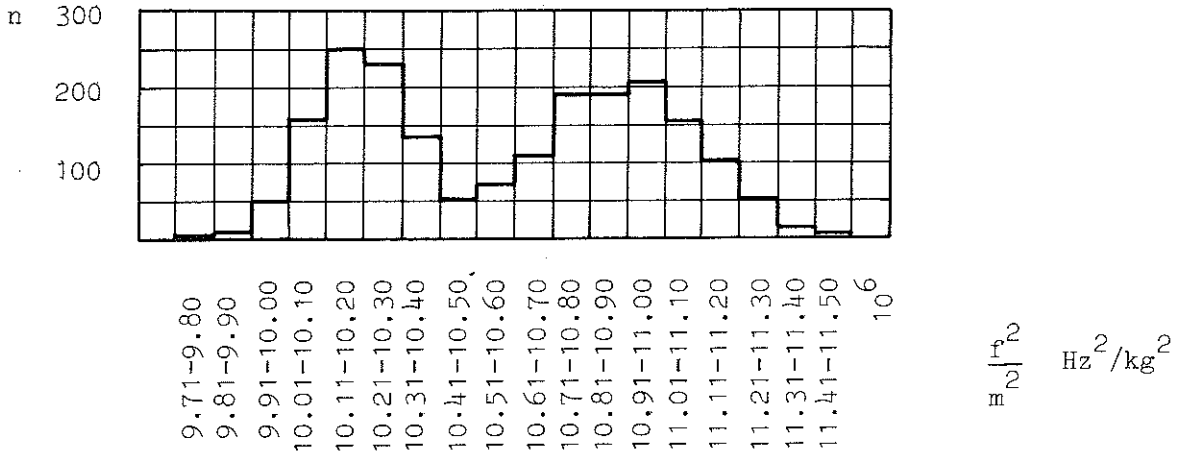

Figure 1.2.3.2c. Histogram of the flexural resonance frequency quantity f^2/m^2 of the F-tiles

The whole population of the quantity f^2/m^2 - left and right distributions - is characterized by the following statistical parameters

$\bar{x} = 10.58 \cdot 10^6$ Hz^2/kg^2
$s = 0.39 \cdot 10^6$ Hz^2/kg^2
$n = 1990$

The probabilistic characteristics of the geometrical measures in mm and of the mass in kg of the F-tiles are summarized in the following table[1].

	length		width		thickness		mass (m)	
	A	B	A	B	A	B	A	B
$\bar{x}$	196.0	195.9	96.6	96.5	12.4	12.4	0.589	0.591
s	0.5	0.5	0.2	0.2	0.1	0.1	0.004	0.004
n	69	68	69	68	69	68	484	520

1. Further information of measures is reported in section 1,5.1.

The values show a good over all uniformity.

The densities, measured according to the mercury method, of tiles A and B are the same: 2340 ± 15 kg/m^3 (n=9).

1.2.3.3. Thin N- and F-tiles

The predominant amount of the tiles, fixed on the test house elements, consisted of tiles type N and F of ordinary thickness of about 15 mm. As complement to this, a few elements were provided with thin N- and F-tiles of a thickness of about 10 mm. These thin tiles were selected in a corresponding manner as the tiles of ordinary thickness.

The thin tiles - A- and B-tiles mixed - had the following mean values of the geometrical measures and of the mass:

N

Length	Width	Thickness
195.7	97.1	10.6 mm

mass 0.430 kg (n = 10)

F

Length	Width	Thickness
195.5	95.6	9.6 mm

mass 0.414 kg (n = 10)

1.2.3.4. Distribution of the tiles on wall and column elements

For the distribution of the tiles on the different wall and column elements of the test houses the following rules were established to be fulfilled, connected to the probabilistic characteristics according to sections 1.2.3.1 and 1.2.3.2.

(1) Both A- and B-tiles should be used and placed in a checkered pattern for each element

(2) The measuring tiles (M) and reference tiles (R), provided with strain gauges, should all be B-tiles (see section 1.4.6). Further, the M and R tiles should be selected from the $\bar{x}$-class(es) of f^2/m

(3) The five vertical tile-rows of a wall element should with regard to f^2/m properties be balanced around the $\bar{x}$-class in the middle. Except M and R tiles, a column element should have all tiles from one and the same class nearest the $\bar{x}$-class.

The rules are further illustrated in application to the measuring, wall and column, test elements in Fig. 1.2.3.4a.

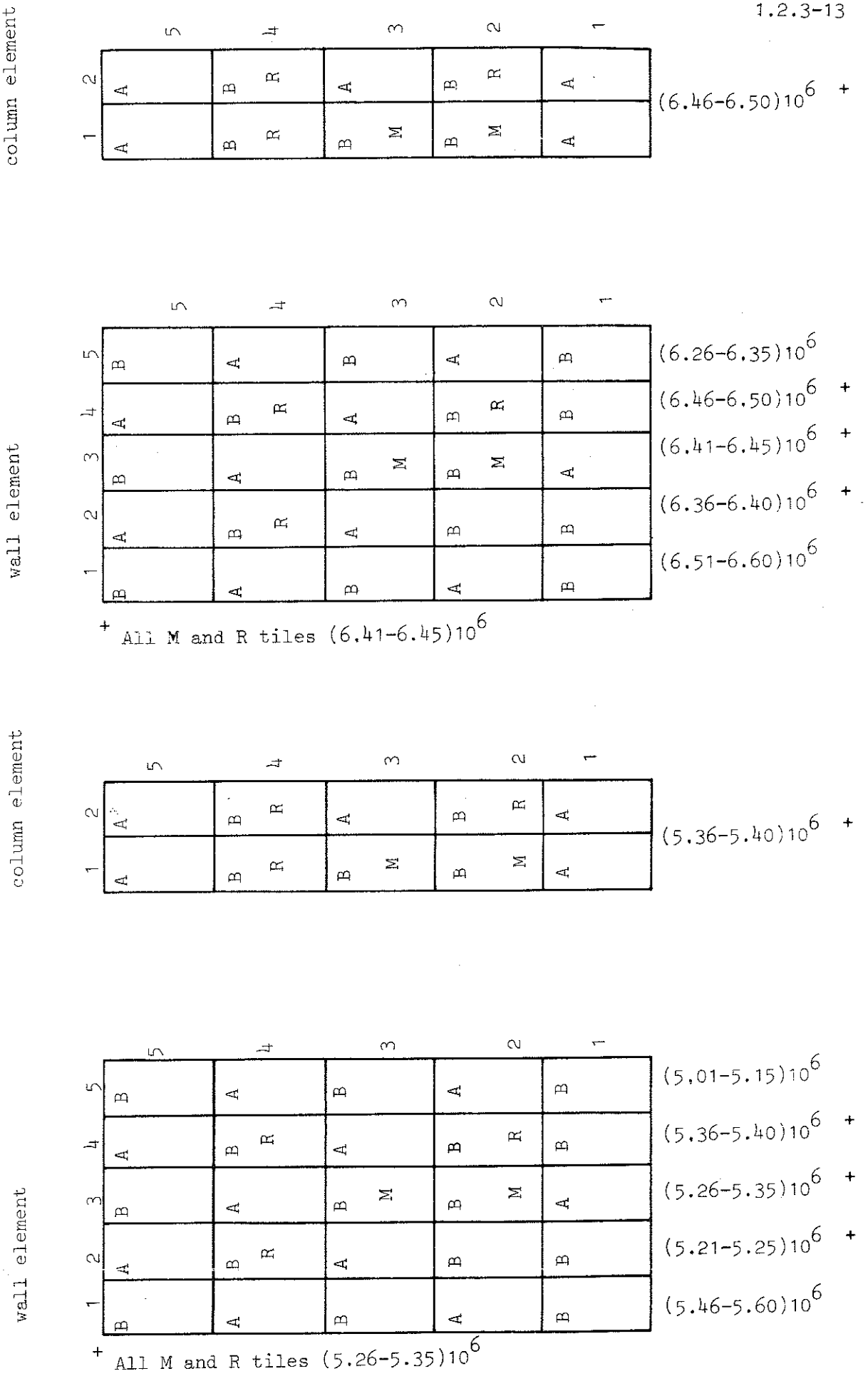

Figure 1.2.3.4a. Distribution of N- and F-tiles on measuring, wall and column, test elements

1.2.4. MATERIAL PROPERTIES

General initial material properties of single tiles, mortars, aerated concrete and concrete used had to be determined, viz.

(1) Measure, density, porosity
(2) Stress-strain relation - modulus of elasticity - creep
(3) Compressive, flexural and tensile strength
(4) Specific heat capacity
(5) Thermal conductivity - dry and wet material
(6) Thermal dilatation - dry and wet material
(7) Moisture fixation and transport
(8) Shrinkage and moisture dilatation
(9) Freezing properties

These initial property data of the different materials used are reported in this volume in sections 1.5.1 to 1.5.5.

The change of the initial properties due to the influence of environment conditions and of time had also to be studied. The collecting and studying of the various material properties, supposed to change are reported in volume 2.

1.2.5. PARALLEL OBSERVATIONS AND SPECIAL INVESTIGATIONS

In addition to the information from the more regular observations of stress and strain, heat, and moisture of the wall and column elements of the two test houses, a series of separate parallel observations and special investigations were planned as follows.

Parallel observations

(1) Single panels inside test house II.
(2) Single panels outside the test houses.

The single panels should partly be used as reference panels, partly as test bodies for heat, moisture and load studies after the main test house period.

Special investigations

(1) Temporary unloading of loaded panels and columns
(2) Dismounting of test house tiles
(3) Artificial heat tests - sun shield tests
(4) High frequency observations of panels and columns during 24 hours
(5) Moisture tests
(6) Freezing studies
(7) Shear studies on brick - mortar - aerated concrete.

1.3. TEST HOUSES

1.3.1. SITE OF TEST HOUSES

The geographic position of the test area is $56^{\circ}12'$N and $12^{\circ}33'$E or the flat industrial area in NW Höganäs, in NW of Scania, Sweden, near the sea shore.

The position of the test houses and surroundings is further described by map sketches and photos on the following pages.

The position gives a typical Scandinavian west coast clima with a clouded, mild winter period with some temperature passages below 0°C, often hard wind with showers of rain, concentrated to the autumn period. The summer period is early bright and its earlier part relatively warm with less wind and rain. To this is to notice the influence of the near salt water and industrial air pollution (sulfur oxides and mineral dust).

Special studies of the local air flow around the test houses were made by the Aeronautical Research Institute of Sweden (FFA) and are reported in appendix 1.3.1a. The studies were performed in the FFA building aerodynamics tunnel on a model of the test houses and the relevant environment in the scale 1:250. The wind speed applied was 20 m/s. The investigation included:

(1) Evaporation tests with naphtalene to locate areas with high flow velocity close to the wall surfaces

(2) Oil-flow tests to determine the flow direction over the building surfaces

(3) Smoke tests to study the vertical extent of the flow separation over that roof of the Central Laboratory building, on which the test houses are located, and

(4) Some calibration flow tests in full scale within the area of the test houses.

The results of the aerodynamic studies are giving a differentiated conception of the wind flow characteristics of the micro environment of the test houses. With regard to the technique of weather-climate measurement, the results are stressing the necessity of using local anemometers near the test houses for the determination of the direction and velocity of the wind, among other things.

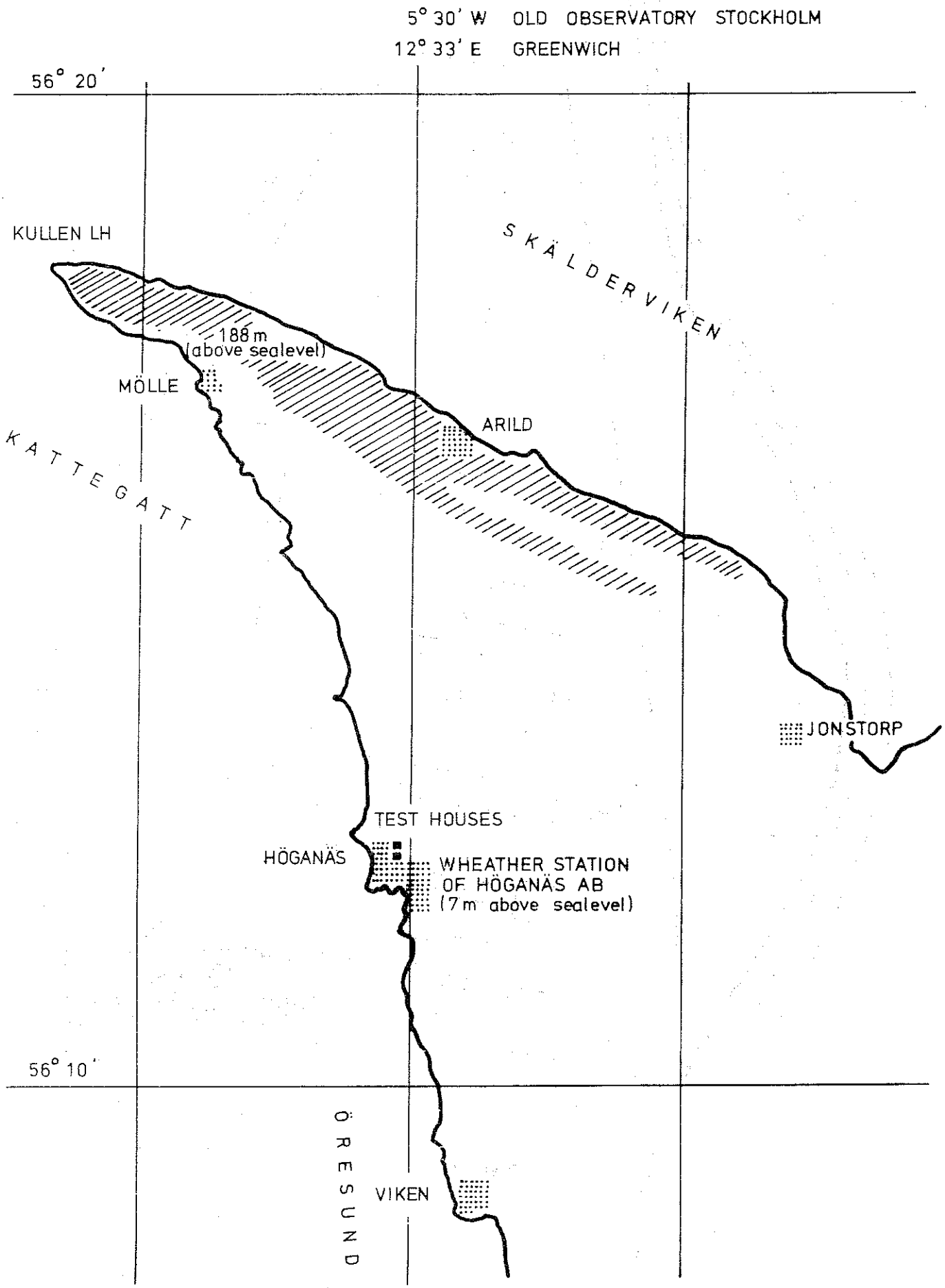

Figure 1.3.1a. Geographic position of test houses. Scale 1:100 000

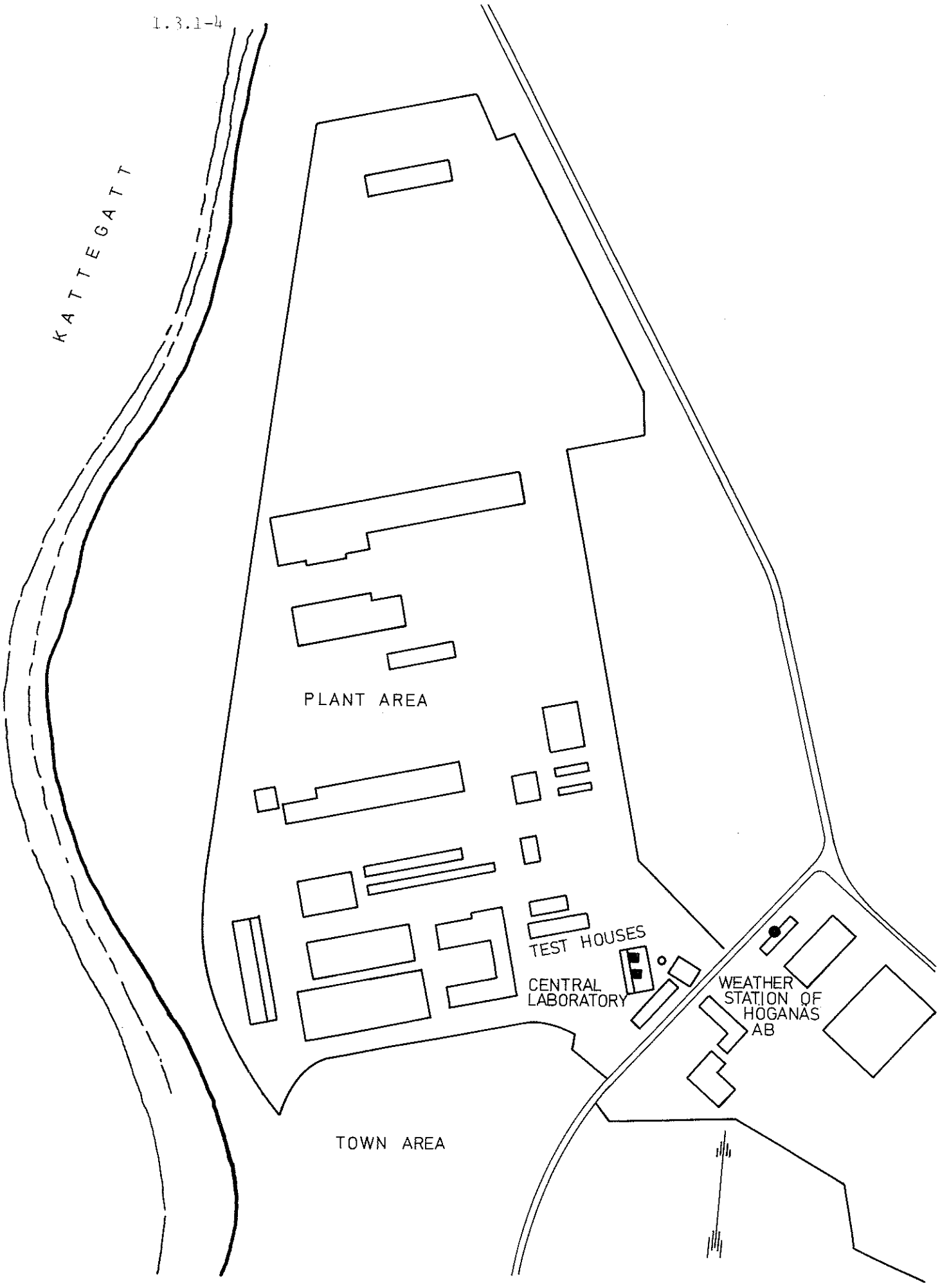

Figure 1.3.1b. Geographic position of test houses. Scale 1:6000

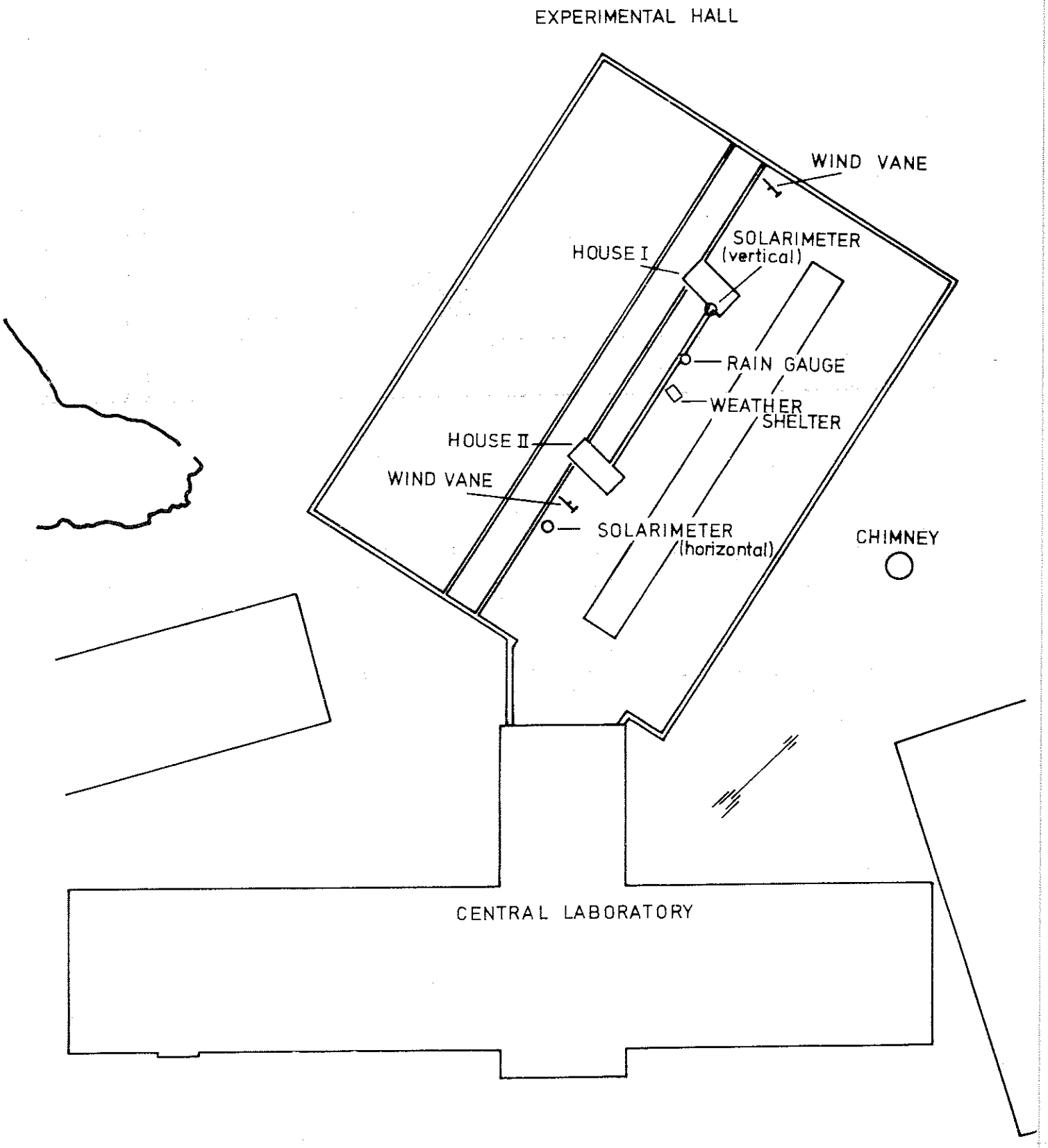

Figure 1.3.1c. Position of test houses on the roof of the Central Laboratory of Höganäs AB. Scale 1:500

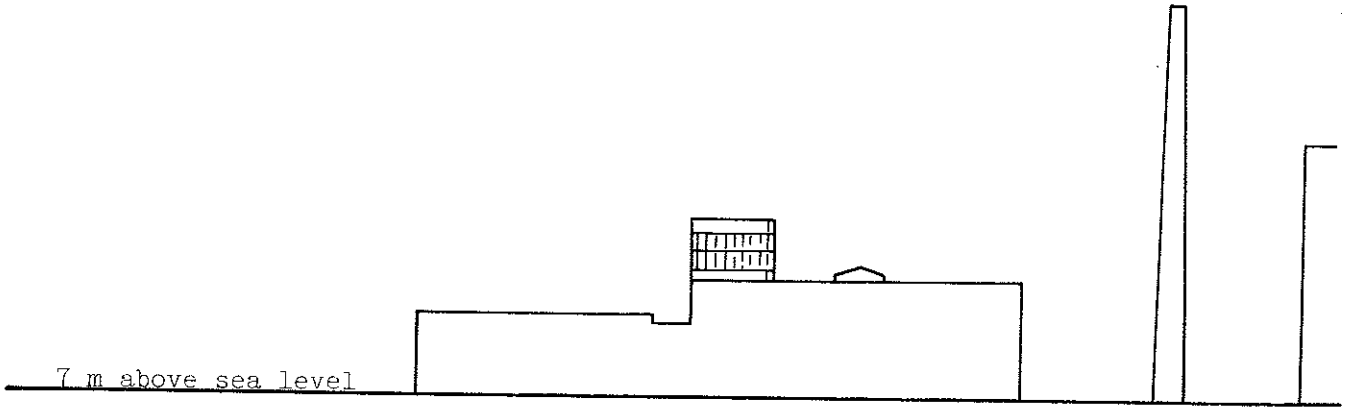

House	I	Length	4570	Width	2560	Height	3525/3260 mm
House	II		4539		2070		3540/3300 mm

Figure 1.3.1d. Vertical view from south, showing the position of the test houses on the roof of the Central Laboratory of Höganäs AB, Scale 1:500

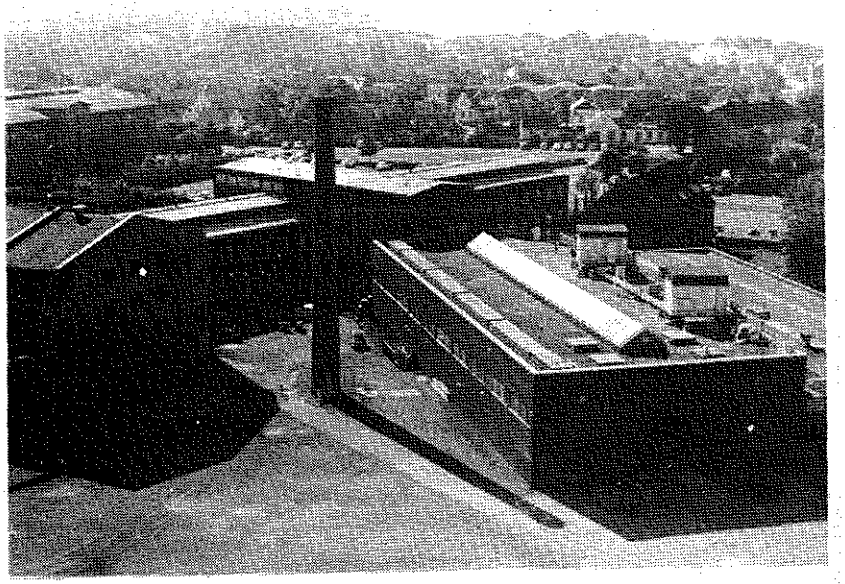

Figure 1.3.1e. View from north

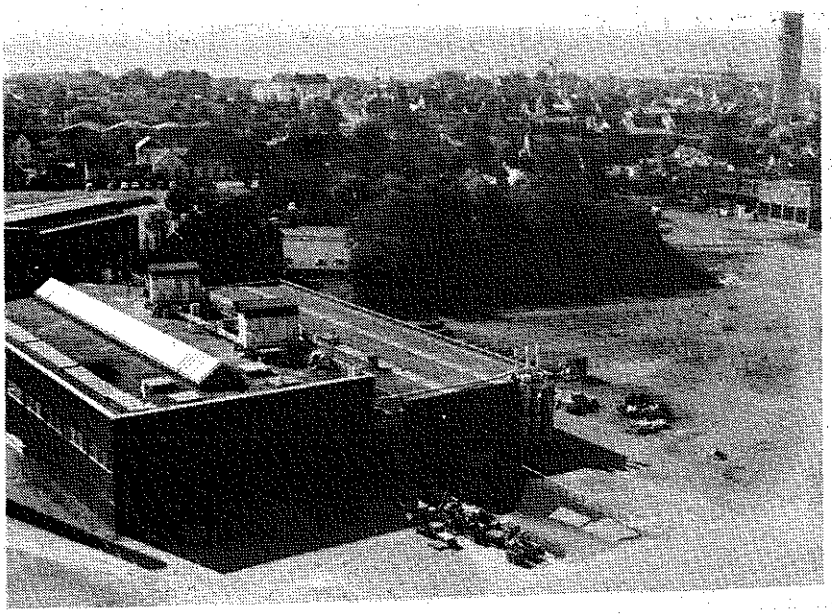

Figure 1.3.1f. View from north

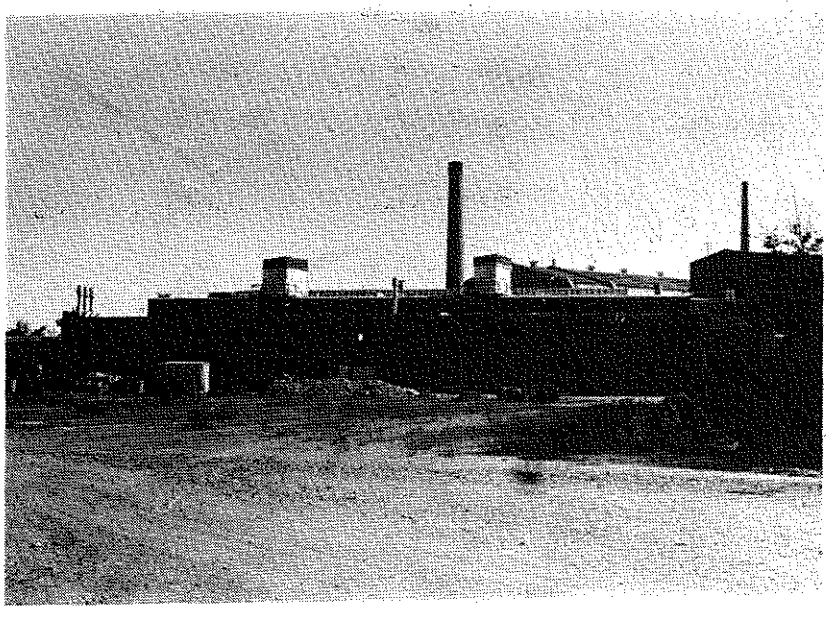

Figure 1.3.1g. View from west

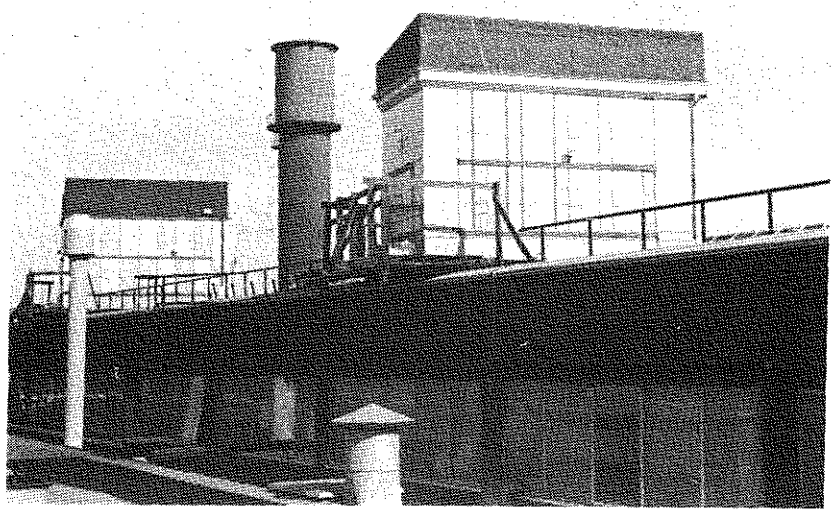

Figure 1.3.1h. View from south-west

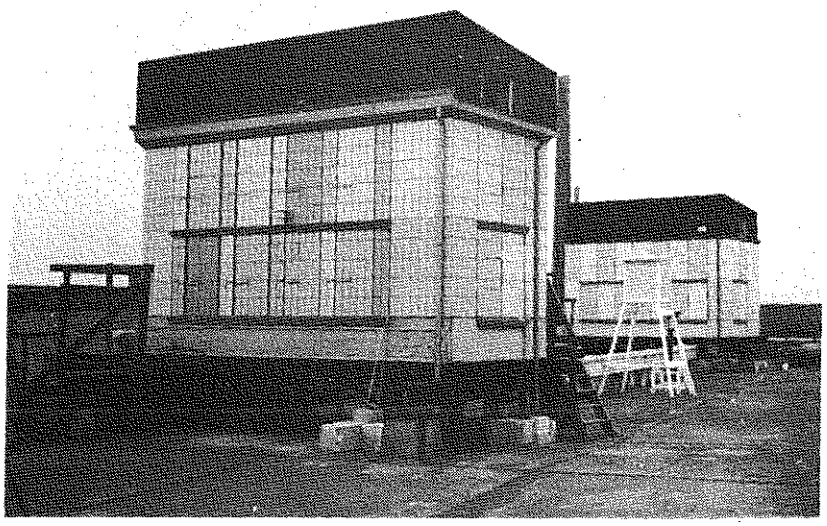

Figure 1.3.1i. View from south

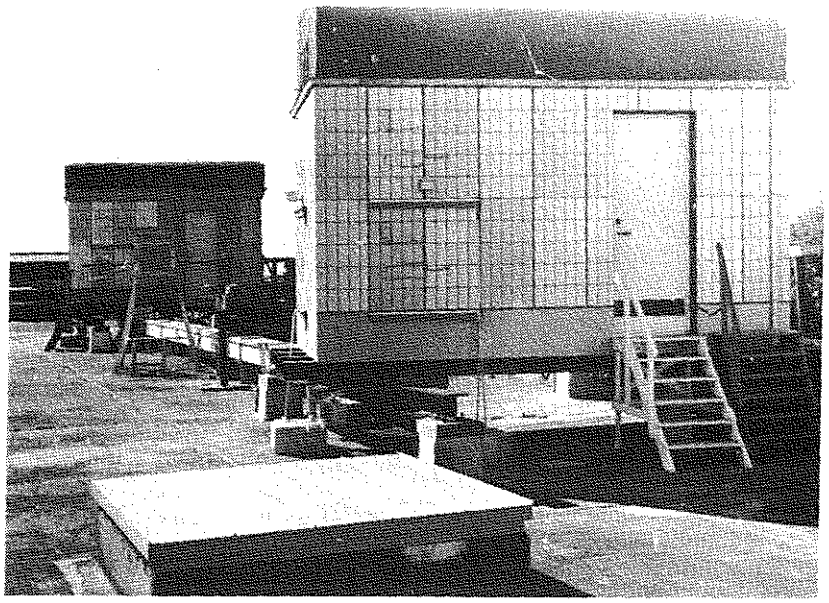

Figure 1.3.1j. View from north

1.3.2. CONSTRUCTION OF THE TEST HOUSES I AND II. DESCRIPTION, DRAWINGS, AND PERFORMANCE

With the main influences and parameters of the investigation being decided upon - see sections 1.2.1 to 1.2.3 - the specifications of the test houses could be drawn up. This was done in February 1966. The specifications are described below with reference to a numbering system according to the Swedish BYGG-AMA 1965.

The main drawings made were:

House I

Nos.	401.290	Fronts
	401.291 C	Horizontal cross section
	401.292 C	S wall, vertical cross section
	401.294 D	Vertical cross section B-B
	401.451 B	Detail C (vertical cross section upper part S wall)
	401.452	Beams and bars
	401.453	Concrete mould
	401.454	Concrete mould section A-A
	401.455	Concrete mould section B-B
	401.456	Insulating elements (top and bottom S wall)
	401.457	Rods, beams, and reinforcing steel
	401.458	Detail D (vertical cross section lower part S wall)

House II

Nos.	401.296 B	Fronts
	401.298 B	S wall, vertical cross section A-A
	401.300 C	Vertical cross sections B-B and C-C
	401.308 B	Horizontal cross section
	401.479	Detail D (vertical cross section upper part S wall)
	401.480 A	Detail E (vertical cross section lower part S wall)
	401.481 A	Rods and beams
	401.482 A	Insulating elements (top and bottom S wall)

The description and the original main drawings are not published in the report, instead an outline of House I is summarized in four drawings (Fig. 1.3.2a - d), and of House II in five drawings (Fig. 1.3.2e - i). Further two drawings (Fig. 1.3.2j - k) and Fig. 1.3.2ℓ show the arrangements with regard to the extra load applied by a hydraulic system on special wall and column elements in the south walls of the test houses.

The different full extra loads (and the accompanying working stresses) were planned as below (cf. Fig. 1.3.2ℓ):

House I,	wall element No. 1/2, 3/4, 5/6	0.36 MN	(5 MPa)
	wall element No. 7/8, 9/10	0.18 "	(2.5 ")
House II,	wall element No. 27/28, 29/30	0.08 "	(0.6 ")
	column element No. 47/48	0.24 "	(8 ")
	column element No. 49/50	0.19 "	(6.5 ")
	column element No. 51/52	0.12 "	(4 ")

The load was applied in four equal steps within 28 days after the tile jointing.

Fig. 1.3.2ℓ also shows the numbering applied to the wall and column elements of the test houses as well as some fundamental characteristics of the elements. The following notations then are used:

F = elements with tiles type F, thickness 15 mm,
Ft= elements with thin tiles type F, thickness 10 mm,
N = elements with tiles type N, thickness 15 mm,
Nt= elements with thin tiles type N, thickness 10 mm,
3 = joints of cement mortar C100/300,
6 = joints of cement mortar C100/600, and
u.j = unfilled joints.

For all wall and column elements, a fixing mortar of lime-cement-mortar type,KC 35/65/550, was used. Cf. also section 1.5.2 and 1.5.3.

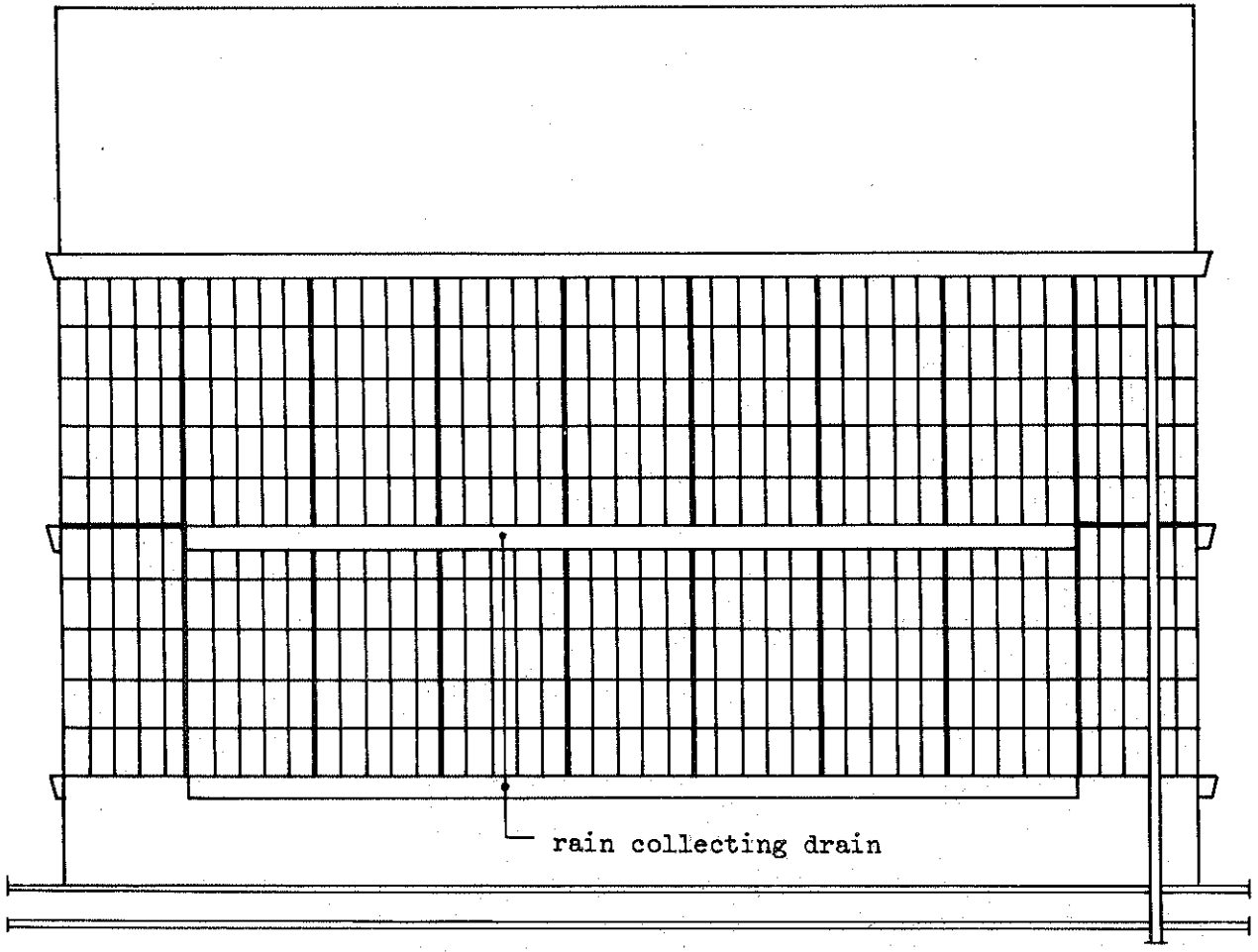

south

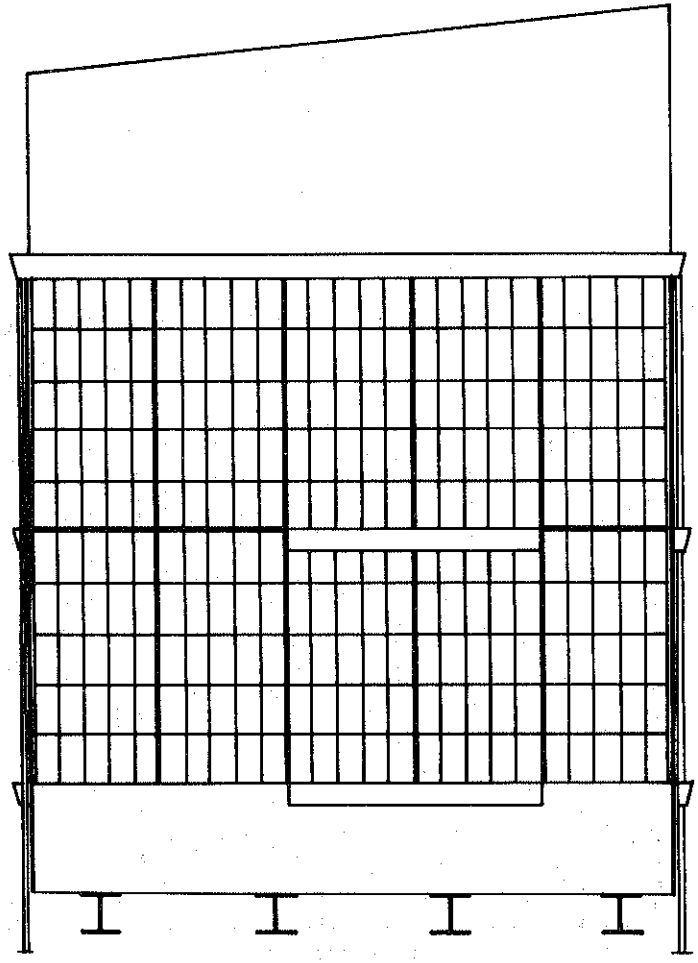

west

Figure 1.3.2a. Test house I, south and west fronts. Scale 1:30

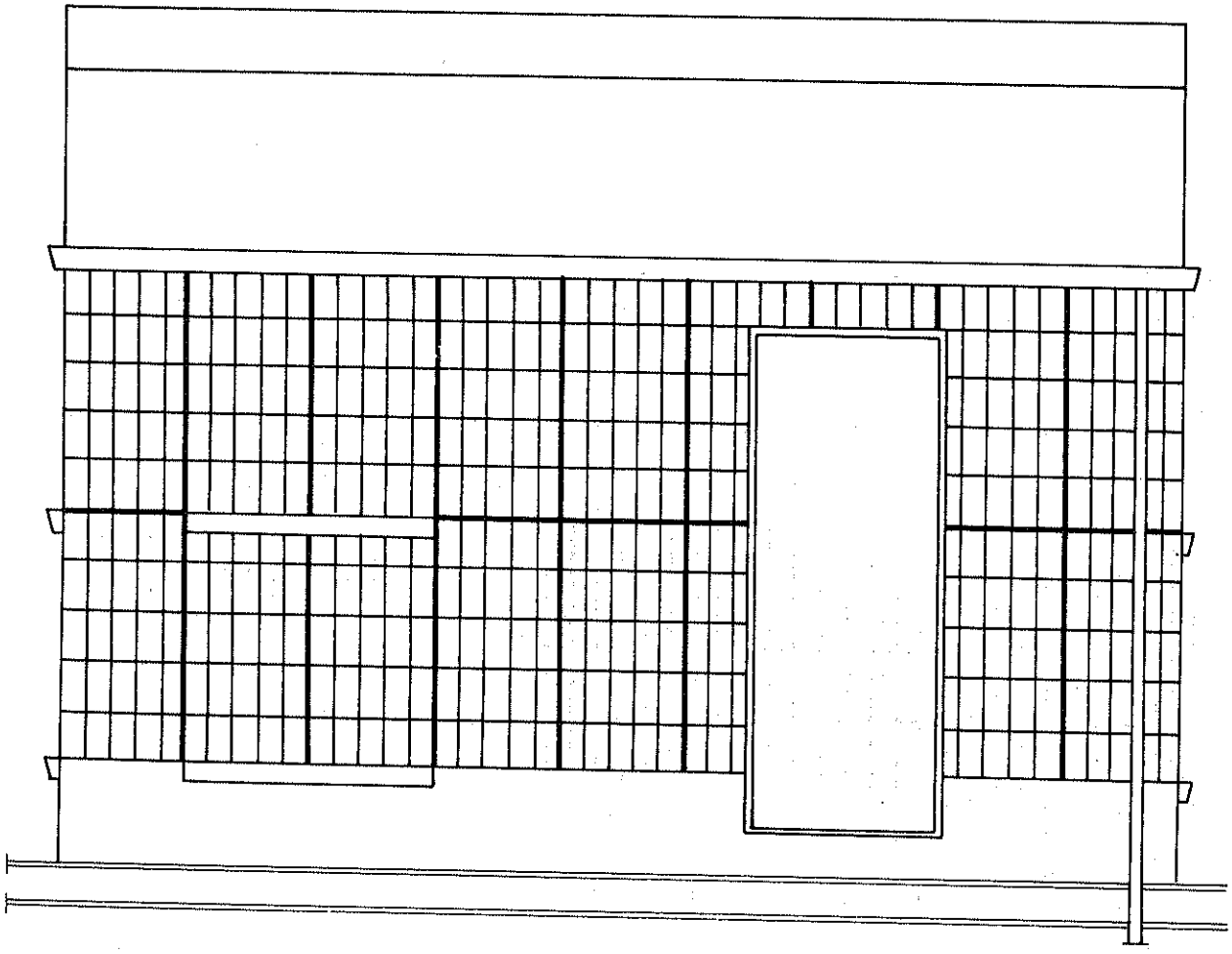

north

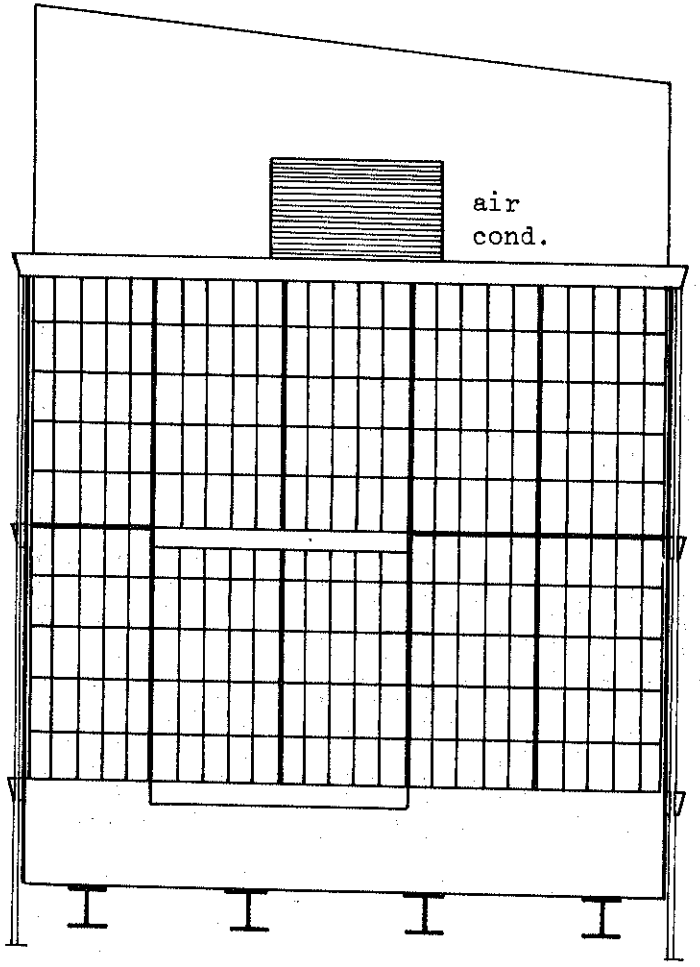

east

Figure 1.3.2b. Test house I, north and east fronts. Scale 1:30

material description on vertical
cross section, page 1.3.2-6

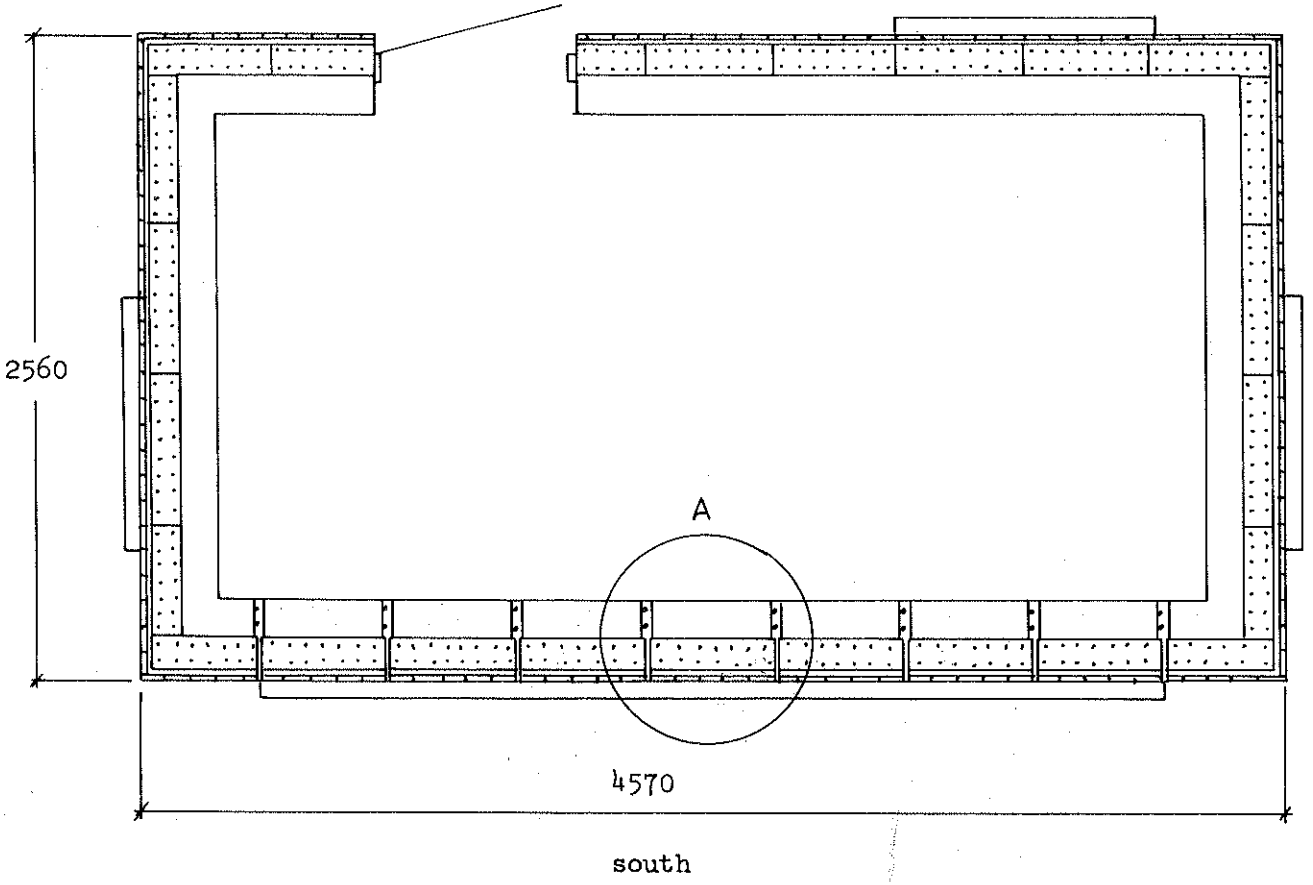

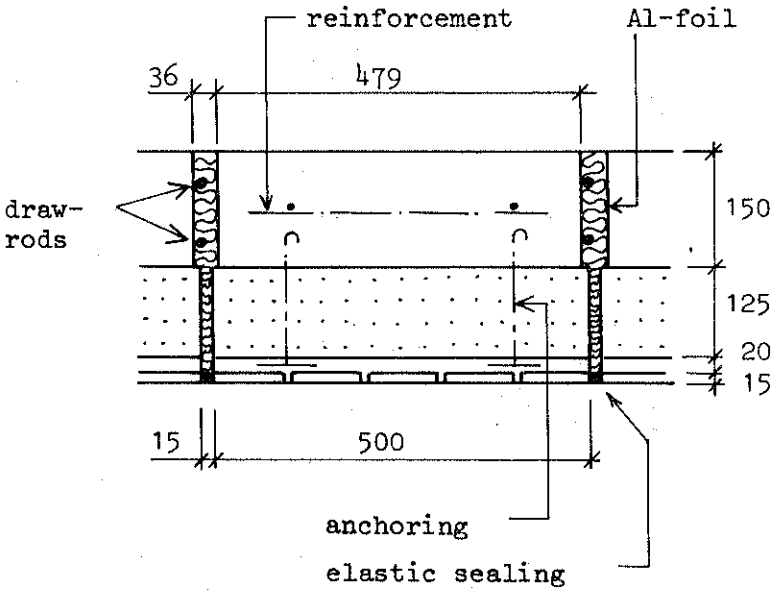

A

measures in mm

1.3.2-5

Figure 1.3.2c. Test house I, horizontal cross section. Scale 1:30 and 1:10 (detail A)

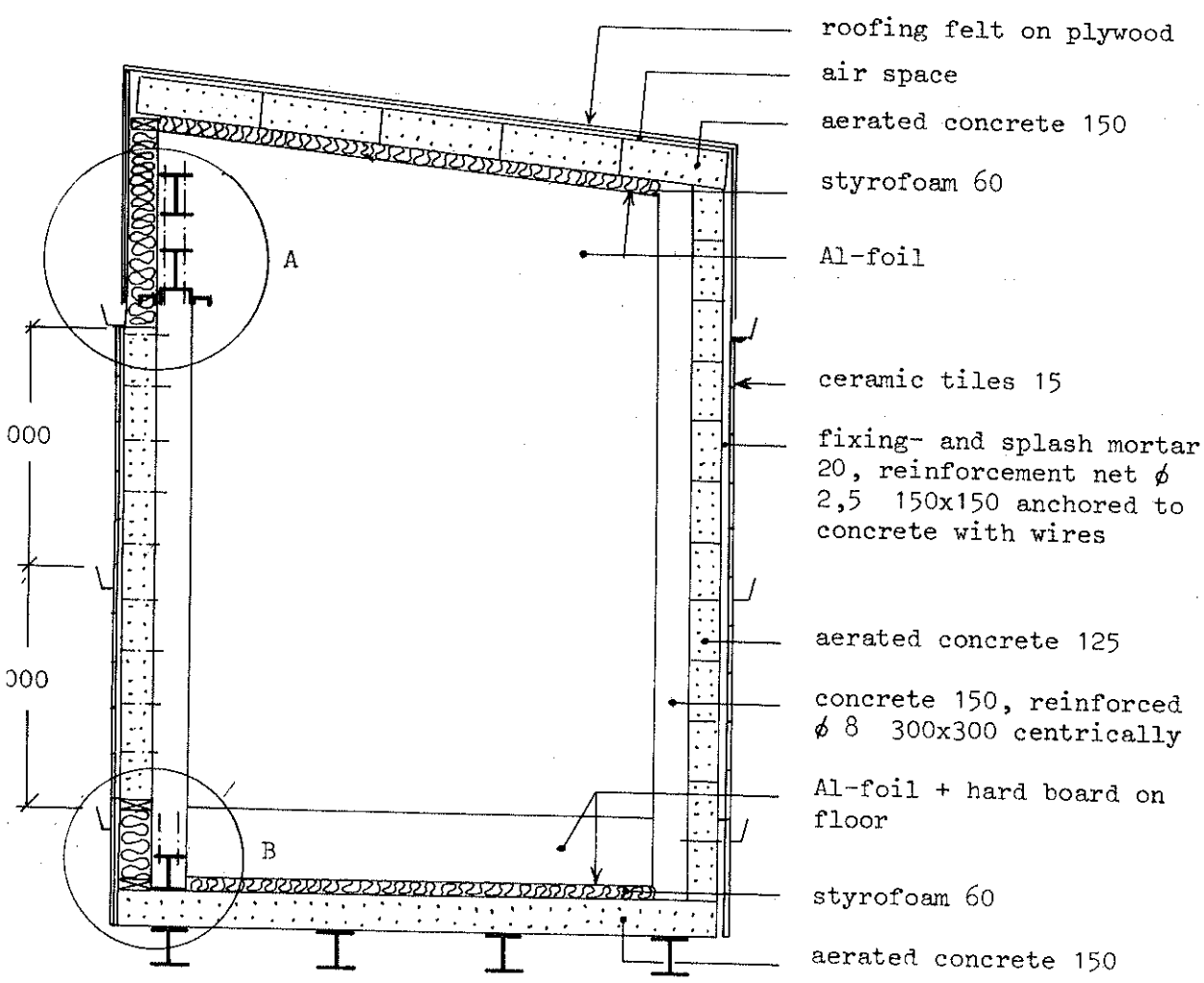

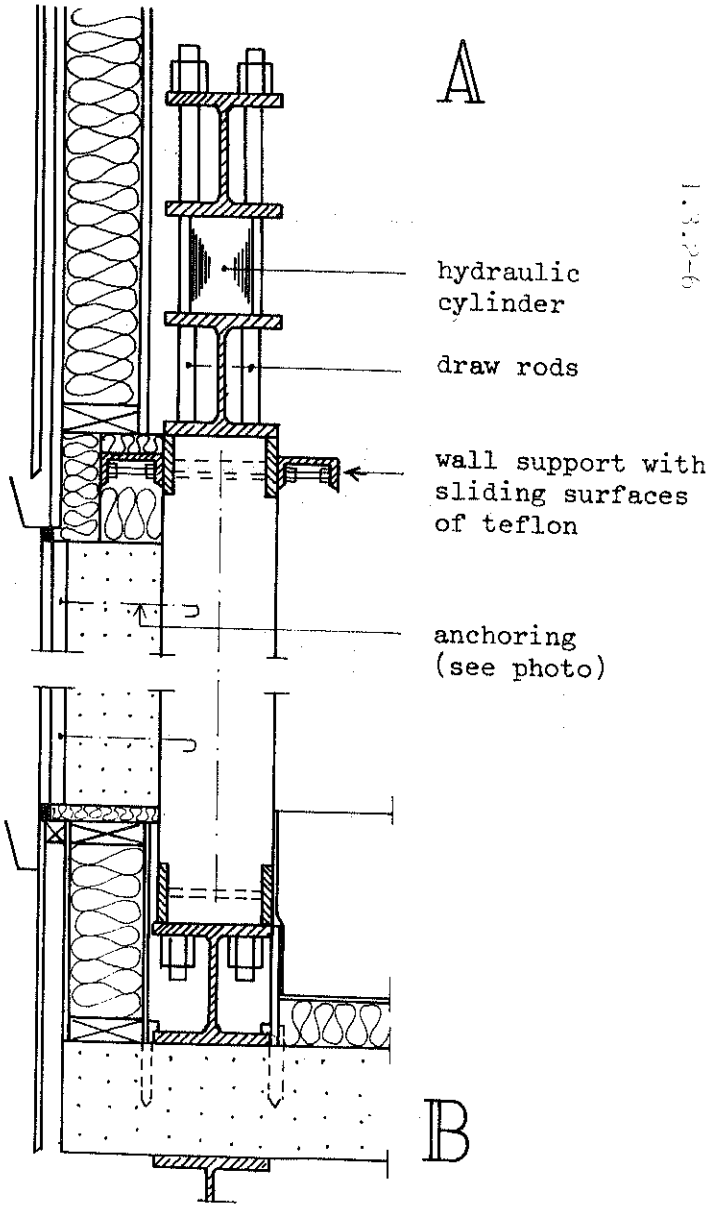

Figure 1.3.2d. Test house I, vertical cross section with hydraulic loading arrangements. Scale 1:30 and 1:10 (details A and B)

measures in mm

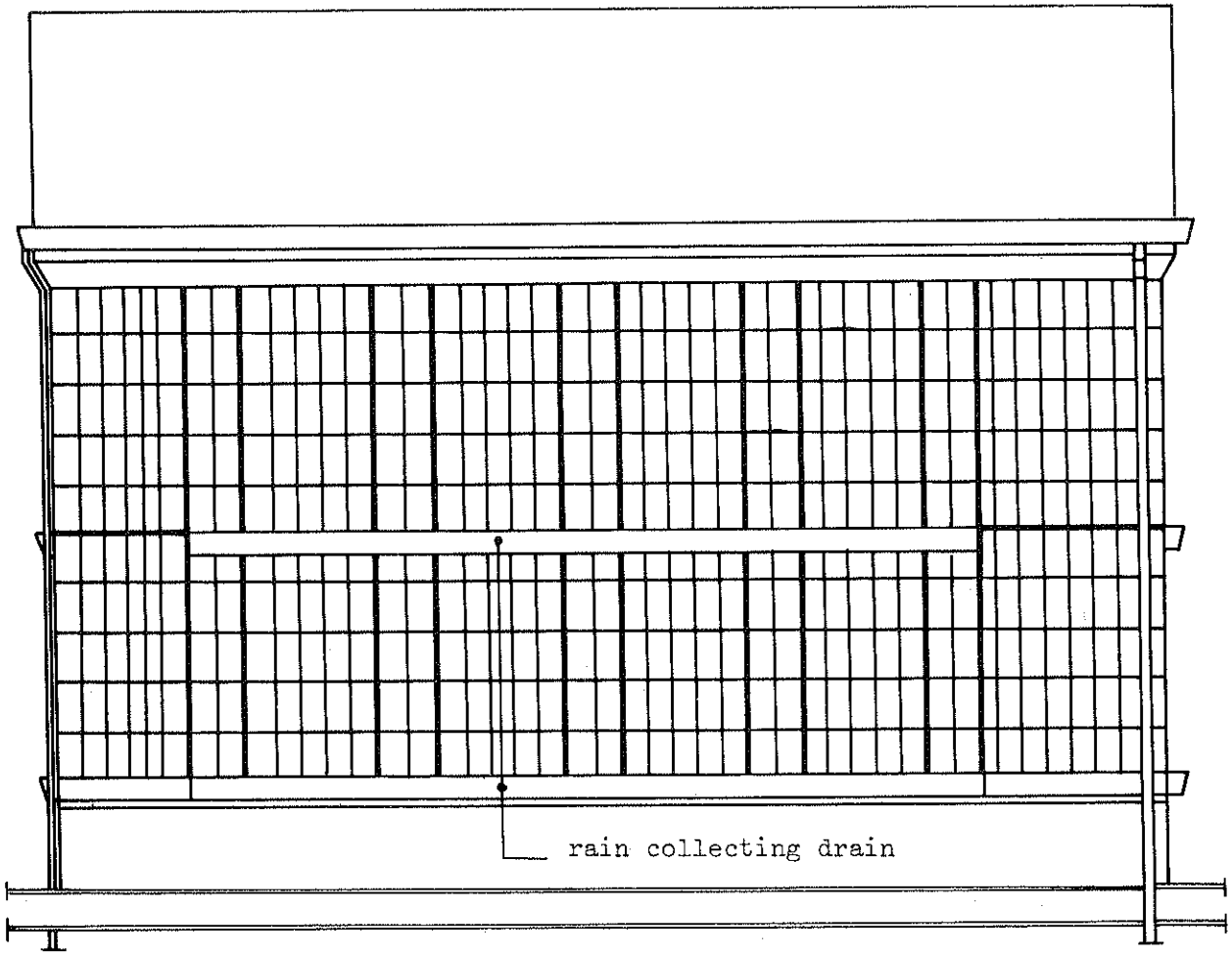

south

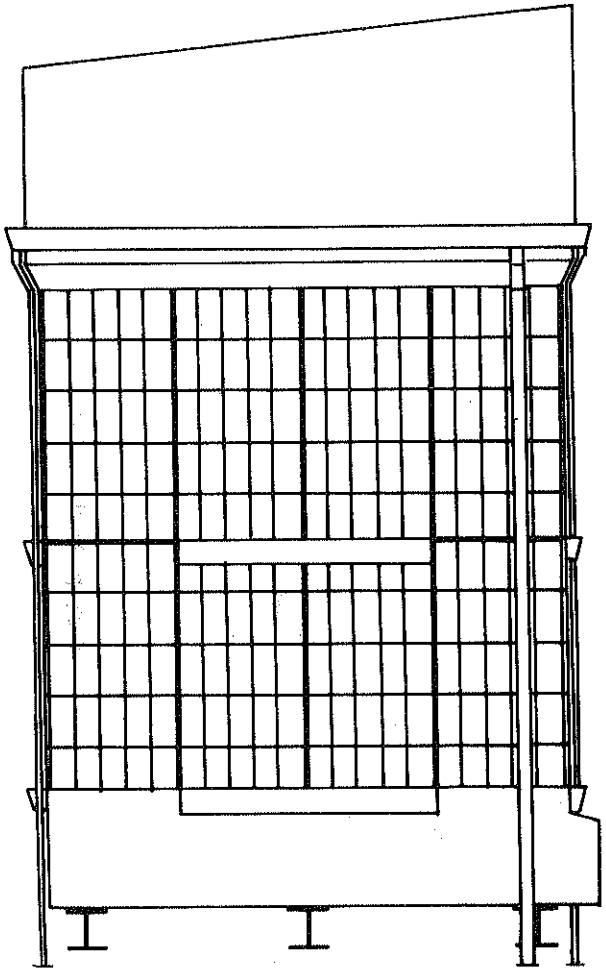

west

Figure 1.3.2e. Test house II, south and west fronts. Scale 1:30

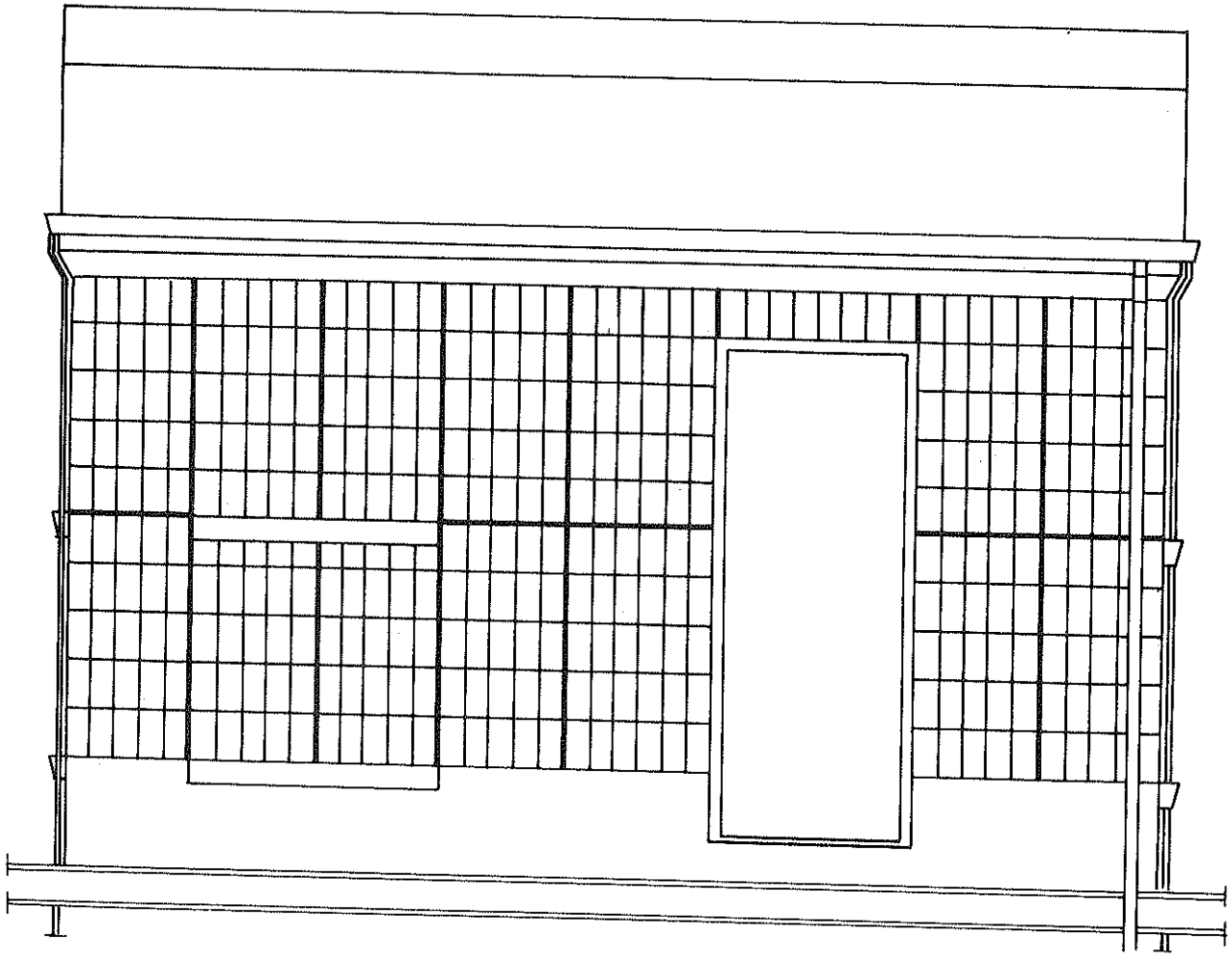

north

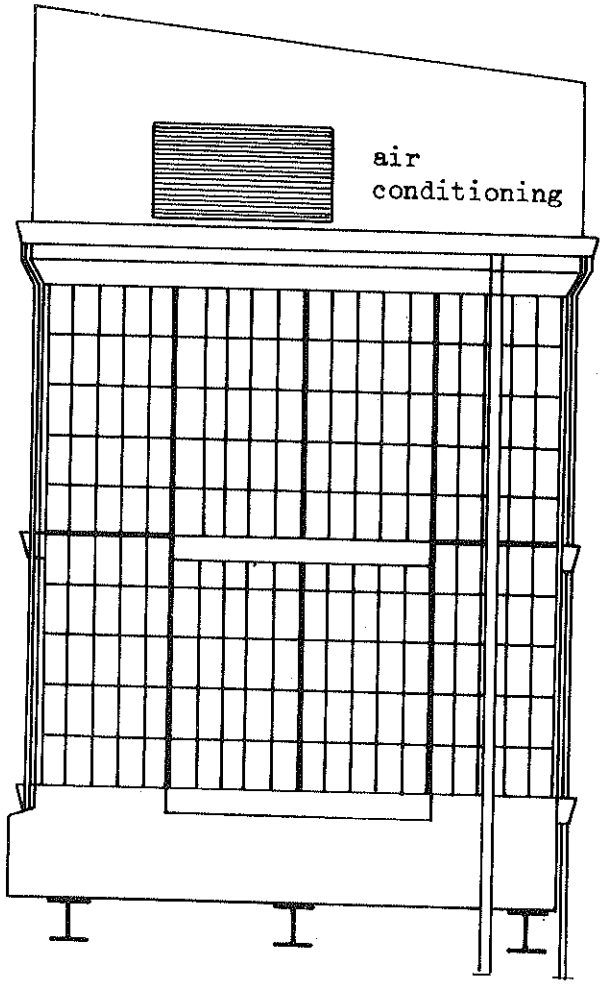

east

Figure 1.3.2f. Test house II, north and east fronts. Scale 1:30

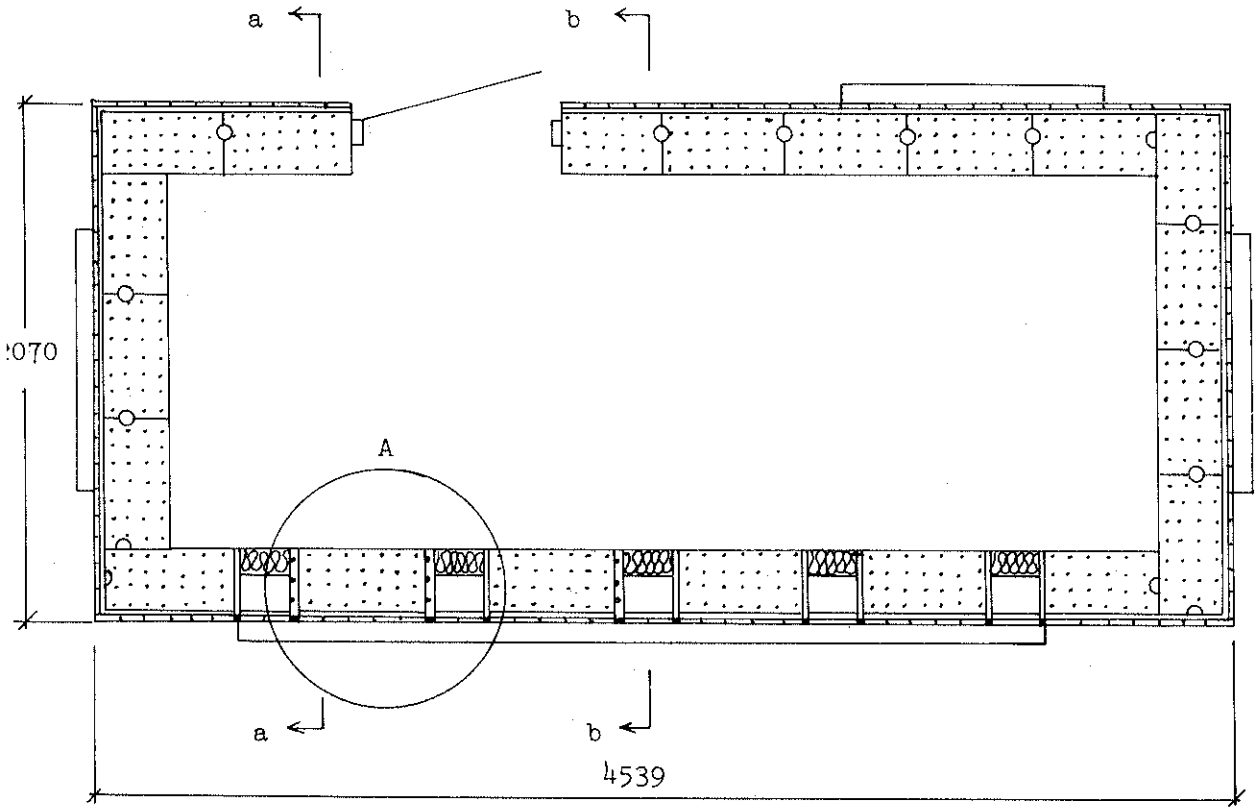

south

material description on vertical
cross section, pages 1.3.2-10 and 11

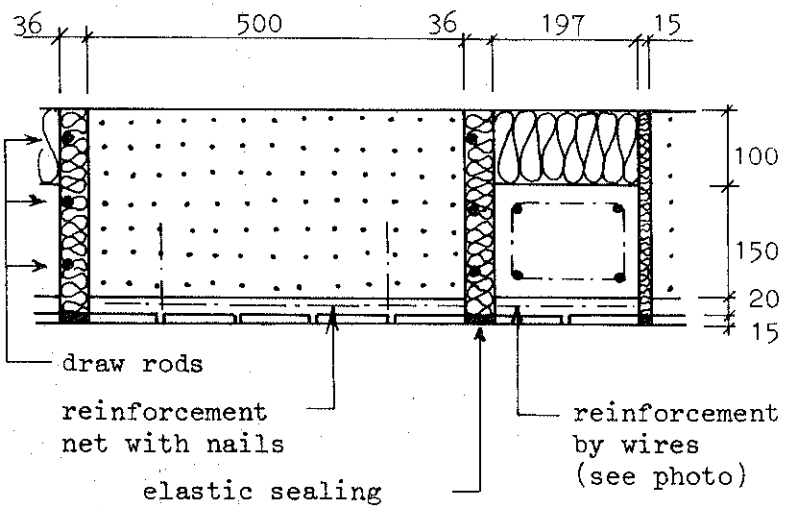

A

measures in mm

Figure 1.3.2g. Test house II, horizontal cross section. Scale 1:30 and 1:10 (detail A)

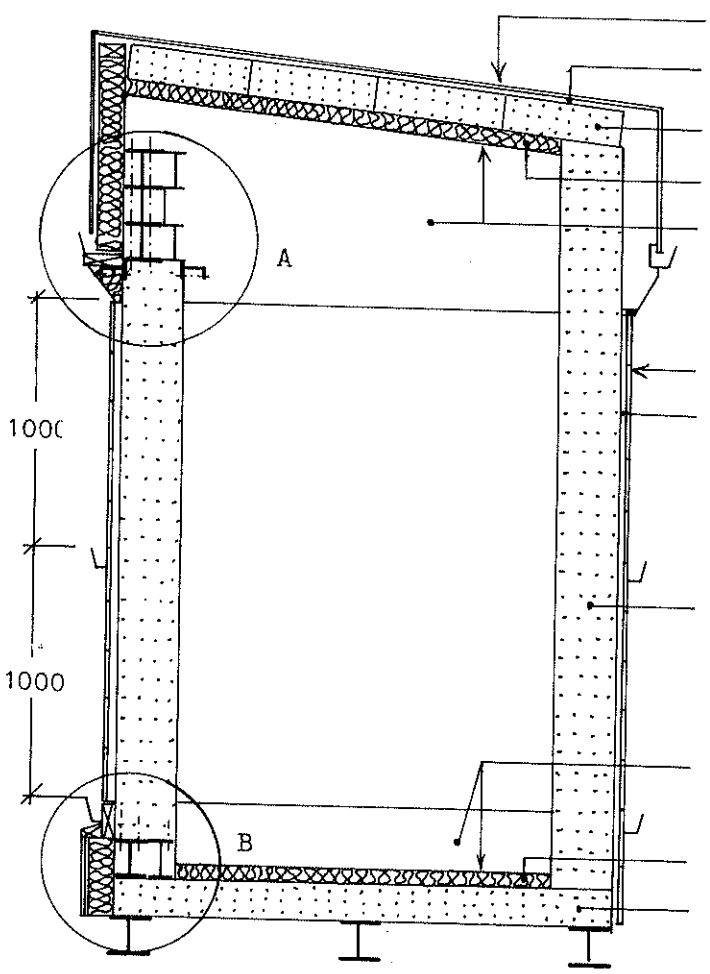

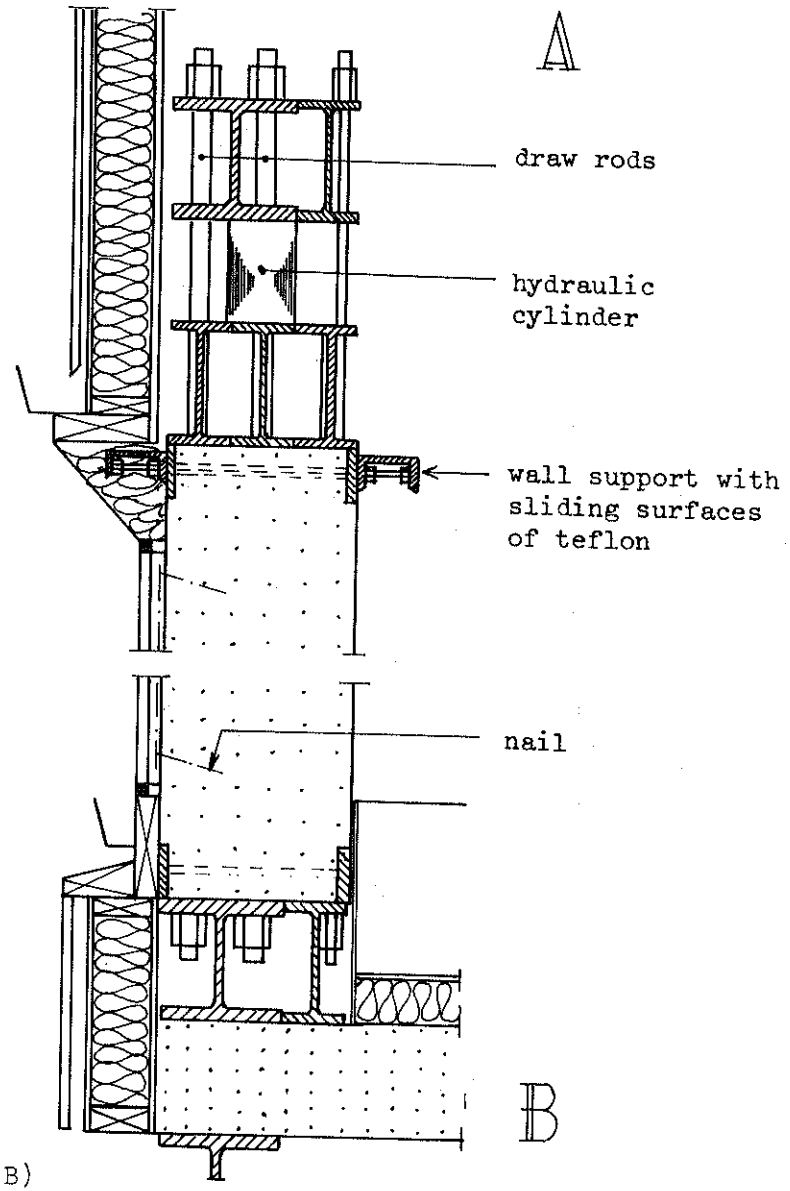

Figure 1.3.2h. Test house II, vertical cross section a-a with hydraulic loading arrangements. Scale 1:30 and 1:10 (details A and B)

measures in mm

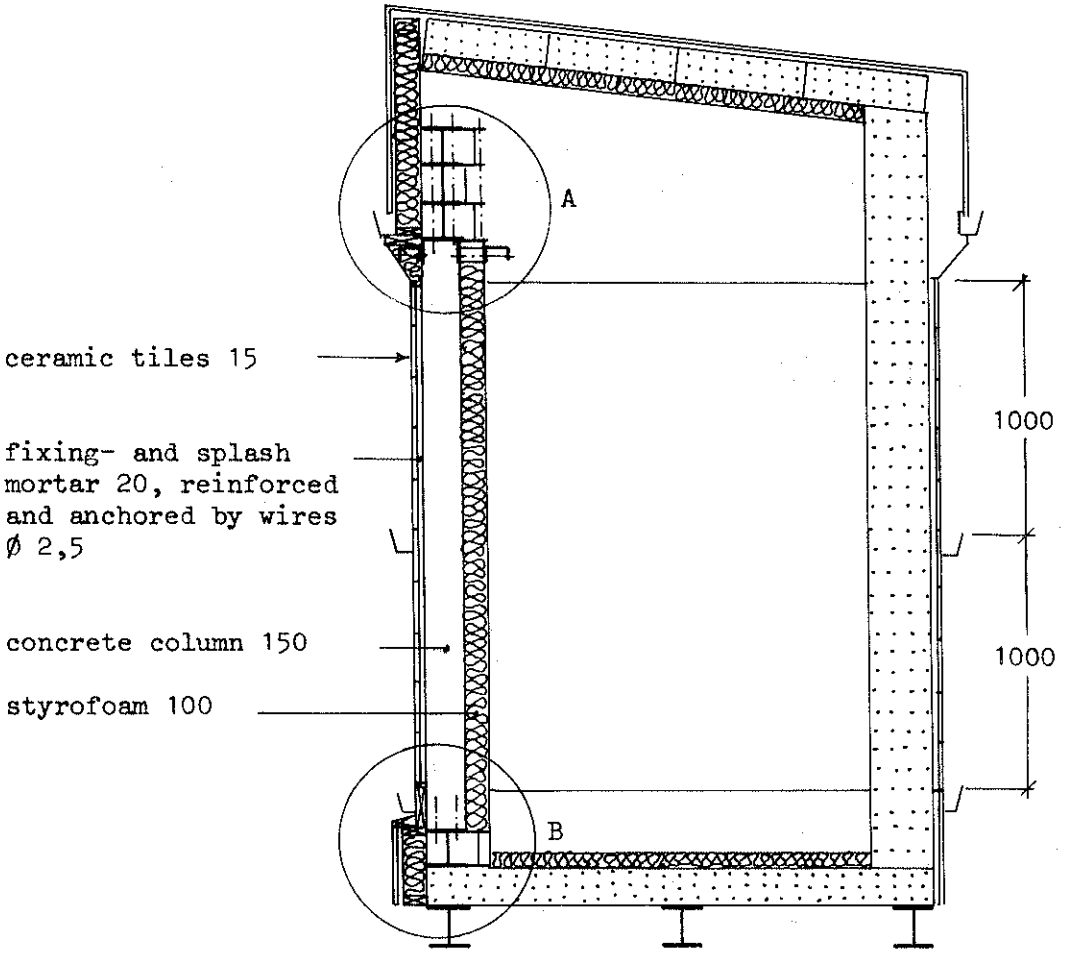

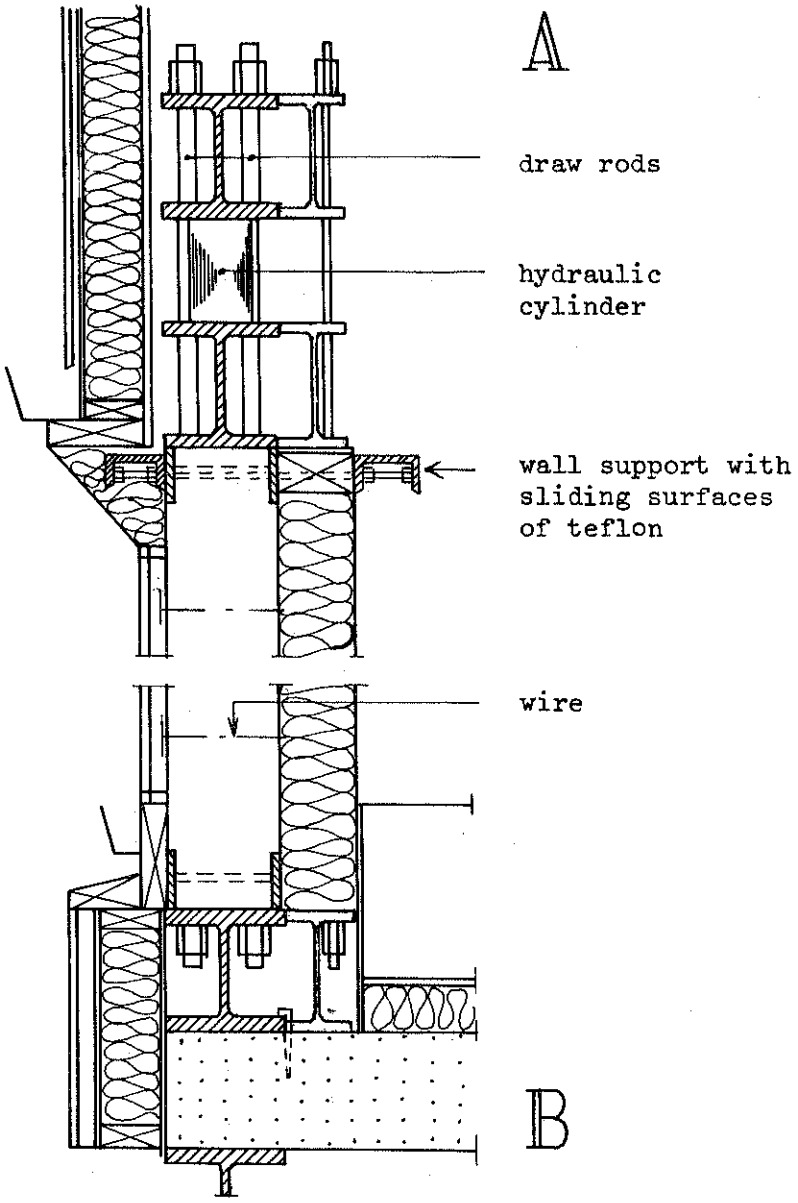

Figure 1.3.2i. Test house II, vertical cross section b-b with hydraulic loading arrangements. Scale 1:30 and 1:10 (details A and B)

measures in mm

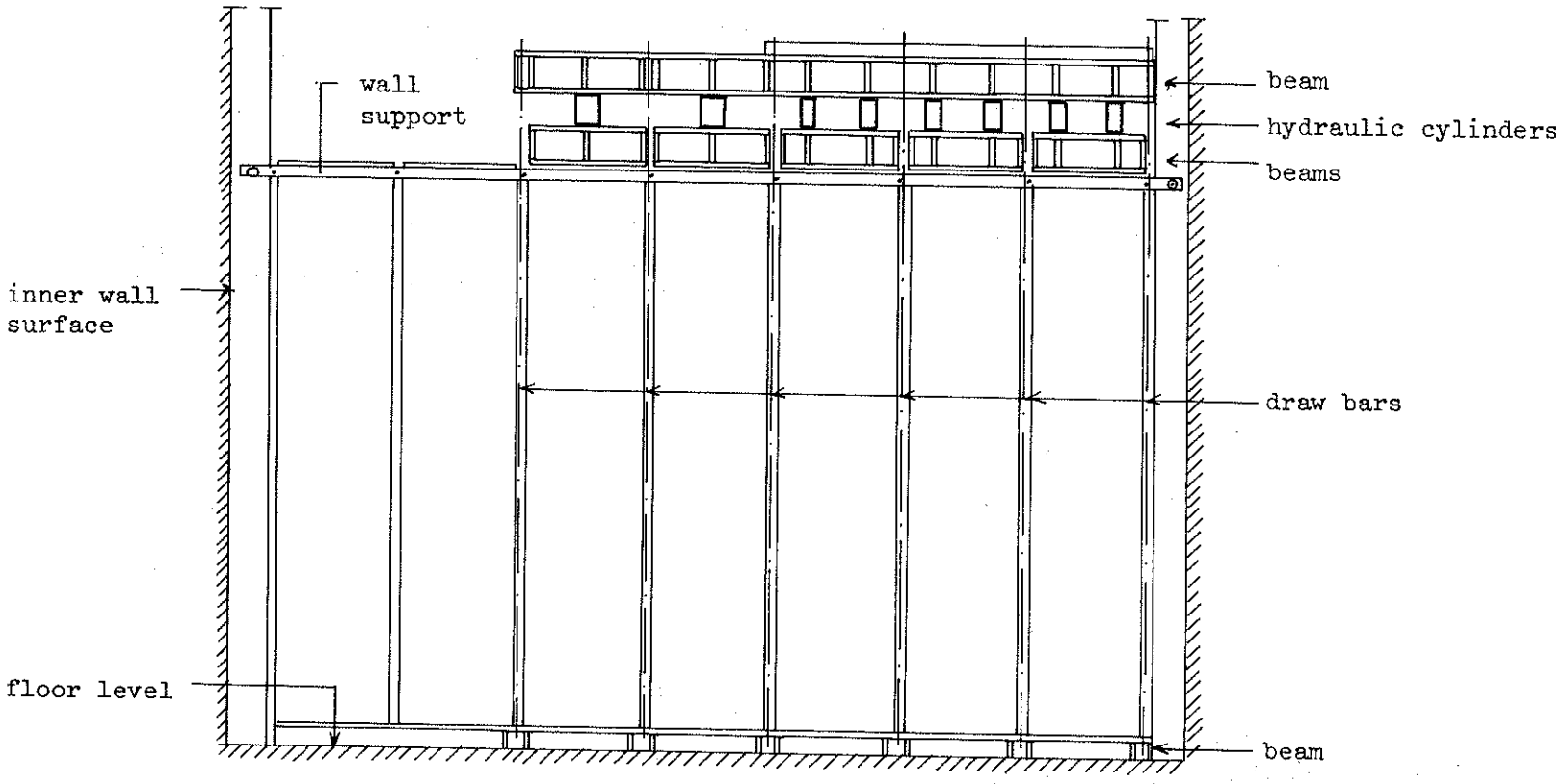

Figure 1.3.2j. Test house I, inside south wall with hydraulic loading arrangements. Scale 1:30

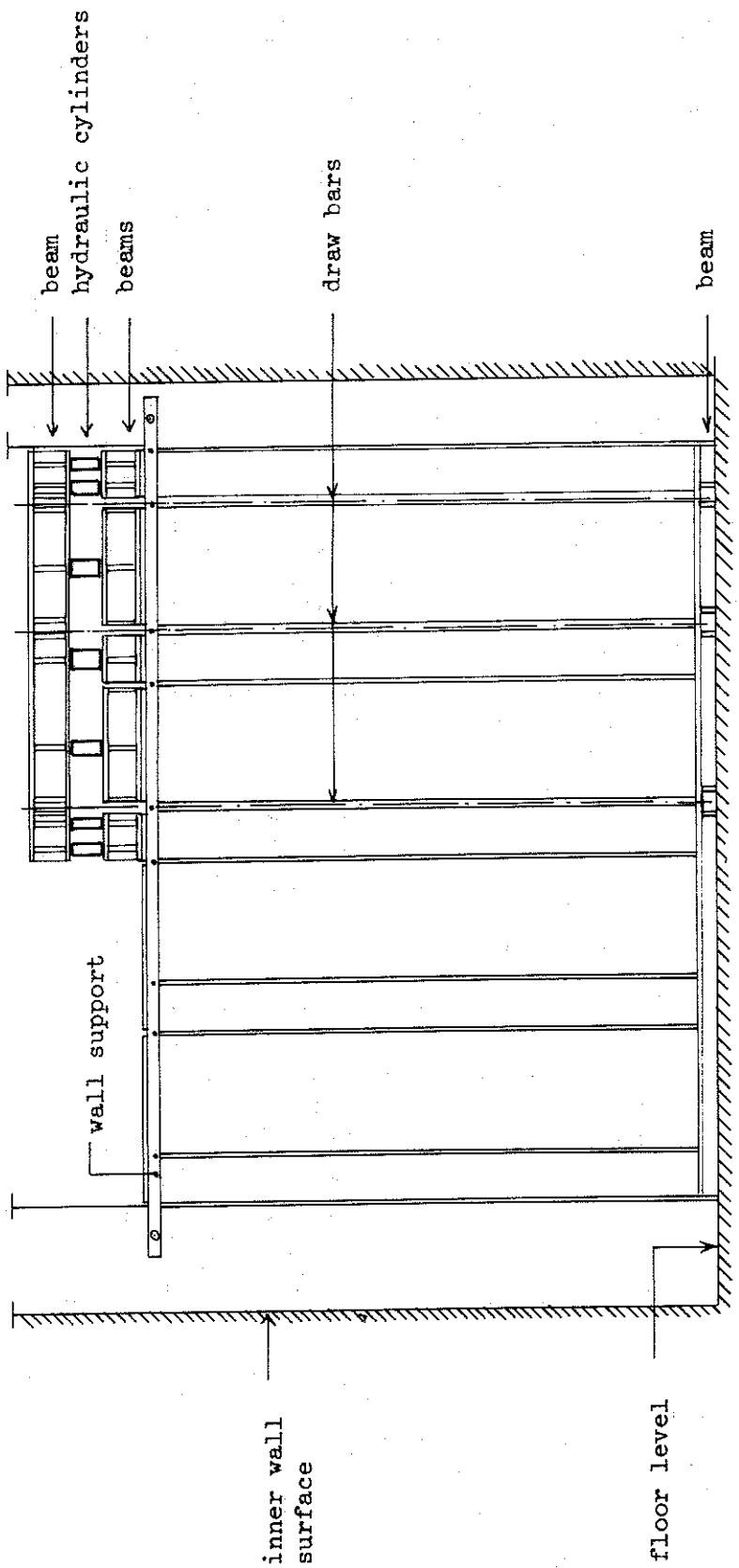

Figure 1.3.2k. Test house II, inside south wall with hydraulic loading arrangements. Scale 1:30

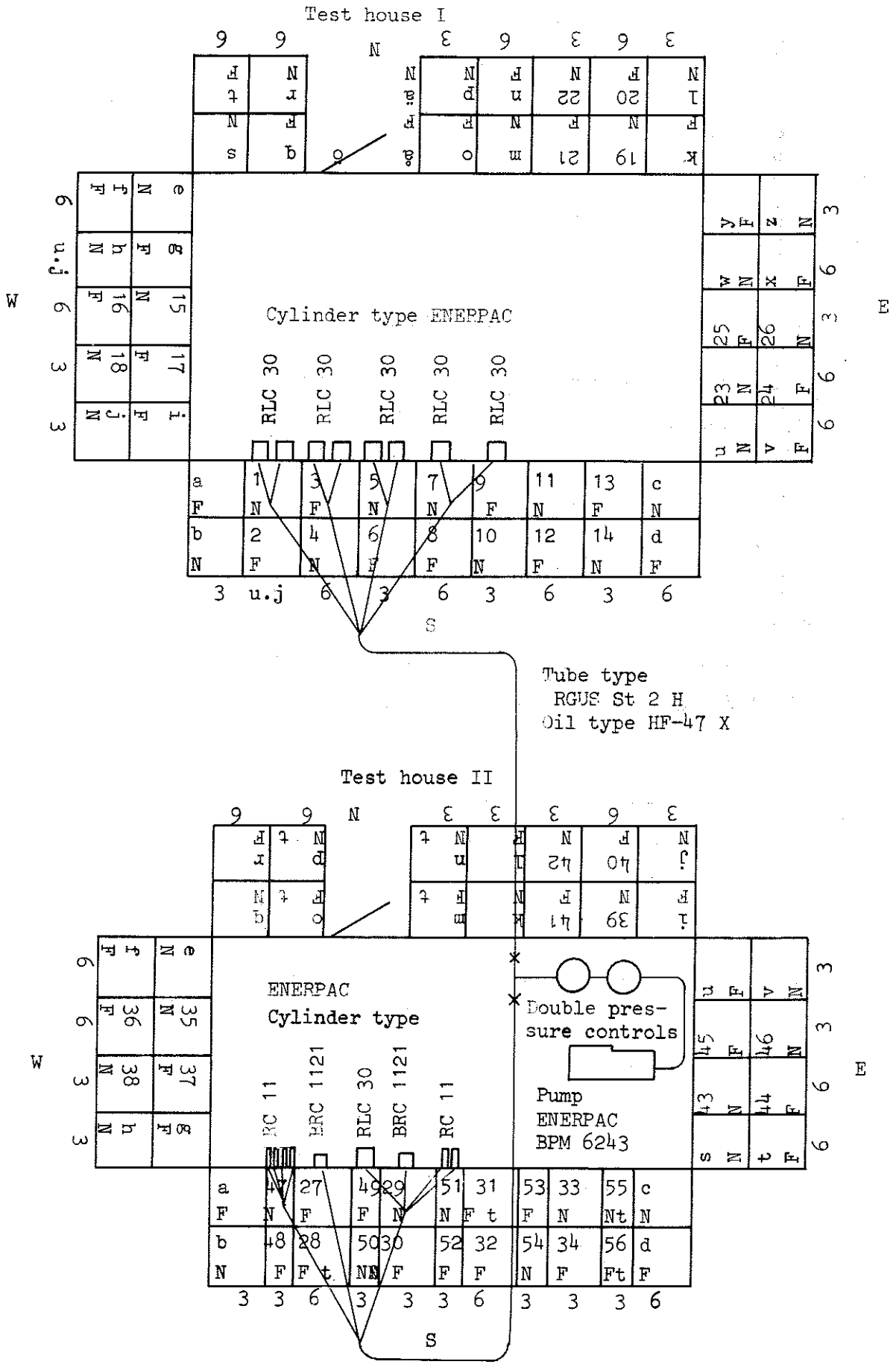

Figure 1.3.2ℓ. Survey of arrangements of different elements and joints. Hydraulic system for extra load on special wall and column elements, shown in unfolded position

The construction of the two test houses followed the chronological order:

1968, autumn	Construction of concrete supports on the roof of the experimental hall (Fig. 1.3.2m)
1969, February	House I: installation of supporting steel beams on the top of the concrete supports. Construction of a floor of aerated concrete, erection of exterior wall insulation of aerated concrete and building of the forms for casting of the concrete wall elements (Fig. 1.2.3n and o)
1969, May 27	House I: concreting.
1969, June 02	House I: removing of concrete forms. Erection of the roof structure and roofing. Installation of the data logging system
1969, June 03	House I: application of splashing mortar
1969, June 05 - 06	tile fixing (Fig. 1.3.2q)
1969, June 09	House I: jointing of the ceramic tiles
1969, June 17	House I: application of 25% of the final level of the hydraulic loading of specified wall elements (Fig. 1.3.2ℓ)
1969, June 17	House II: concreting and construction of column and wall elements (except aerated concrete elements of south wall) on previously installed supporting steel beams and floor elements of aerated concrete (Fig. 1.3.2r and s)
1969, June 23	House II: removing of the forms from the concrete columns and raising the aerated concrete elements on the south wall (Fig. 1.3.2t). Erection of the roof structure and roofing
1969, June 24-25	House I: increase of the hydraulic loading of specified wall elements to 50% of the final load level
1969, June 24-27	House II: application of splashing mortar and fixing of the tiles (Fig. 1.3.2u and v)
1969, July 01	House I: increase of the hydraulic loading of specified wall elements to 75% of the final load level

1969, July 01	House II: jointing of the ceramic tiles
1969, July 08	House I: increase of the hydraulic loading of specified wall elements to the final load level
1969, July 08	House II: application of 25% of the final level of the hydraulic loading of the column elements and of some specified wall elements (Fig. 1.3.2ℓ)
1969, July 15	House II: increase of the hydraulic loading of specified elements to 50% of the final load level
1969, July 22	House II: increase of the hydraulic loading of specified elements to 75% of the final load level
1969, July 29	House II: increase of the hydraulic loading of specified elements to the final load level

Figure 1.3.2m. 1968, autumn. 4+4 concrete supports, 0.4 by 0.4 m, height 0.5 m, just above existing building columns below the roof of the experimental hall, were cast and plated

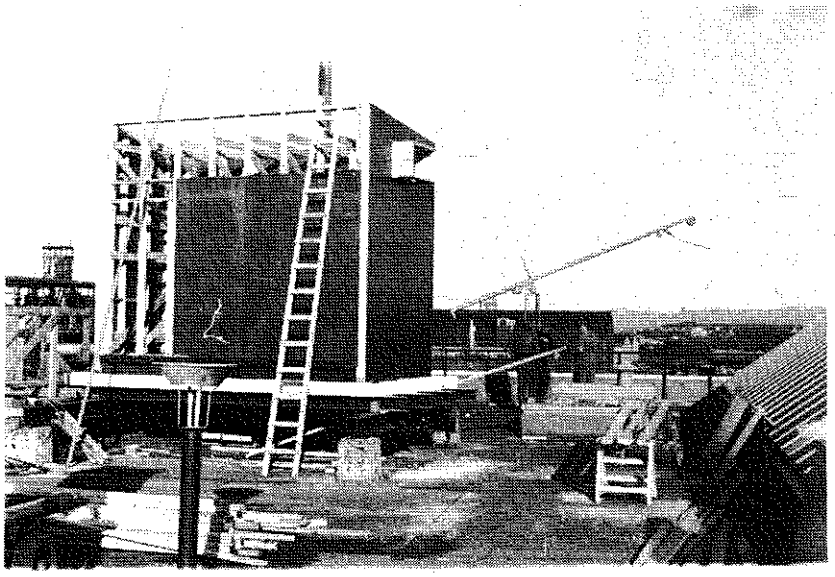

Figure 1.3.2n. 1969, February. Steel beams are placed on the top of the concrete supports and on a floor of aerated concrete the concrete forms of House I were built. No oil was used on the mould surfaces

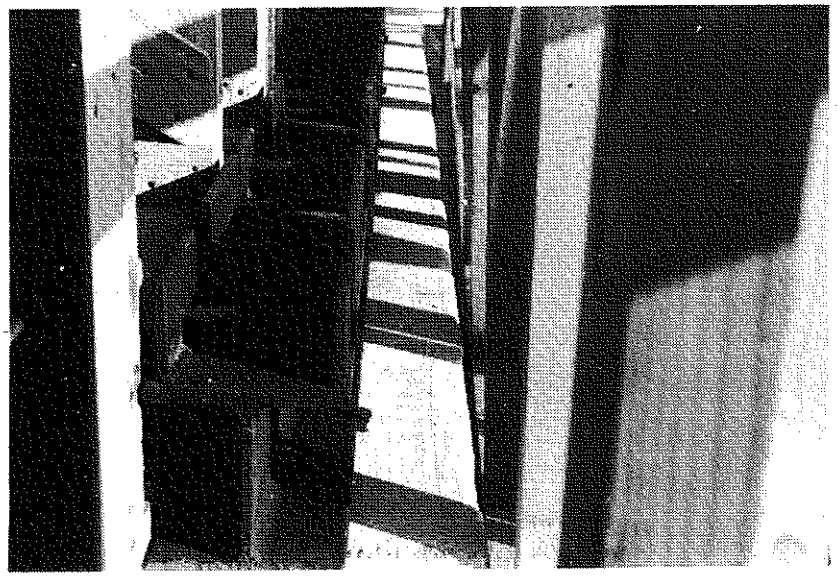

Figure 1.3.2o. Bottom beam in south wall of House I to support the unloaded and loaded wall elements

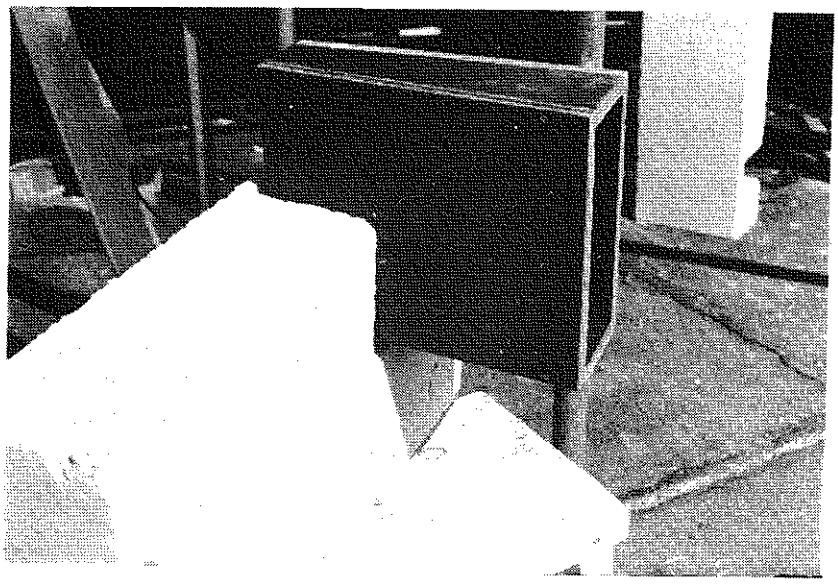

Figure 1.3.2p. House I: openings, two in each wall, left free for moisture observations by use of wedge-shaped test specimens

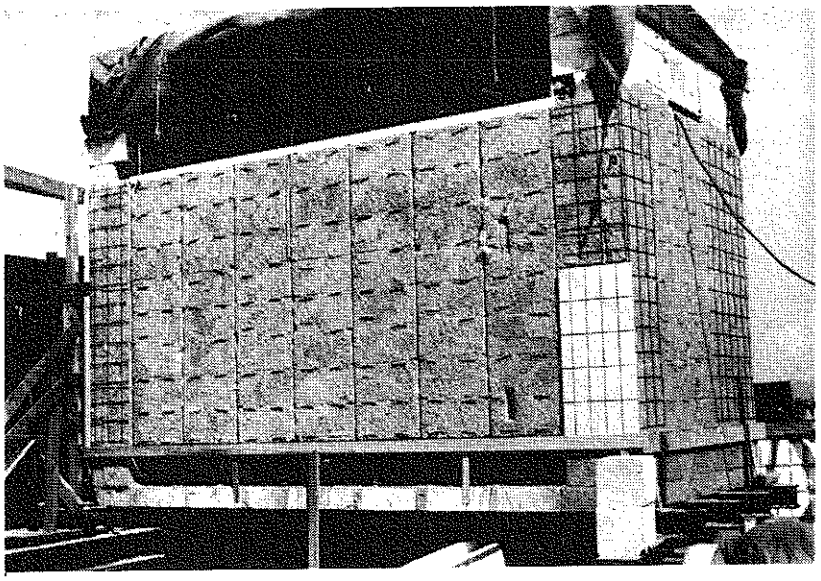

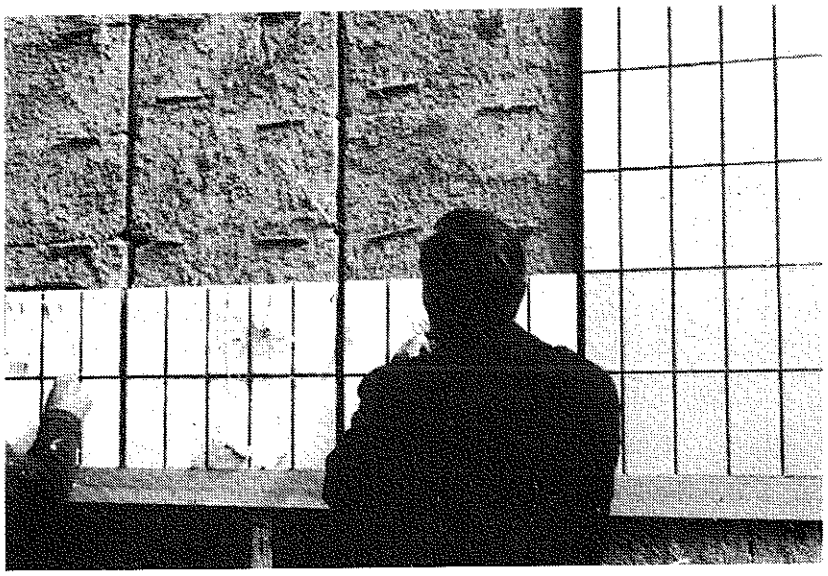

Figure 1.3.2q. Tile fixing, House I, south wall. Observe the special anchors for the fixing mortar. All wall elements in House I to be observed by strain-gauges etc were provided with these anchors while rest of the wall surfaces were provided with a normal net. The two vertical slots on each wall are holes intended for the moisture observations by use of wedge-shaped test specimens

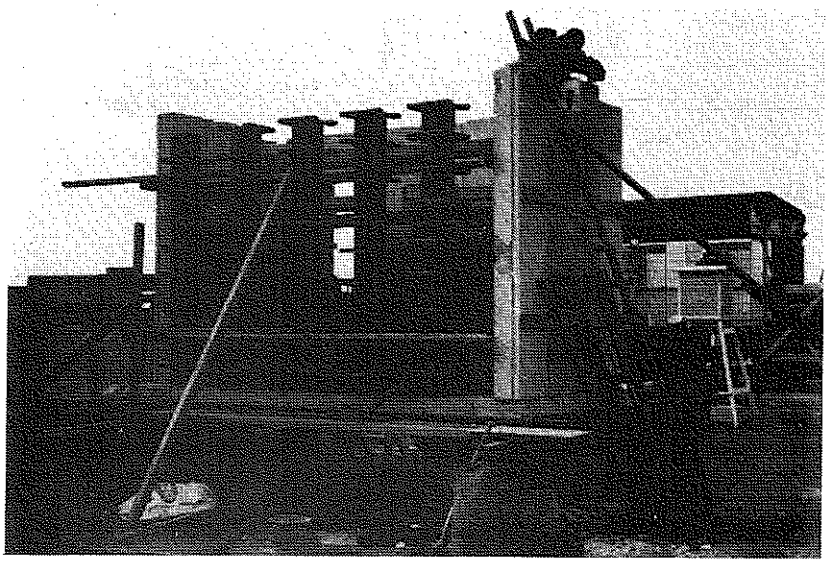

Figure 1.3.2r. Concreting and constructing, south and east walls of test house II

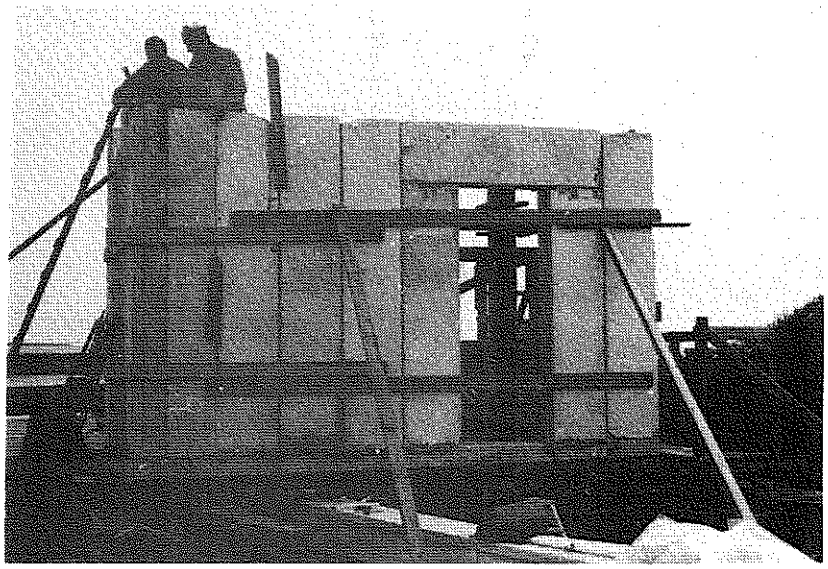

Figure 1.3.2s. Constructing, north wall of test house II

Figure 1.3.2t. House II, south wall: removing the forms from the concrete columns and raising the aerated concrete elements

Figure 1.3.2u. House II, south wall: a splashed aerated concrete wall element and a splashed concrete column element with its anchoring wires

Figure 1.3.2v. House II, south wall: tile fixing on the column elements

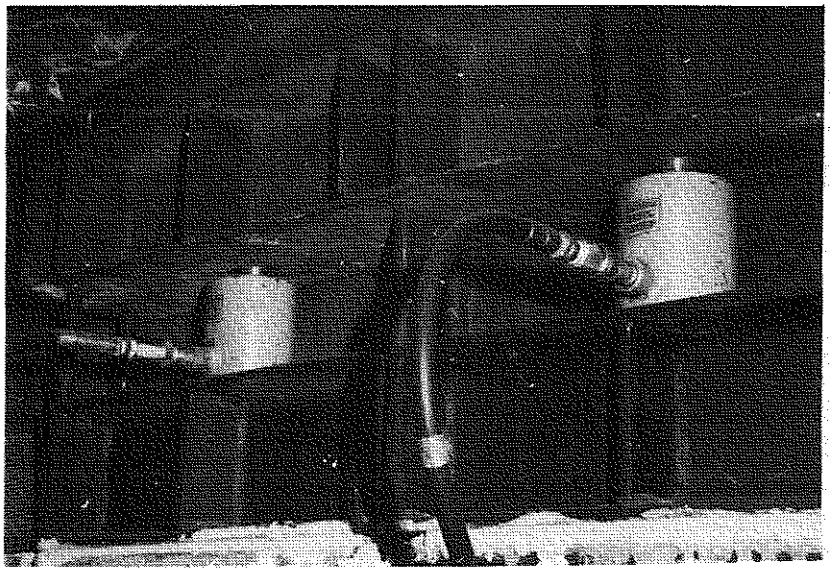

Figure 1.3.2x. House I: detail of the equipment for application of hydraulic loading on specified wall elements

1.4. GENERAL OBSERVATIONS TECHNIQUE AT THE TEST HOUSES

Below are noted the different groups of the performed observations, starting with the first day of the application of the tiles on the 3rd June, 1969.

Weather-climate data were observed and collected principally as is made internationally at weather stations, i.e. the data are partly registered manually in a meteorological journal and partly continuously by instruments in graphs, all data intended for a possible later computer processing.

Heat, moisture and deformation data, emanating at the test houses themselves from a total number of 500 measuring points had to be collected on a great number of occasions and on each occasion within a few minutes. For temperature and deformation measurements these conditions were fulfilled by use of electrical resistance measuring sensors and a data logging system, the digital data received in printed form and as punched paper tapes for further computer treatment. Due to well-known difficulties associated with moisture flow and intensity measurements, the required moisture data could not be included in this system within reasonable efforts and had thus to be observed separately and registered manually.

Some observations of wall deformation and the ocular observations of the wall surfaces also had to be registered manually.

A journal containing different notes as regards the running of the test houses was written, starting with the concreting of House I on the 27th May, 1969.

The weeks of the observations are numbered consecutively, starting with the week of the 1st to 7th June, 1969 to be test week No. 1.

1.4.1. WEATHER-CLIMATE

The Swedish Meteorological and Hydrological Institute (SMHI), Stockholm, has in a report M 739/1967 given some aspects on equipment, times and techniques for climate and weather observations and recommended weather stations to serve as reference or calibration points. The recommendations given could in general be followed.

The main test place, the roof of the experimental hall where the test houses are situated, has been the main place of the macro-micro meteorological observations. Regarding eventual local disturbances of the observation, see, the different types of observations below and also the observation reports in volume 2.

The nearest situated weather station for a comparison of data is that of Höganäs AB, situated about 200 m ENE the test houses but on ground level. The official SMHI weather station at Kullen, 12.5 km NNW the test houses at Höganäs, has by kind permission been used for continuous comparisons with regard to clouds, air temperature, atmospheric pressure, wind, humidity and precipitation. Information concerning air pollution is taken from observations made at the weather station of Höganäs AB.

The geographic positions of the stations and positions of the instruments are given in the section 1.3.1.

The observation technique, used for a determination and description of the near- and micro-climate of the test houses, is reported in the sections 1.4.3 and 1.4.4.

1.4.1.1. Meteorological observations at the test houses

1.4.1.1.1. Discontinuous registrations

By routine, visual observations were made daily of

(1) Clouds
(2) Air temperature

(3) Atmospheric pressure
(4) Wind
(5) Air humidity, and
(6) Precipitation

at 07.00, 13.00. 16.00 and in summer 19.00 o'clock, Swedish standard time (central European time). Some observations also were made at 10.00 o'clock. All these observations are registered in the meteorological journal, drawn up according to appendix 1.4.1.1.1a.

Pelting rain on the test house walls was measured periodically.

Air temperature, in the weather shelter and at a distance of 10 cm from the test house walls, was measured each time strain-temperature measurements were made with the data logger.

1.4.1.1.2. Continuous registrations

The continuous weather-climate registrations comprise solar radiation to different planes, and air temperature and humidity, outside and inside the test houses.

Solar radiation

was followed by

(1) Continuous registrations from solarimeters in the horizontal and the S vertical planes, and from photocells in the S,W,N and E vertical planes

(2) Intermittent cloud observations, completing the registration of the solar radiation

The solarimeters consist of two Kipp & Zonen Moll thermopiles for outdoor installment. The horizontally arranged pile was of the type CM3 with a glass dome and screen, the vertical pile of the type CM2 with a glass dome but without any screen, both piles connected to a 12-point mV-recorder (Philips PR 3210 A/00). According to the calibration certificate, referring to the international pyrheliometer

scale 1956, a radiation of 1 gcal · $cm^{-2}.min^{-1}$ produces an EMF of 8.6 mV.

The horizontally arranged solarimeter gives the global radiation, viz. the direct solar radiation + the indirect diffuse sky radiation. The position of this solarimeter was 8 m S of S wall for the test house II and, 1.8 m above the ground level of the test houses (the top level of the roof of the experimental hall).

The vertical solarimeter had its position just above panel 13 on the S wall of test house I.

The four vertical photocells on the S,W,N and E wall of the test house I, positioned just above the panels 13, 17, 19 and 23, respectively, were of the type Ferranti silicon photocells Ms 40, connected to the mV-recorder mentioned. The cells have a maximum spectral response at 0.8 to 0.9 µm with a 40 to 80 % sensitivity between 0.45 and 0.7 µm. These cells were installed for comparative measurements of radiation on the four walls of the test house I and for a correlation to the vertical solarimeter.

The influence of interfering local reflexes etc is evaluated not to exceed 3 % of the observed value. The shadowing of the adjacent buildings E and S of the test houses and especially the shadowing of the stack E of the test house I (cf. Fig. 1.3.1b and c) have to be considered.

Cloud picture

was visually observed on routine times mentioned and registered in the meteorological journal with regard to the quantity of clouds in a scale 0 to 10 and with regard to the height of the clouds in the classes 1 = low, 2 = medium and 3 = high. Further, notes were made with regard to fog, haze, thunder etc.

Air temperature

was observed on routine times mentioned

(1) In the weather shelter by a "dry" mercury thermometer
(2) In the weather shelter by maximum and minimum mercury thermometers

continuously

(3) In the weather shelter by a thermohygrograph

and further, when strain-temperature measurements were collected

(4) In the weather shelter by a resistance thermometer, and
(5) On the outsides of the S,W,N and E wall of the test house I and of the S wall of the test house II by resistance thermometers on a distance of 10 cm of the walls.

As regards the type of resistance thermometers, see section 1.4.3.

The observations of the types (1) and (2) were noted in the meteorological journal, the type (3) registered on a curve chart/week, and (4) and (5) registered in the Saab data logger.

Atmospheric pressure

was observed on routine times mentioned by a precision aneroid barometer, system Paulin, in level of the test houses and indoors, in a distance of about 35 m S. Readings in millibar (mbar) were noted in the meteorological journal with no corrections to sea level.

Wind

was observed on routine times mentioned with regard to direction by use of weather vanes around the test houses, also smoke from neighbouring stacks being used, when possible. The wind velocity was observed by an anemometer, Lambrecht, type 1438. All observations were noted in the meteorological journal.

A special study of the air flow conditions around the test houses made by the Aeronautical Research Institute of Sweden (FFA) is reported in appendix 1.3.1a.

Air humidity

was observed on routine times mentioned

(1) In the weather shelter by wet and dry bulb thermometer readings with notes in the meteorological journal, and

continuously

(2) In the weather shelter, and inside the test houses, by a thermohygrograph giving a curve chart/week.

Precipitation

was observed generally at 07.00 and 16.00 o'clock (summer time 19.00) by readings at a rain gauge between the test houses. Notations were made in the meteorological journal, together with remarks of the type of precipitation (rain, snow, hail etc). Pelting rain on the test house walls was collected by gutters placed below the test house panels, the quantities normally noted at 07.00 o'clock (special forms). Dust precipitation etc was followed, the general observations made by the weather station of Höganäs AB.

1.4.1.2. Meteorological observations at the weather station of Höganäs AB

At the neighbouring weather station of Höganäs AB observations were made daily of

(1) Air temperature, by a thermograph
(2) Wind, by a direction and velocity recorder, and
(3) Precipitation, by a normal rain gauge.

Air pollution observations are made for sulfur dioxide and dust together with the wind observations and are generally valid for an area 500 m N the test houses.

1.4.1.3. Meteorological observations at the SMHI weather station at Kullen

For a comparison of data, those observations recorded at the official SMHI weather station at Kullen were noticed which directly correspond to the data in the meteorological journal of the test houses, cf. appendix 1.4.1.1.1a.

1.4.2. DATA LOGGING SYSTEM FOR TEMPERATURE SENSORS AND STRAIN-GAUGES

According to the observation plan 100 measuring points of temperature and 400 measuring points of strain (deformation) had to be scanned and this within such a short time that the values of one scanning round practically could be regarded as simultaneous.

Extensive trial experiments with temperature sensors and strain-gauges, all of the resistance type, together with technical and economical considerations and the requirements mentioned on scanning of the measuring points, resulted in the choice of a data logging system, Saab DLS 550, made by Saab-Scania AB, Sweden. The function of the data acquisition system follows general principles - physical quantities observed are changed by use of appropriate transducers to electrical analogous DC-voltages, these being converted to digital values and recorded by a printer as well as by a punch (Fig. 1.4.2a-c).

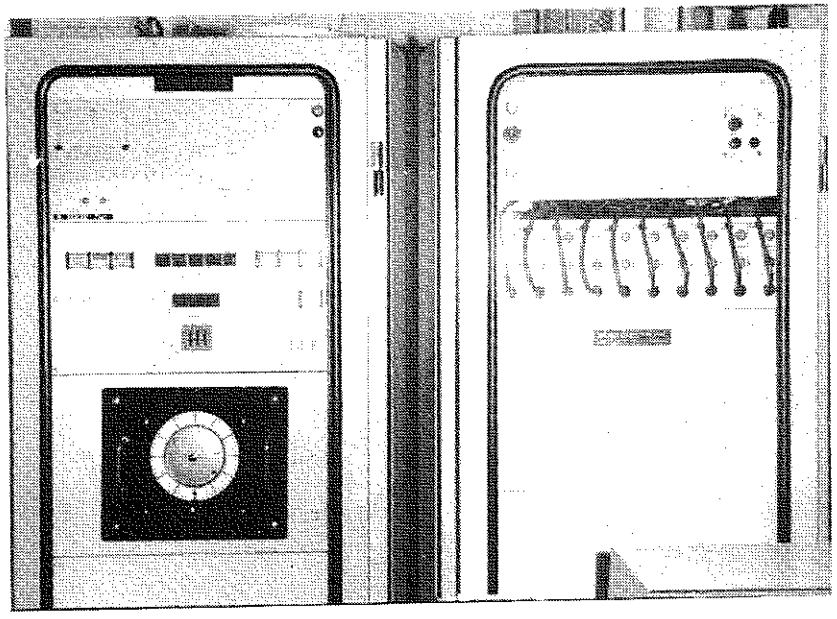

Figure 1.4.2a. Data logging system, Saab DLS 550. The right cabinet contains bridge completion, scanner, amplifier and bridge power supply, the left contains the control unit, A/D-converter display, program unit, digital clock, output unit and power supply

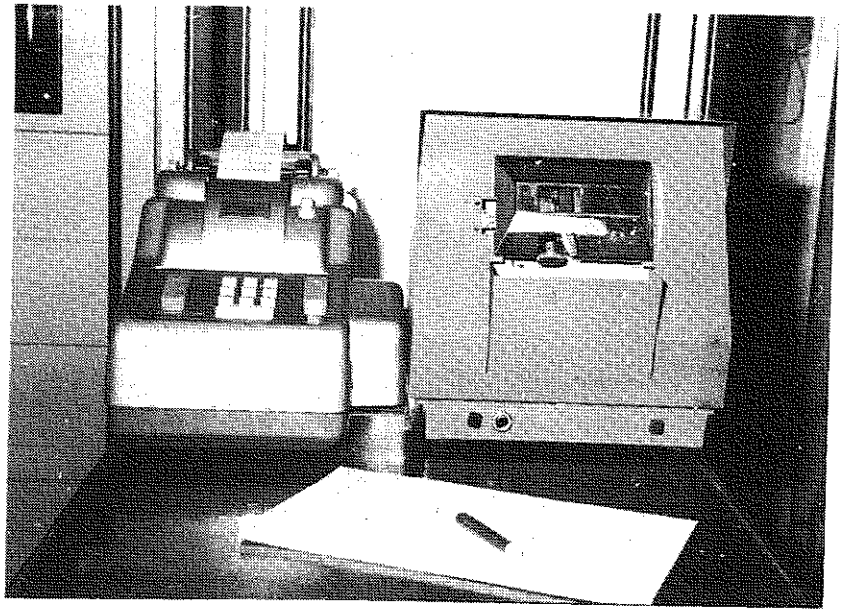

Figure 1.4.2b. The printer and the punch of the data logging system

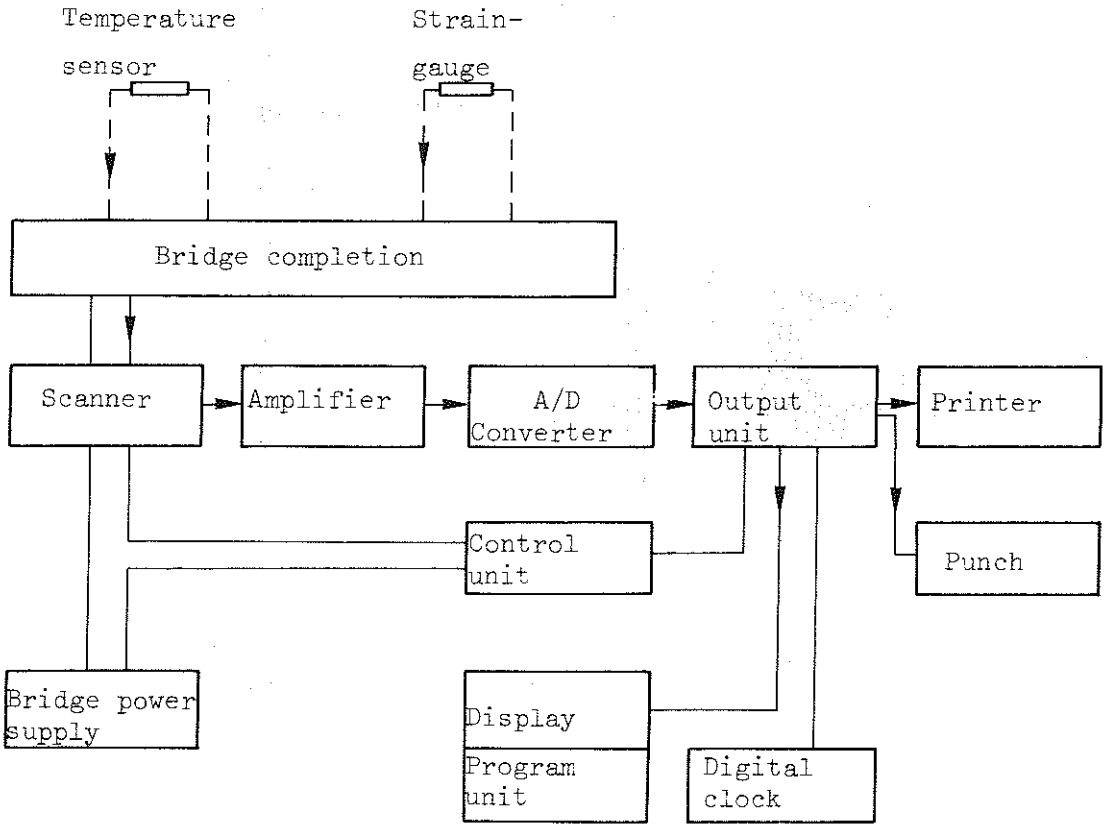

Figure 1.4.2c. Block diagram of the data logging system, the arrows showing the way of the measuring signals

The data logging system, Saab DLS 550, is characterized by the following main specifications:

Number of channels	500 (bridges)
Stability	± 0.01 % at D.C.
Resolution (used)	5 μV/digit (corresponding to 0.01°C and 1 μ-strain)
Measuring range	± 5000 in digits
CMR	more than 150 dB at D.C.
Printer	Addo-X mod 41 E (1.02 s/reading)
Punch	Automatic Punched Tape Ltd mod P 3 U (0.27 s/reading) Telexcode (5 channel tape)

Normal reading of 500 measuring points with printer and punch gives a scanning time of 510 s.

The input circuit of each channel consists of three fixed resistors R_1, R_2 and R_3 (wire wound precision type Ultrom 207 A), which together with the transducer at the measuring point R_4 are constituting a Wheatstone bridge (Fig. 1.4.2d).

To get the best long-term stability of the measuring system, all connections were soldered and - instead of using potentiometers - an individual approximate balancing of the bridges was made in the following manner, some week before the fixing of the tiles on the walls.

The strain-gauge, being bonded to the tile, was connected with its specific bridge via the terminal board and the cable material intended for the final installation. After connecting a resistor of known value in the R_1-position (Fig. 1.4.2d) the un-balance was measured and from a batch of precision measured and classified resistors the

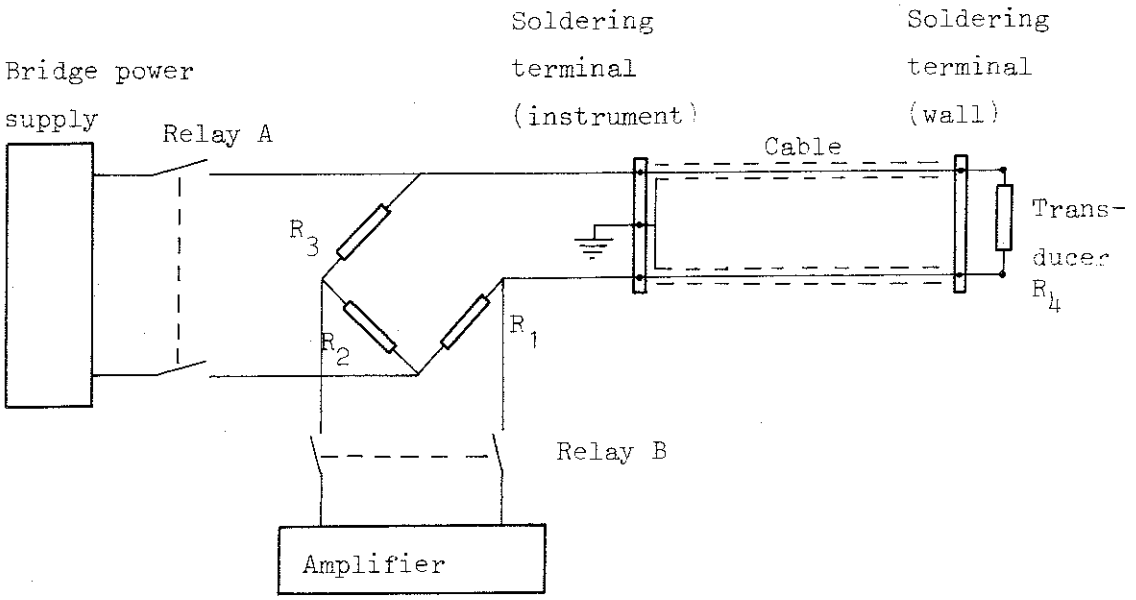

Figure 1.4.2d. Bridge circuit for one channel

final R_1- resistor was so selected as to give an output voltage from the bridge of less than ± 1500 μV for an unloaded strain-gauge.

The strain-gauges, intended for the concrete, were balanced when applicating the gauges. For the temperature sensor bridges no special balancing was necessary.

The bridge excitation voltage of the strain-gauges was 10 V and that of the temperature sensors 0.5 V.

By use of the shunt calibration method, the gain of the amplifier was adjusted to give a resolution for the instrument of 1 μ-strain ($1 \cdot 10^{-6}$) for the strain-gauges and a resolution of about 0.01°C for the temperature sensors.

The wiring from transducers to the data logger consisted

between transducer and the terminal board just inside the wall of a pair of twisted not shielded, 1.25 m long PVC insulated 0.25 mm^2 (30 x 0.1) tinned Cu-wires, type Soflex TQ, manufactured by Schweizerische Isola-Werke, Breitenbach, and

between the terminal board and the data logger of cables, containing 15 or 19 individually shielded pairs of tinned Cu-wires, AWG 22, polypropylene and vinyl insulated, type Belden, trade no. 8776 and 8769, respectively, manufactured by Belden Corp,Chicago.

The Saab DLS 550 data logger, the printer and the punch were all installed in House I and the cables from the measuring points in House II were placed in a thermally insulated drum, fed with the 22°C air from both test houses. The measuring points in House II were connected to the data logger at the beginning of test week no. 5. Up to the test week no. 33, air leakages occured along the drum, but from this week the required stability of the drum temperature was attained. A correction table for the strain-gauge measurements in test weeks no. 5 to 32 is given in appendix 1.4.2a.

The following control arrangements of the instrument were made:

Four bridges, one in the temperature sensor series, viz. measuring point no. 99, and three in the strain-gauge series, viz. measuring points no. 440, 441, and 442, were selected and the transducer and its cabling was changed to a fixed resistor (type Ultrom 207 A), giving checking values of the measuring points no. 99, 440, 441, and 442.

An arrangement to check the function of the relays A and B of the different bridges was made according to Fig. 1.4.2e. The signal enters the A/D-converter directly.

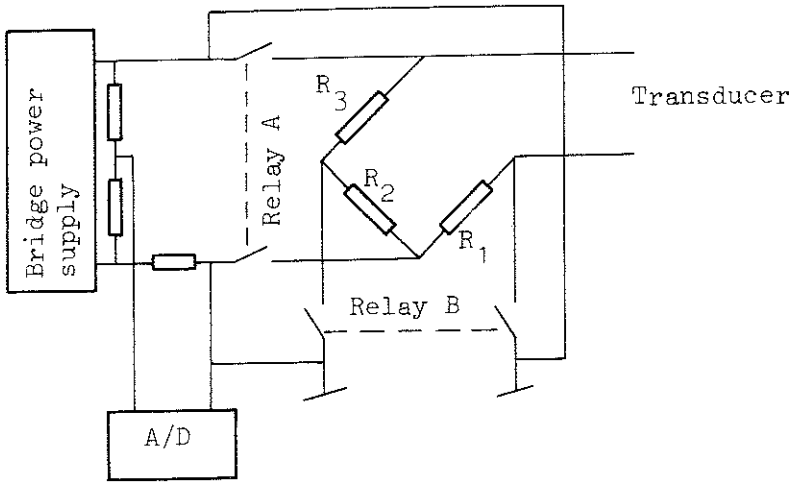

Figure 1.4.2e. Check of the contact resistance of the relays A and B

1.4.3. HEAT IN WALLS

According to the test plan, temperature measurements were to be carried out - in accordance with Fig. 1.4.3a to c - immediately below the glaze layer on the front of the tile, further, on the back surface of the tile, in the layer between fixing mortar and aerated concrete, in the layer between aerated concrete and concrete, and on the surface of concrete respectively of aerated concrete inside the test houses. In addition, temperature measurements were to be taken on distances of 10 cm outside and inside the walls of the test houses.

Taking into account the desired accuracy of the temperature measurements, the different positions which in some cases called for a small mass of the sensors, and the type of data logging system to be used, electrical resistance thermometers were decided upon.

Of the capacity of the data logging system used, 100 measuring points (no. 0 to 99) were selected for the temperature measurements.

The types of the sensors, all of the quality Minco Products, Inc. U S A, used were:
model S 27 metal enclosed cylinder 14.5 x dia 4.8 mm
model S 60 metal enclosed cylinder 3.1 x dia 5.6 mm
model S 2B plastic enclosed ribbon 100 x 10 x 0.5 mm
all nickel-iron alloys, with a nominal resistance at $0^{\circ}C$ of 604 ± 0.5 ohms and with a mean sensitivity of 2.9 ohms/$^{\circ}C$ in the actual operating range.

An example of the choice and positioning of different sensor models in a wall cross section of House I is given by Fig. 1.4.3a.

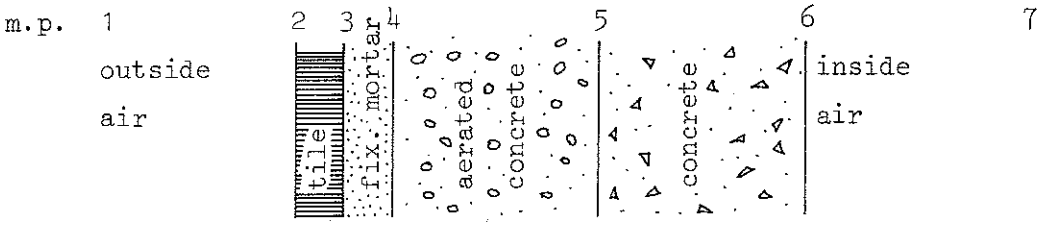

Figure 1.4.3a. Positions of temperature sensors in a typical wall section

Further details regarding the specific temperature sensors in the wall section according to Fig. 1.4.3a are given below.

M.p. 1: sensor model S 27, in the air 0.10 m from outside wall surface, protected against precipitation and direct radiation of sun

M.p. 2: sensor model S 60, in the centre of the tile in a cavity, drilled from the backside. The cavity has a diameter of 6 mm and ends 1 $\pm$ 0.1 mm from the outside surface of the glaze. The hole with the sensor in bottom was filled with crushed tile material (< 0.5 mm) and sealed with silicon rubber RTV

M.p. 3: sensor model S 2B, fixed and moisture insulated by a 0.2 mm layer of silicon rubber RTV on a smoothed back surface area of the tile

M.p. 4 and 5 : sensor model S 2B, fixed and insulated as for measuring point 3 on outer and inner surface of the aerated concrete

M.p. 6: sensor model S 2B, fixed and insulated as for measuring point 3 on the inside surface of the concrete, and

M.p. 7: sensor model S 27, in the air 0.10 m from the inside wall surface, not especially protected.

The connection from a sensor to the data logging system was realized by two separately shielded wires, cable Belden type 8769 (Cu-AWG no. 22), each sensor being one of the resistances in a Wheatstone bridge circuit, energized by 0.5 V DC.

The readings are linearized and converted to ^{o}C by use of the formula

$$\vartheta = \frac{2000 - B + s}{10^2} \left(1 + \frac{2000 - B + s}{10^5}\right) \qquad (1.4.3a)$$

where

B = reading, when calibrated at 20°C, and

s = actual reading at ϑ°C.

Each sensor, including the cable connections, was calibrated at four different temperatures between - 10 and + 40°C.

The accuracy of the whole measuring system is approximately ± 0.2°C.

The distribution of the temperature sensors no. 1 to 98 outside and in the walls of the test houses is given in Fig. 1.4.3b and c, in Fig. 1.4.6a and in section 1.4.7.

The temperature sensor no. 0 (type S 27) was installed, not especially protected, inside the weather shelter - as mentioned in the section 1.4.1 - between the test houses.

The measuring point no. 99 was selected as a control point, cf. section 1.4.2.

The calibration values (base values) of the temperature sensors, recorded by the data logging system at 20°C for the measuring points 0 to 99, are reported in volume 2.

cross section of wall elements

Wall element	outside of wall		tile	fix	aerated concrete	concrete	inside of wall
11	1	2	3		4	5 6	7
12		8	9		10	11 12	
15	13	14	15		16	17	18
16		19	20		21		
19	22	23	24		25	26	27
20		28	29		30		
23	31	32	33		34	35	36
24		37	38		39		
a,		40	41				
b,		42	43				
c,		52	53				
e,							
i,		44	45				
l,		46	47				
t,							
u,		50	51				
z,		48	49				

Figure 1.4.3b. Temperature sensors in cross section of wall elements in test House I. Figures 1 to 53 designate the numbering of the measuring points

cross section of wall elements

Wall element	outside of wall		tile	fix	aerated concrete		inside of wall
31		54	55		56	57	
32	58	59	60		61	62	63
35		64	65			66	
36		67	68		69		
39		70	71		72		
40		73	74		75	76	
43		77	78		79[x]		
44		80	81			82	

[x] out of order

cross section of column elements

Column element	outside of column		tile	fix	concrete		inside of column (insulation)
47		83	84		85	86	
50		87	88		89	90	
52		91	92		93	94	
53		95	96		97	98	

Figure 1.4.3c. Temperature sensors in cross sections of wall and column elements in test House II. Figures 54 to 98 designate the numbering of the measuring points

1.4.4. MOISTURE IN WALLS

An accurate knowledge of the prevailing moisture content and moisture transfer phenomenon is essential in any performance evaluation of external wall systems. As a consequence, substantial effort was made to investigate the possibilities and limitations of the various measurement methods in use. Special attention was paid to the numerous physical methods based upon dielectric constant, microwave absorption, neutron diffusion, etc.

In an early stage, a serious attempt was made to use an instrumentation based on the change of frequency in a microwave resonant circuit. An instrumentation was developed by the Institute of Microwave Technique at the Royal Institute of Technology in Stockholm. Three different measuring cells - antennas - were used, giving and taking signals from one and the same side of the material to be tested and to different depths from about 5 to 50 mm. Difficulties arose regarding the calibration and evaluation of the values received, but it was more the inconvenient handling of the measuring cells and the long cables to supply and data collecting instruments which made us to decide not to use this instrumentation.

The finally chosen method was based upon the radio frequency power loss by absorption and the instrument, a model A-8, was manufactured by Moisture Register Company, Alhambra, California - Fig. 1.4.4a.

17 spring knobs function as testing electrodes and cover a circular surface with a diameter of 80 mm and a penetration depth of about 25 mm. A figure is readable in few seconds on a numerical scale and four different moisture range settings are possible. The instrument has a weight of about 1 1/2 kg, has no cable connections and is very handy. The instrument is in the report called the "A"-meter and the normally used moisture range is no. 2.

In Fig. 1.4.4b are reproduced, as orientation, some calibration curves of the "A"-meter with reference to tiles, aerated concrete, and concrete, having a homogeneous moisture distribution, which situation, however, seldom exists in practice.

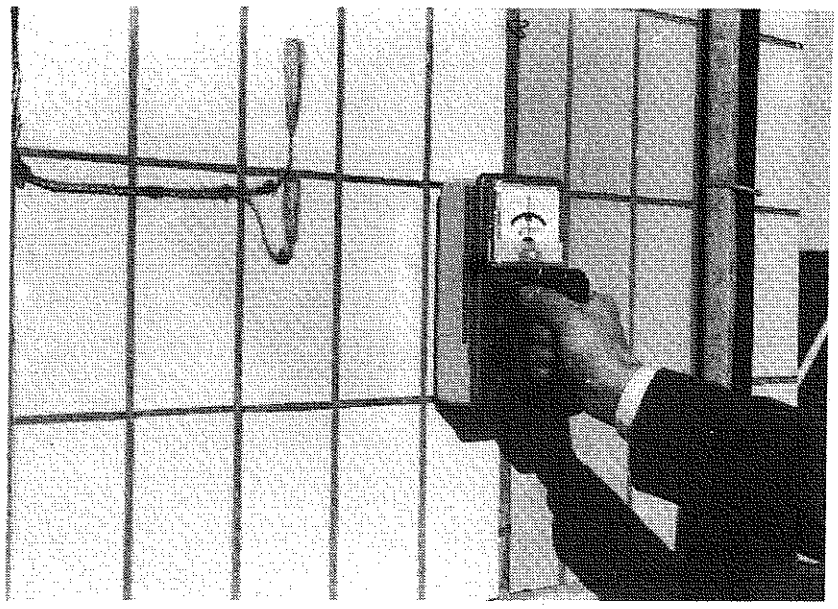

Figure 1.4.4a. The "A"-meter, model A-8

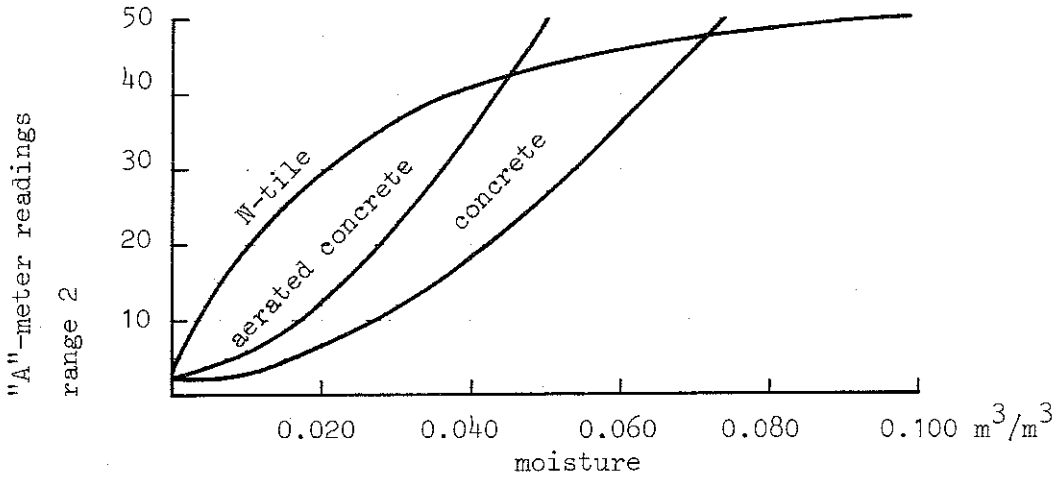

Figure 1.4.4b. Calibration curves of the "A"-meter, determined for N-tiles, aerated concrete, and concrete, having a homogeneous moisture distribution

Observations made with the "A"-meter are reported in instrument readings and an estimation of the moisture picture of a wall section at a given moment has to consider the sources of additional information before and at this moment.

The investigations carried out regarding the applicability and reliability of different measurement methods made it clear that the more advanced methods would have to be confirmed and complemented by the

procedure of continuously weighing material samples. As a final check, the test bodies would have to be dried at 110°C and weighed, providing values of the true moisture content, averaged over the test body volume.

The test bodies for the weighing procedure are taken from the concrete and aerated concrete walls (Fig. 1.4.4c to e). In test house I concrete wedges of a volume of about 0.0025 m^3 were installed, one in each of the inside of the wall elements no. 13, 14, 17, 18, 21, 22, 25, and 26 (cf section 1.4.5). Behind these concrete wedges, aerated concrete wedges of a volume of about 0.0012 m^3 were placed. The wedges and corresponding holes were adjusted to best possible fitting.

In test House II only aerated concrete wedges of a volume of about 0.0035 m^3 were installed, one in each of the inside wall behind the elements no. 34, 37, 42, and 46.

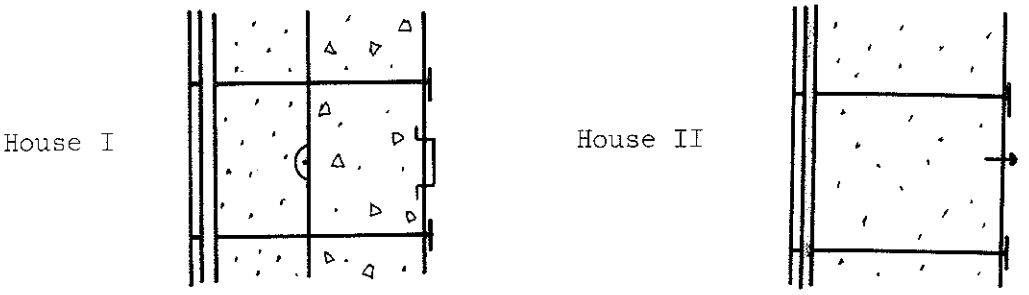

Figure 1.4.4c. Cross section of the wedge test body arrangement

The narrow slit around the wedges was sealed with an adhesive paper tape between wall and wedge surfaces.

In this way, the change of moisture in the wedges was followed by weighing - and also by use of the "A"-meter. As mentioned before, the true moisture content could only be calculated when the wedge was heated at 110°C to get the dry weight and thus destroyed for further use as test body. Even if the moisture of a test wedge almost never is in equilibrium with the moisture of the surrounding wall, the use of this method was still considered well worth making.

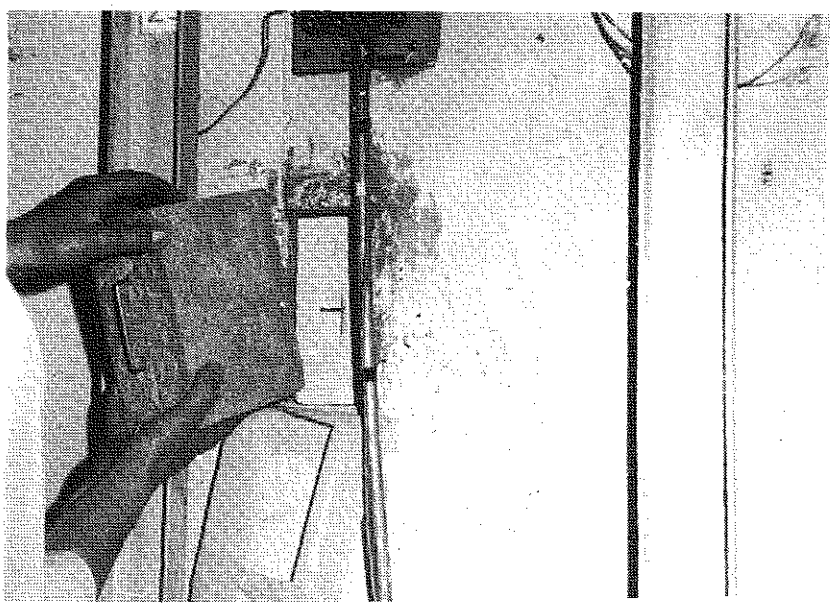

Figure 1.4.4d. The concrete test wedge is pulled out and the aerated concrete wedge is pulled forwards in the slit

Figure 1.4.4e. The concrete test wedge in wall element no. 25, House I

Information regarding built-in deformations and stresses as well as moisture condition in the wall sections is produced by the different observation techniques accounted for in section 1.4. The data, produced by this measuring system, have been followed up and checked by a partial, step-by-step release or dismounting of specific tiles from the fixing mortar. These dismounting studies, the details of which will be given in volume 2, make possible an investigation of the moisture gradient through the wall, resulting in diagrams exemplified by Fig. 1.4.4f.

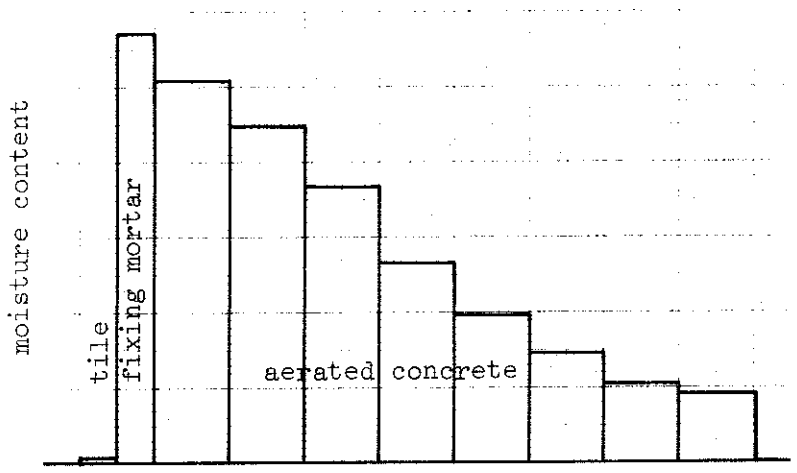

Figure 1.4.4f. Example of moisture gradient through wall profile

1.4.5. INSIDE WALL DEFORMATION. MACRO LINEAR AND STRAIN-GAUGE MEASUREMENTS

For a determination of the time variation of the change of the length and the change of the vertical curvature of the wall and column elements, macro-micro measurements were carried out on the inner wall and column surfaces, on one hand by use of metallic vertical bars with a measuring equipment of fixed micrometer clocks or of hand clock calipers, on the other by use of strain-gauges, applicated on the interior surfaces of the walls.

The measuring bars were made of AlSiMg-alloy 6508-06 with a thermal dilatation of $23 \cdot 10^{-6}$/K (SIS 4212 - F 10154). They were arranged for the deformation measurements according to Fig. 1.4.5a. The bars were fixed to the wall and column elements at one end and the change of the element length was measured by micrometer clocks at the other end of the bars. The change of the vertical curvature of the elements was determined at the centre of the bars on the measuring length by micrometer clocks - Fig. 1.4.5b. The positions of the measuring bars are given in Fig. 1.4.5c, showing also the measuring length and the use of the alternative equipment for the macro deformation measurements of the different wall and column elements.

The fixed micrometer clocks were of the type Somet, manufactured in Czechoslovakia, scale 0-1 mm, each scale part giving 0.01 mm, 0.001 mm estimated.

The hand clock caliper was of the type Kröplin, manufactured in West Germany, scale 40-50 mm, each scale part giving 0.05 mm, 0.01 mm estimated.

To complete and check the linear macro measurements strain-gauge measurements were used for the vertical deformations in the centre of the back surface of each of the main wall elements (no. 1-46) and of the main column elements (no. 47-54).

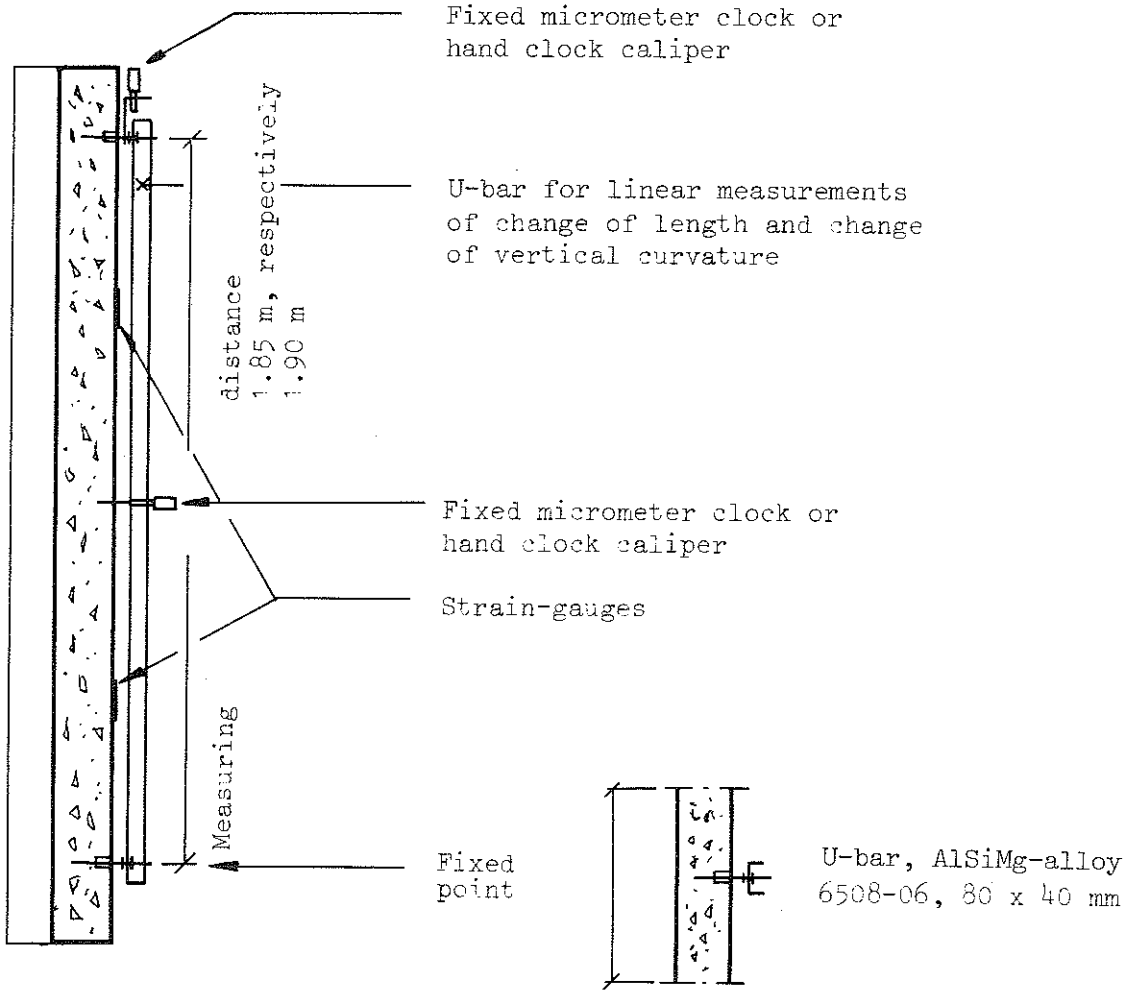

Figure 1.4.5a. Arrangements for bar and strain-gauge measurements of the deformations on the inside of wall and column elements

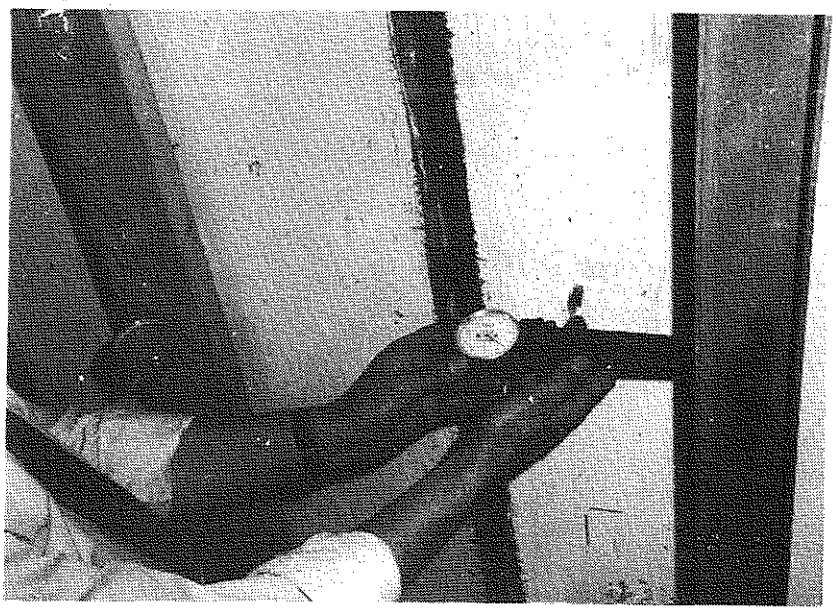

Figure 1.4.5b. The hand clock caliper being used to measure the vertical curvature of a wall element

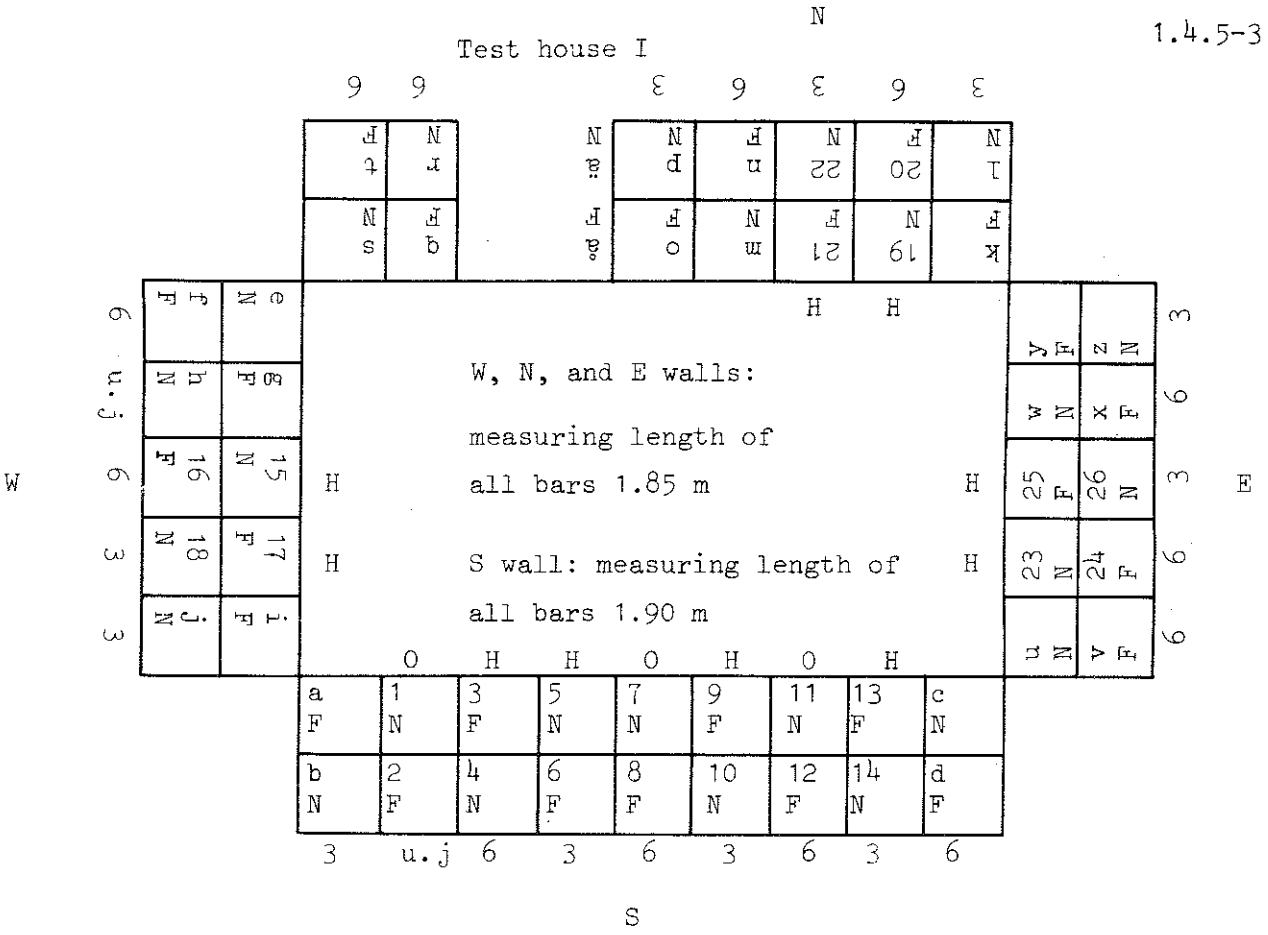

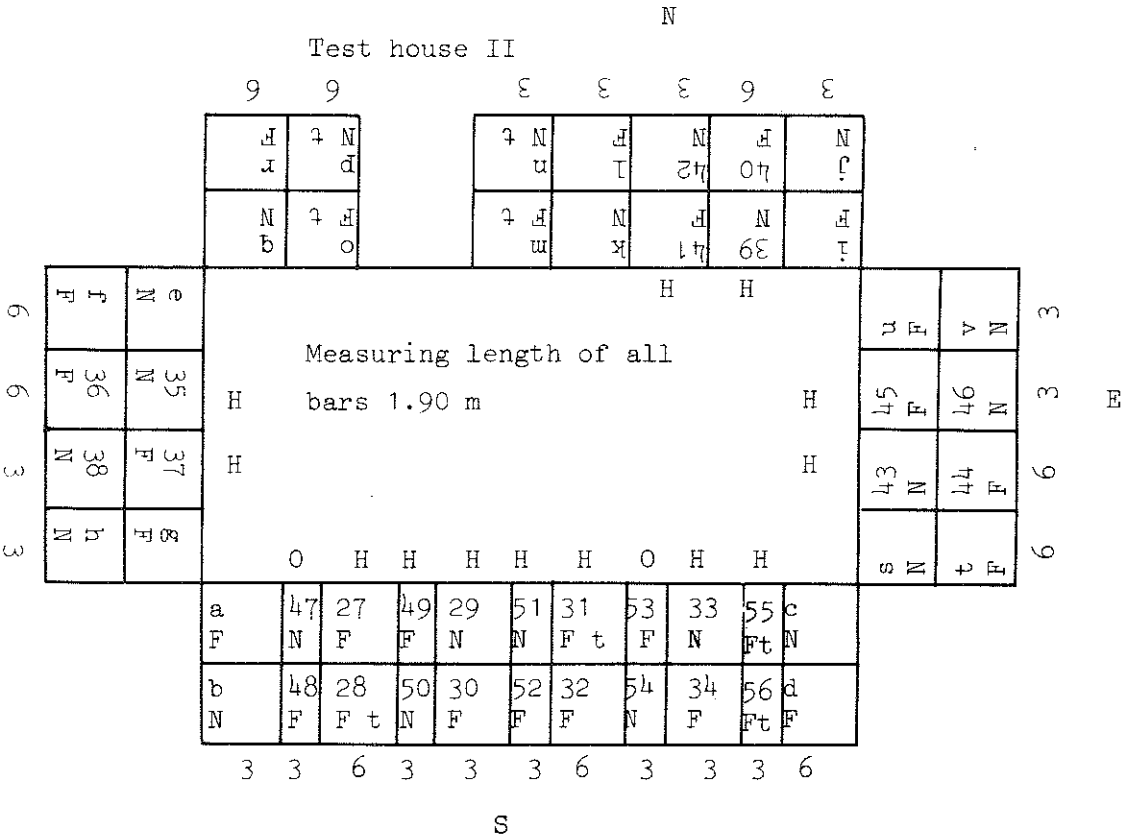

Figure 1.4.5c. Positions of bars for deformation measurements on the inside of wall and column elements, shown in unfolded manner. 0 = Measurements of fixed micrometer clocks, H = Hand clock caliper measurements

Three reference bodies - two wall elements and one aerated concrete brick - were provided with the same type of strain-gauges and were placed inside House II.

The strain-gauges used had the following characteristics: Hottinger 150/300 LP 21, active length 150 mm, resistance 300 ohm, thermal compensation $12 \cdot 10^{-6}$/K. The gauge factor at 20°C is 2.12. To get the true value of the strain in the concrete a factor of 0.96 had to be used on the figures from the logger. The strain-gauges were attached to the elements and reference bodies by cement, Hottinger X 60, rapid room temperature curing.

The numbering of the 57 strain-gauges, placed on the inside surface of wall and column elements and on the reference bodies is summarized in Table 1.4.5a.

Wall element	Position no.	Wall element	Position no.	Wall element	Position no.
1	446	3	448	5	450
2	447	4	449	6	451
7	452	9	454	11	456
8	453	10	455	12	457
13	458				
14	459				
15	460	17	462		
16	461	18	463		
19	464	21	466		
20	465	22	467		
23	468	25	470		
24	469	26	471		
27	472	29	474	31	476
28	473	30	475	32	477
33	478				
34	479				
35	480	37	482		
36	481	38	483		
39	484	41	486		
40	485	42	487		
43	488	45	490		
44	489	46	491		

Column element		Column element		Column element	
47	492	49	494	51	496
48	493	50	495	52	497
53	498				
54	499				

Reference bodies inside House II wall elements		free aerated concrete
type N	443	444
type F	445	

Table 1.4.5a. Positions and numbering of the strain-gauges on the back surface of wall and column elements and on the reference bodies (positions no. 443 to 499)

1.4.6. TILE DEFORMATION. STRAIN-GAUGE MEASUREMENTS

The time variation of the vertical strain of the tiles was studied by strain-gauge observations on wall elements no. 1 to 46, column elements no. 47 to 54, and some corner elements, a, b, c, f, i, j, l, t, u, z of test house I; cf. Fig. 1.3.2ℓ, 1.4.5c, and section 1.4.7. The observations comprise the state of strain on the glazed side as well as on the back side of the tiles. The strain-gauge measurements were arranged in a way to give explicit informations on the effect of different influences - instantaneous and time dependent deformations of the structure behind the tiles, temperature variation of the tiles, and moisture variation of the tiles.

The following five types of measuring points were chosen - cf. Fig. 1.4.6a to c:

M1, comprising one strain-gauge on the glazed side and one strain-gauge on the back side of a tile (for corner elements only one strain-gauge on the glazed side) in the centre of a wall, column or corner element, giving the total vertical strain in the centre of such a tile,

M2, comprising one strain-gauge on the glazed side and one strain-gauge on the back side of a tile (for corner elements only one strain-gauge on the glazed side) near to the centre of a wall, column or corner element, giving the total vertical strain at the edge of such a tile, close to a horizontal joint,

R1, comprising two strain-gauges according to the type M1, but with the tile insulated against moisture transfer and included in and simultaneously separated from the wall and column element so that no deformations of the structure behind reached the tile - the type of measuring points thus giving the influence of the temperature variations of the tile alone,

R2, comprising one strain-gauge on the glazed side of a tile near to the centre of a wall or column element, giving the combined influence of temperature and moisture variations on the vertical strain in the centre of such a tile, and

R3, principally arranged as type R2, but giving the combined influence of temperature and moisture variations on the vertical strain at the edge of a centre tile, close to a horizontal joint.

In order to fulfil the requirement to give the influence of temperature and moisture variations of the tiles and to simultaneously exclude the influence of the deformations of the structure behind the tiles, the reference tiles with the measuring points R2 and R3 were prepared in the following way. Around each strain-gauge position a circle was drilled with a diameter about four times the active length of the strain-gauge. The depth of the drilled circles finished about 1 mm from the back of the tiles - to keep the drilled "test cylinders" in position. The drilled slots were softly filled with finely crushed tile material and sealed by a white adhesive tape.

About half of the elements with measuring points of type M1 and M2 were provided with reference strain-gauges R1, R2 and R3, too.

Experience of outdoor strain-gauge measurements during long test periods, reported in the literature and also received at previous own investigations at Höganäs, has verified the clima-safe application of the strain-gauges as a main problem.

New work, carried out in connection with this investigation, of development on gauge application technique was started in 1968 and after some time The Aeronautical Research Institute of Sweden (FFA), known for its advanced experiences of similar problems, was consulted and consequently, an investigation was carried out at FFA for the special strain-gauge problems in

connection with our test house project.

The work of FFA is described in the FFA-reports MU-398:0-4 and later presented by G Scherling at the Fourth International Conference on Stress Analysis in Cambridge 1970 as paper nr 40: Longterm Strain-Gauge Measurements in Outdoor Environment on Ceramic Tiles. This paper is enclosed here as appendix 1.4.6a.

The finally selected strain-gauges were manufactured by Micro Measurements, Michigan, USA, and of the type EK-03-500 BC-600, all gauges of the same lot. The active gauge length was 12.7 mm and pre-tests had shown that this length was appropriate with regard to the material structure of the tiles. The code of the gauge says further: open-faced general purpose gauge with polyimide backing, nickel-chromium alloy high-performance, self-temperature compensated for the material with a thermal expansion coefficient approximately $5.4 \cdot 10^{-6}$/K, special-resistance pattern, primarily for transducer use, 600 ohm ($\pm$ 0.3). The gauge factor at 20.4°C is 2.03 ($\pm$ 1.0%) and the transverse sensitivity 1.9%.

The strain-gauge application technique used is characterized by the following sub-operations:

(1) All measuring positions on the glaze side of the tiles slightly blasted by a fine grain steel sand and all measuring positions on the back side of the tiles ground flat in level with the bottom of the rills, followed by a drying at 120°C

(2) Precoating-cementing (in three layers) with FFA V-cement

(3) Application of the strain-gauge with a pressure on the gauge and a first curing at 80 to 90°C during 3 hours at slight evacuation

(4) A second curing at 180°C during 1 hour

(5) Covering with cemented aluminium foil

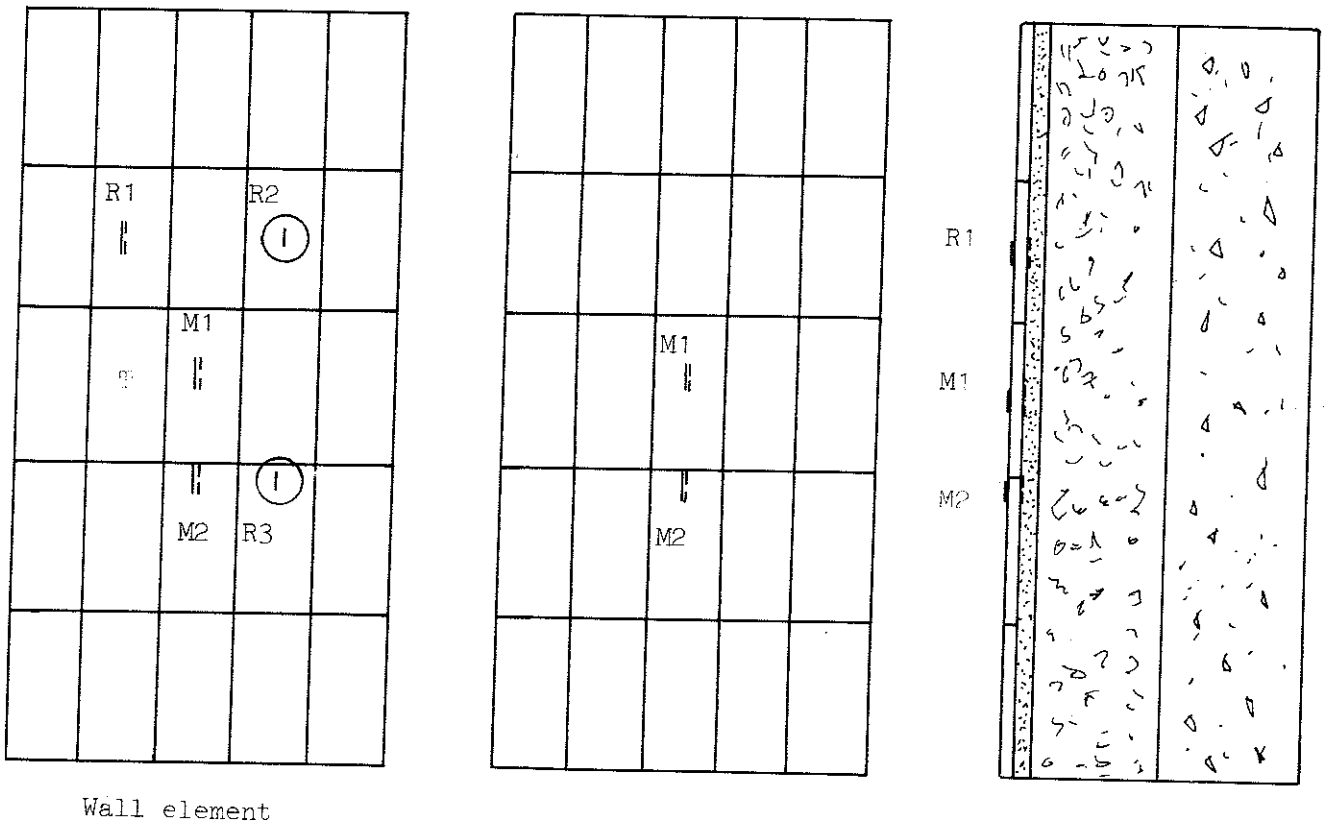

Wall element

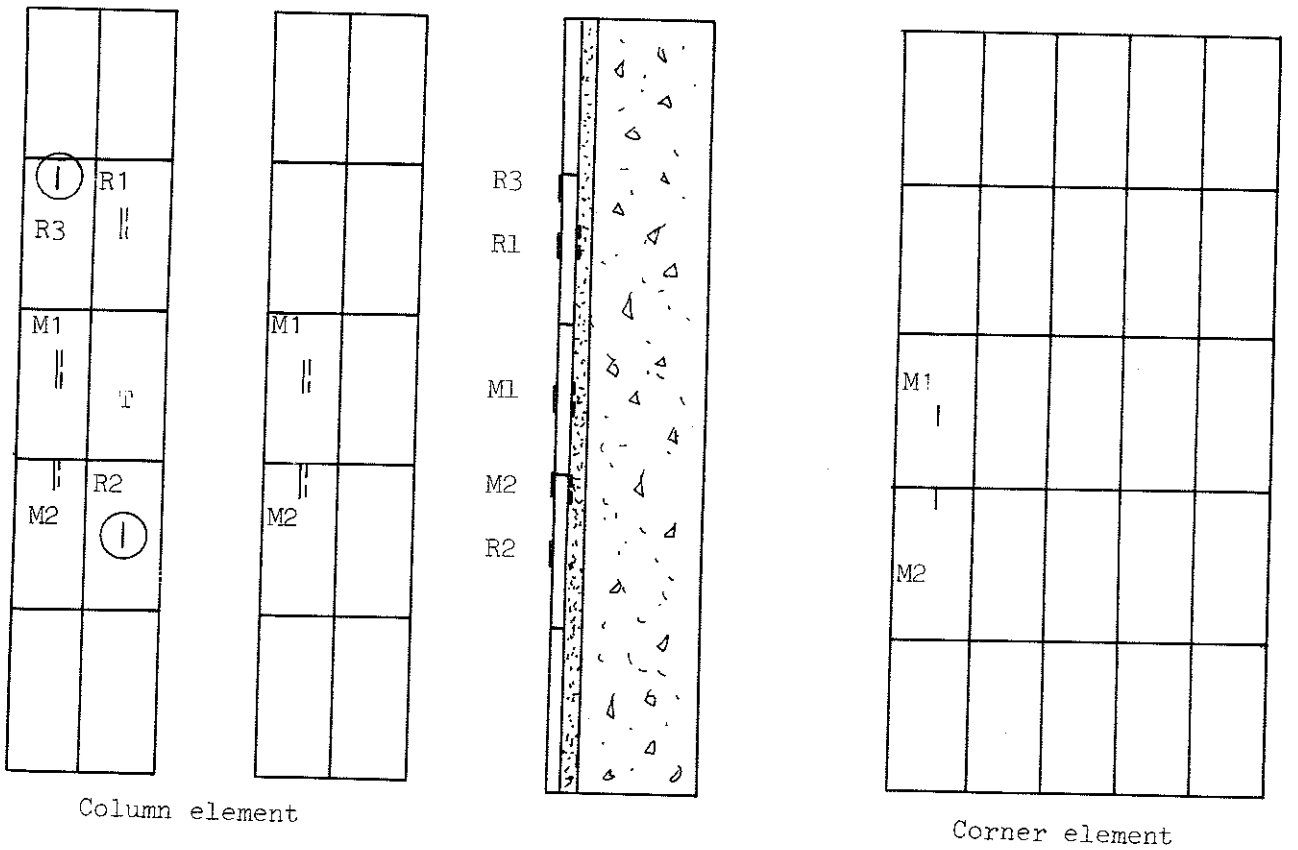

Column element

Corner element

Figure 1.4.6a. Positions of the different types of strain-gauge measuring points for tiles on wall, column and corner elements. M1 and M2 are giving the total vertical strain, R1, R2 and R3 reference values, connected to the influence of temperature and moisture variations of the tiles. | glazed side position, ¦ back side position. T = position of temperature sensors, cf. Fig. 1.4.3a-c

(6) Lead wire installation, total length 1.25 m, and insulation

(7) Sealing with Araldite PZ 820 plus HZ 820 and finally Rhodorsil, CAF 3, Elastomers

(8) Mechanical protection of the gauges on the back side of the tiles by a 1 mm layer of Epoxylite No. 222 and painting of the gauges on the glazed side to get about the same light absorption of the gauge surface as of the tile surface.

The moisture insulation of the R1 reference tiles was made by immersing the tiles, dried at 75°C and with the strain-gauges applicated, in a melt of a paraffin with a solidifying point between 69 and 73°C (Merck) for 30 minutes. The N-tiles were by this treatment impregnated to a depth of 1 to 2 mm. No corresponding penetration was observed for the F-tiles.

The strain-gauge application on the tiles was followed by a pre-aging by heating the tiles three times during about 16 hours at 70°C. Thus treated, the strain-gauges showed no zero drift after an overnight treatment at 50°C.

As described in section 1.2.3.4, all measuring tiles M and all reference tiles R are B-tiles, selected from the $\bar{x}$-classes of f^2/m. This gives a comparatively narrow probabilistic scatter of the elastic properties of the tiles. In spite of these circumstances, a further check was decided of the strain-gauge signals of these M- and R-tiles. This check was made with the total cable equipment intended for the final installation, being soldered to the strain-gauges and with the signals being evaluated with the Saab data logger. The check comprised cooling-heating tests and a longitudinal compression test of the tiles.

The cooling-heating tests were made by conditioning the tiles to a stabilized state of strain at, normally, three temperatures from about +4°C to +40°C, and for some tiles also at a temperature of about -11°C. Values down to -20°C were estimated by

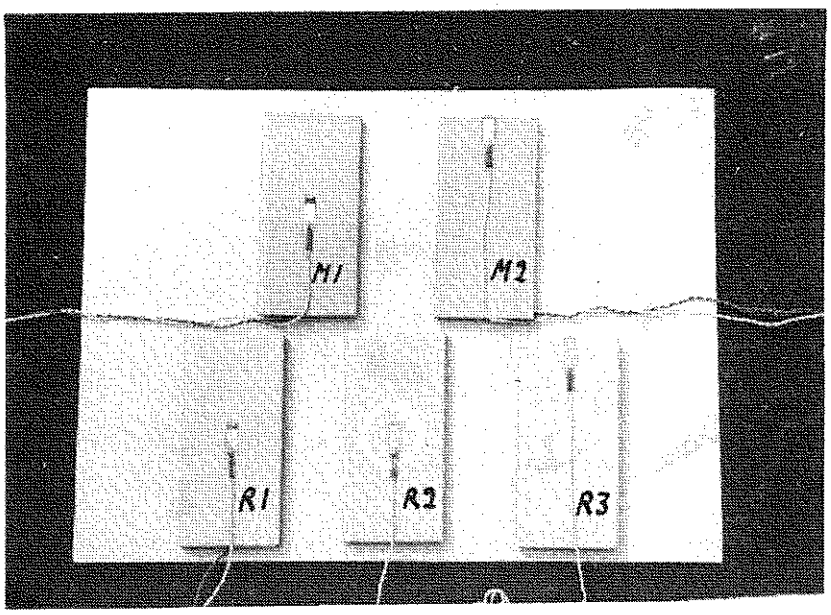

Figure 1.4.6b. The strain-gauges, applicated to the glazed side of the tiles, for the different types of measuring points (before final covering)

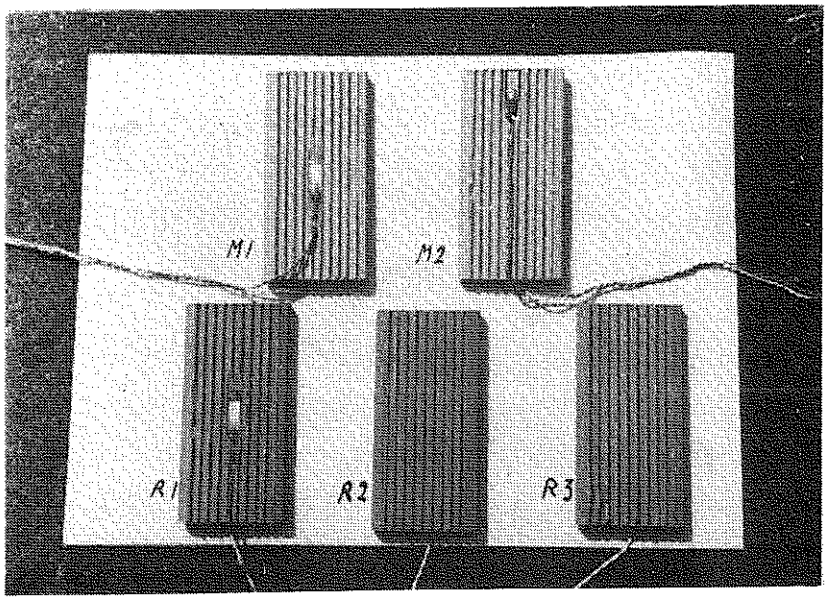

Figure 1.4.6c. The strain-gauges, applicated to the back side of the tiles, for the different types of measuring points (before final covering)

extrapolation. Due to delayed deliverances of M- and R-tiles for test house II the check had to be limited to M- and R-tiles for test house I.

The temperature induced apparent strain in 10^{-6} thus observed on free tiles and calculated around the value for $+21^{\circ}C$ as a base value is as follows - G = strain-gauge on the glaze side, B = strain-gauge on the back side of the tiles:

$^{\circ}C$	-20	-15	-5	+4	+12	+21	+30	+40
N-tile M1G								
$\bar{x}$	-164	-141	-96	-59	-29	0	+25	$+49 \cdot 10^{-6}$
s	18	15	9	5	2	-	2	$5 \cdot 10^{-6}$
n	13	13	13	13	13	-	13	13
N-tile M2G								
$\bar{x}$	-169	-146	-97	-60	-30	0	+25	$+48 \cdot 10^{-6}$
s	18	13	9	5	3	-	2	$4 \cdot 10^{-6}$
n	13	13	13	13	13	-	13	13
N-tile R1G								
$\bar{x}$	-133	-114	-79	-49	-25	0	+22	$+42 \cdot 10^{-6}$
s	11	9	6	4	2	-	1	$3 \cdot 10^{-6}$
n	6	6	6	6	6	-	6	6
N-tile R2G								
$\bar{x}$	-163	-139	-95	-59	-30	0	+24	$+47 \cdot 10^{-6}$
s	13	11	7	4	2	-	1	$3 \cdot 10^{-6}$
n	6	6	6	6	6	-	6	6
N-tile R3G								
$\bar{x}$	-166	-142	-97	-60	-31	0	+24	$+47 \cdot 10^{-6}$
s	19	16	11	7	3	-	2	$3 \cdot 10^{-6}$
n	6	6	6	6	6	-	6	6
N-tile M1B								
$\bar{x}$	-188	-160	-108	-66	-33	0	+27	$+52 \cdot 10^{-6}$
s	23	20	11	6	3	-	3	$4 \cdot 10^{-6}$
n	13	13	13	13	13	-	13	13

°C	-20	-15	-5	+4	+12	+21	+30	+40
N-tile M2B								
$\bar{x}$	-187	-162	-108	-66	-33	0	+26	$+51 \cdot 10^{-6}$
s	29	24	14	8	4	-	2	$3 \cdot 10^{-6}$
n	13	13	13	13	13	-	13	13
N-tile R1B								
$\bar{x}$	-198	-170	-115	-71	-36	0	+30	$+57 \cdot 10^{-6}$
s	14	12	8	3	1	-	1	$3 \cdot 10^{-6}$
n	6	6	6	6	6	-	6	6
F-tile M1G								
$\bar{x}$	-127	-107	-72	-44	-22	0	+18	$+35 \cdot 10^{-6}$
s	9	7	5	3	2	-	2	$4 \cdot 10^{-6}$
n	13	13	13	13	13	-	13	13
F-tile M2G								
$\bar{x}$	-123	-104	-71	-44	-22	0	+18	$+35 \cdot 10^{-6}$
s	11	9	6	4	2	-	2	$5 \cdot 10^{-6}$
n	13	13	13	13	13	-	13	13
F-tile R1G								
$\bar{x}$	-123	-105	-71	-44	-22	0	+18	$+35 \cdot 10^{-6}$
s	11	9	6	4	2	-	2	$4 \cdot 10^{-6}$
n	6	6	6	6	6	-	6	6
F-tile R2G								
$\bar{x}$	-128	-109	-74	-46	-23	0	+19	$+37 \cdot 10^{-6}$
s	10	8	4	2	1	-	1	$2 \cdot 10^{-6}$
n	6	6	6	6	6	-	6	6
F-tile R3G								
$\bar{x}$	-124	-105	-71	-44	-22	0	+17	$+34 \cdot 10^{-6}$
s	10	8	6	3	1	-	2	$3 \cdot 10^{-6}$
n	6	6	6	6	6	-	6	6
F-tile M1B								
$\bar{x}$	-123	-105	-71	-44	-22	0	+18	$+34 \cdot 10^{-6}$
s	12	10	7	4	2	-	2	$4 \cdot 10^{-6}$
n	13	13	13	13	13	-	13	13

°C	-20	-15	-5	+4	+12	+21	+30	+40
F-tile M2B								
$\bar{x}$	-128	-108	-74	-46	-23	0	+19	$+36 \cdot 10^{-6}$
s	9	7	6	4	2	-	2	$5 \cdot 10^{-6}$
n	13	13	13	13	13	-	13	13
F-tile R1B								
$\bar{x}$	-125	-106	-72	-45	-22	0	+18	$+35 \cdot 10^{-6}$
s	11	9	7	4	2	-	1	$2 \cdot 10^{-6}$
n	6	6	6	6	6	-	6	6

The table shows a good conformity for all positions of the strain-gauges for the F-tiles. Also for the N-tiles the conformity is good, except the R1 position. The deviation in this case is probably caused by the paraffin impregnation.

The average values of the temperature induced apparent strain of M1, M2, R2 and R3 positions on the N- and F-tiles are summarized in Fig. 1.4.6d.

The longitudinal compression test for the strain-gauge applicated tiles was primarily developed to have a final check of the gauge signals for a well-defined load of the tiles but was also used to get information on the modulus of elasticity of the tiles.

In the longitudinal test, the tile was placed horizontally, the glazed side down, on a bed between two jaws, one fixed and the other one feeded hydraulically giving a well-defined load. The requirement of a uniformly distributed load on the both end surfaces of the tile was solved by the use of waterfilled canvas tubes as pads. In spite of substantial efforts to apply the longitudinal compressive load centrically, it was not possible to avoid some bending of the tiles at the tests. However, when calculating the average value of the signals from the both sides of the tile this value varied only within $\pm$ 2 % even if the bending curvature showed some variation from test to test on the same tile. The variation is considered mainly to emanate from the mechanics of the test equipment.

The checking of the strain-gauge signals according to above showed all gauge applications sane.

The strain values of the longitudinal compression tests, but for the tiles of the measuring types M1 and R1 only, where the strain-gauges have a centre tile position, are used for the static modulus of elasticity in section 1.5.1.

The positions of the strain-gauges on the wall, column and corner elements of the two test houses and the corresponding numbering of the measuring points are given in tables 1.4.6a and b where G and B mark a glaze or a back position of the strain-gauges for the tiles of measuring types M1, M2, and R1. The tiles of measuring types R2 and R3 have only glaze positioned strain-gauges.

The initial values of the unbalance of strain-gauge bridges for free, dry tiles at 21°C (base values) are reported in volume 2.

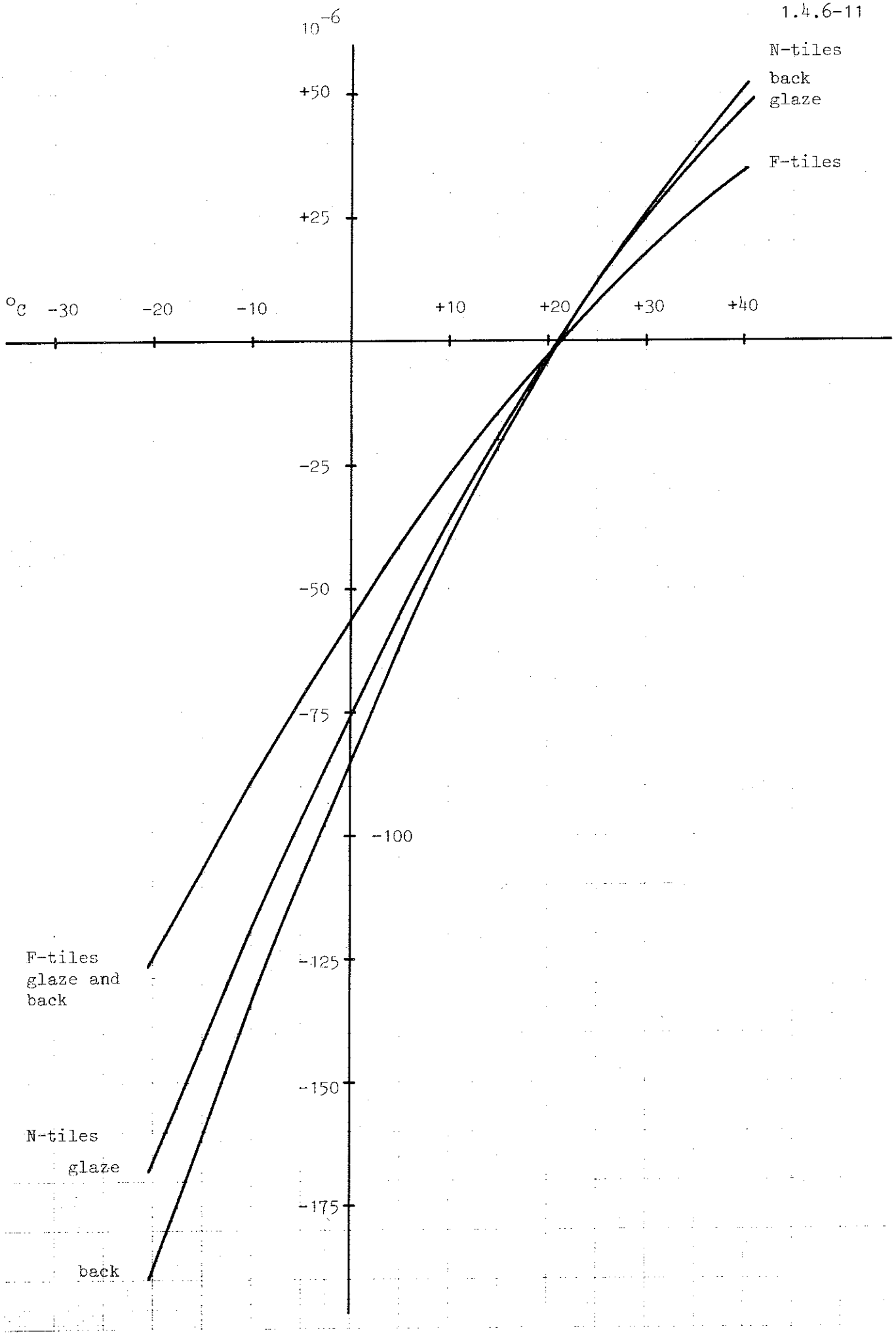

Figure 1.4.6d. Temperature-induced apparent strain of M1, M2, R2, and R3 positions on N- and F-tiles, average values

Wall element	Type of strain-gauge position							
	M1G	M1B	M2G	M2B	R1G	R1B	R2	R3
1	124	125	174	175				
2	224	225	274	275				
3	116	117	118	119	120	121	122	123
4	104	105	106	107	108	109	110	111
5	100	101	102	103				
6	112	113	114	115				
7	126	127	128	129				
8	138	139	140	141				
9	142	143	144	145	146	147	148	149
10	130	131	132	133	134	135	136	137
11	154	155	156	157	158	159	160	161
12	166	167	168	169	170	171	172	173
13	162	163	164	165				
14	150	151	152	153				
15	180	181	182	183	184	185	186	187
16	192	193	194	195	196	197	198	199
17	188	189	190	191				
18	176	177	178	179				
19	204	205	206	207	208	209	210	211
20	216	217	218	219	220	221	222	223
21	212	213	214	215				
22	200	201	202	203				
23	230	231	232	233	234	235	236	237
24	242	243	244	245	246	247	248	249
25	238	239	240	241				
26	226	227	228	229				
a corner	324		325					
b "	374		375					
c "	438		439					
f "	428		429					
i "	424		425					
j "	426		427					
l "	432		433					
t "	430		431					
u "	436		437					
z "	434		435					

Table 1.4.6a. House I: The numbering of the strain-gauge measuring points for the tiles (100 to 249, 274, 275, 324, 325, 374, 375, 424 to 439)

Wall element	Type of strain-gauge position							
	M1G	M1B	M2G	M2B	R1G	R1B	R2	R3
27	380	381	382	383	384	385	386	387
28	392	393	394	395				
29	254	255	256	257	258	259	260	261
30	376	377	378	379				
31	388	389	390	391				
32	266	267	268	269	270	271	272	273
33	250	251	252	253				
34	262	263	264	265				
35	280	281	282	283	284	285	286	287
36	292	293	294	295	296	297	298	299
37	288	289	290	291				
38	276	277	278	279				
39	304	305	306	307	308	309	310	311
40	316	317	318	319	320	321	322	323
41	312	313	314	315				
42	300	301	302	303				
43	330	331	332	333	334	335	336	337
44	342	343	344	345	346	347	348	349
45	338	339	340	341				
46	326	327	328	329				
Column element								
47	366	367	368	369				
48	416	417	418	419	420	421	422	423
49	370	371	372	373				
50	362	363	364	365				
51	354	355	356	357	358	359	360	361
52	408	409	410	411	412	413	414	415
53	400	401	402	403	404	405	406	407
54	350	351	352	353				

Table 1.4.6b. House II: The numbering of the strain-gauge measuring points for the tiles (250 to 273, 276 to 323, 326 to 373, 376 to 395, 400 to 423)

1.4.7. SURVEY OF MEASURING POINTS FOR TEMPERATURE AND STRAIN

The main characteristics of the wall and column elements of the test houses are given in Fig. 1.3.2a-i and in Fig. 1.3.2ℓ, which also shows the numbering of the elements. The following notations then are used:

F = elements with tiles type F, thickness 15 mm,
Ft = elements with thin tiles type F, thickness 10 mm,
N = elements with tiles type N, thickness 15 mm,
Nt = elements with thin tiles type N, thickness 10 mm,
3 = joints of cement mortar C 100/300,
6 = joints of cement mortar C 100/600, and
u.j= unfilled joints.

The hydraulic system for applying a permanent external axial load on some special wall and column elements in the south walls of the test houses is described in Fig. 1.3.2j-ℓ with the different load levels specified on p. 1.3.2-2.

The positions of the sensors for the temperature measurements are shown in Fig. 1.4.3a-c, as concerns the direction in depth of the wall and column elements. In Fig. 1.4.3b and c then also the numbering of the temperature measuring points is indicated. The different temperature sensors of an element are located along a perpendicular to the front surface of the element with a position of this perpendicular as marked by T in Fig. 1.4.6a. A compilation of the complete location and numbering system of the temperature sensors (no. 1 to 98) is found in Fig. 1.4.7b-e, connected to a notation procedure according to Fig. 1.4.7a. A temperature sensor (no. 0) was installed inside the weather shelter between the test houses, cf. section 1.4.1, and another additional temperature sensor (no. 99) was selected and used for control purposes, cf. section 1.4.2.

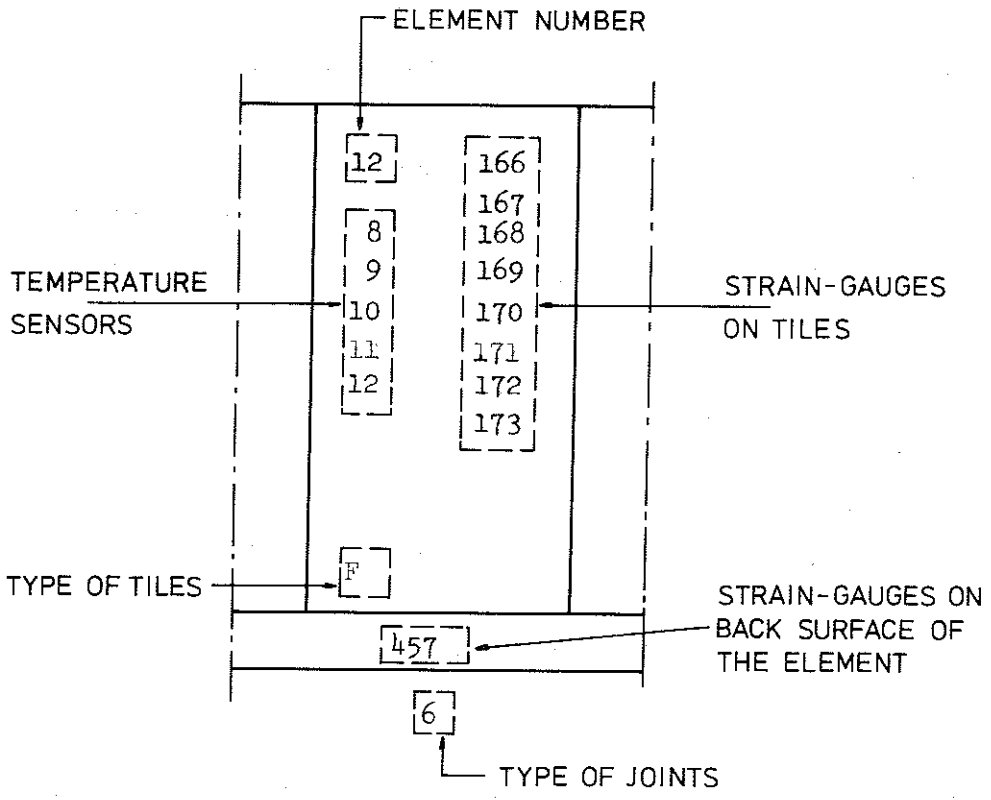

Figure 1.4.7a System of notation applied in Fig. 1.4.7b-e for specifying element number, type of tiles, type of joints, and positions of temperature sensors and strain-gauges

For a determination of the vertical strain on the glazed side and the back side of the tiles, five types of strain-gauge measuring points were used - the types M1 and M2, giving the total vertical strain, the type R1, giving separately the influence of the temperature variations, and the types R2 and R3, giving the combined influence of the temperature and moisture variations, Fig. 1.4.6a-c. About half of the wall and column elements with measuring points of type M1 and M2 then were provided with reference strain-gauges of type R1, R2 and R3. The extent of the strain-gauge measuring points on the tiles (no. 100 to 439) is given in tables 1.4.6a and b, and in Fig. 1.4.7b-e, for the different elements of the test houses with the detailed position of the measuring points on the elements according to Fig. 1.4.6a. The measuring points no. 396 to 399 were used for observations on free single panels inside test house II, cf. section 1.2.5. Three additional strain-gauge measuring points (no. 440 to 442) were arranged for checking against a fixed resistor, cf. section 1.4.2.

For a determination of the change in length and vertical curvature of the wall and column elements, metallic vertical bars with a connected measuring equipment were used with a design according to Fig. 1.4.5a and positions according to Fig. 1.4.5c. These arrangements were completed with strain-gauge measurements of the vertical deformations in the centre of the back surface of each of the main wall and column elements (no. 1 to 54). The numbering and positions of these complementary measuring points (no. 446 to 499) are shown summarily in table 1.4.5a and Fig. 1.4.7b-e. The strains of reference bodies, placed inside House II, were followed by the strain-gauge measuring points no. 443 to 445.

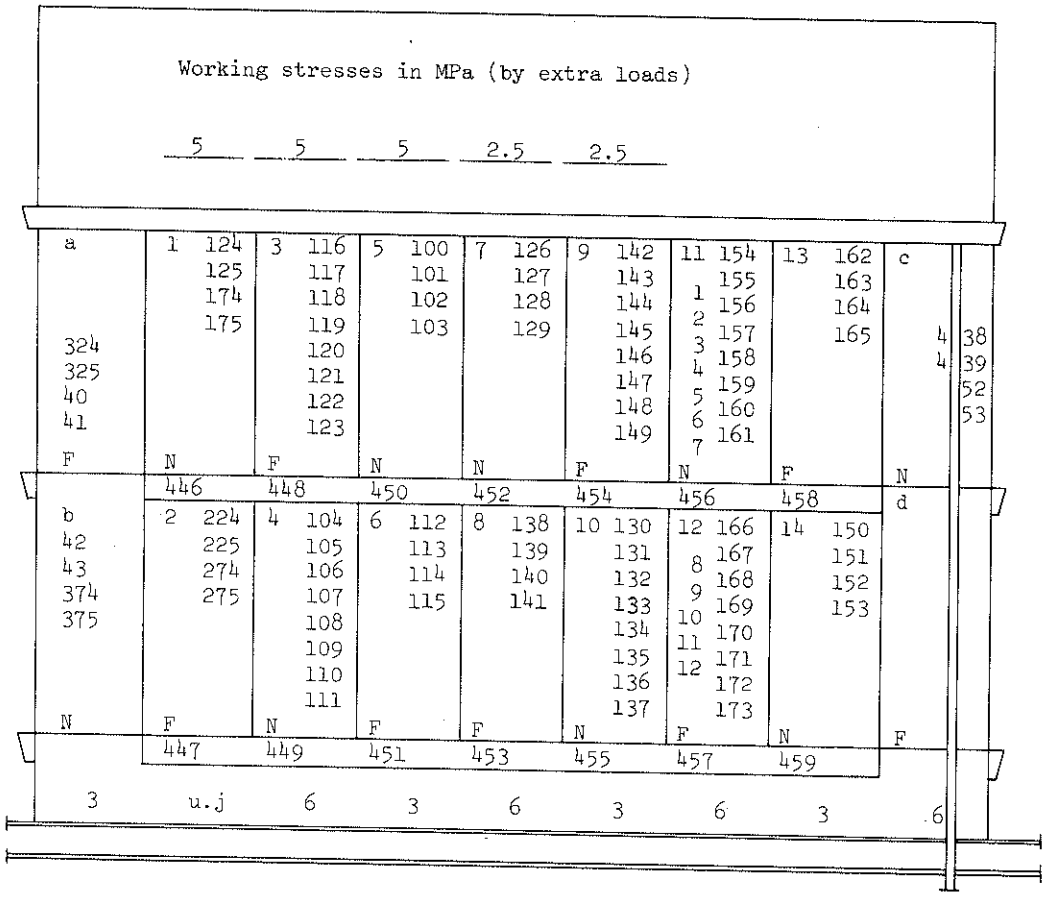

Figure 1.4.7b. Element number, type of tiles, type of joints, and positions and numbering of temperature sensors and strain-gauges. Test house I, south and west fronts

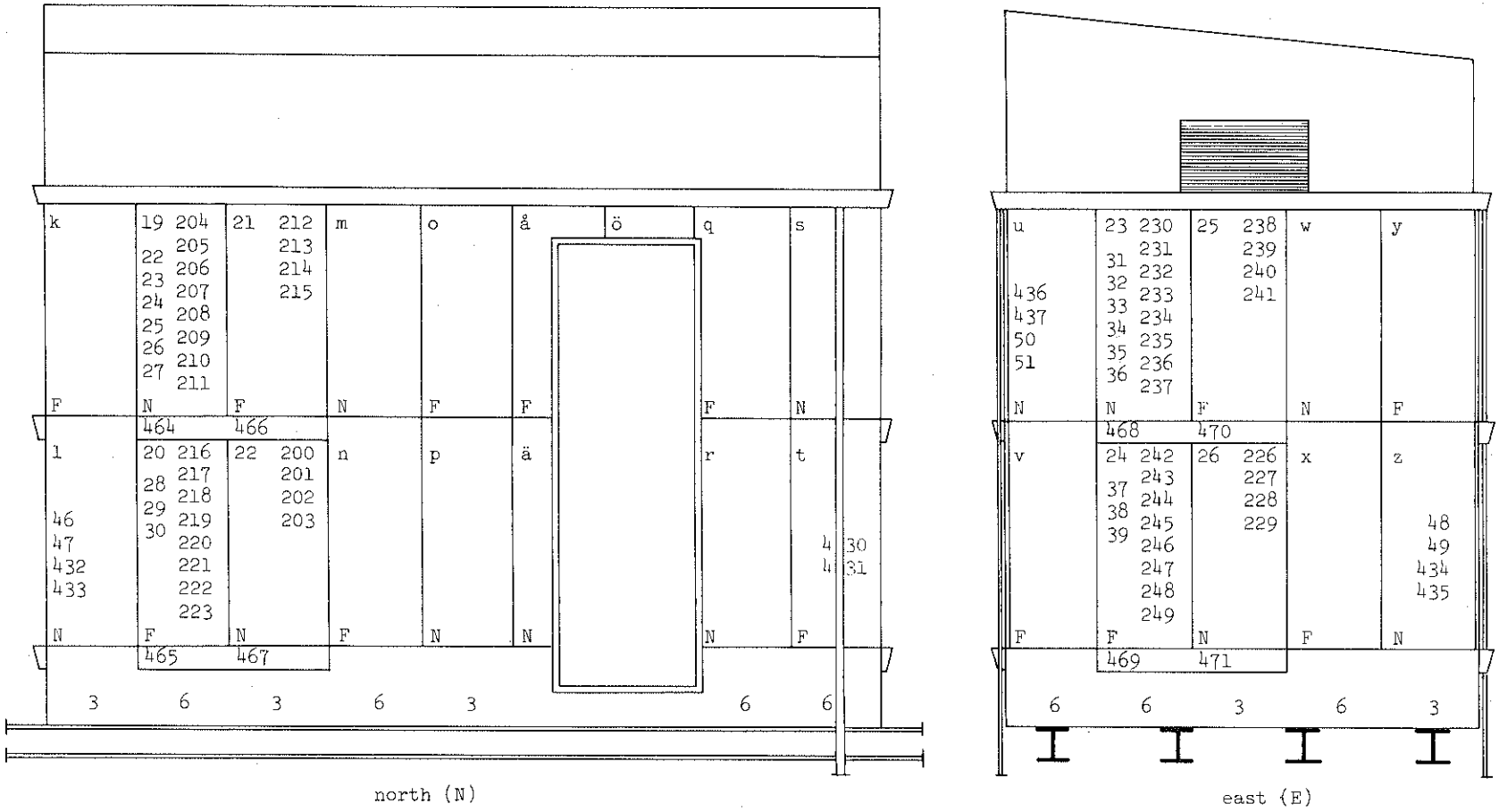

Figure 1.4.7c. Element number, type of tiles, type of joints, and positions and numbering of temperature sensors and strain-gauges. Test house I, north and east fronts

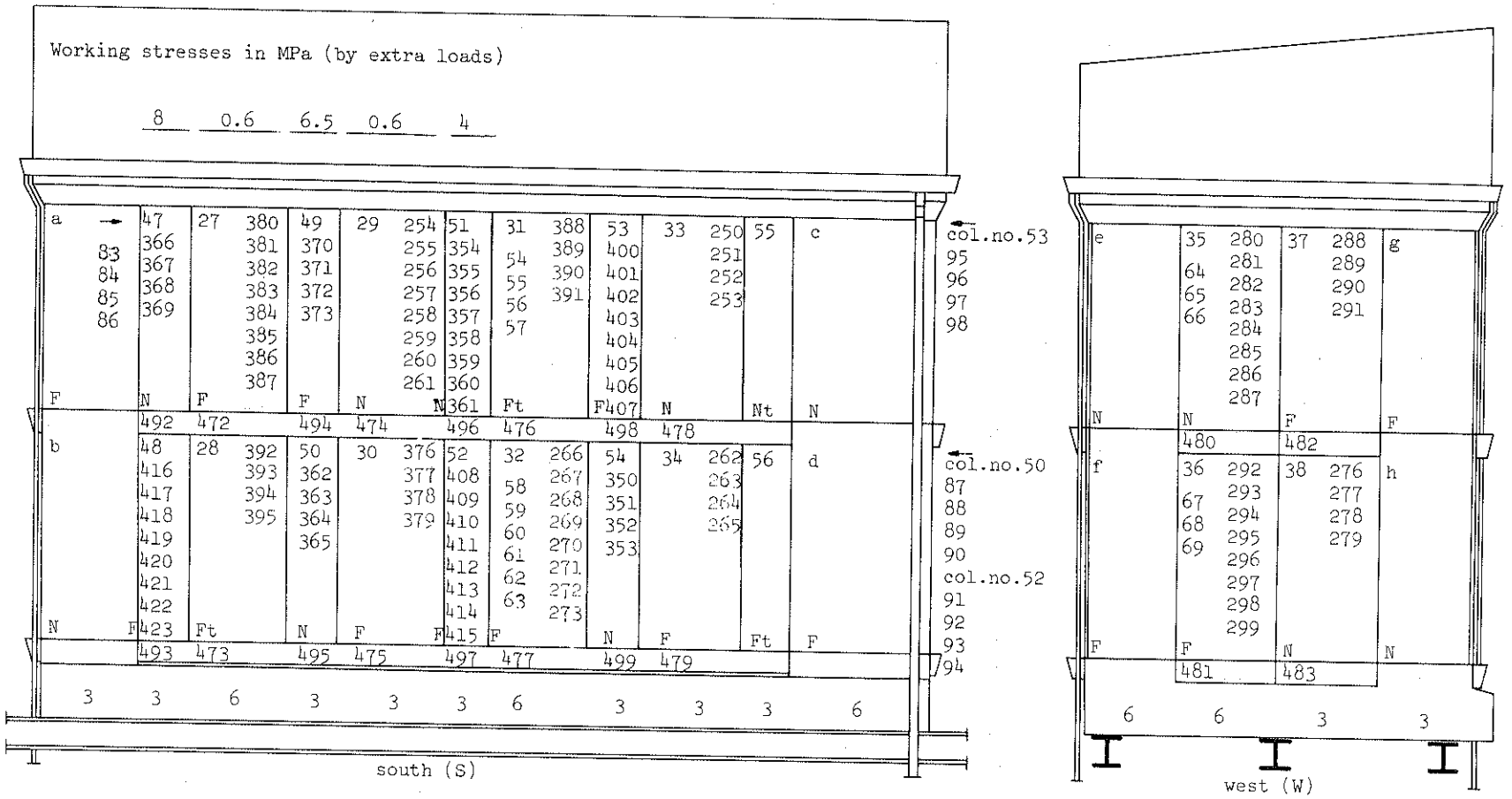

Figure 1.4.7d. Element number, type of tiles, type of joints, and positions and numbering of temperature sensors and strain-gauges. Test house II, south and west fronts

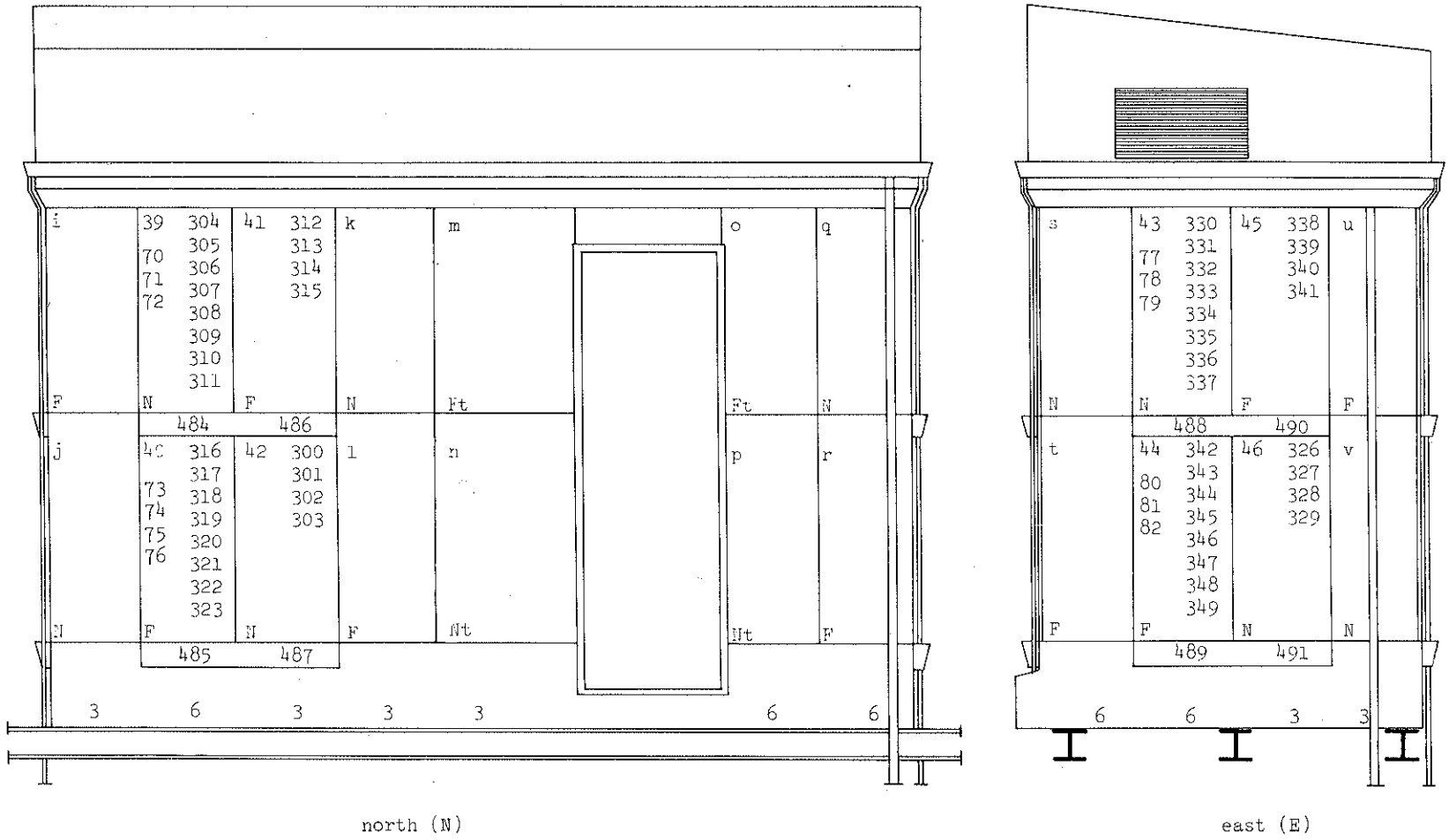

Figure 1.4.7e. Element number, type of tiles, type of joints, and positions and numbering of temperature sensors and strain-gauges. Test house II, north and east fronts

1.4.8. DAMAGES IN CERAMIC WALL FACINGS, IF ANY

Intermittently, the ceramic wall facings were observed visually regarding cracks and partial scaling off in the glazing and portions of the body of the tiles, and regarding cracks in the joints. Parallelly, possible bond failures between the ceramic tiles and the fixing mortar or between the fixing mortar and the material behind as well as possible cracks in the fixing mortar itself were investigated by listening to the character of the sound at a careful knocking on the tiles with a steel rod.

The time-schedule of these observations was:

twice a month	during the first six months,
once a month	subsequently.

A more thorough study of the state of damage in the ceramic wall facings was referred to an individual dismounting of the tiles, comprising a determination of the change of strain for defined steps of the dismounting procedure and the change of the initial material properties due to the influence of environment conditions and time, cf. volume 2.

1.5. INITIAL MATERIAL PROPERTIES

1.5.1. INITIAL PROPERTIES OF TILES

The two types of ceramic tiles used for the exterior covering on the wall surfaces of the test houses are - as mentioned in section 1.2.3 - denominated N and F.

The tile type N is manufactured since about 1950 and of mainly native clays, wet extruded in pairs giving twins, back to back (split tiles), and dried. The outside surfaces are sprayed with a glaze composition and the body and glaze are simultaneously fired. The result is a cream-yellow, to some extent porous body with a glazed non-porous outside layer. After splitting, the single tile has a rough back with rills oriented along the tile.

The tile type F is manufactured since 1961-1962, principally in the same way as type N, but of mainly imported clays, giving a grey body with a low porosity. The final glaze is more or less transparent.

Fig. 1.5.1a shows the cross sections across the rills of the two types of tiles before splitting, and Fig. 1.5.1b the tiles after splitting, as concerns the predominating tiles of ordinary thickness.

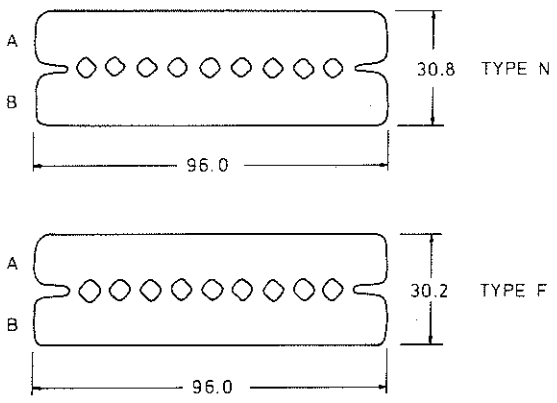

Figure 1.5.1a. Cross section of twin tiles, type N and F. Scale 1:2

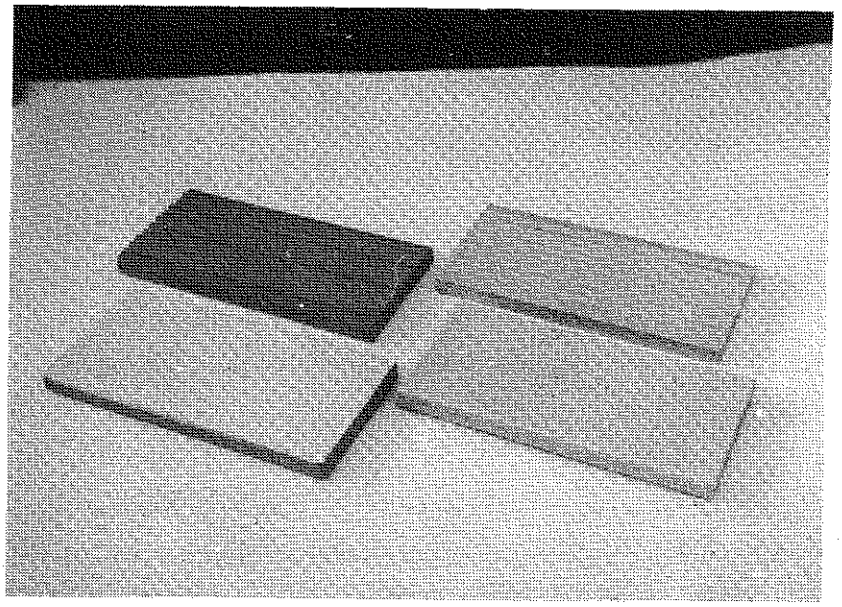

Figure 1.5.1b. Split tiles, type N and F

A few elements of the test houses were provided with thin N- and F-tiles, i.e. tiles of a thickness of about 10 mm. The material properties of these tiles, which principally are the same as for the normal N- and F-tiles, are not further reported in this section.

1.5.1.1. Physical average data of split N- and F-tiles

Due to the character of the raw materials and the manufacturing processes, there is a slight tendency of an anisotropic structure for the tiles of type N and, in less degree, also for the tiles of type F. If not otherwise mentioned, the data below refer to the properties with reference to the longitudinal direction of the tiles and to dry tiles at normal storage conditions (temperature 20°C, relative humidity ~60%). As concerns the N-tiles, the data have to be seen in the light of the differences in thickness, mass and flexural resonance frequency of the A- and B-twins, noted in section 1.2.3.1.

	N-tiles	F-tiles
(1) Colour scale guide, according to Fédération Européenne des fabricants des carraux céramiques	A3(glaze) C-D8(body)	A4(glaze) A5(body)

	N-tiles	F-tiles
(2) Light absorption factor, %, for 0.7 µm, at angle near the perpendicular	30 ± 2	39 ± 1
(3) Dimensions of tile, length x width x thickness, mm, thickness measured from glaze surface to bottom of rills. Height of longitudinal bars between rills ~2.6 mm. Due to splitting the top of bars is very rough and can vary up to ± 2 mm. Regarding scatter of tile dimensions, see section 1.2.3.1 and 1.2.3.2	A: 196.1x96.0x12.6 B: 195.9x96.0x13.1	A: 196.0x96.6x12.4 B: 195.9x96.5x12.4
(4) Thickness of glaze, mm,	~0.32	~0.40
(5) Area of cross section, mm^2, calculated value, bars included	A: 1330 B: 1370	1310
(6) Weight of tile, kg,	A: 0.576 B: 0.592	0.590
(7) Density, mercury displacement, kg/m^3, similar to ASTM C 493	A: 2230 B: 2220	2340

	N-tiles	F-tiles
(8) True density, xylene displacement, kg/m^3, similar to DIN 51057	A: 2660 B: 2670	A: 2570 B: 2560
(9) Porosity, total, m^3/m^3 from densities above	0.165	0.088

(10)Stress-strain characteristics in compression

Stress-strain curves, determined in longitudinal compression tests on parallelepipedal test specimens without glaze, size 62.5 x 25.2 x x 11.2 mm^3, one specimen per type of tile, are shown in Fig. 1.5.1.1a and b for N-tile and F-tile, respectively. In the figures, the curves ① are giving the relation between stress and longitudinal compressive strain, the curves ② the relation between stress and lateral expansion parallel to the width direction, and the curves ③ the relation between stress and lateral expansion parallel to the thickness direction.

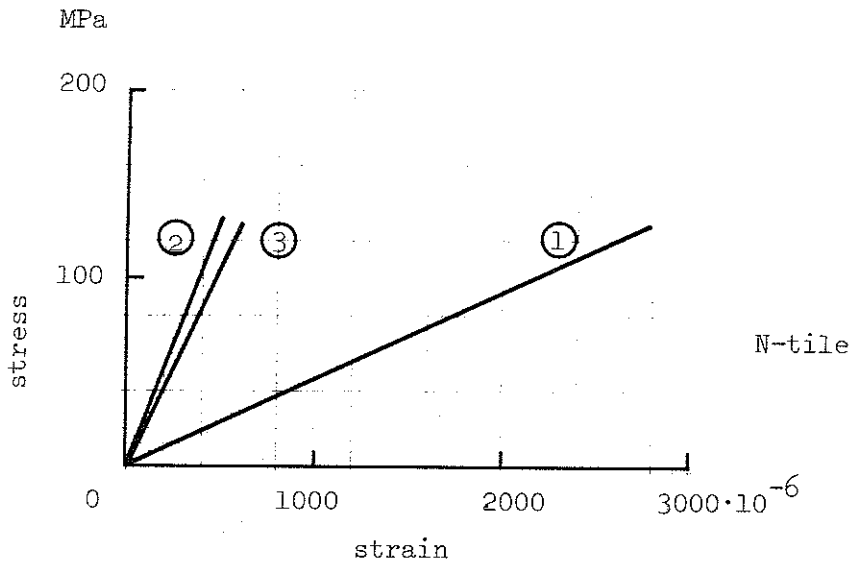

Figure 1.5.1.1a. Stress-strain curves of N-tile body in compression. ①longitudinal compressive strain, ②and ③lateral expansion in width and thickness direction, respectively

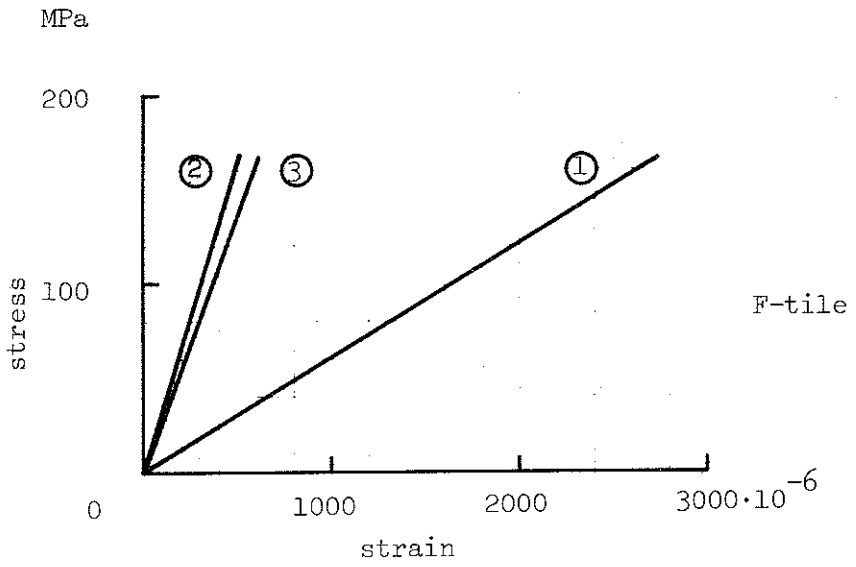

Figure 1.5.1.1b. Stress-strain curves of F-tile body in compression. ① longitudinal compressive strain, ② and ③ lateral expansion in width and thickness direction, respectively

From the tests according to Fig. 1.5.1.1a and b, the following quantities are obtained:

	N-tile	F-tile
Modulus of elasticity, GPa,	44.8	61.5
Poisson's ratio, width direction	0.173	0.186
Poisson's ratio, thickness direction	0.207	0.214
Ultimate compressive strength, MPa,	131	175

Complementary, the static modulus of elasticity was determined also in the compression tests of the strain-gauge applicated tiles, measuring types M1 and R1, described in section 1.4.6, see pp 1.4.6-9 and 10. The determination then was made for two load levels, corresponding to the stress values 2.3 and 4.6 MPa. The dynamic modulus of elasticity was evaluated from the flexural

resonance measurements, carried out in connection with the tile material selection and reported in section 1.2.3. The mean value $\bar{x}$ and the standard deviation s received in these tests are given in the following table - n = number of observations.

	N-tile	F-tile
Static modulus of elasticity, GPa,	$\bar{x}$ = 48 s = 2 n = 31	$\bar{x}$ = 65 s = 1 n = 33
Dynamic modulus of elasticity, GPa,	$\bar{x}$ = 47 s = 1.4 n = 1984	$\bar{x}$ = 65 s = 1.0 n = 1117

Determinations of the ultimate compressive strength of hard and brittle materials, such as ceramic tile materials, are normally characterized by a high standard deviation. In not inconsiderable extent, this scatter is due to the conditions around the load application in the test. Some studies were performed at this problem leading to a test procedure, reducing the standard deviation to be influenced predominantly by the tile material. The studies are described briefly in appendix 1.5.1a. Applied to cut, not split twin tiles of full cross section, compressed in the longitudinal direction of the tiles, the test procedure gave the following values of the ultimate compressive strength.

	N-tile	F-tile
Ultimate compressive strength, MPa,	$\bar{x}$ = 241 s = 9.3 n = 6	$\bar{x}$ = 270 s = 10.1 n = 6

(11) Ultimate flexural strength, MPa, tested similar to DIN 51090 but with tensile strain on glaze side

	N-tile	F-tile
(a) dry tile	$\bar{x}$ = 38.3 s = 1.7 n = 10	$\bar{x}$ = 22.2 s = 2.0 n = 10
(b) wet tile	$\bar{x}$ = 36.0 s = 2.1 n = 10	$\bar{x}$ = 21.5 s = 2.5 n = 10
(12) Ultimate tensile strain of glaze in bending of the tile, 10^{-6},	740	310
(13) Ultimate tensile strength, MPa, splitting tension test according to appendix 1.5.1b, applied to tiles without rills and glaze	$\bar{x}$ = 17.2 s = 0.9 n = 5	$\bar{x}$ = 17.6 s = 1.0 n = 5
(14) Creep deformation	Negligible at test house conditions	
(15) Specific heat capacity, J/(kg·K),	710	710
(16) Thermal conductivity, W/(m·K),		
(a) dry tile	0.95	0.98
(b) total water saturation	1.51	1.03
(c) at 0.25 of total water saturation	1.23	-
(d) at 0.5 of total water saturation	1.35	-
(17) Thermal dilatation, 10^{-6}/K,		
(a) dry tile, -15 to +40°C	5.2	4.2
(d) wet tile, 0 to +40°C	5.2	4.2

	N-tile	F-tile
(18) Water absorption in vacuum, m^3/m^3, similar to DIN 51056	0.147	0.003
(19) Moisture absorption equilibrium at 20°C and 60% relative humidity, m^3/m^3,	≈0.0013	≈0.0002

For N-tiles, the rate of moisture absorption from dry state to a saturation between 0.5 and 0.7 of the total saturation strongly depends on the wetting conditions. Under equivalent conditions, the rate of drying is much slower than the rate of absorption.

(20) Moisture permeability

Can be considered negligible in all directions for the F-tiles and perpendicular to the glaze surface for the N-tiles. In other directions of the N-tiles, the permeability is estimated to the order of $2 \cdot 10^{-6}$ m^2/s within the hygroscopic range.

(21) Moisture dilatation in presence of mortar ions

The moisture dilatation of ceramic tiles is to its character a combined physical-chemical reaction, only partly reversible.

For free, new N-tiles, not earlier wetted, the moisture dilatation, observed at ordinary room temperature, is of the magnitude $(120-150) \cdot 10^{-6}$. The moisture dilatation has a considerable delay in comparison with the corresponding water absorption. For F-tiles, the appurtenant value of the moisture dilatation is $(5-10) \cdot 10^{-6}$.

In fixing mortar water at ordinary room temperature, the moisture dilatation of the N- and F-tiles, free from glaze, grows according to Fig. 1.5.1.1c. The dilatation-time curves are approaching limits which correspond to a final degree of water saturation of 0.73 and 1.0 for the N-tile and F-tile, respectively.

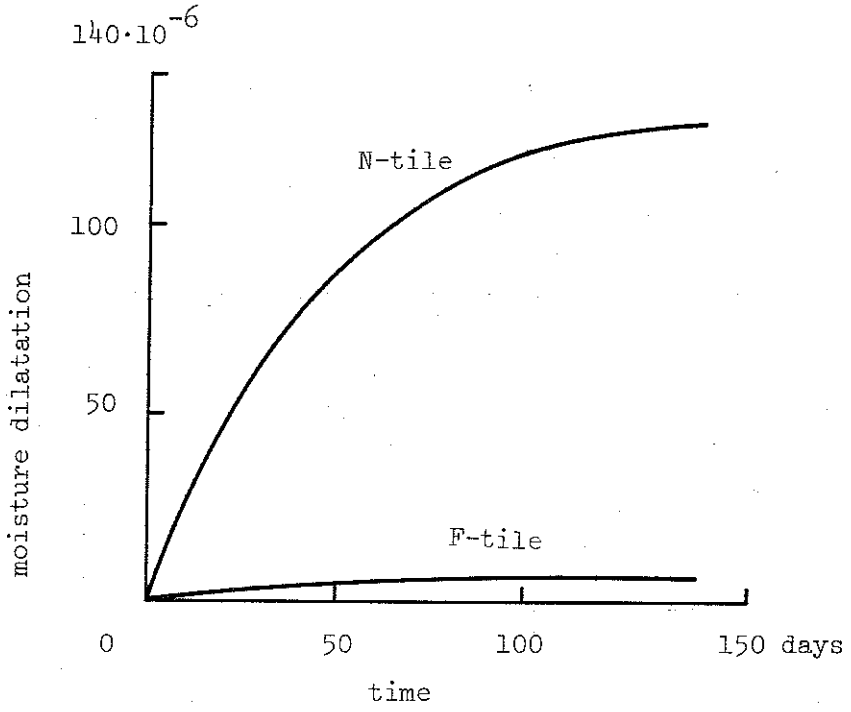

Figure 1.5.1.1c. Moisture dilatation-time curves for N- and F-tiles, free from glaze, in fixing mortar water at ordinary room temperature

An increase of the ion concentration in the water from the mortar gave rise to a still further increase of the observed dilatation of the tiles.

	N-tile	F-tile
(22) Temperature, initiating ice formation in the tiles in the presence of mortar ions, °C,	-2 to -3	-1 to -3

(23) Frost dilatation

Examples of frost dilatation, obtained at the first freezing cycle for free split tiles, size 0.2x0.1x0.015 m^3, are given in Fig. 1.5.1.1d and e. The figures show the time curve of dilatation and the connected temperature-time variation for the N- and F-tiles, preconditioned with destilled water in vacuum similar to the DIN 51056 procedure.

Additional information is planned to be given in volume 2.

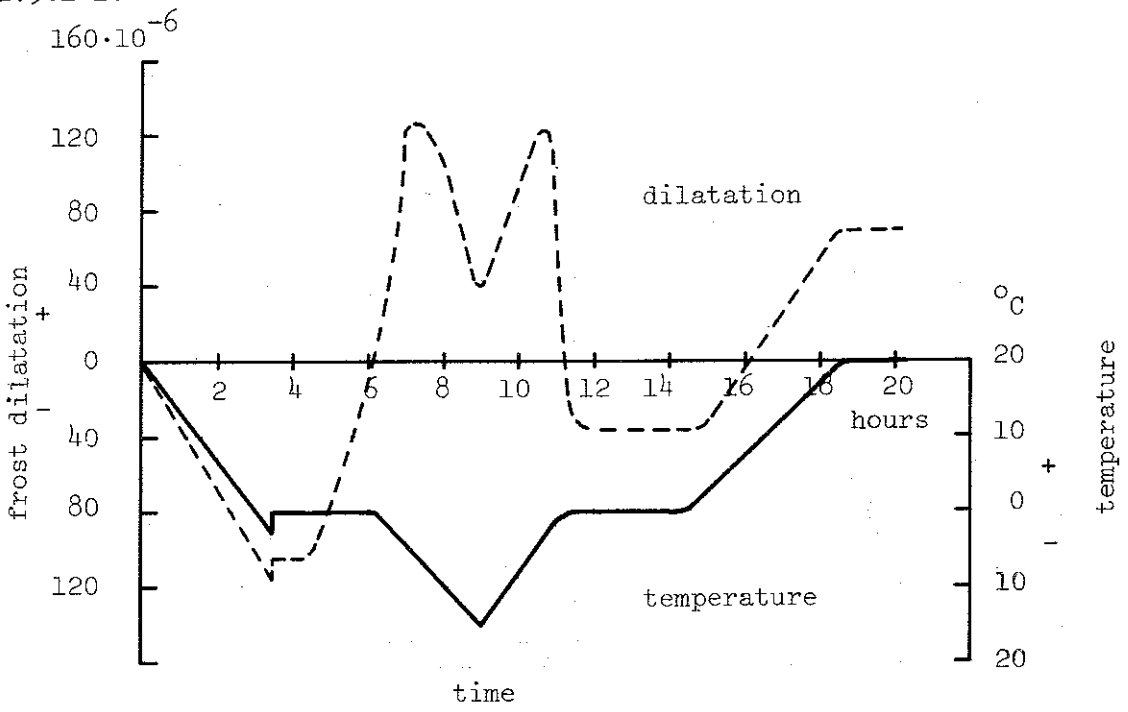

Figure 1.5.1.1d. Frost dilatation and connected temperature variation at the first freezing cycle for free split N-tile. Water content 0.15 m^3/m^3, saturation near 1.0

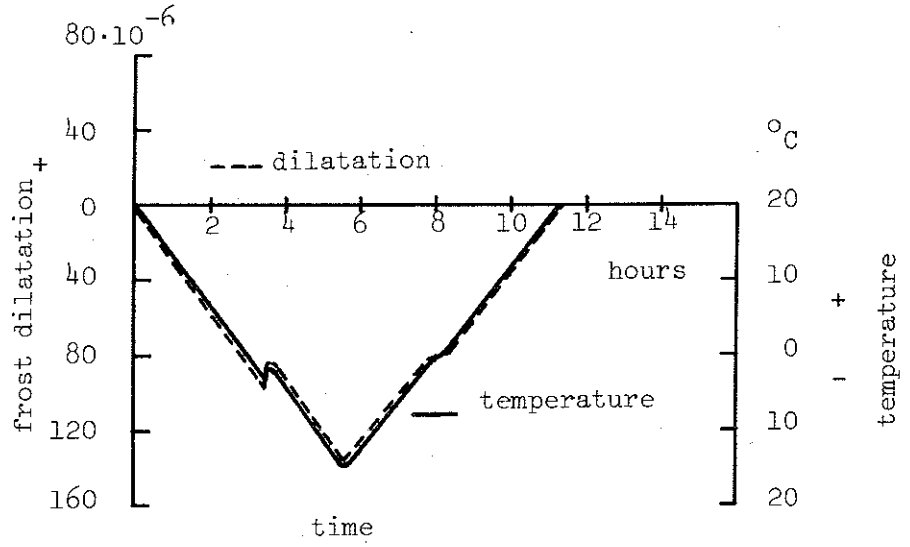

Figure 1.5.1.1e. Frost dilatation and connected temperature variation at the first freezing cycle for free split F-tile. Water content 0.003 m^3/m^3, saturation near 1.0

	N-tile	F-tile
(24) Critical degree of water saturation for frost damage, cf. appendix 1.5.1c	0.91	0.91, aged tiles 1.0, new tiles

(25) Micro material structure of the tiles

In Fig. 1.5.1.1f, representative cross sections of the N- and F-

-tiles are shown at a magnification of 25 and in Fig. 1.5.1.1g scanning microscope photos of fracture surfaces of the tiles at two different degrees of magnification.

The photos confirm well the reported material data of the two types of tiles. The N-tile has in comparison with the F-tile about the double total porosity. Of the total porosities about 90% are accessible to water for the N-tile, but only about 4% for the F-tile. Further, the inner surfaces are "finely" distributed as small pores in the N-tile but in the F-tile, concentrated to irregularly distributed large, few pores.

N-tile F-tile

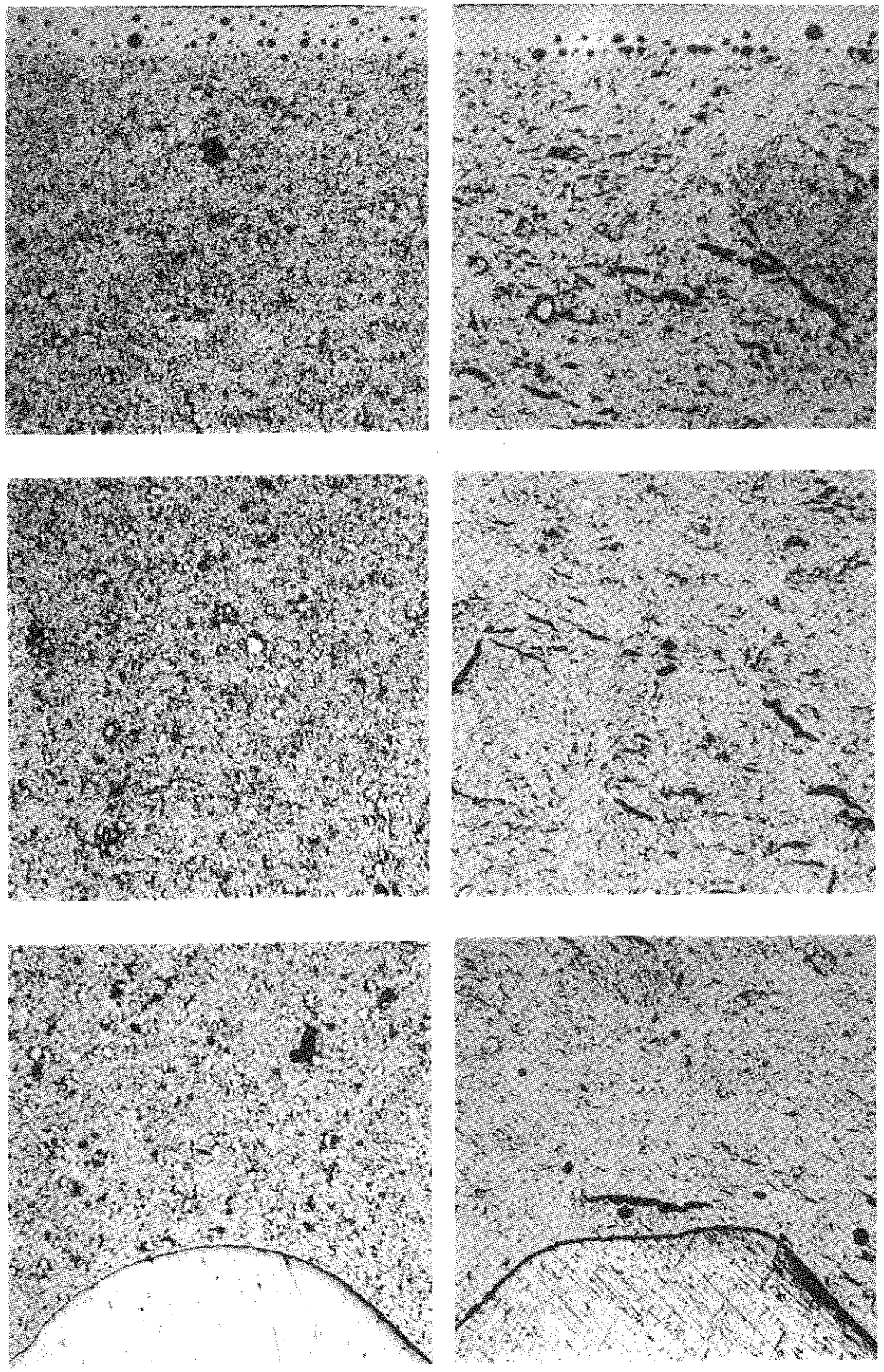

Figure 1.5.1.1f. Cross sections of N- and F-tiles at a magnification of 25. Scale: 2.5 mm in photo correspond to 100 µm in reality. Each square corresponds to 3 by 3 mm and the sections are, from top to bottom, the glaze side, the middle part and the back, inclusive part of rills, of the tiles

N-tile F-tile

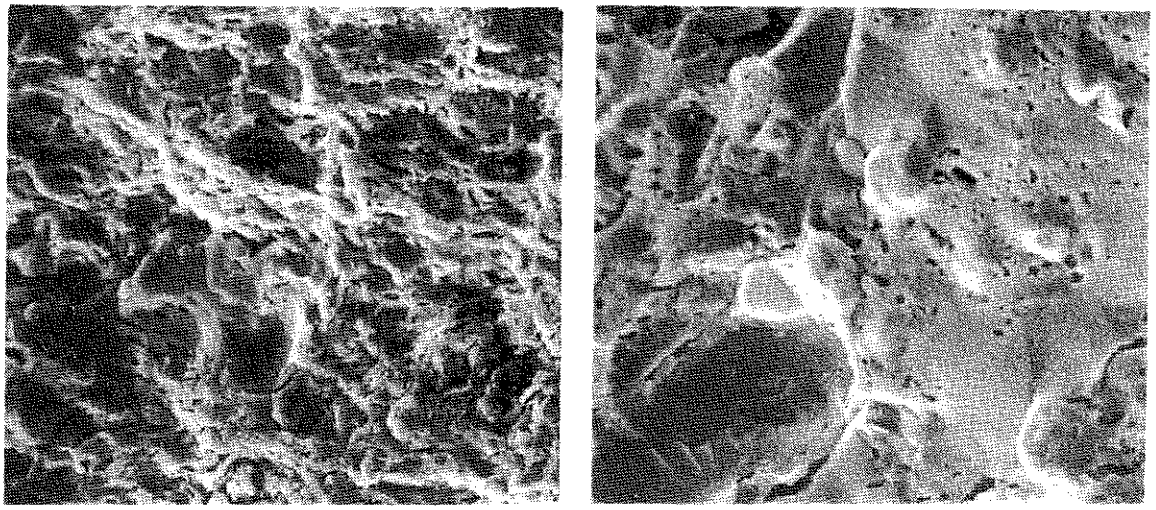

100 µm

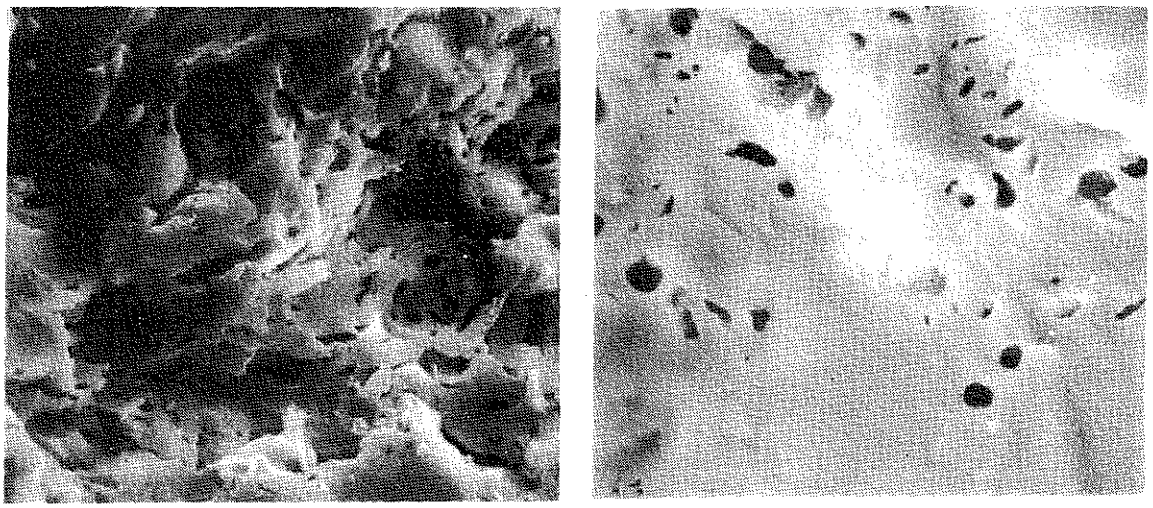

100 µm

Figure 1.5.1.1g. Scanning microscope photos of fracture surfaces of N- and F-tiles, orientation as for the micro photos in Fig. 1.5.1.1f

1.5.2. INITIAL PROPERTIES OF FIXING MORTAR

Before the fixing of the ceramic tiles to the wall and column elements of the test houses, the bedding surface of the elements was ground by a thin splash mortar of the type KC 10/90/325, composed of 10 parts lime powder + 90 parts standard Portland cement (equivalent mixture KC 14) + 325 parts sand no-3, all parts by weight. The ceramic tiles then were fixed by a fixing mortar with a thickness of about 20 mm, cf. Fig. 1.3.2d, 1.3.2h and 1.3.2i. The fixing mortar used was a lime-cement-mortar of the type KC 35/65/550, composed of

35 parts by weight lime powder
65 parts by weight standard Portland cement
} equivalent mixture KC 11

550 parts by weight sand no-3,
moisture 4%.

The sand no-3 is characterized by the sieve analysis

above 4 mm	2% by weight
2-4 mm	8%
1-2 mm	16%
0.5-1 mm	28%
0.25-0.5 mm	29%
0.125-0.25 mm	12%
0.062-0.125 mm	4%
less than 0.062 mm	1%

The equivalent mixture KC 11 and the sand were mixed in dry condition during 5 min, after which water was added to the prescribed workability - about 13% by weight.

1.5.2.1. Physical average data of fixing mortar

(1) Density, kg/m^3, at moisture 0.026 m^3/m^3 1870

(2) Stress-strain characteristics in compression

Stress-strain curves, determined in a longitudinal compression test on a parallelepipedal test specimen, size 159.0x40.2x39.9 mm^3, age 5.5 years, are shown in Fig. 1.5.2.1a. In the figure, curve ① gives the relation between stress and compressive strain and curve ② the relation between stress and lateral expansion.

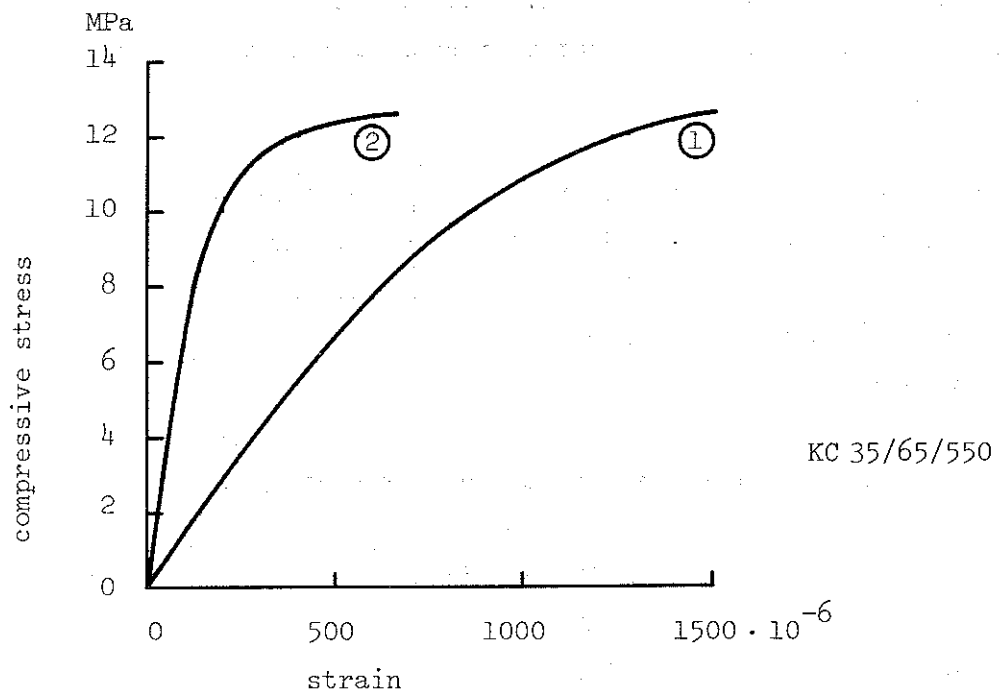

Figure 1.5.2.1a. Stress-strain curves of fixing mortar in compression. ① longitudinal compressive strain and ② lateral expansion, respectively

From the test according to Fig. 1.5.2.1a, the following quantities are obtained:

Initial modulus of elasticity, GPa,	13.9
Poisson's ratio, evaluated at 50% of ultimate compressive strength	0.213
Ultimate compressive strength, MPa,	12.5

Complementary, the initial modulus of elasticity and the ultimate compressive strength of the fixing mortar were determined at different age of the test specimens. The results of these tests are

given in Fig. 1.5.2.1b and c.

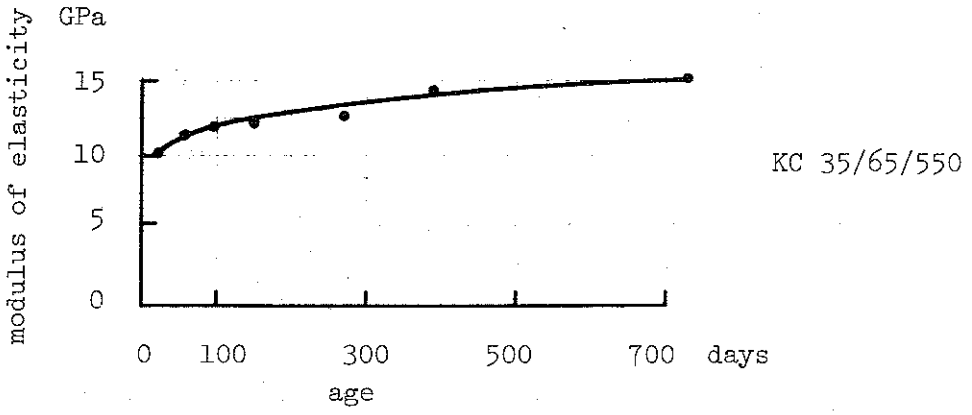

Figure 1.5.2.1b. Initial modulus of elasticity of fixing mortar at different age

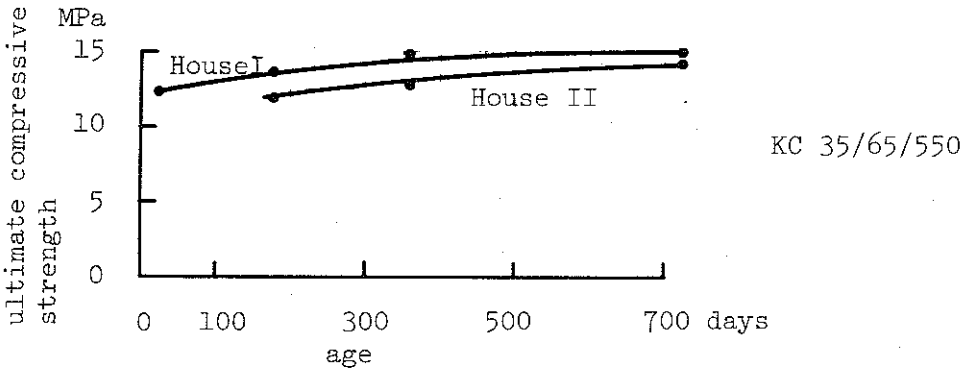

Figure 1.5.2.1c. Ultimate compressive strength of fixing mortar at different age - similar to DIN 1164

(3) Ultimate flexural strength at different age - according to Fig. 1.5.2.1d.

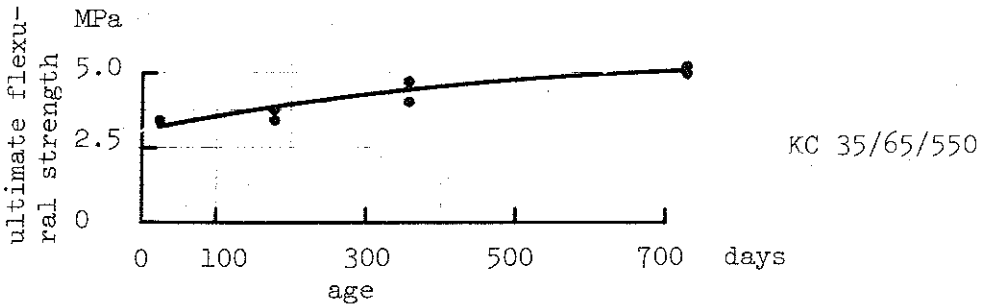

Figure 1.5.2.1d. Ultimate flexural strength of fixing mortar at different age - similar to DIN 1164

(4) Ultimate tensile strength at different age - determined in splitting tension test according to ASTM C 496, Fig. 1.5.2.1e.

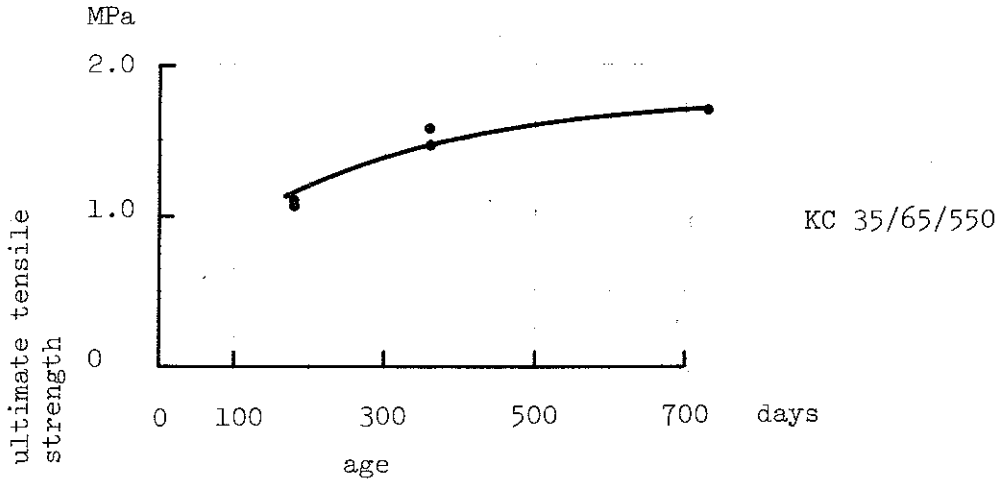

Figure 1.5.2.1e. Ultimate tensile strength of fixing mortar at different age - similar to ASTM C496

(5) Creep deformation - to be dealt with in volume 3

(6) Specific heat capacity, J/(kg·K), dry material, estimated value ~850

(7) Thermal conductivity, W/(m·K),
(a) dry material, estimated value 0.8
(b) water content 0.036 m^3/m^3, estimated value 1.05

(8) Thermal dilatation, 10^{-6}/K, dry material 8.1

(9) Water absorption in vacuum, m^3/m^3, 0.29

(10) Moisture permeability as a function of relative humidity, determined at 25°C, Fig. 1.5.2.1f [1]

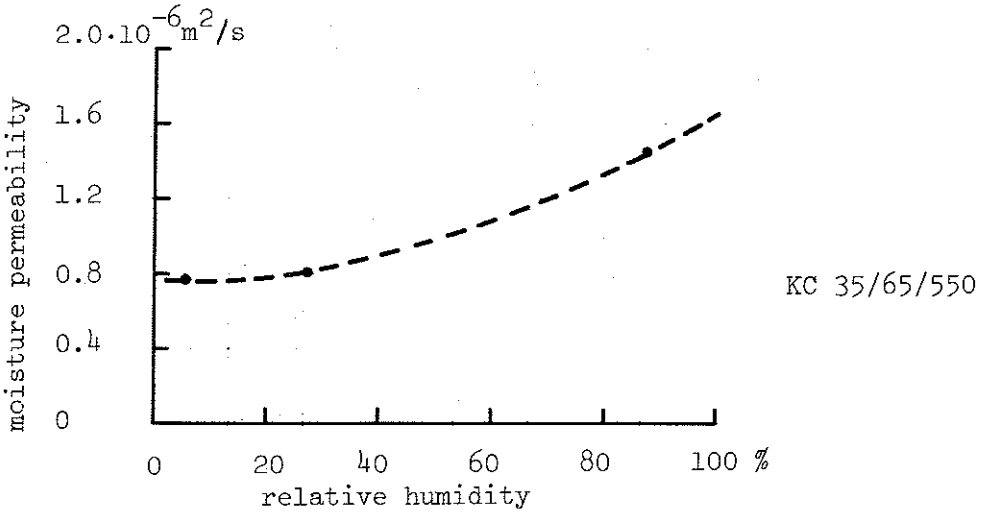

Figure 1.5.2.1f. Moisture permeability of fixing mortar at varying relative humidity [1]

(11) Moisture dilatation - determined for test specimens wetted at equilibrium with 65% relative humidity, Fig. 1.5.2.1g.

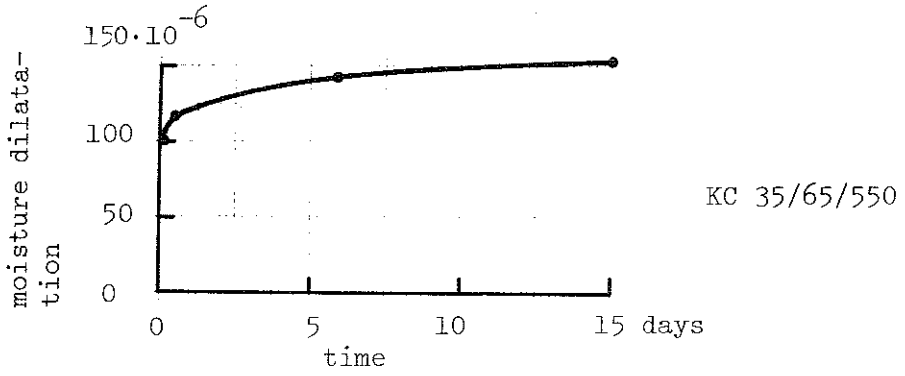

Figure 1.5.2.1g. Time curve of moisture dilatation for fixing mortar wetted at equilibrium with 65% relative humidity

(12) Shrinkage

At the hardening of a mortar, a primary shrinkage takes place parallelly with the increase in strength. This shrinkage starts directly when the mortar is applied on the bedding and begins to get stiff. This shrinkage, however, seldom gives rise to any visible consequences since the mortar then is plastic and formable. As the hardening process and the strength increases, the shrinkage causes stresses in the mortar which can result in a crack formation.

The free, primary shrinkage of a fixing mortar of the type used for the ceramic tiles on the test houses - KC 35/65/550 - is shown in Fig. 1.5.2.1h [2].

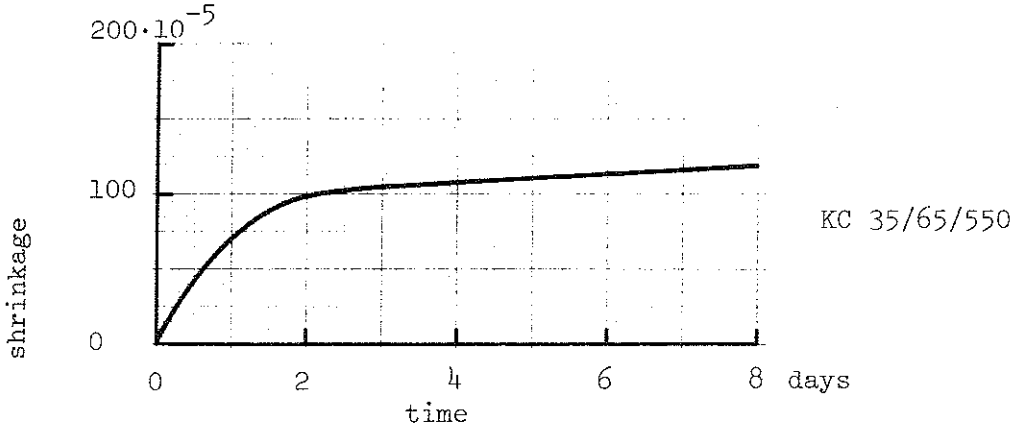

Figure 1.5.2.1h. Free, primary shrinkage of fixing mortar of type KC 35/65/550 [2]

For an analysis of the stress-strain behaviour of a fixing mortar between a ceramic tile layer and the underlying bedding, the data on the free shrinkage have to be supplemented with data on the restrained shrinkage, giving the stresses induced in the mortar at a complete deformation restraint. This problem will be further dealt with in volume 3 where also shrinkage-time curves related to a longer time period will be presented.

(13) Temperature, initiating ice formation in the fixing mortar in the presence of mortar ions, °C, -2 to -4

(14) Frost dilatation

An example of frost dilatation, obtained at the first freezing cycle for a free test specimen of the fixing mortar, size 0.16 x 0.04 x x 0.04 m^3, is given in Fig. 1.5.2.1i. The figure shows the time curve of dilatation and the connected temperature-time variation for the test specimen evacuated and kept in destilled water, giving a water content of 0.30 m^3/m^3 - a water saturation of 1.0. At the freezing, the fixing mortar had an age of about 300 days.

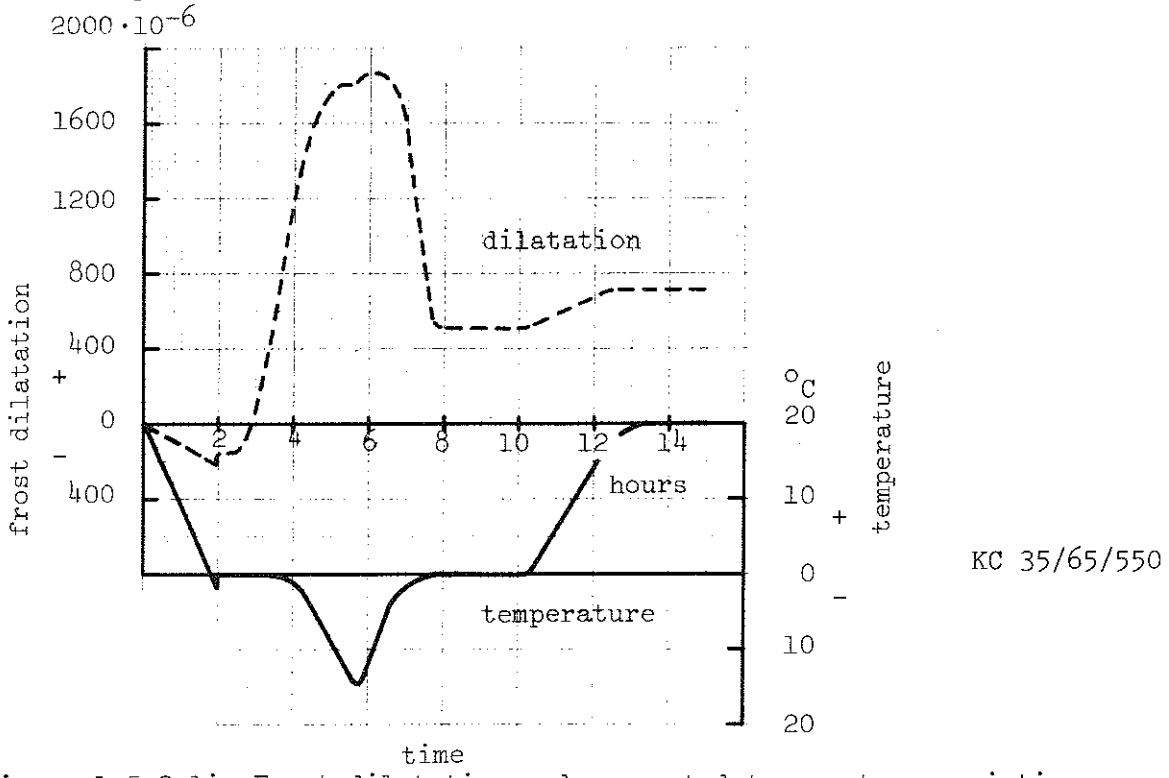

Figure 1.5.2.1i. Frost dilatation and connected temperature variation at the first freezing cycle for free fixing mortar specimen. Water content 0.30 m^3/m^3, saturation 1.0

Additional information is planned to be given in volume 2.

(15) Critical degree of water saturation for frost damage, estimated value 0.8

REFERENCES

[1] TVEIT, A., Measurement of Moisture Sorption and Moisture Permeability of Porous Materials. Swedish Building Research, Report 8: 1966, Stockholm.

[2] DÜHRKOP, H. - SARETOK, V. - SNECK, T. - SVENDSEN, S.D., Bruk-Murning-Putsning (Mortar-Masonry-Rendering). Stockholm, 1966.

[3] BYGG, Huvuddel 2, Materiallära. Stockholm, 1968.

1.5.3. INITIAL PROPERTIES OF JOINT MORTARS

For the joining of the ceramic tiles, two types of joint mortar were used, viz. a cement mortar C 100/300 and a cement mortar C 100/600, in the report denominated "1:3" and "1:6", respectively. The mortars were composed of:

"1:3"	"1:6"
100	100 parts by weight standard Portland cement
300	600 parts by weight sand
87	170 parts by weight water.

The sand is characterized by the sieve analysis

above 1 mm	0% by weight
0.5 - 1 mm	13%
0.25 - 0.5 mm	39%
0.125 - 0.25 mm	29%
0.062 - 0.125 mm	8%
less than 0.062 mm	11%

The cement and the sand were mixed in dry condition during 2 min, after which water was added and the mortar further mixed during 5 min to a good workability.

1.5.3.1. Physical average data of joint mortars

	"1:3"	"1:6"
(1) Density, kg/m^3, at moisture 0.050 m^3/m^3	1940	1840

(2) Stress-strain characteristics in compression

Stress-strain curves, determined in longitudinal compression tests on one parallelepipedal test specimen of each joint mortar type, size 159.5 x 40.4 x 40.0 mm^3, age 150 days, are shown in Fig. 1.5.3.1a and b. In the figures, curve (1) gives the relation between stress and compressive strain and curve (2) the relation between stress and lateral expansion.

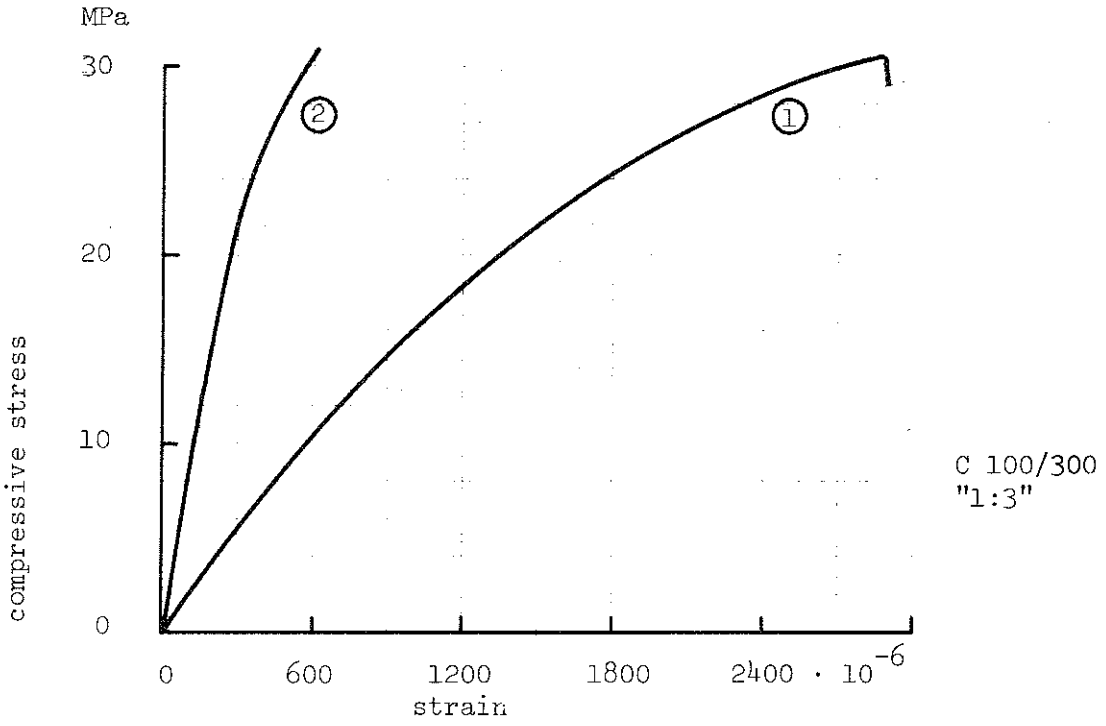

Figure 1.5.3.1a. Stress-strain curves of joint mortar C 100/300 in compression. (1) longitudinal compressive strain and (2) lateral expansion, respectively

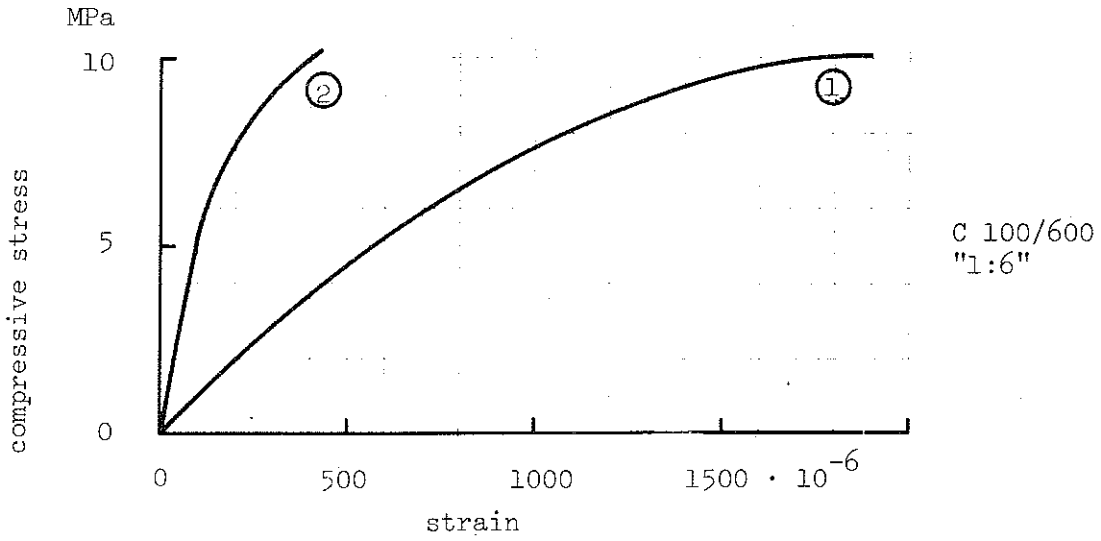

Figure 1.5.3.1b. Stress-strain curves of joint mortar C 100/600 in compression. (1) longitudinal compressive strain and (2) lateral expansion, respectively

From the tests according to Fig. 1.5.3.1a and b, the following quantities are obtained:

	"1:3"	"1:6"
Initial modulus of elasticity, GPa,	17.3	9.3

	"1:3"	"1:6"
Poisson's ratio, evaluated at 50% of ultimate compressive strength	0.145	0.150
Ultimate compressive strength, MPa,	31	10.5

Complementary the initial modulus of elasticity and the ultimate compressive strength of the joint mortars were determined at different age of the test specimens. The results of these tests are given in Fig. 1.5.3.1c and d.

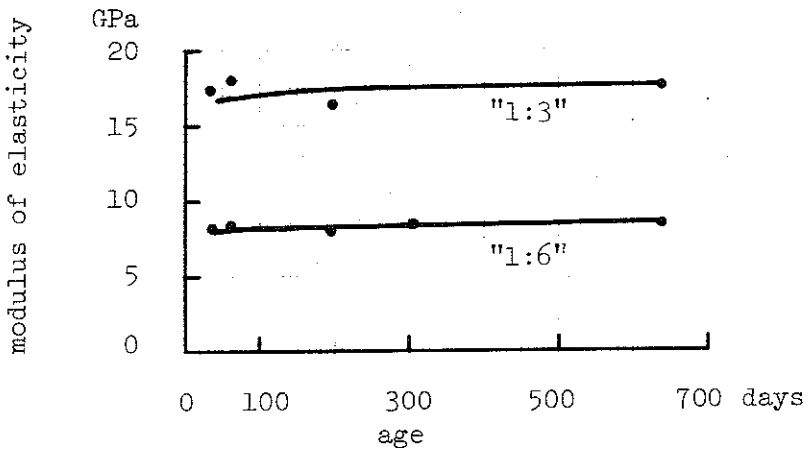

Figure 1.5.3.1c. Initial modulus of elasticity of joint mortars at different age

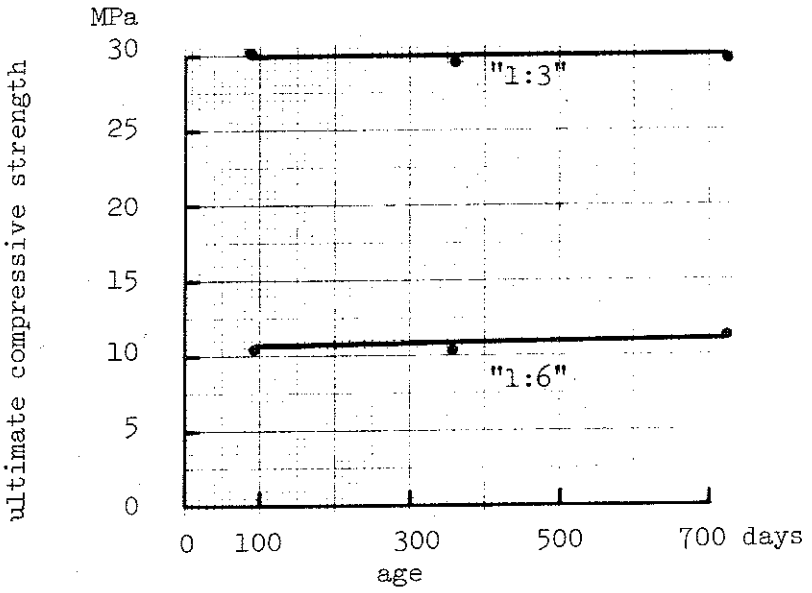

Figure 1.5.3.1d. Ultimate compressive strength of joint mortars at different age - similar to DIN 1164

(3) Ultimate flexural strength at different age - according to Fig. 1.5.3.1e.

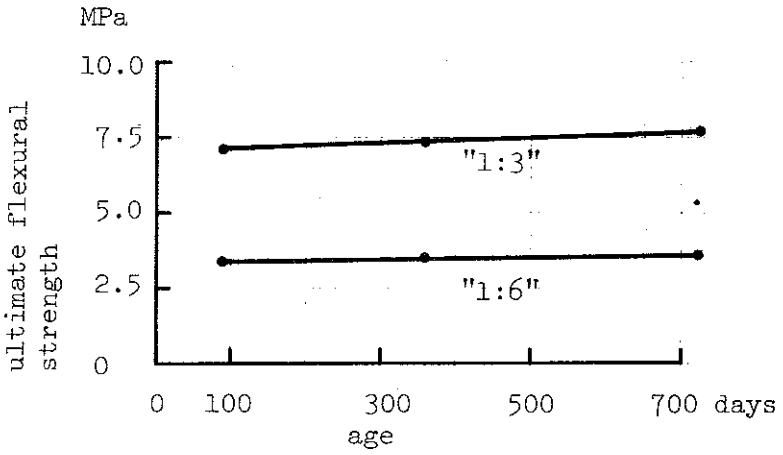

Figure 1.5.3.1e. Ultimate flexural strength of joint mortars at different age - similar to DIN 1164

	"1:3"	"1:6"
(4) Ultimate tensile strength, MPa, age 360 days, determined in splitting tension test according to ASTM C 496	1.9	1.1

(5) Creep deformation

For linear creep, the creep strain ε_{cr} can be evaluated according to the formula

$$\varepsilon_{cr} = \phi_t \varepsilon_\sigma \qquad (1.5.3.1a)$$

where

ε_σ = the instantaneous, stress related strain, and
ϕ_t = the creep coefficient, describing the time variation and magnitude of the creep strain.

In Fig. 1.5.3.1f, the creep coefficient ϕ_t is given for the two joint mortars, determined in compression tests on test specimens of the size 160 x 40 x 40 mm^3 and of an age of 90 days at the load application. The creep tests were performed at 20°C and 65% relative humidity and

at a compression stress of 10.3 MPa for the joint mortar C 100/300 and 3.5 MPa for the joint mortar C 100/600.

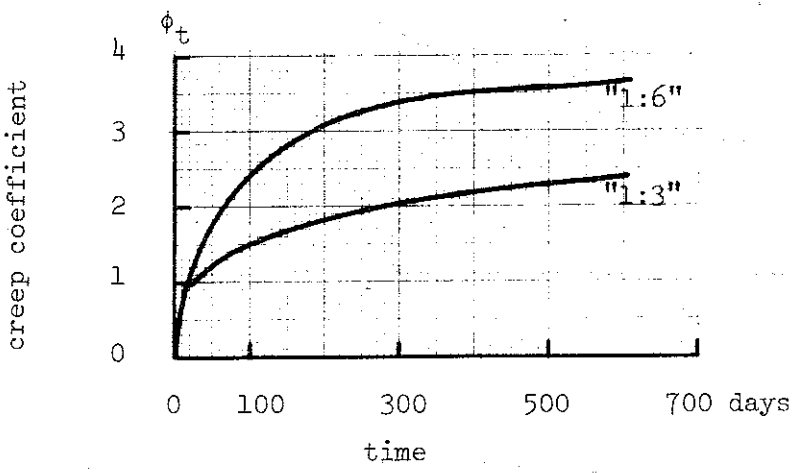

Figure 1.5.3.1f. Creep coefficient ϕ_t for joint mortars, defined according to Eq. (1.5.3.1a)

	"1:3"	"1:6"
(6) Specific heat capacity, J/(kg·K), dry material	~850	~850
(7) Thermal conductivity, W/(m·K),		
(a) dry material, estimated values	~0.7	~0.6
(b) water content ~0.1 m^3/m^3, estimated values	~1.2	~1.0
(8) Thermal dilatation, 10^{-6}/K, at 0 to 20°C, age of test specimens 5.5 years, conditioned at 20°C and 60% relative humidity	9.2	8.9
(9) Water absorption in vacuum, m^3/m^3	0.27	0.32

(10) Moisture permeability as a function of relative humidity, determined at 25°C - according to Fig. 1.5.3.1g which is roughly valid for joint mortar C 100/300 as well as C 100/600 [1].

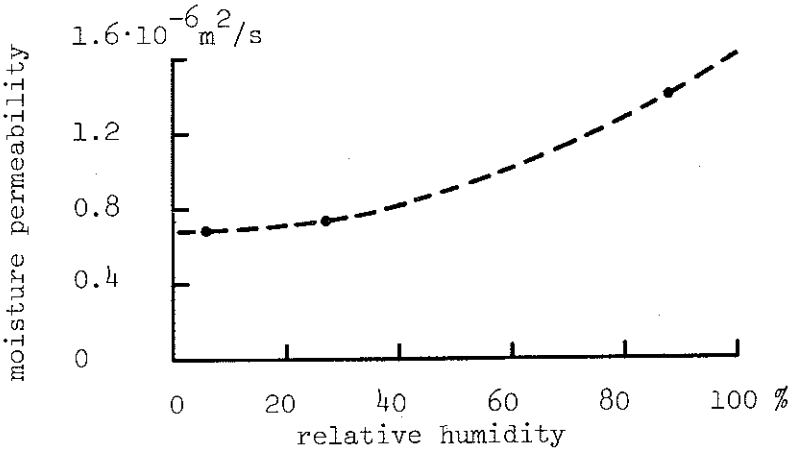

Figure 1.5.3.1g. Moisture permeability of joint mortars at varying relative humidity [1]

(11) Moisture dilatation

The moisture dilatation of the two joint mortars is shown in Fig. 1.5.3.1h by the full-line curves for a time period of 30 days. The curves are determined for test specimens wetted at equilibrium with 65% relative humidity and at 20°C. After 60 days, the moisture dilatation amounts to $\sim 450 \cdot 10^{-6}$ for the joint mortar C 100/300 and to $\sim 180 \cdot 10^{-6}$ for the joint mortar C 100/600. A drying of the test specimens at 20°C and 65% relative humidity - after 60 days wetting - gave a decrease in moisture dilatation according to the dash-line curves in the figure. For the joint mortar C 100/300, the drying did not give a fully reversible dilatation process but a remaining dilatation of $\sim 140 \cdot 10^{-6}$. For the joint mortar C 100/600, the moisture dilatation turned out to be over-reversible with a remaining contraction of $\sim 75 \cdot 10^{-6}$ after drying to equilibrium.

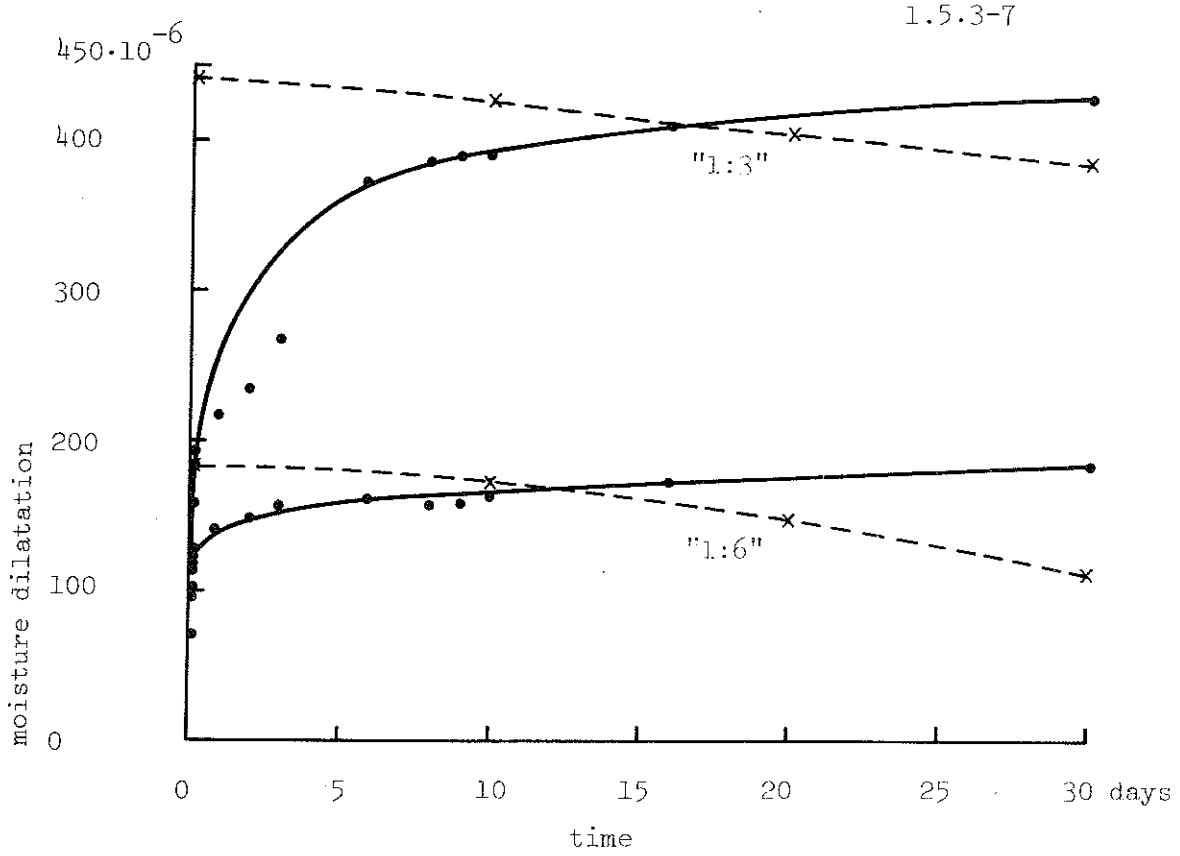

Figure 1.5.3.1h. Time curves of moisture dilatation for joint mortars. Full-line curves give the dilatation for test specimens wetted at equilibrium with 65% relative humidity, dash-line curves the decrease in dilatation at a subsequent drying, after 60 days wetting

(12) Shrinkage - determined for test specimens, size 160 x 40 x 40 mm^3, age 90 days, at 20°C and 65% relative humidity, Fig. 1.5.3.1i.

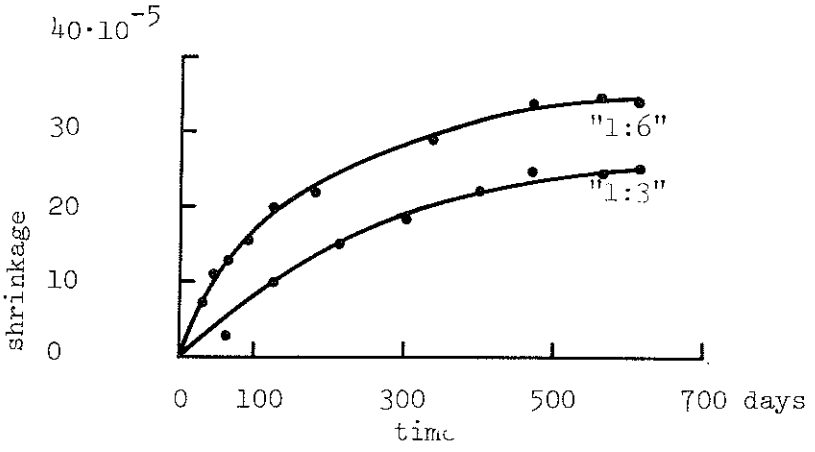

Figure 1.5.3.1i. Free shrinkage of joint mortars

(13) Temperature, initiating ice formation in the joint mortars in the presence of mortar ions, °C, -3 to -5

(14) Frost dilatation

Examples of frost dilatation, obtained at the first freezing cycle

for free test specimens of the joint mortars, size 0.16 x 0.04 x x 0.04 m^3, are given in Fig. 1.5.3.1j and k. The figures show the time curve of dilatation and the connected temperature-time variation for the test specimens evacuated and kept in destilled water, giving a water content corresponding to a saturation of 1.0. At the freezing, the joint mortar specimens had an age of about 300 days.

Additional information is planned to be given in volume 2.

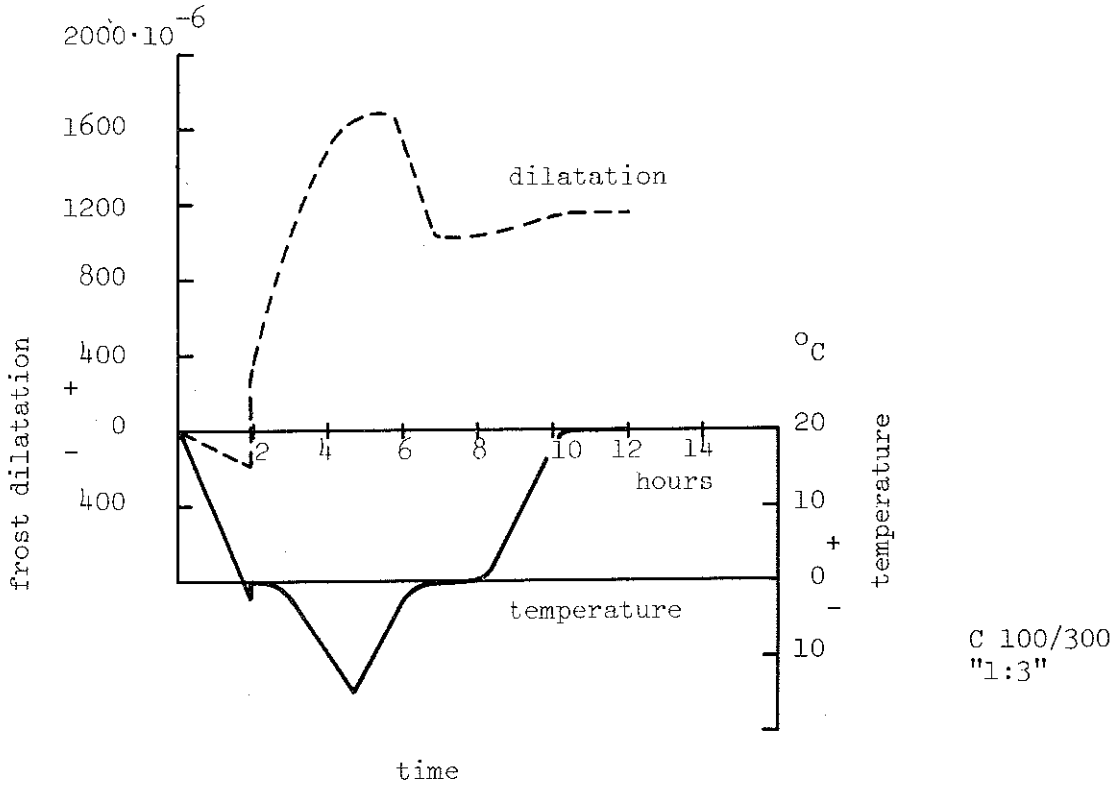

Figure 1.5.3.1j. Frost dilatation and connected temperature variation at the first freezing cycle for free specimen of joint mortar C 100/300. Water content 0.28 m^3/m^3, saturation 1.0

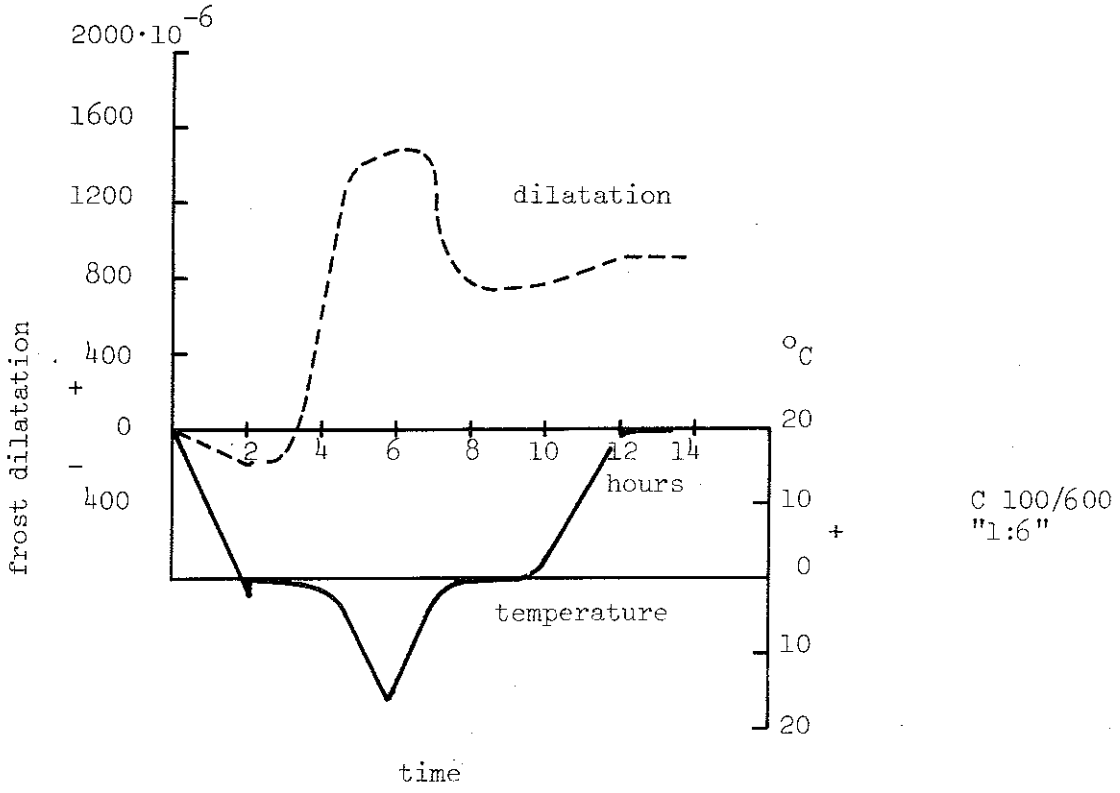

Figure 1.5.3.1k. Frost dilatation and connected temperature variation at the first freezing cycle for free specimen of joint mortar C 100/600. Water content 0.34 m^3/m^3, saturation 1.0

	"1:3"	"1:6"
(15) Critical degree of water saturation for frost damage, estimated value	0.7	0.7

REFERENCES

[1] TVEIT, A., Measurement of Moisture Sorption and Moisture Permeability of Porous Materials. Swedish Building Research, Report 8: 1966, Stockholm.

[2] BYGG, Huvuddel 2, Materiallära, Stockholm, 1968.

1.5.4. INITIAL PROPERTIES OF AERATED CONCRETE

The aerated concrete, used for the wall, roof and floor structures of the test houses, was of the type sand SIPOREX and manufactured at Dalby, Sweden.

The product was delivered to Höganäs under the type marks BE 0.5/230, TE 0.5/110, VL 0.5/80, SV 0.5/30, M 0.5/30, ME 0.5. The shape for masonry blocks was 0.125x0.250x0.500 m^3, for reinforced floor and roof panels 0.150x0.500 m^2 in cross section, and for reinforced wall panels 0.250x0.500 m^2 in cross section.

Cf. Fig. 1.3.2c, d, g, h and i.

1.5.4.1. Physical average data of aerated concrete

The physical data, presented below for the aerated concrete used for the test houses, are based partly on literature information [1]-[7], partly on tests carried out in connection with this investigation.

(1) Density, kg/m^3, at moisture 0.015 m^3/m^3 510

(2) Stress-strain characteristics in compression

A stress-strain curve of the aerated concrete used, determined in a longitudinal compression test on a parallelepipedal test specimen, size 0.5 x 0.15 x 0.15 m^3, moisture content 0.015 m^3/m^3, is shown in Fig. 1.5.4.1a.

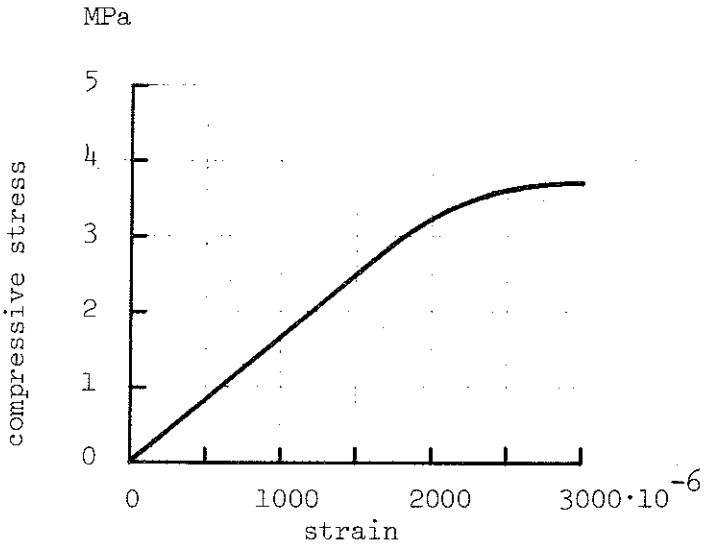

Figure 1.5.4.1a. Stress-strain curve of aerated concrete 0.5 in compression

Initial modulus of elasticity, GPa, at moisture 0.015 m^3/m^3 — 1.65 ± 0.092

The influence of moisture on the modulus of elasticity in compression E_{cu} is given approximately by the formula

$$E_{cu} = 1.55 + \frac{0.27}{1 + u} \quad \text{GPa} \qquad (1.5.4.1a)$$

where

u = the moisture ratio in percentage of volume.

Poisson's ratio — 0.19

Ultimate compressive strength, MPa, prism strength, at moisture 0.015 m^3/m^3 — 3.71 ± 0.15

The influence of moisture on the ultimate compressive strength σ_{cu} is given approximately by the formula

$$\sigma_{cu} = 2.86 + \frac{2.12}{1 + u} \quad \text{MPa} \qquad (1.5.4.1b)$$

where

u = the moisture ratio in percentage of volume.

(3) Ultimate flexural strength, MPa, at moisture 0.015 m^3/m^3 — 1.09 ± 0.020

(4) Ultimate tensile strength, MPa,

(a) determined in direct tension test

$\approx 0.25 \cdot$ ultimate compressive strength (1.5.4.1c)

(b) determined in splitting tension cylinder test

$\approx 0.080 \cdot$ ultimate compressive strength (1.5.4.1d)

(5) Creep deformation

The creep strain of aerated concrete in compression ε_{cr} follows approximately the formula

$$\varepsilon_{cr} = \alpha \sigma t^b \qquad (1.5.4.1e)$$

where

σ = the compressive stress, MPa,
t = the time, days, and
α and b = material coefficients.

For aerated concrete 0.5 of the type used in the test houses

$\alpha = 3.9 \cdot 10^{-5}$, $b = 0.21$ for dry material
$\alpha = 9.4 \cdot 10^{-5}$, $b = 0.20$ for wet material.

(6) Specific heat capacity, J/(kg·K), dry material — ~ 950

(7) Thermal conductivity, W/(m·K),

(a) dry material — 0.12

(b) water content 0.030 m^3/m^3 — 0.16

The influence on the thermal conductivity of variations in the moisture content u and the temperature is illustrated in Fig. 1.5.4.1b, valid for an aerated concrete with a density of 540 kg/m^3.

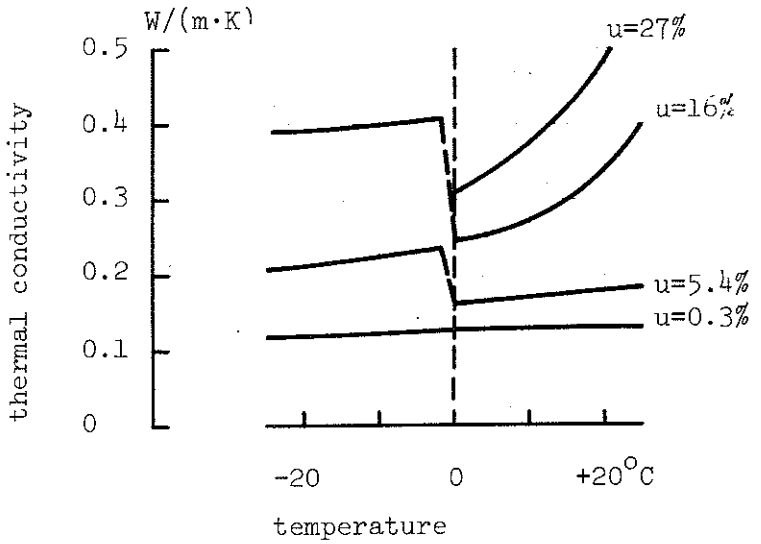

Figure 1.5.4.1b. Variation of thermal conductivity with temperature and moisture content u for an aerated concrete, density 540 kg/m^3. u is the moisture content in percentage of volume [6]

Fig. 1.5.4.1c shows an approximately linear variation of the thermal conductivity with the moisture content for an aerated concrete 0.5 at a constant temperature of 20°C.

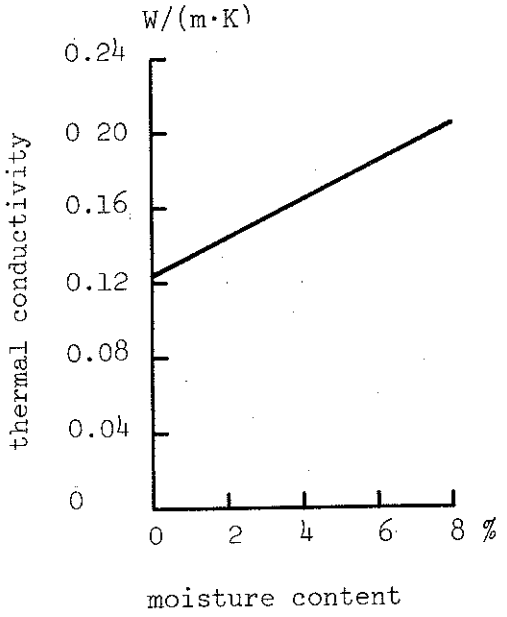

Figure 1.5.4.1c. Variation of thermal conductivity with moisture content for an aerated concrete 0.5. The moisture content is defined in percentage of volume [6]

(8) Thermal dilatation, 10^{-6}/K,
dry material

(9) Water absorption, m^3/m^3, at full saturation 0.7 - 0.8

The average moisture content of the aerated concrete at the time of the construction of the test houses was 0.075 m^3/m^3 for test house I and 0.080 m^3/m^3 for test house II. At equilibrium with a relative humidity of 40-70% at ordinary room temperature, the moisture content of the aerated concrete used is about 0.02 m^3/m^3.

(10) Moisture permeability as a function of relative humidity, determined at 25°C, Fig. 1.5.4.1d

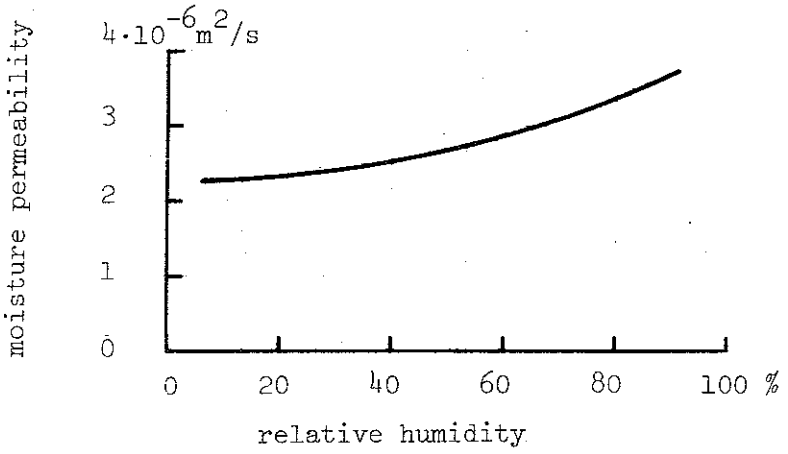

Figure 1.5.4.1d. Moisture permeability of aerated concrete 0.5 at varying relative humidity [5]

(11) Moisture dilatation

The moisture dilatation characteristics of aerated concrete 0.5 are illustrated fragmentarily in Fig. 1.5.4.1e, which shows the relation between the shrinkage and the moisture ratio at drying of a test specimen from a totally saturated state to equilibrium with 43% relative humidity. The rate of drying depends strongly on the dimensions of the structure and on the temperature, humidity and motion characteristics of the surrounding air.

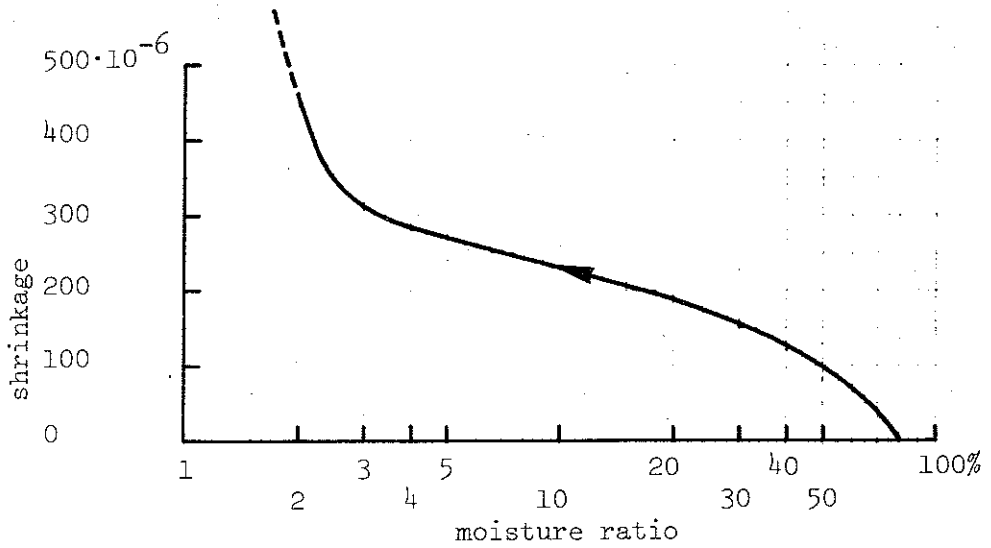

Figure 1.5.4.1e. Relation between shrinkage and moisture ratio at drying of aerated concrete 0.5 from a fully saturated state to equilibrium with 43% relative humidity at ordinary room temperature. Moisture ratio defined in percentage of weight [7]

Own strain-gauge observations on a free aerated concrete test specimen, size 0.5 x 0.12 x 0.12 m^3, located inside test house II - measuring point 444, cf. appendix 1.4.2a, Fig. Aa - showed a reversible moisture dilatation at a varying relative humidity of the air, ranging between 25 and 75 %. This is verified by Fig. 1.5.4.1f, based on observations during a test period of about 100 weeks, i.e. two annual climatic cycles. In the figure, also the corresponding moisture ratio of the aerated concrete is indicated.

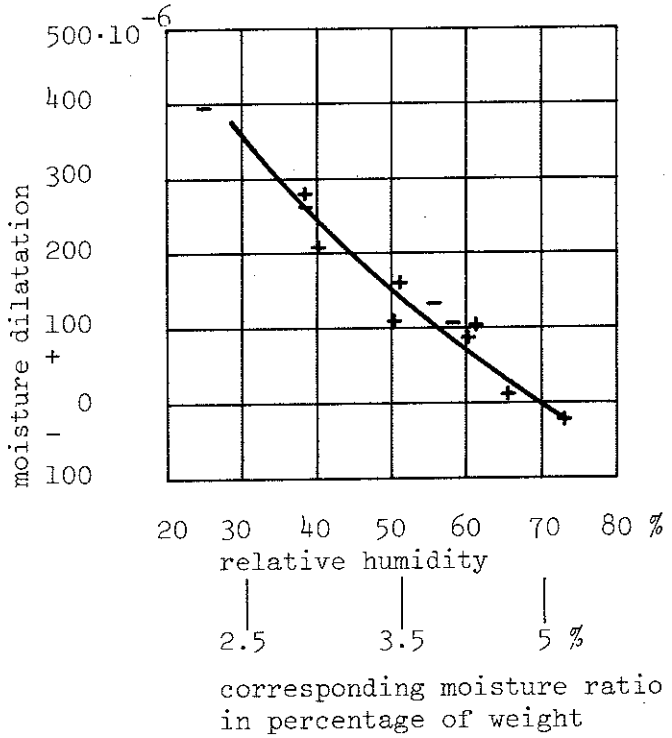

Figure 1.5.4.1f. Reversible moisture dilatation of aerated concrete 0.5 at varying relative humidity and corresponding moisture ratio. Air tem-

(12) Temperature, initiating ice formation in aerated concrete 0.5 in the presence of water, °C, -3 to -5

(13) Frost dilatation

An example of frost dilatation, obtained at the first freezing cycle for a free test specimen of aerated concrete 0.5, size 0.16 x 0.04 x x 0.04 m^3, is given in Fig. 1.5.4.1g. The figure shows the time curve of dilatation and the connected temperature-time variation for the test specimen evacuated and kept in destilled water for 24 h, then left open at ordinary room condition for 24 h and finally the moisture equalized with the specimen within a plastic bag for 48 h. The preconditioning process gave a water content of 0.50 m^3/m^3 corresponding to a degree of saturation of about 0.7.

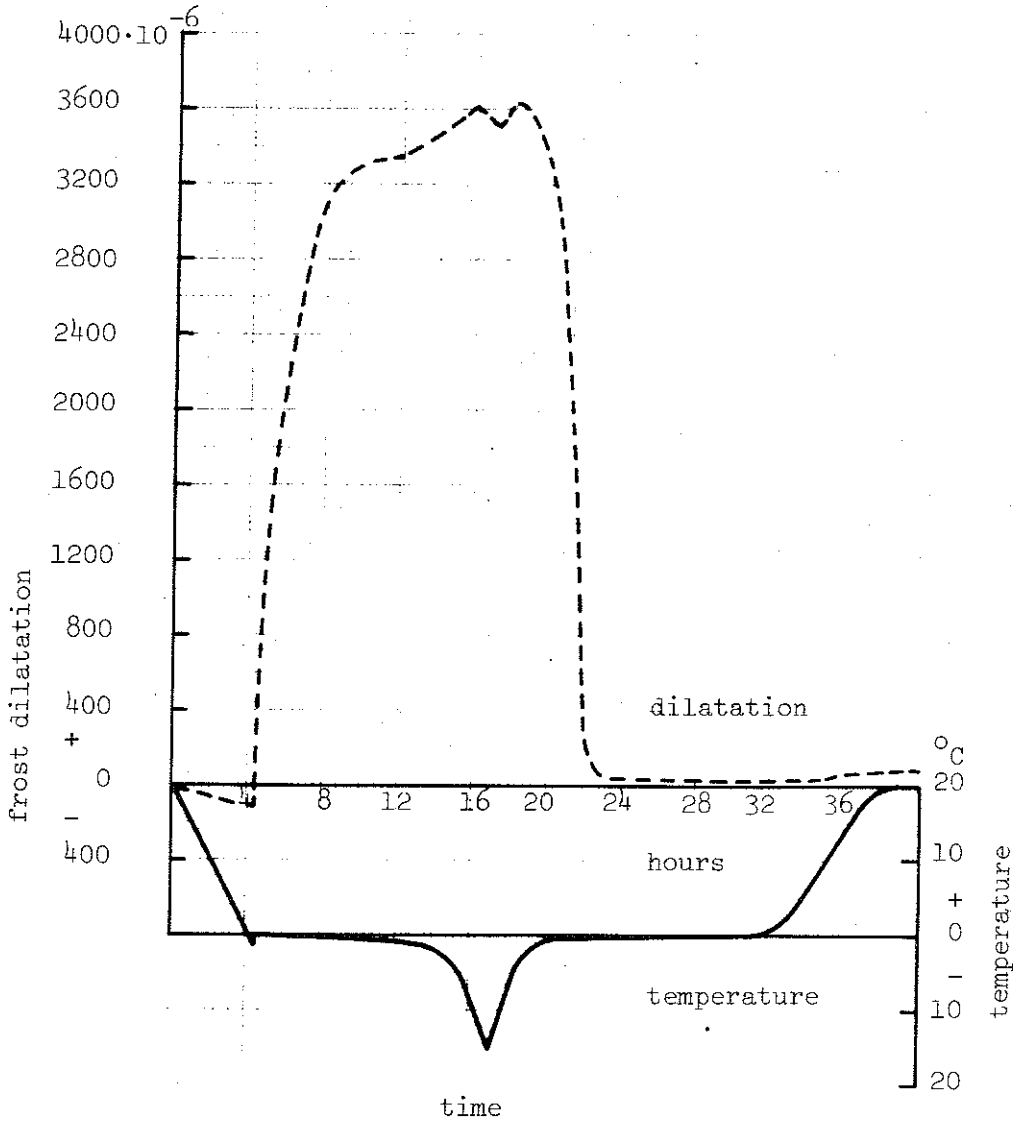

Figure 1.5.4.1g. Frost dilatation and connected temperature variation at the first freezing cycle for free specimen of aerated concrete 0.5. Water content 0.50 m^3/m^3, saturation 0.7

(14)	Critical degree of water saturation for frost damage	~ 0.45

REFERENCES

[1] NIELSEN, A., Krypning hos högtrycksånghärdad gasbetong (Creep of Autoclaved Aerated Concrete). Byggnadsteknik, LTH, Lund, 1962.

[2] VINBERG, H., Murade lättbetongväggars hållfasthet (The Strength of Built Up Walls of Aerated Concrete). Byggnadsstatik, KTH, Meddelande Nr 13, Stockholm, 1953.

[3] PURINS, E., Gasbetongens tryck- och draghållfasthet som funktion av fuktkvoten (The Compressive and Tensile Strength of Cellular Concrete as a Function of the Moisture Ratio). Byggforskningen, Rapport R52:1972, Stockholm.

[4] BRIESEMANN, D., Spaltzugfestigkeit des Gasbetons. Die Bautechnik 5, 1974.

[5] TVEIT, A., Measurement of Moisture Sorption and Moisture Permeability of Porous Materials. Swedish Building Research, Report 8:1966, Stockholm.

[6] RILEM Symposium on Light Weight Concrete, held in Gothenburg 1960, Proceedings. Akademiförlaget-Gumperts, Göteborg, 1961.

[7] Lättbetonghandboken (Light Weight Concrete Manual). Stockholm, 1974.

1.5.5. INITIAL PROPERTIES OF CONCRETE

Ready mixed concrete from Granitbetong, Åstorp, with the quality mark K 250-T-15 was used. The mix was composed of ordinary Portland cement 280 kg/m^3 and washed aggregate of sand and crushed aggregate 8-16 mm 1870 kg/m^3. Water-cement ratio 0.71, semi-fluid consistency (vebe = 2), AEA 0.01%.

1.5.5.1. Physical average data of concrete

(1) Density, kg/m^3, at moisture 0.065 m^3/m^3 — 2280

(2) Stress-strain characteristics in compression

Stress-strain curves of the concrete used, determined in longitudinal compression tests on parallelepipedal test specimens, size 0.5 x 0.15 x 0.15 m^3, age of specimens 1 year, are shown in Fig. 1.5.5.1a for a specimen stored indoors and in Fig. 1.5.5.1b for a specimen stored in outdoor climate.

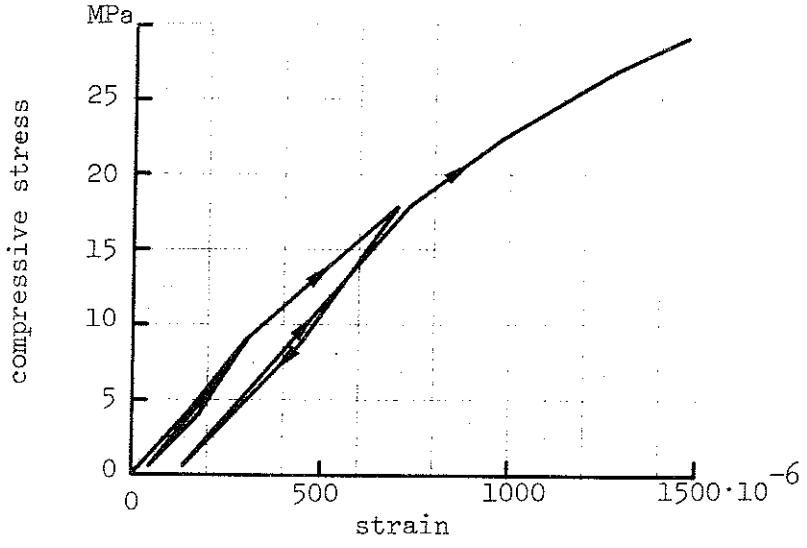

Figure 1.5.5.1a. Stress-strain curve of concrete in compression, stored indoors (temp. = 20°C, rel. humidity ~ 60%)

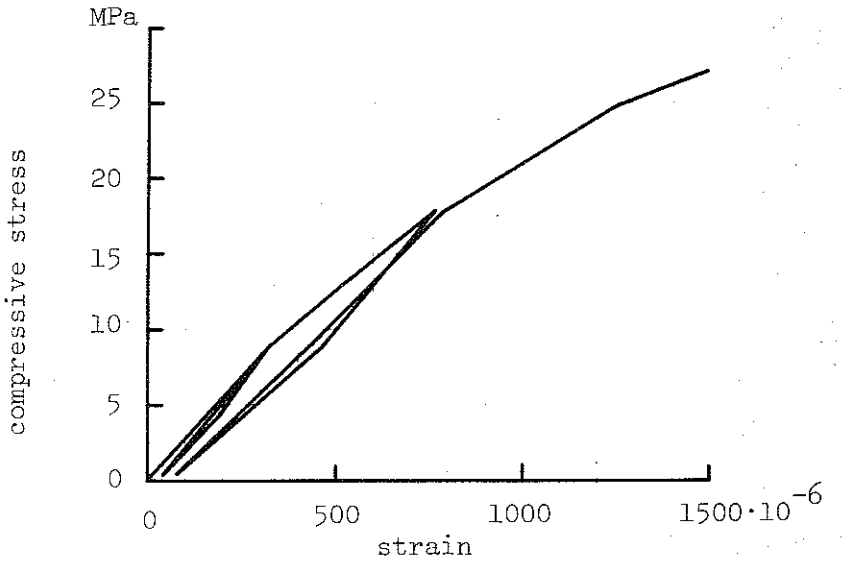

Figure 1.5.5.1b. Stress-strain curve of concrete in compression, stored in outdoor climate

Modulus of elasticity, GPa

The influence of age on the modulus of elasticity in compression E_{cu} is shown in Fig. 1.5.5.1c.

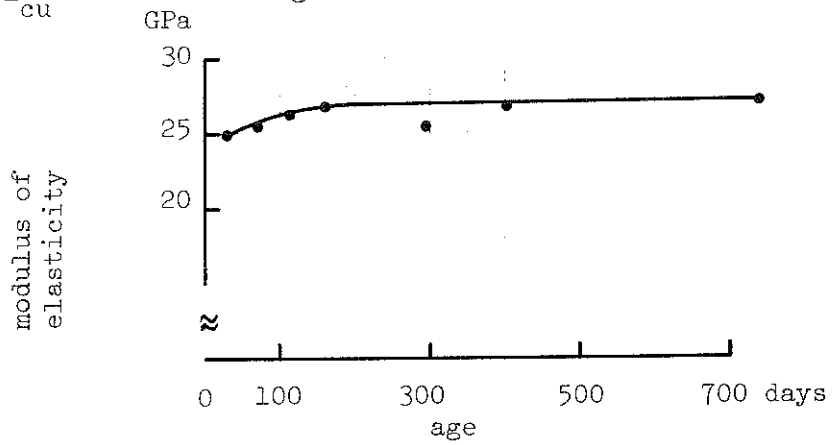

Figure 1.5.5.1c. The influence of age on the modulus of elasticity in compression as measured by static tests at low stress level (σ=1.75 MPa)

The influence of the cube strength (σ_{cube}) on the modulus of elasticity in compression E_{cu} is given approximately by the formula[1]

$$E_{cu} = 4.65 \cdot \sqrt{\sigma_{cube}} \quad \text{GPa} \qquad (1.5.5.1a)$$

with σ_{cube} in MPa.

The formula will give values which may diverge from the real ones by about ± 20 - 25 %.

E_{cu} calculated by the formula
with σ_{cube} given below at a
specimen age = 1 year

Poisson's ratio [3] varies within the range 0.11 to 0.21 when determined from strain measurements. Under biaxial stress, it has been measured to be 0.20 in compression - compression, 0.18 in tension - tension and between 0.18 and 0.20 in compression - tension.

Ultimate compressive strength, MPa

The influence of age on the ultimate compressive strength σ_{cube} is shown in Fig. 1.5.5.1d.

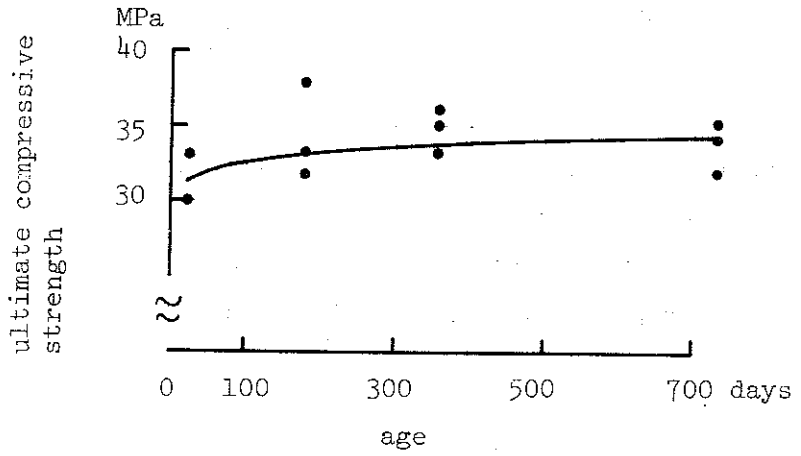

Figure 1.5.5.1d. The influence of age on the ultimate compressive strength measured on cubes with side = 0.15 m

(3) Ultimate flexural strength, σ_{bt}, MPa

The relation between σ_{cube} and σ_{bt} is assumed to be [1]

$$\sigma_{bt} = 0.36 \cdot \sigma_{cube}^{2/3} \qquad (1.5.5.1b)$$

The formula is supposed to be valid independently of the age of concrete with the restriction that the ultimate flexural strength is not supposed to increase after 90 days. The stated value of σ_{bt} is valid for a beam depth of about 0.1 - 0.15 m. At a small depth the value will increase considerably (about twice as high for a depth of about 0.04 m) and for a large depth the value will decrease slightly.

(4) Ultimate tensile strength, σ_t, MPa

The relation between σ_{cube} and σ_t is assumed to be [1]

$$\sigma_t = 0.24 \cdot \sigma_{cube}^{2/3} \qquad (1.5.5.1c)$$

The ultimate tensile strength is not supposed to increase after 90 days.

The influence of the size of the specimen is much smaller than for the ultimate flexural strength.

(5) Creep deformation [1]

Basic creep at constant temperature and pore humidity may be determined by

$$\varepsilon_{cr} = \sigma \cdot f(H) \cdot f(t_o) \cdot \alpha_{cr} \cdot t^{0.24} \qquad (1.5.5.1d)$$

with σ in MPa and t in days.

A linear relation has been assumed between stress and creep.

The relation between the magnitude of basic creep upon equilibrium relative humidity at lower pore humidity than 100 % and the magnitude at 100 % is given by

$$f(H) = 1 \qquad H \geq 0.8$$
$$f(H) = 2H - 0.6 \qquad 0.35 \leq H \leq 0.8 \qquad (1.5.5.1e)$$

there H = the pore humidity of concrete.

The influence of age at loading (t_o) on basic creep is given by

$$f(t_o) = 2.54 \cdot t_o^{-0.28} \qquad (1.5.5.1f)$$

with t_o in days.

If the temperature at storage deviates much from 20°C then time should be adjusted

$$t_o = \Sigma\, \Delta t\, (T + 10)/30 \qquad (1.5.5.1g)$$

The parameter α_{cr}, shown in Fig. 1.5.5.1e, takes into account the influence of the composition of the concrete and can be described as a function of the water-cement ratio and the original water content of the mix (W_o).

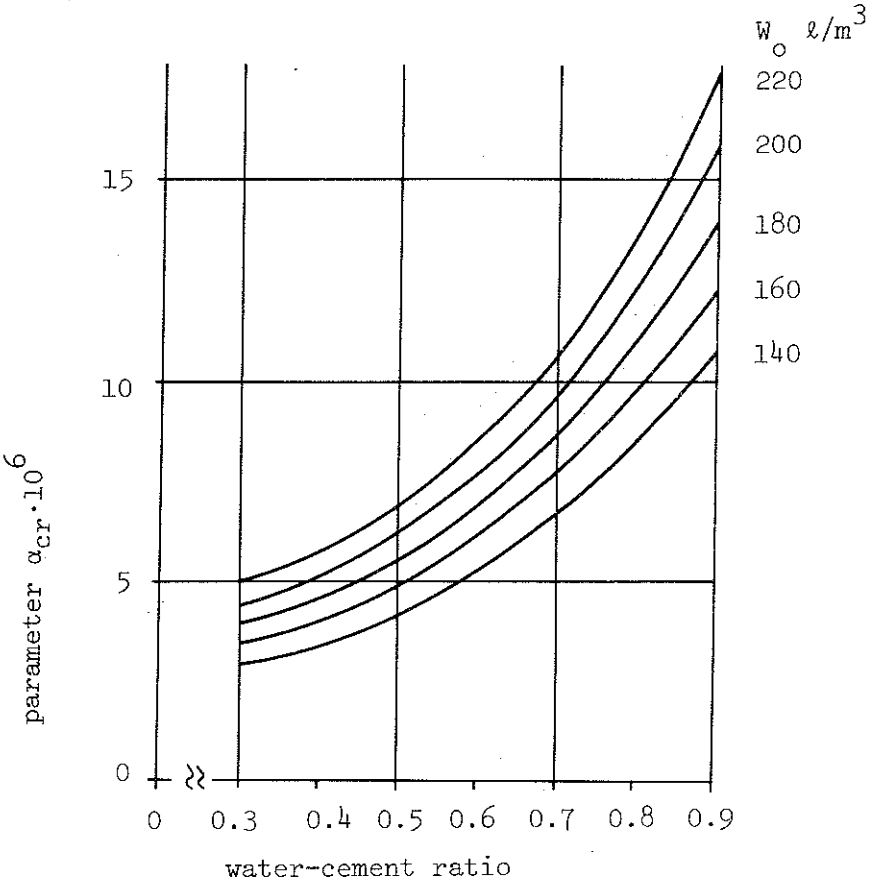

Figure 1.5.5.1e. The parameter α_{cr} in Eq. (1.5.5.1d) as a function of the water-cement ratio and the original water content of the mix (W_o)

Concrete is assumed to be strain hardening at the calculation of basic creep at stress and pore humidity changes. This means that the creep, after a time step Δt when the stress is equal to σ_n and the pore humidity H_n, may be calculated by the formula

$$\varepsilon_{crn} = \sigma_n \cdot f(H_n) \cdot \varepsilon'_{cr}\ (t' + \Delta t) \qquad (1.5.5.1h)$$

where $\varepsilon'_{cr}\ (t' + \Delta t)$ is equal to the specific creep at 100 % relative pore humidity after $t' + \Delta t$ days and t' is determined from

$$\sigma_n \cdot f(H_n) \cdot \varepsilon'_{cr}(t') = \varepsilon_{crn-1} \qquad (1.5.5.1i)$$

where ε_{crn-1} is equal to the accumulated basic creep before the time step.

Sorption creep is called that part of creep which can be assigned to changes in the pore humidity. The model for sorption creep is built up in such a way that the additional sorption creep, at the

stress σ and the time t days after the beginning of drying when the pore humidity of concrete is changed by ΔH, may be expressed as

$$\Delta\varepsilon_{crs} = \sigma \cdot f(\Delta H) \cdot f(t_o) \cdot \alpha_{cr} \cdot f(t) \qquad (1.5.5.1j)$$

A linear relation between sorption creep and stress has been assumed as for basic creep. The influence of the change of the pore humidity may be expressed as

$$f(\Delta H) = 16.6 \cdot \Delta H \qquad (1.5.5.1k)$$

The influence of age at loading $f(t_o)$ is supposed to be the same as for basic creep. The same matter is valid for the influence of the composition of the concrete (α_{cr}). A correction factor producing that the sorption creep will be smaller at a pore humidity change at a later event has been introduced

$$f(t) = \max\begin{Bmatrix} 1 - 0.15 \cdot \ln(1 + t/28) \\ 0 \end{Bmatrix} \qquad (1.5.5.1\ell)$$

The base is small for a judgement of the influence of temperature on basic creep and transient creep at a temperature intervall of -20 - + 70°C expecially as the temperature influence is linked to the moisture content. These kinds of creep will be treated later in volume 3.

(6) Specific heat capacity, J/(kg·K),
dry material [2] 880

(7) Thermal conductivity, W/(m·K)

The influence on the thermal conductivity of variations in the moisture content u is illustrated in Fig. 1.5.5.1f.

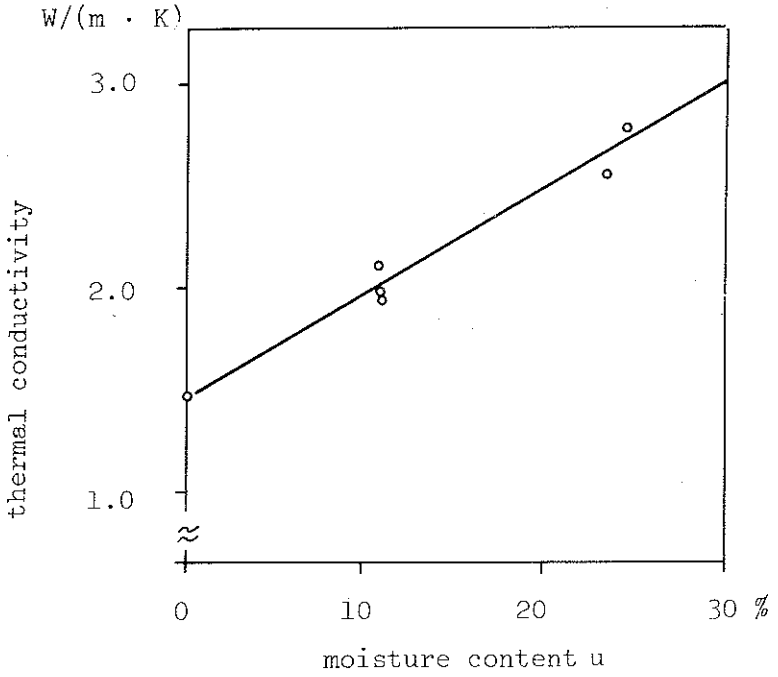

Figure 1.5.5.1f. Variation of thermal conductivity with moisture content u for conrete. u is the moisture content in percentage of volume [2]

(8) Thermal dilatation, 10^{-6}/ K,
for specimen in equilibrium
with 60% rel. humidity at 20°C,
age of specimen = 5.5 years

(9) Water absorption, m^3/m^3,
in vacuum (similar to DIN 51056)

(10) Moisture permeability, m^2/s [1]

The moisture permeability at high pore humidity varies much with the composition of the concrete (Fig. 1.5.5.1g). As a rough approximate $(K_{vc})_{max}$ may assumed to be equal to $2.5 \cdot 10^{-10}$ m^2/s. The moisture permeability at low pore humidity is about 1/20 of the permeability at high pore humidity.

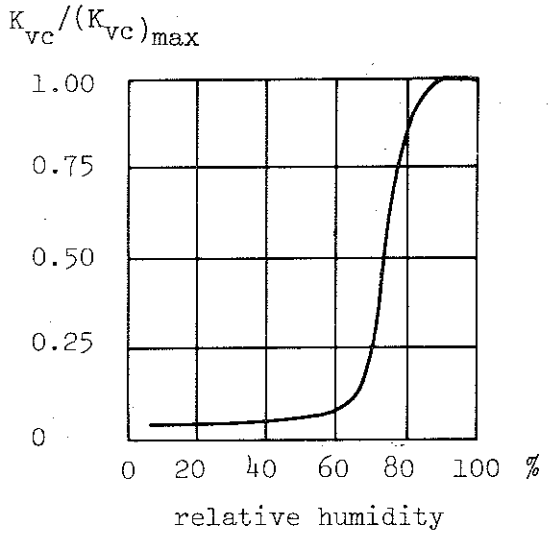

Figure 1.5.5.1g. The ratio between the moisture permeability at other relative pore humidities than 100% and the one at 100%

(11) Moisture dilatation[1]

The moisture dilatation is the same as the drying shrinkage. For ordinary concrete structures the effect of the carbonization on shrinkage is small and therefore shrinkage will be treated as consisting only of drying shrinkage.

The final shrinkage deformation at 50 % relative humidity of the environment may be determined by

$$\varepsilon_s = 3.75 \cdot (W_o - 50) \cdot 10^{-6} \qquad (1.5.5.1m)$$

where W_o denotes the original water content in ℓ/m^3.

The final shrinkage at other relative humidities may be calculated by the aid of Fig. 1.5.5.1h.

The time function for the development of the shrinkage is supposed to be the same as the drying process. The influence of the temperature on shrinkage will be treated in volume 3.

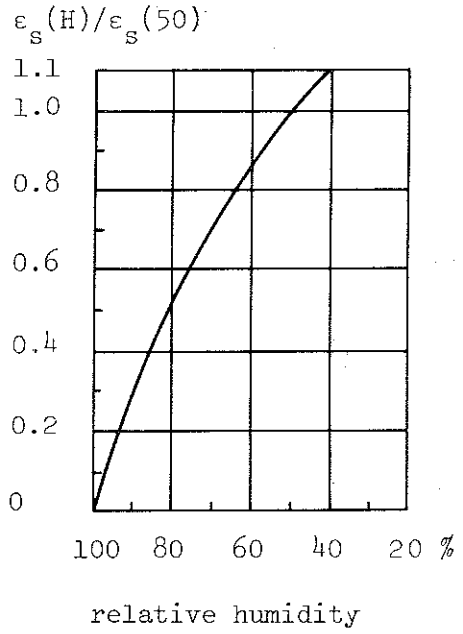

Figure 1.5.5.1h. The ratio between the final shrinkage at other relative humidities of the environment than 50% and the one at 50%

(12) Temperature, initiating ice formation in the presence of water, °C — -1 to -3

(13) Frost dilatation

An exemple of frost dilatation, obtained at the first freezing cycle for a free test specimen, size 0.16 x 0.04 x 0.04 m^3, is given in Fig. 1.5.5.1i. The figure shows the time curve of dilatation and the connected temperature-time variation for the test specimen evacuated and kept in destilled water giving a water content of 0.16 m^3/m^3 corresponding to a degree of saturation of 1.0.

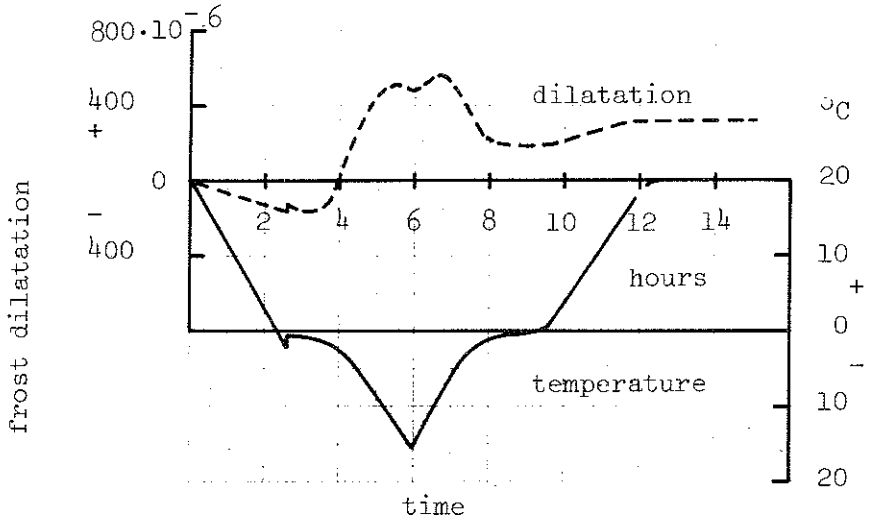

Figure 1.5.5.1i. Frost dilatation and connected temperature variation at the first freezing cycle for a free specimen. Water content 0.16 m^3/m^3, saturation 1.0. Age of specimen 5.5 years, stored at 20°C and 60% relative humidity

(14)	Critical degree of water saturation for frost damage (estimated value)	0.85

REFERENCES

[1] ALEMO, J., The Effects of Imposed Deformations on the Behaviour of Loaded Concrete Structures. Bulletin 53, Division of Structural Mechanics and Concrete Construction, Lund Institute of Technology, Lund, 1976.

[2] THELANDERSSON, S., Betongkonstruktioner vid höga temperaturer - en översikt (Concrete Structures at Elevated Temperatures - A Survey). Kraftverksföreningens utvecklingsavdelning, VAST, Stockholm, 1974.

[3] NEVILLE, A.M., Hardened Concrete: Physical and Mechanical Aspects. Monograph No. 6, American Concrete Institute, Detroit, 1971.

Studies of local flow around the test houses in Höganäs[1)]

By Tommy Lovén
The Aeronautical Research Institute of Sweden (FFA), Stockholm

A1. PRESENTATION OF THE PROBLEM

On the roof of the Central Laboratory building of Höganäs AB, two test houses have been built for a long-range study of the behaviour of multilayer, external walls with an outer layer of ceramic tiles when exposed simultaneously to a long-term loading and a fluctuating exterior climate, cf. Fig. 1.3.1a-j. For a practical application of the results of the study, it is important to know if the wind environment of the test houses can be considered as representative of the corresponding wind environment for ordinary buildings. Especially important then it is to know if some observed local environment effects are caused by the base laboratory building. Furthermore, it is also important to know if there are any systematic differences between the wind, to which the test objects are exposed, and the wind measured at the main place of the macro wind observations, viz. the roof of the experimental hall of the Central Laboratory.

---

1) Translation of Report AU-948, The Aeronautical Research Institute of Sweden, Stockholm, 1972.

A2. PURPOSE AND SCOPE OF THE INVESTIGATION

The purpose of the aerodynamics-tunnel tests is to give an approximate idea of the flow around the test houses.

The following test methods were used:

(1) Evaporation tests with naphtalene in order to locate areas with high or low flow velocity nearest to the wall surfaces.

(2) Oil-flow tests to vizualize the flow directions over the test house surfaces. The method applied is satisfactory for the horizontal surfaces but for the vertical ones, the gravity has a disturbing influence at the used tunnel wind speed.

(3) Smoke tests to study the vertical extent of the separated flow regions over the Central Laboratory building on which the test houses are located.

A3. MODEL AND TEST EQUIPMENT

A model of the base laboratory building and the two test houses was made in scale 1:250 at FFA. It includes the nearest surrounding buildings and the small "ash-heap" of a height of about 10 m west of the laboratory, see Fig. A3a.

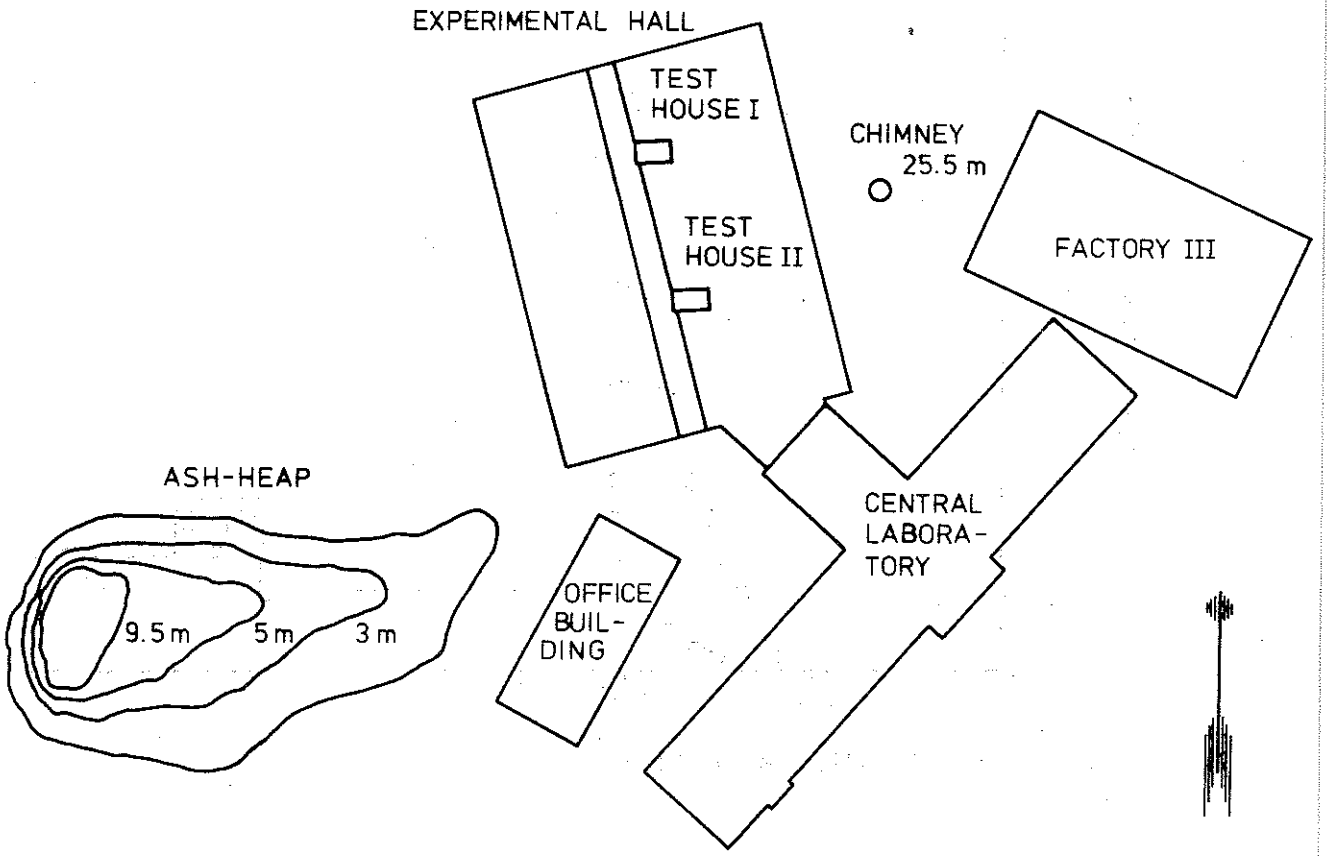

Figure A3a. Geographic position of test houses and nearest surroundings. Scale 1:1000

The model scale tests were done in the FFA building aerodynamics-tunnel, cross section 0.4 x 1.0 m^2, having a maximum wind speed of 23 m/s. For a simulation of the atmospheric boundary layer, a generator consisting of 200 mm high triangular wedges was used. The generator has been turned out according to instructions given by J. Counihan [1]. In order to further increase the braking of the

flow in the lower regions of the boundary layer, a distributed ground roughness, consisting of small-sized stones glued on a sheet-metal, was placed immediately downstream the boundary layer generator.

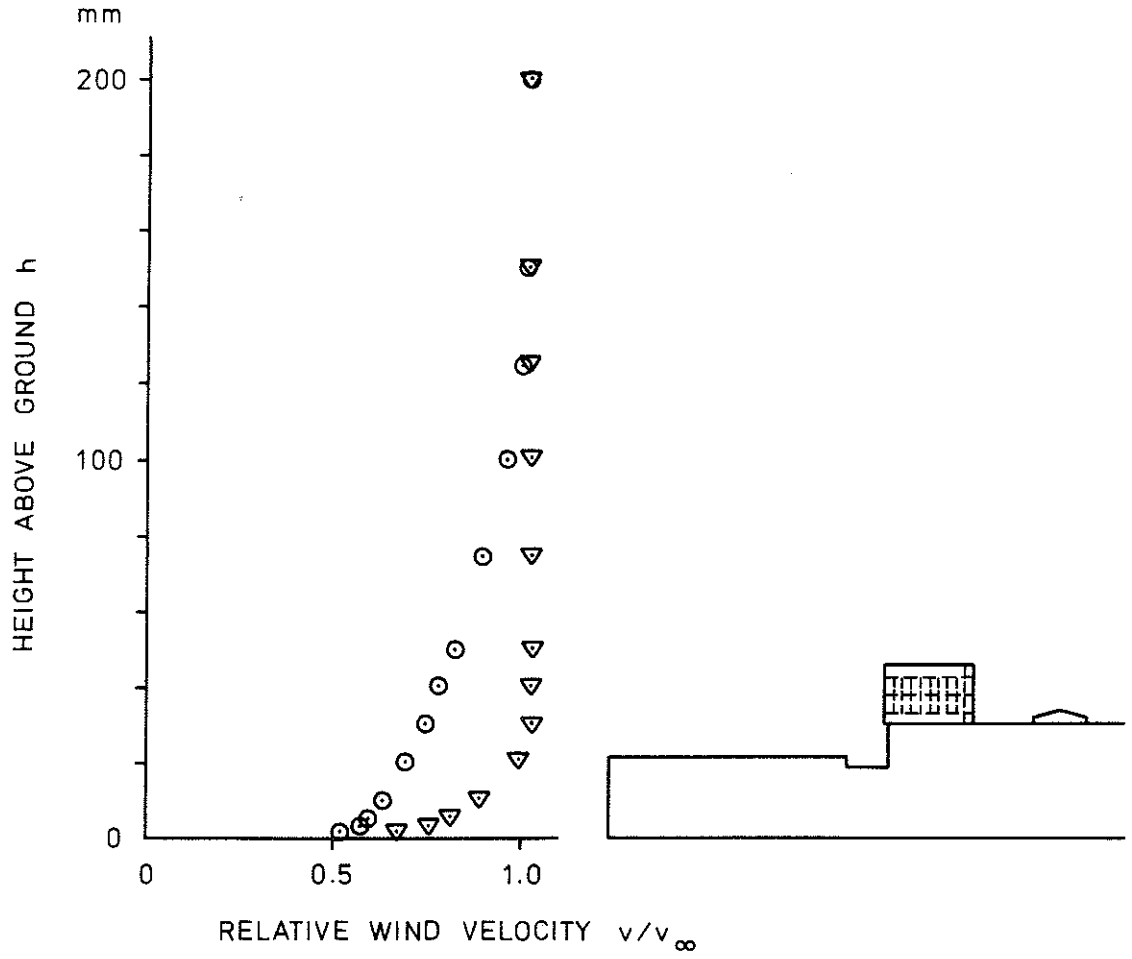

Figure A3b. Wind velocity profile at the place of the model. v = local wind velocity, v_∞ = wind velocity above boundary layer, ⊙ artificial boundary layer caused by generator and ground roughness, ▽ ="natural" boundary layer on a smooth tunnel floor

Fig. A3b shows the flow velocity profile at the place of the model, as concerns the boundary layer caused by the generator and the ground roughness, compared to the flow velocity profile of a "natural" boundary layer formed by only the smooth tunnel floor. Fig. A3c shows the model put up in the tunnel as well as the wedge shaped generator and the ground roughness area.

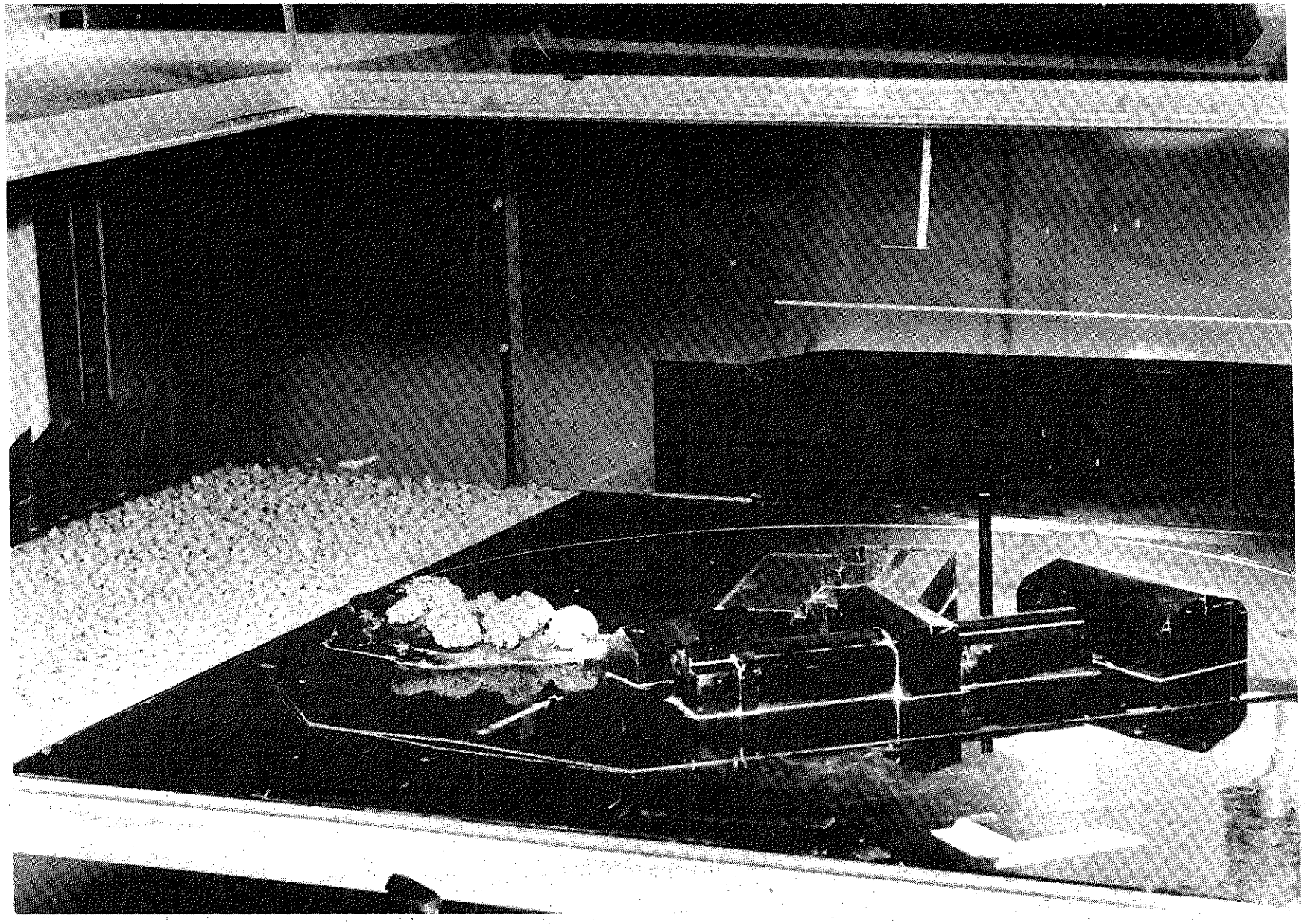

Figure A3c. The model in the test section of the FFA building aerodynamics-tunnel

A4. PERFORMANCE OF TEST

In the main, the tests were done for the four principal wind directions, i.e. wind from north, east, south and west, but in a few cases also for some further wind directions.

In the evaporation tests, the model was sprayed with naphtalene, dissolved into benzine, until a uniformly distributed layer of a white cover was produced. The model was then placed in the building aerodynamics-tunnel and exposed to an air flow with a velocity of about 20 m/s, as measured above the boundary layer. The test was interrupted at various stages of evaporation and photographs were taken until, after 20 to 30 min, all the naphtalene had disappeared. In this way, an illustration was obtained of the evaporation process or, in other words, a qualitative impression of the flow velocity variation over the wall and roof surfaces of the model. In the areas with the most rapid evaporation, close to the wall surfaces, the highest values of the flow velocity occur.

The oil-flow tests were done in a similar way. The model was covered by a flowing white paint, consisting of a mixture of kerosene and zincoxide with some linseed oil added. The model was then placed in the aerodynamics-tunnel and exposed to an air flow until the paint got dry. A characteristic paint pattern was produced, enabling a study of the flow directions within the boundary layer near to the surfaces of the model. Paint accumulations indicate separated areas with a low flow velocity. Due to the comparatively low wind velocity, about 20 m/s, it was not possible to get a completely correct current pattern on the vertical surfaces - the influence of the gravity was too strong, giving rise to a tendency of the paint flowing downwards. For the horizontal and only slightly inclined surfaces, representative current patterns occured. The evaporation tests and the oil-flow tests complete each other in a useful way.

Supplementary, smoke flow tests were carried out in order to give an illustration of the vertical extent of the separated flow regions. The smoke outlets were mainly located on the roof of the central

laboratory building within the separated flow region. In tests made at an east wind direction, smoke outlets were performed also in front of the laboratory building. The extent of the separated regions within the vertical plane was photographed by a highspeed polaroid film. Using a narrow slot, the model was lighted up by an approximately parallel light beam. The source of light consisted in a discharge tube with a very short flash time of the magnitude of 1/30000 s. Thus, a frozen picture of the momentary spread of the smoke was received and by lighting up the model a number of times for each photo, an averaged picture of the smoke extension could be produced. The narrow light slot was generally located in the main wind direction and in a plane through the test houses and consequently, the photos show the extent of the separated flow regions in such vertical planes through the test houses and parallel to the wind direction. The location of the smoke outlets can be seen in Fig. A4a.

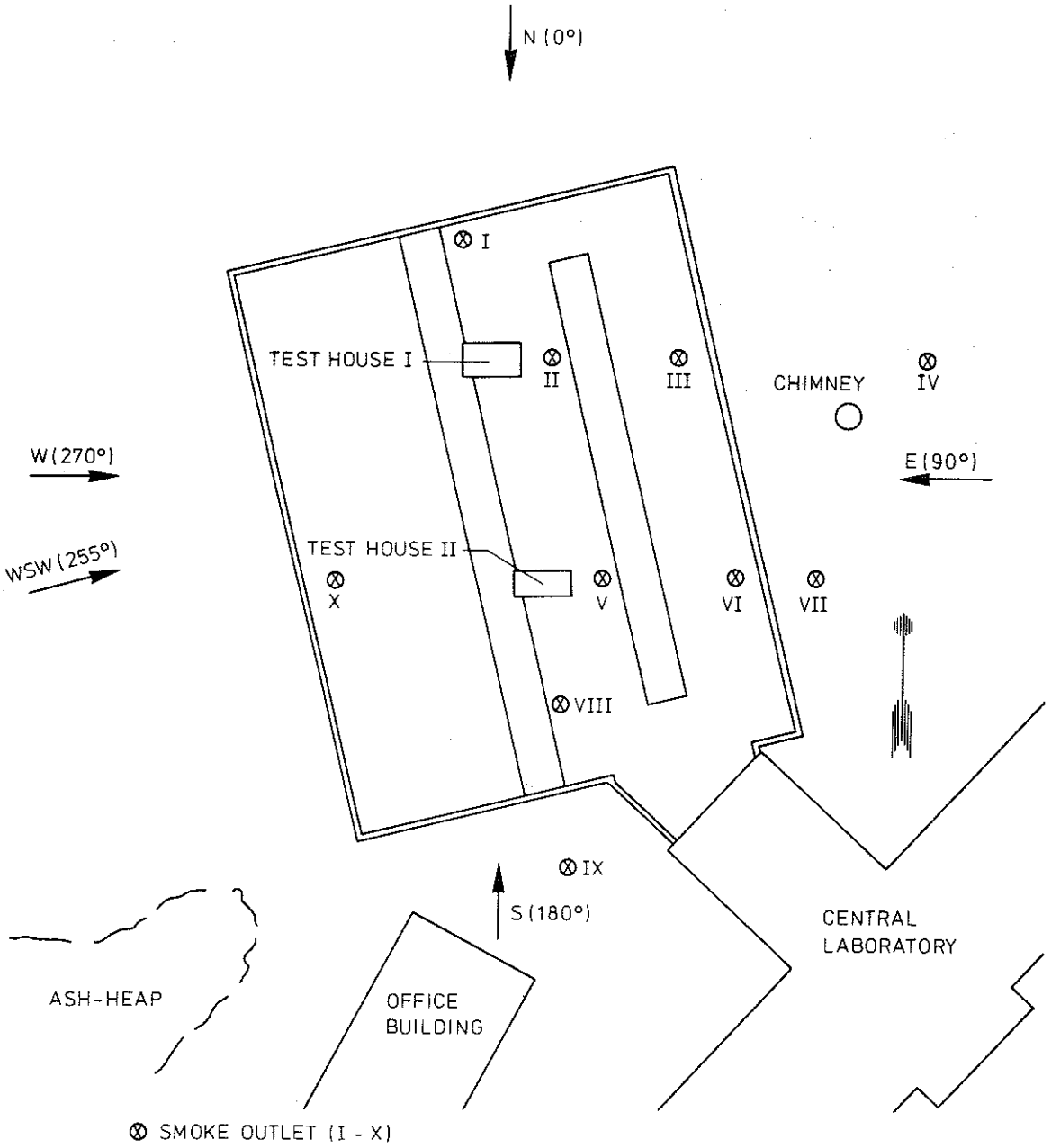

Figure A4a. Smoke flow tests. Location of smoke outlets

A5. TEST RESULTS

The results of the different types of tests are reported in Fig. A5a-n in the form of photos. The pictures from the evaporation and oil-flow tests are taken from northeast showing the north and east fronts of the test houses as well as from southwest showing the corresponding south and west fronts. The evaporation tests are illustrated in this report for 2 to 3 different stages of the evaporation. Further photos from other stages are available and can be obtained from FFA at request.

On each photo from the evaporation and oil-flow tests, the wind direction is defined by an arrow and by a figure giving its value in degrees.

The different photos, Fig. A5a-n, are not discussed in detail in this report but only generally commented on. Especially, the pictures of the oil-flow patterns contain a lot of information regarding the general characteristics of the flow conditions around the buildings, but this particular information is of minor importance for the test house problem itself.

Fig. A5a shows the model, sprayed with naphtalene, before the start of an evaporation test. There were some difficulties to get the naphtalene spray uniformly distributed over the model surfaces. Nevertheless, the starting conditions were probably tolerably the same in this respect for the different tests. The napthalene tests were carried out for wind from the four main compass headings and also from NNW, i.e. for a wind direction parallel with the length direction of the laboratory building.

The photos illustrate that the naphtalene starts evaporating from the upper parts of the windward wall surfaces of the test houses. At wind from north or south and the two test houses shading each other, the evaporation occured most rapidly on the windward test house, which then gave some shelter for the other test house. At wind from east or west, the evaporation was fairly similar for the two test houses. Besides the directly exposed windward wall surfaces of the test houses, the evaporation was also relatively fast

on the side wall surfaces but essentially slower on the leeward wall surfaces.

On the slightly inclined roof surfaces, the evaporation generally was generated more slowly than on the vertical windward wall surfaces and then started somewhat downstream of the windward edge. This shows that the roofs of the test houses were found to be exposed to a lower local wind velocity near the front edge than further downstream.

At wind from north, east and south, the evaporation was relatively fast on the roof of the base laboratory building within the area immediately in front of the test houses and also on the lower parts of the windward wall surfaces of the test houses. This was probably caused by the vortex developed directly windward of the test houses.

The oil-flow tests were made for the same wind directions as for the evaporation tests and also for some additional wind directions - these additional tests, however, are not dealt with in this report. Examples of the recorded oil-flow patterns are given in Fig. A5g-k, showing the flow directions of the air flow in the boundary layer close to the various surfaces of the model. Areas of an oil accumulation, indicating a low flow velocity, are as a rule concentrated to the corresponding areas as obtained in the naphtalene evaporation tests. For the vertical surfaces, the oil-flow patterns must be analysed with some caution because - as noted in section A4 - the influence of the gravity could be considerable at the relatively low wind velocity applied, causing the paint flowing downwards.

The results of the smoke tests are exemplified in Fig. A5ℓ-n. The Roman numerals in the figures refer to the various smoke outlet locations, as specified in Fig. A4a. This figure also gives an idea of the location of the narrow photolight slots, considering that the individual slot lies in a vertical plane, parallel with the wind direction and passing through the test houses. The photos, taken by using a very sensitive polaroid film, were repro-photographed for this report which resulted in certain fine details being lost. If desirable, the original photos can be borrowed from FFA.

The photos from the smoke flow tests show the vertical extent of the separated flow regions above the roof of the Central Laboratory building. It can be seen that the test houses mainly are located within these regions. The floor separation regions generated by the roof window and the roof edge barrier are illustrated in Fig. A5ℓ and m, applicable to east wind direction.

The smoke flow patterns according to Fig. A5ℓ can be interpreted by stating that test house I is located within three superimposed flow separation regions. The test house lies inside a local separation region caused by the roof window. The roof window in its turn lies inside a separation region caused by the eastern roof edge barrier of the base laboratory building which in its turn is inside a separation region caused by the factory building III, cf. Fig. A3a.

Analogously, test house II - Fig. A5m - also is located within three superimposed separation regions. The smoke outlet VII gives the roof edge barrier an air of being exposed to a relatively stationary wind although a turbulence is to be expected from the factory building III and the central laboratory building. In contrast to Fig. A5m, Fig. A5ℓ shows the roof edge barrier of the base laboratory building as exposed to a turbulent flow for smoke outlet IV. The flow conditions ought to be similar in the two cases. The difference in the received flow patterns could be a consequence of the difference in the smoke outlet location in relation to the vortex, probably existing between the factory building III and the central laboratory building.

The smoke flow patterns are stressing the necessity of using local anemometers near the test houses in the full scale investigation for a determination of the direction and velocity of the wind, even if certain errors can be induced by an interference with the test houses themselves.

The tests were generally made with an artificially thickened ground boundary layer. For one specific wind direction, a complementary test was carried out with a natural thin boundary layer generated by only the smooth tunnel floor, cf. Fig. A3b. This test did not

show any noticeable difference in the vertical extent of the flow separation regions and consequently no more test was considered necessary for a further examination of the sensitivity to variations in the boundary layer profile.

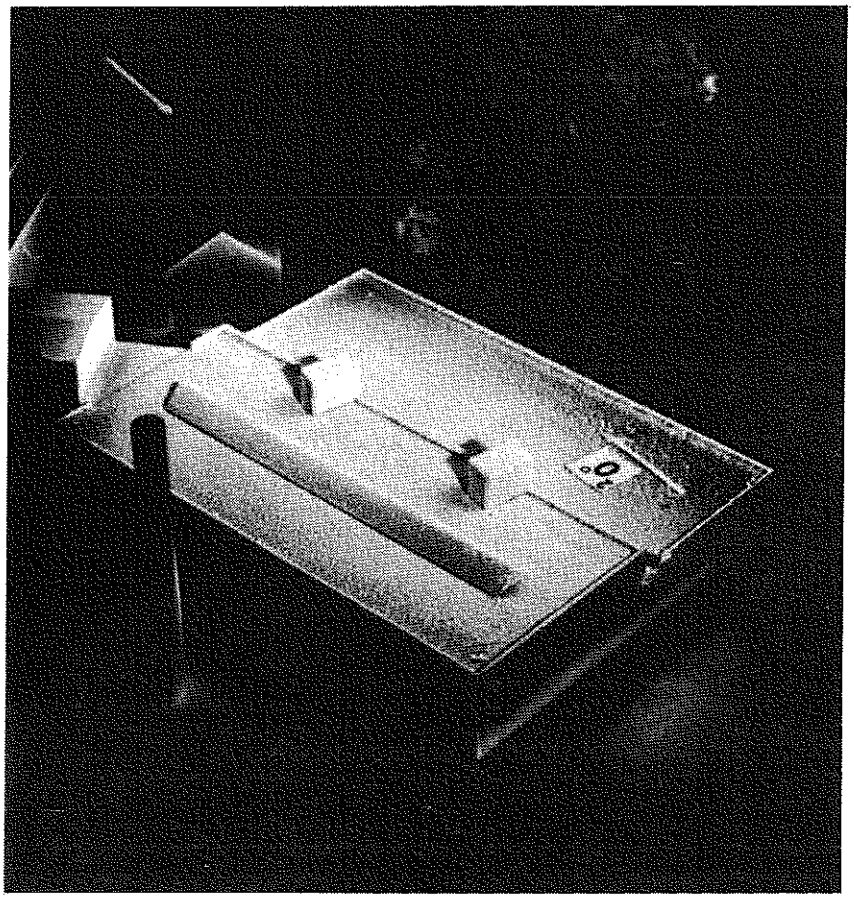

View from NE

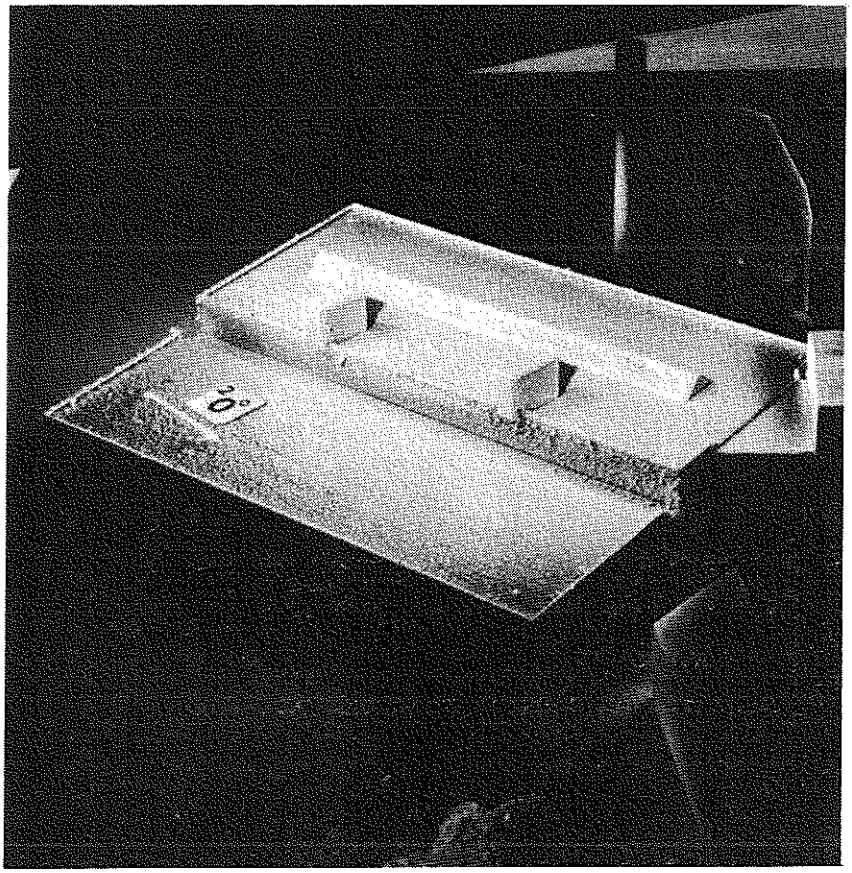

View from SW

Figure A5a. Evaporation tests. The model sprayed with naphtalene before exposure to wind

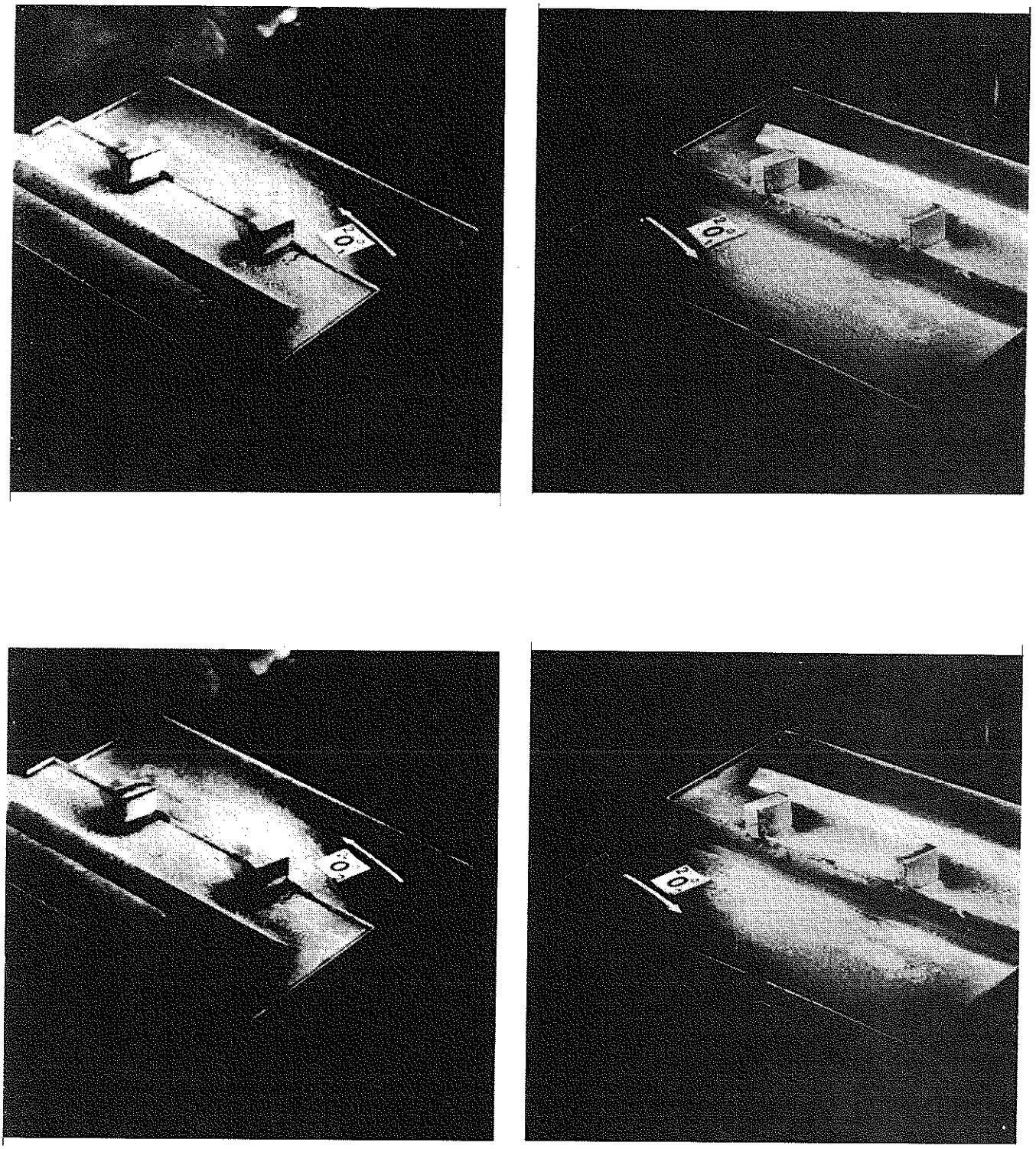

Figure A5b. Evaporation tests. Wind from north (0°)

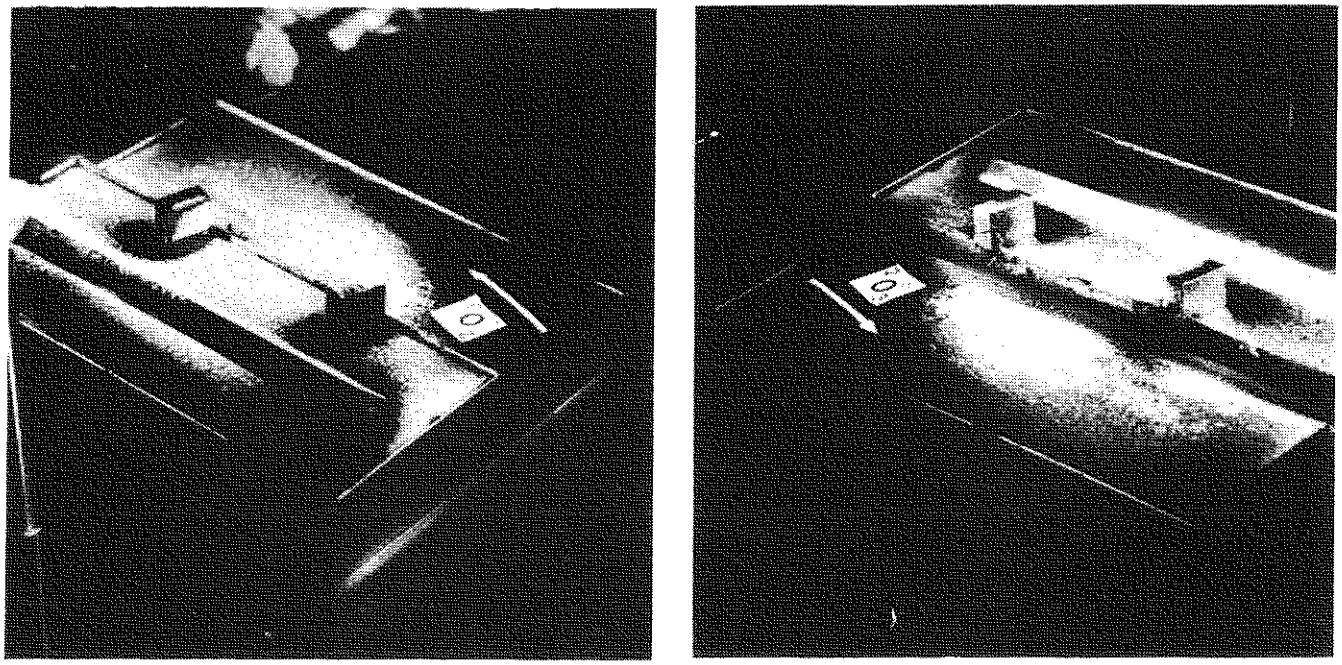

Figure A5b. Cont.

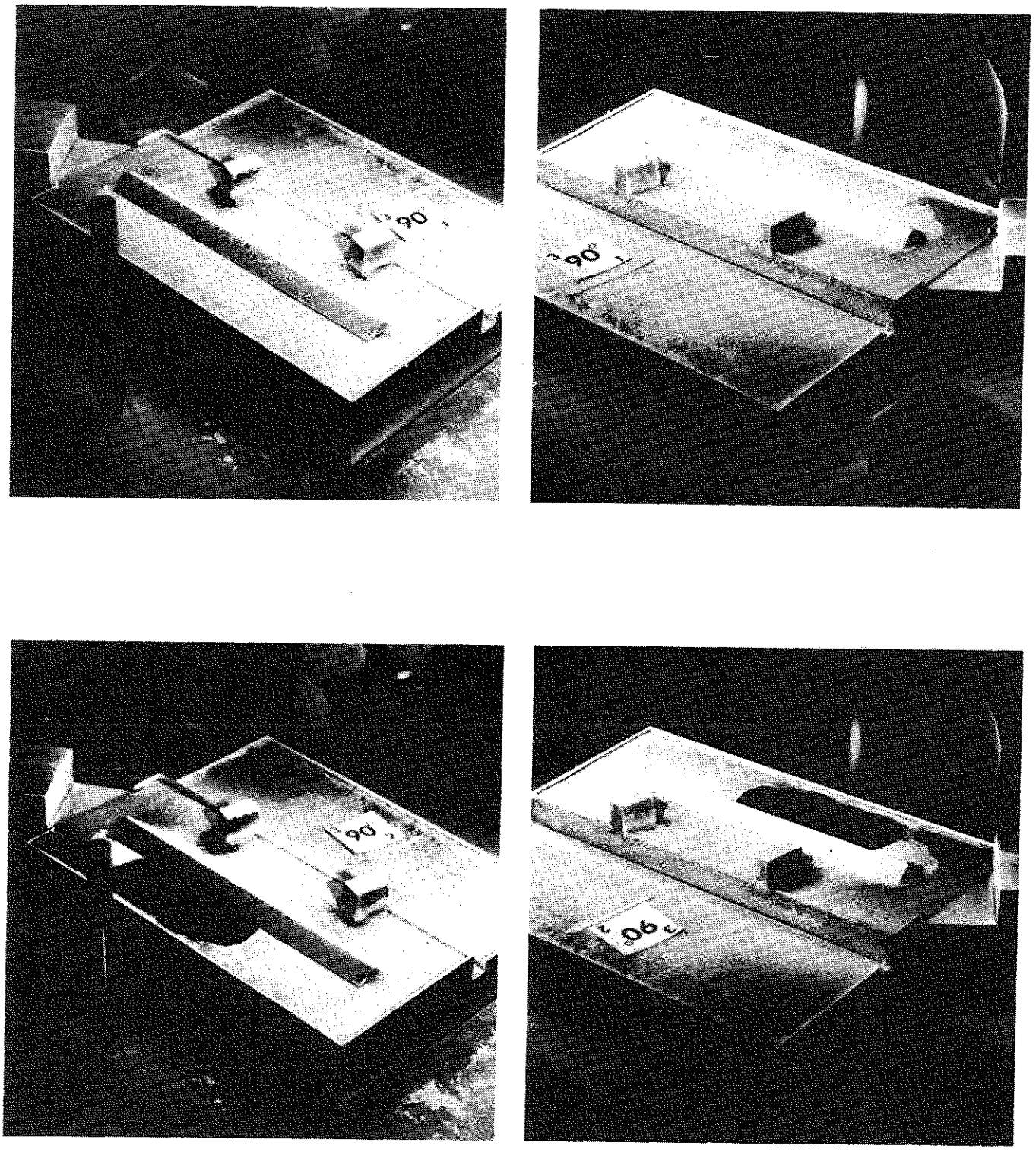

Figure A5c. Evaporation tests. Wind from east (90°). In the dark area windward of the roof window, the naphtalene spray was blown away due to insufficient bond

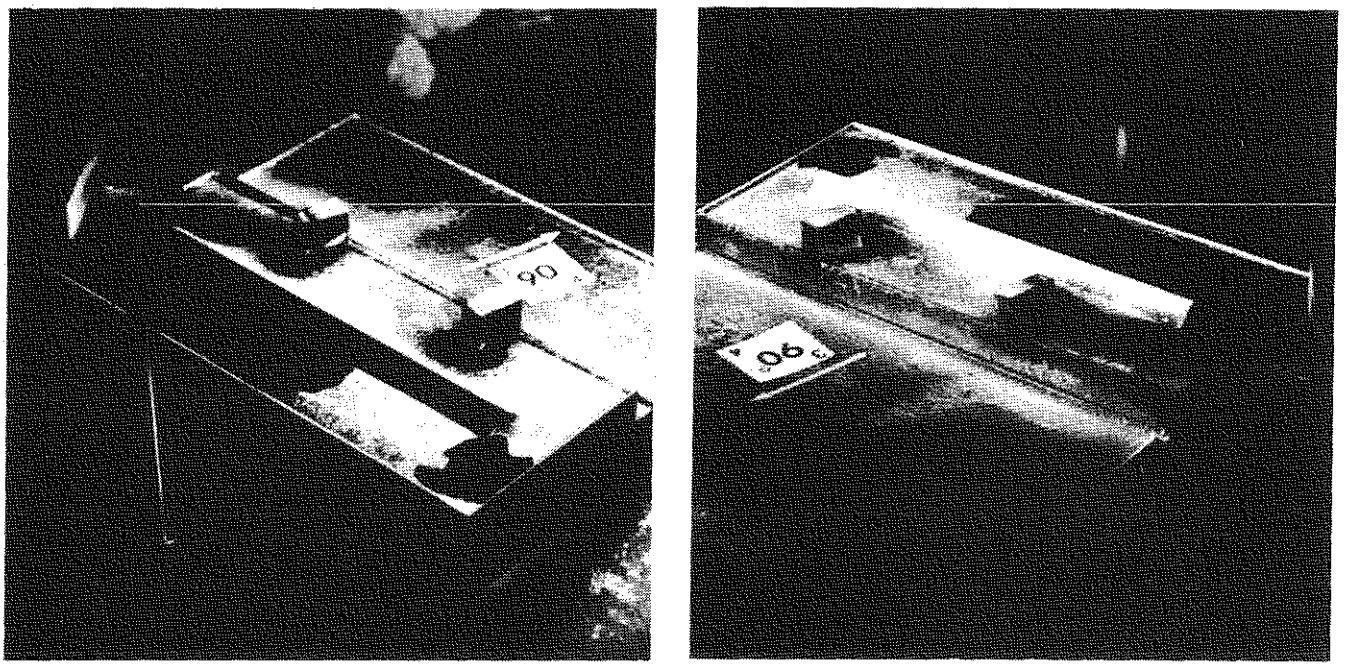

Figure A5c. Cont.

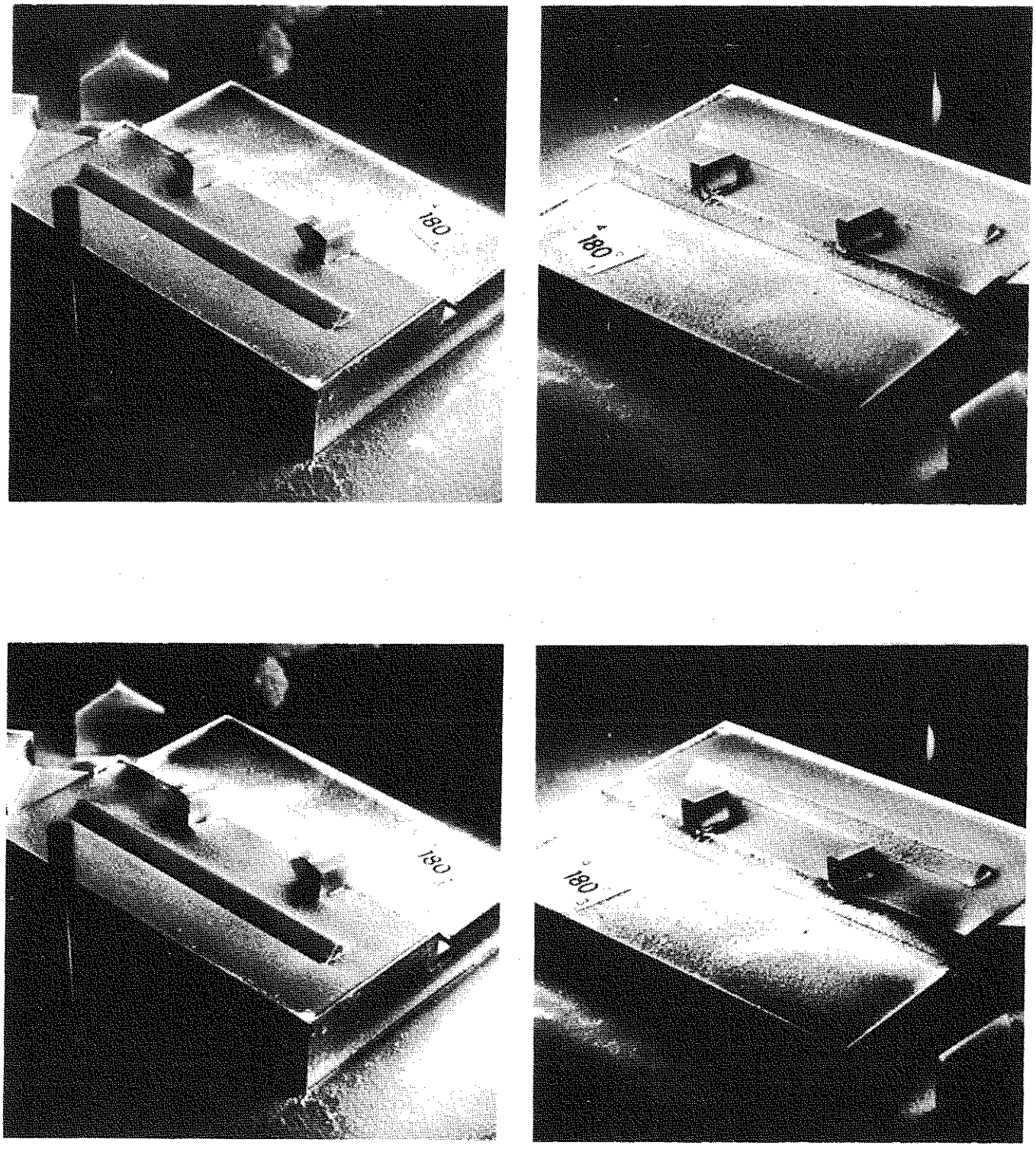

Figure A5d. Evaporation tests. Wind from south (180°)

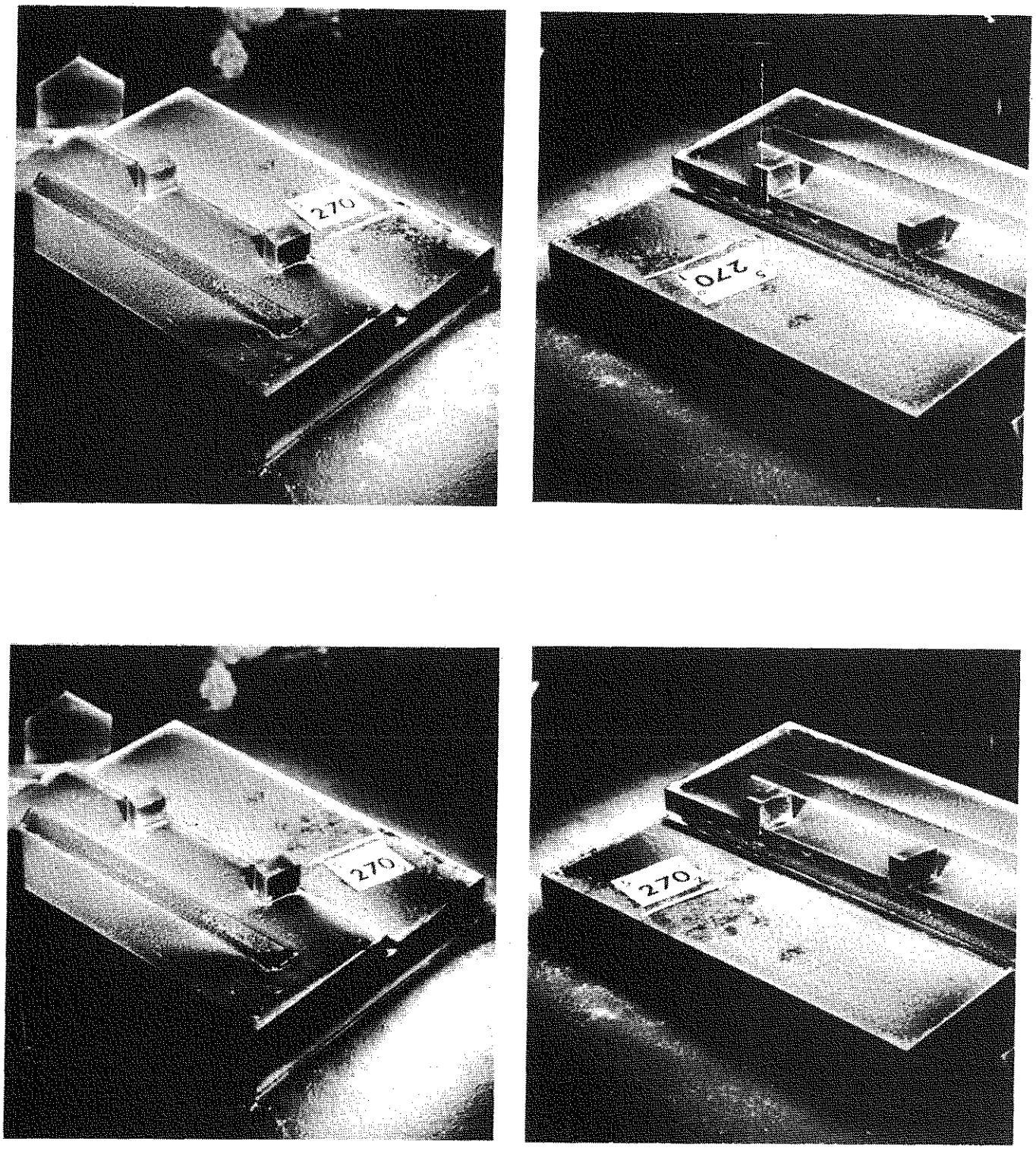

Figure A5e. Evaporation tests. Wind from west (270°)

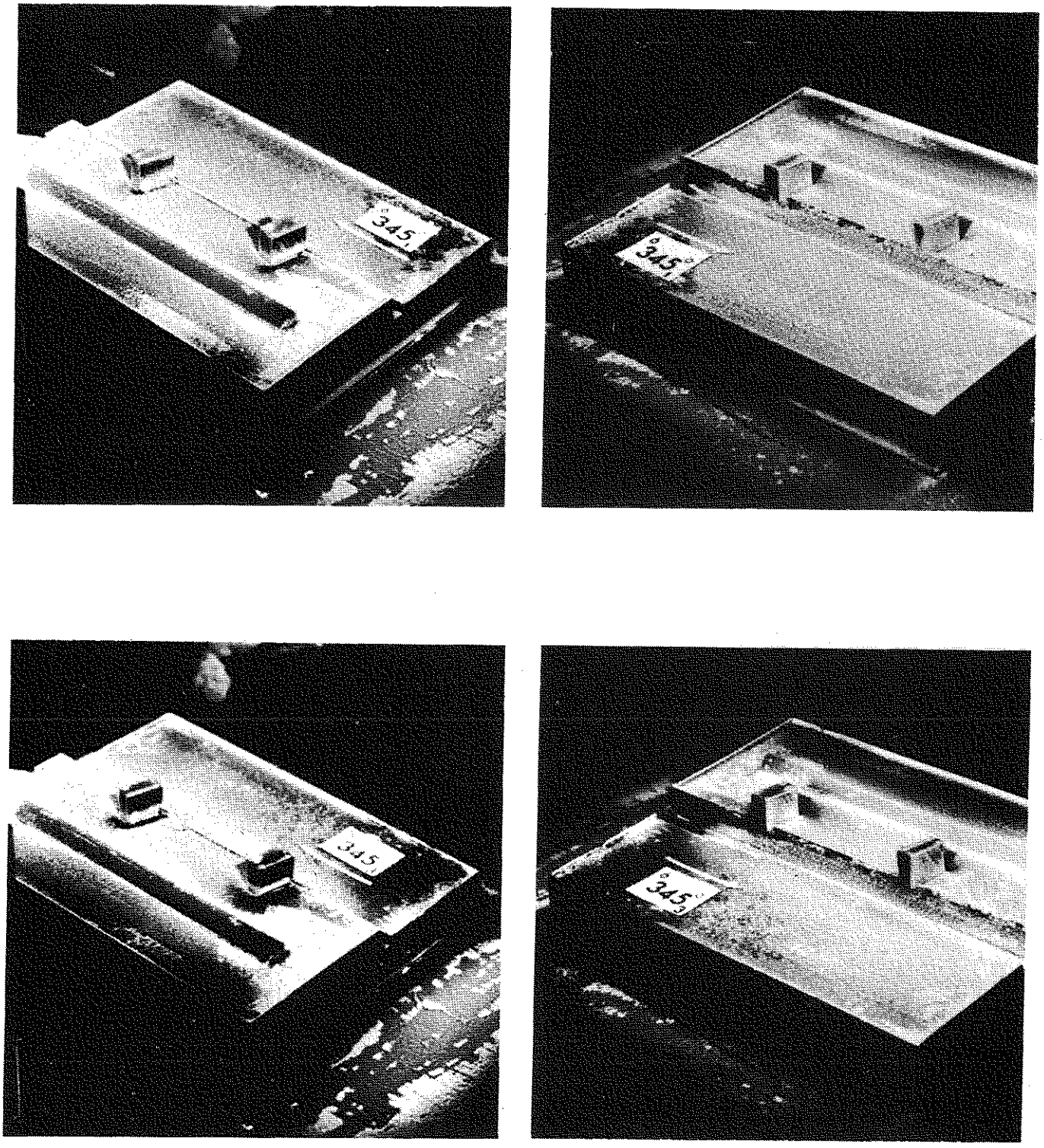

Figure A5f. Evaporation tests. Wind from NNW (345°), parallelly to the length direction of the central laboratory building

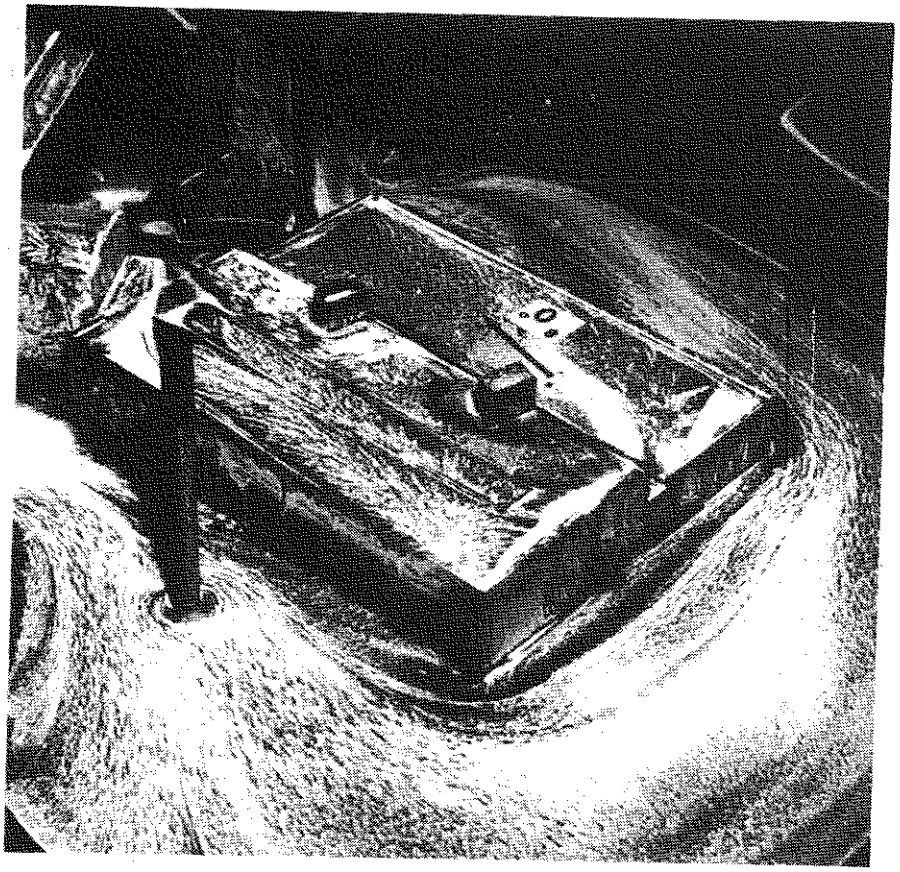

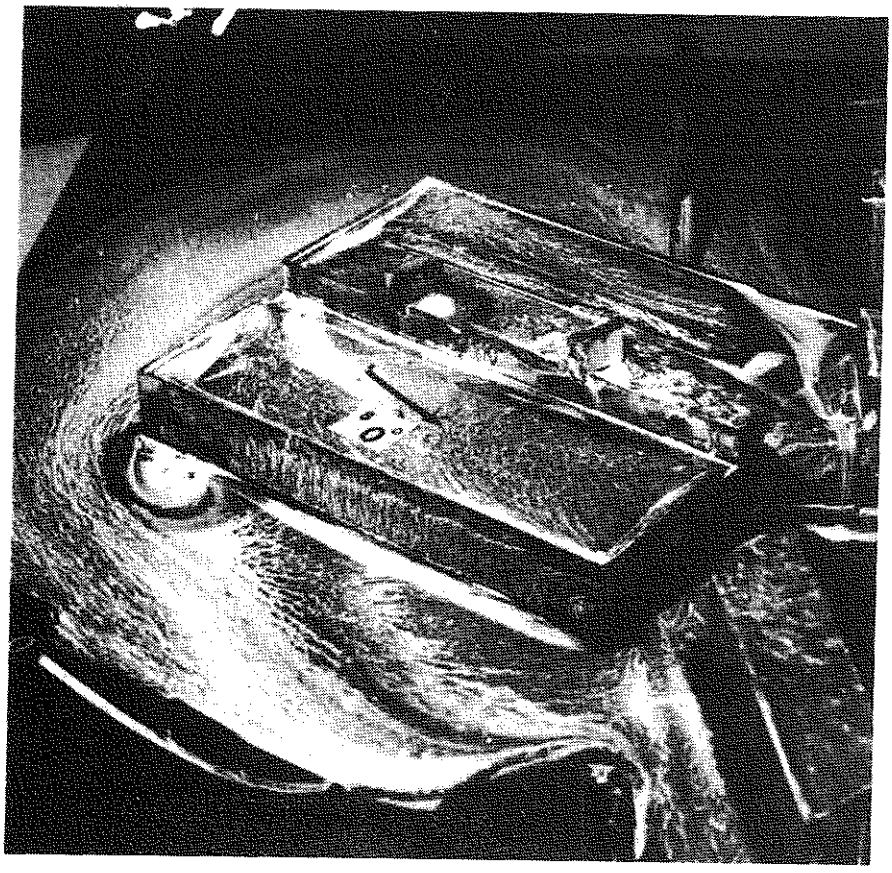

Figure A5g. Oil-flow tests. Wind from north (0^{o})

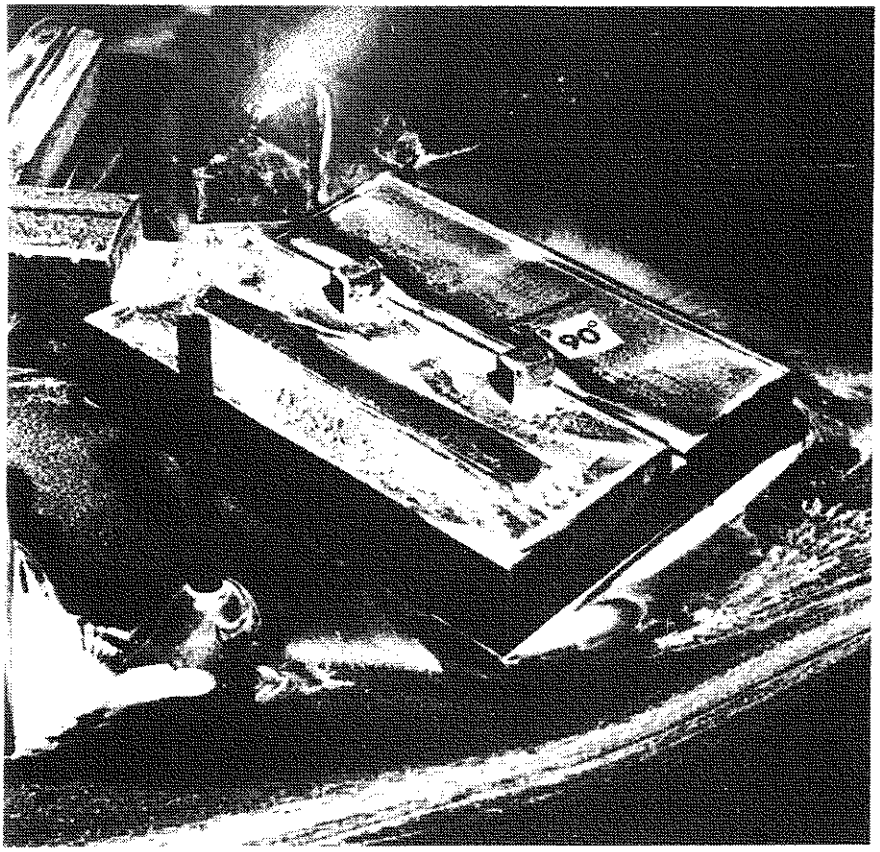

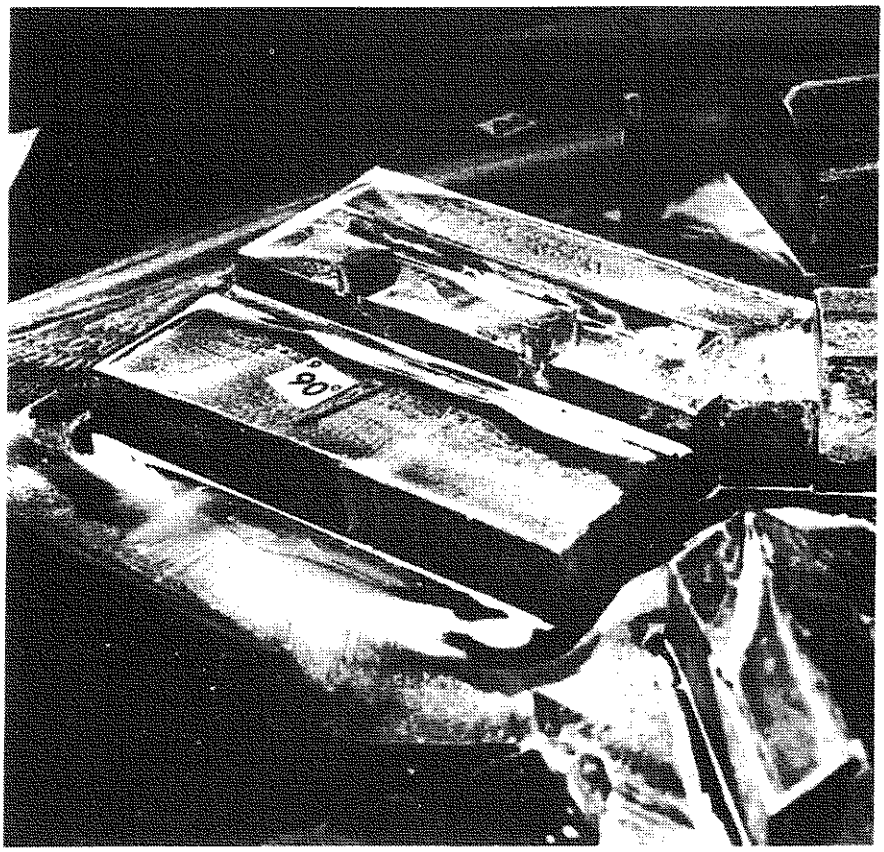

Figure A5h. Oil-flow tests. Wind from east (90^{o})

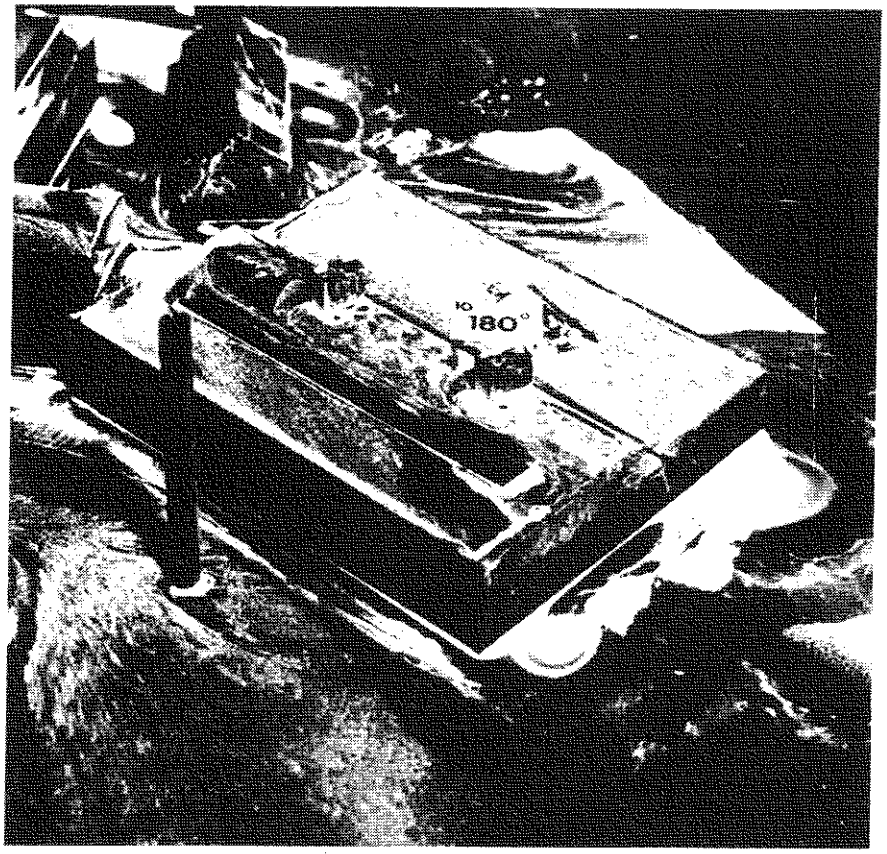

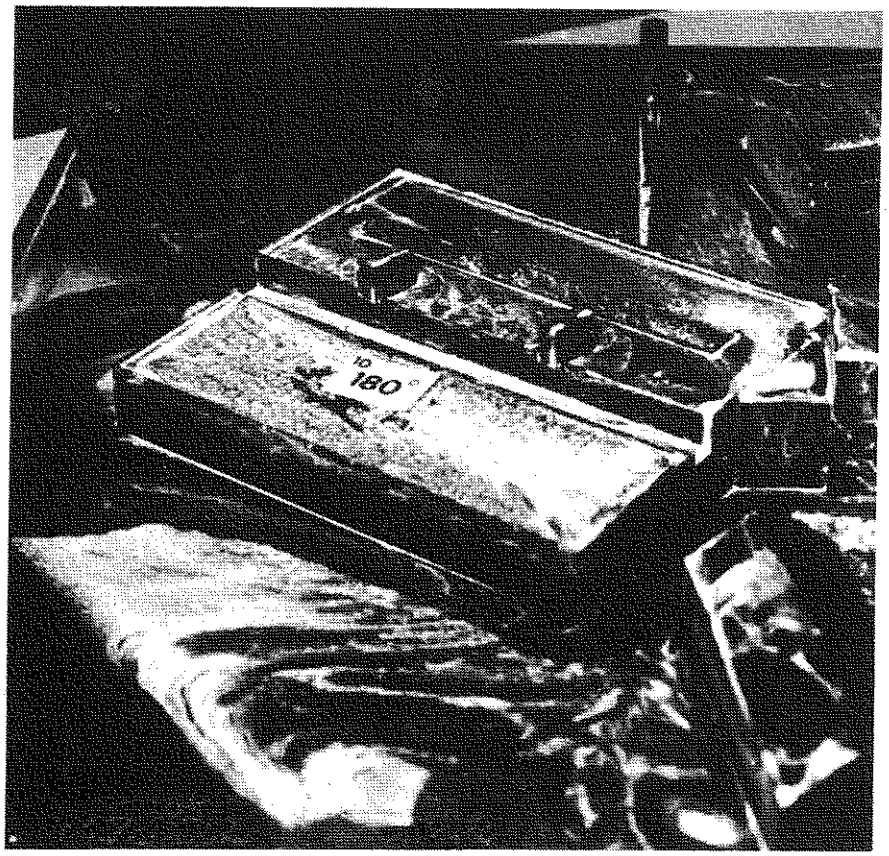

Figure A5i. Oil-flow tests. Wind from south (180°)

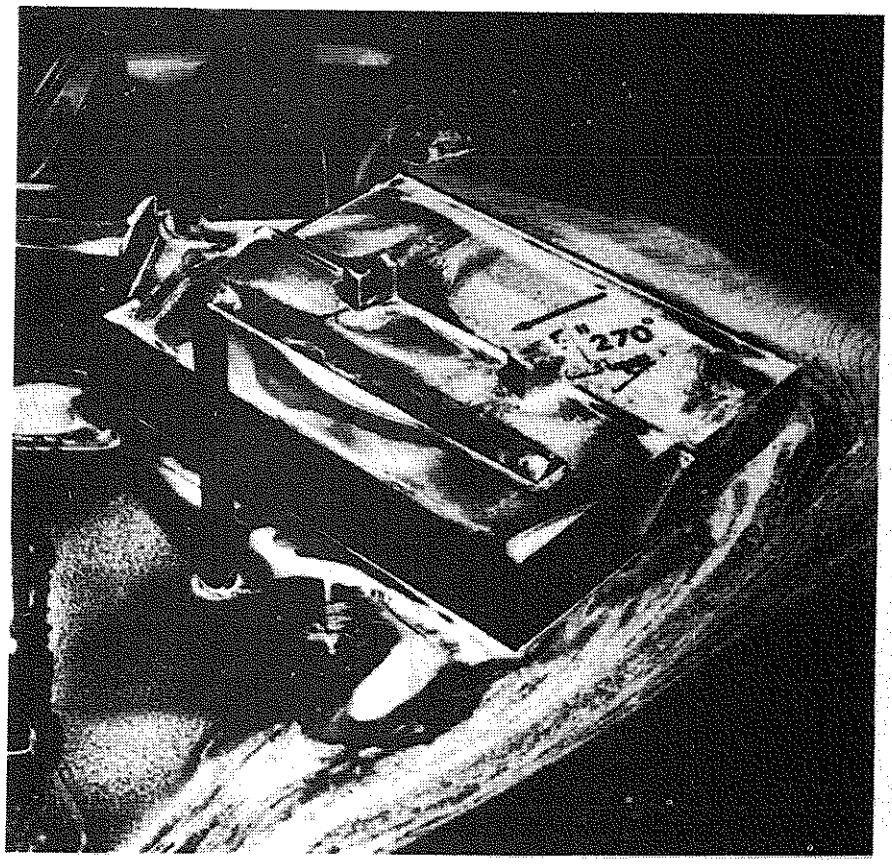

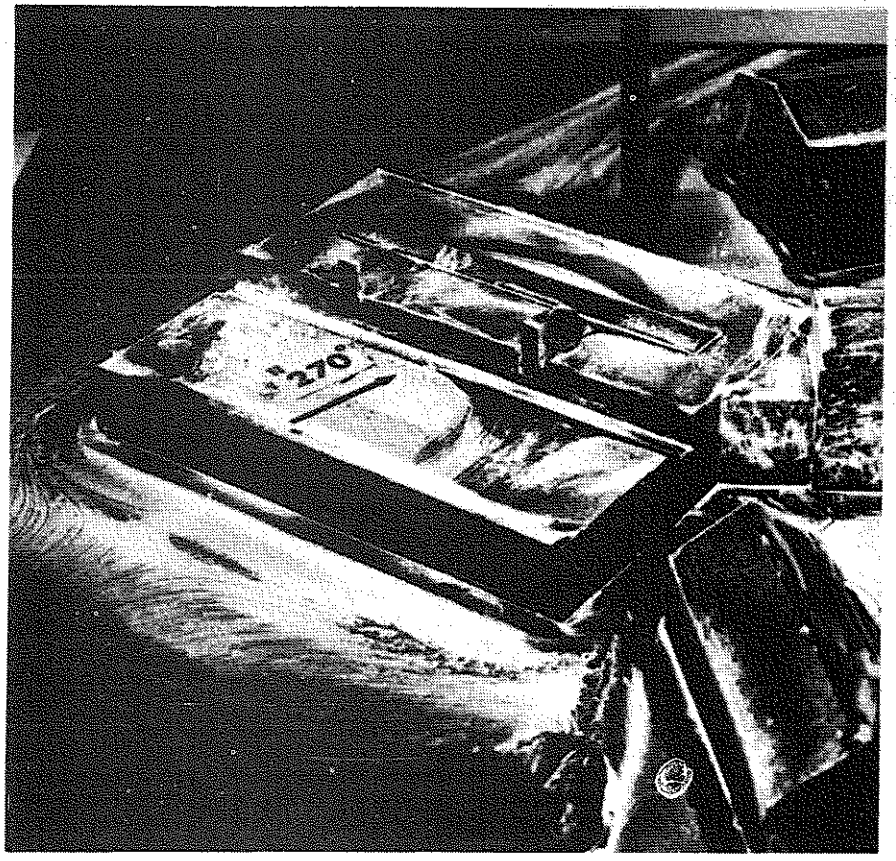

Figure A5j. Oil-flow tests. Wind from west (270°)

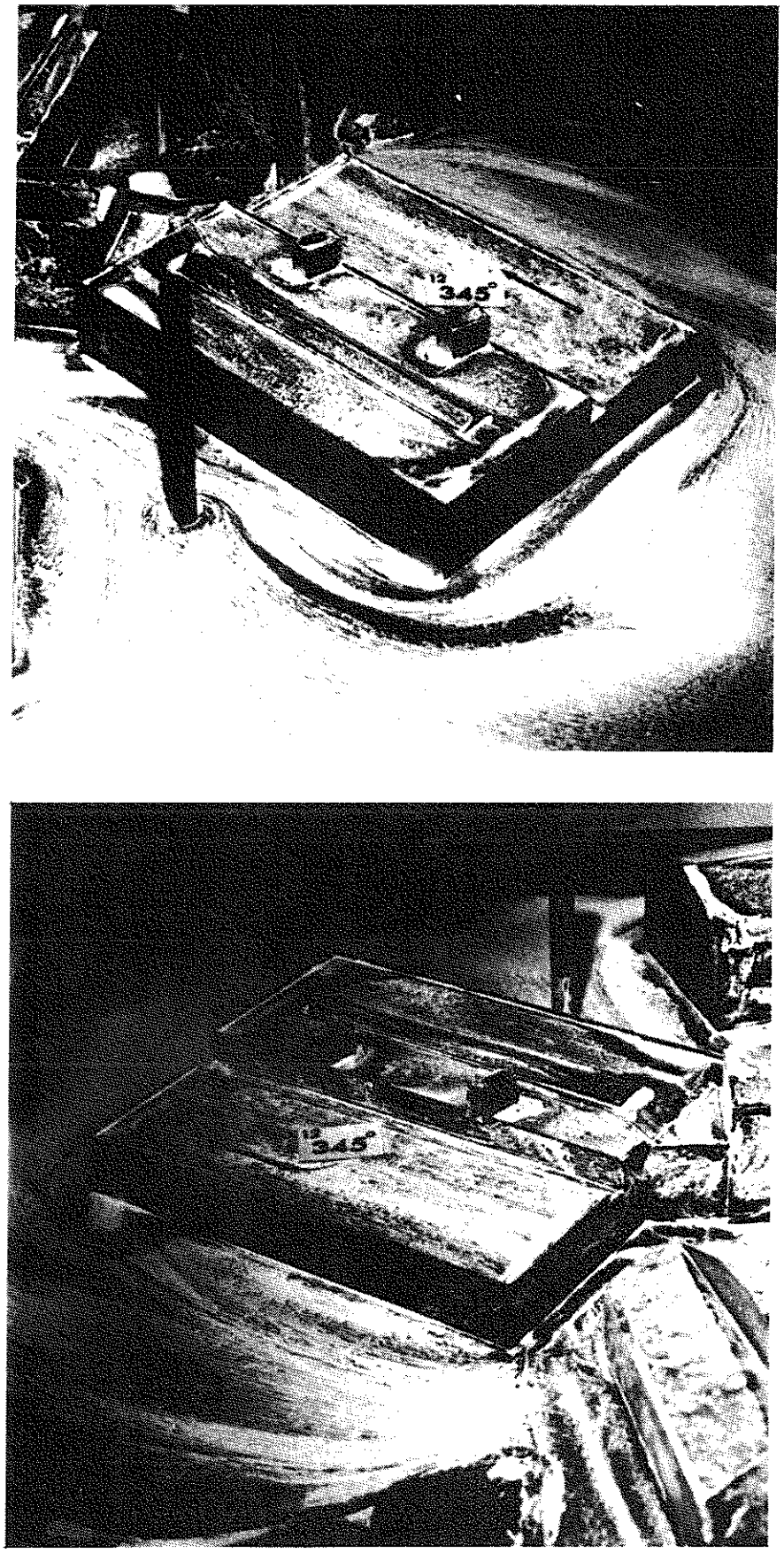

Figure A5k. Oil-flow tests. Wind from NNW (345°), parallelly to the length direction of the central laboratory building

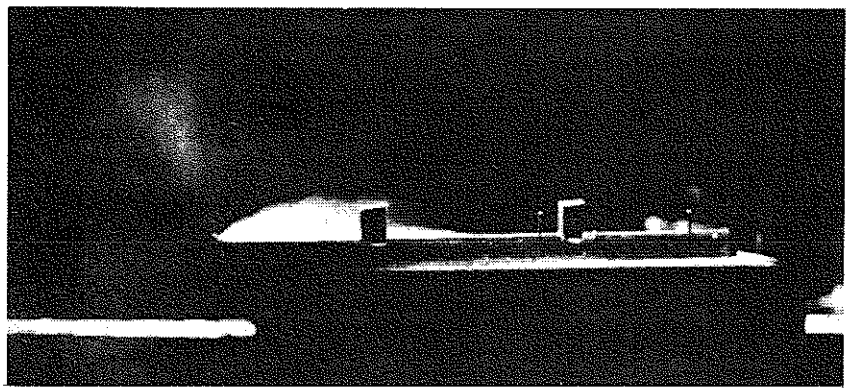

Outlet I

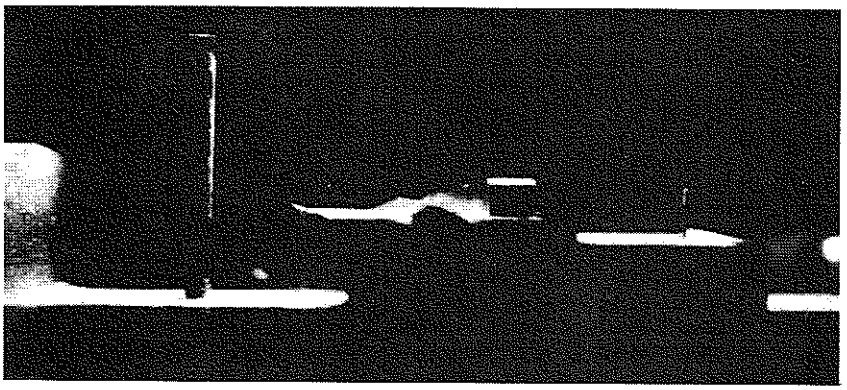

Outlet II

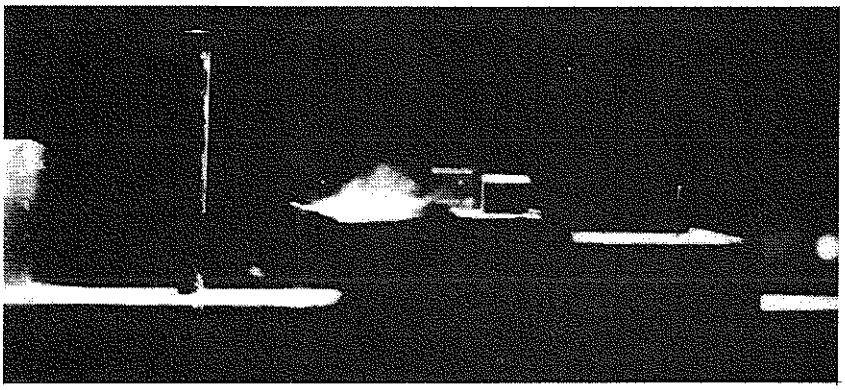

Outlet III

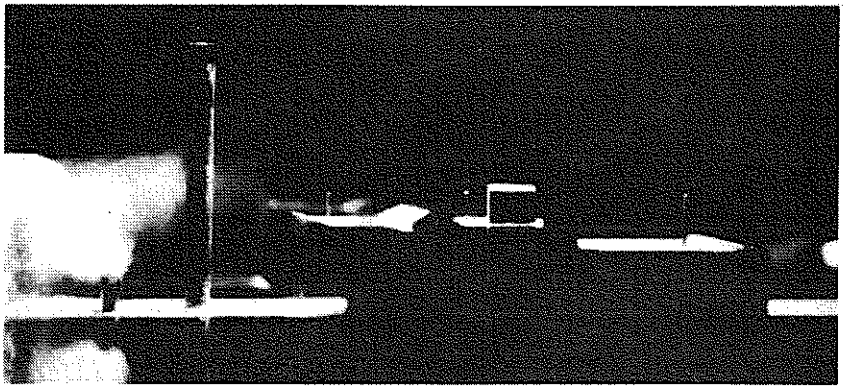

Outlet IV

Wind from east (90°). Light section through test house I

Figure A5ℓ. Smoke flow tests

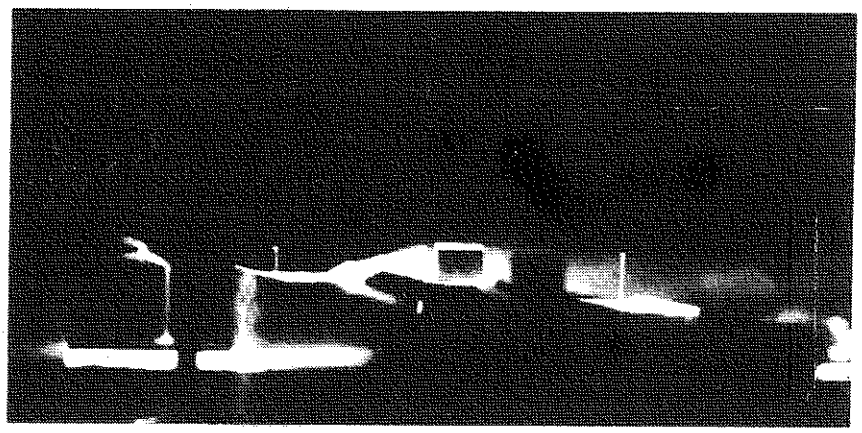

Outlet V

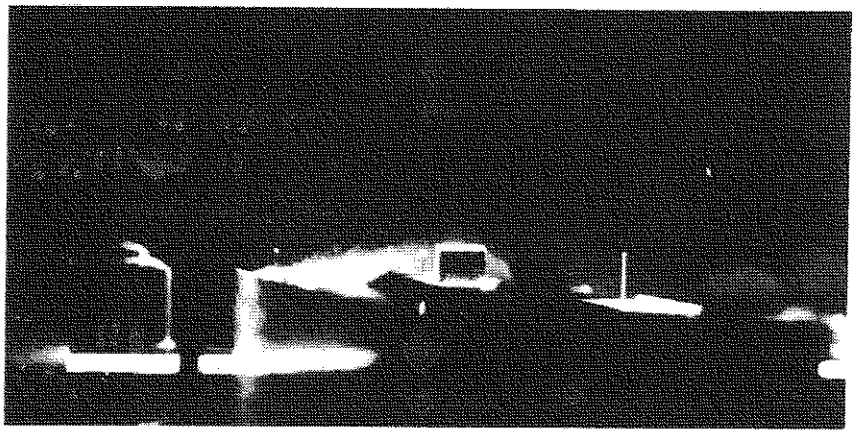

Outlet VI

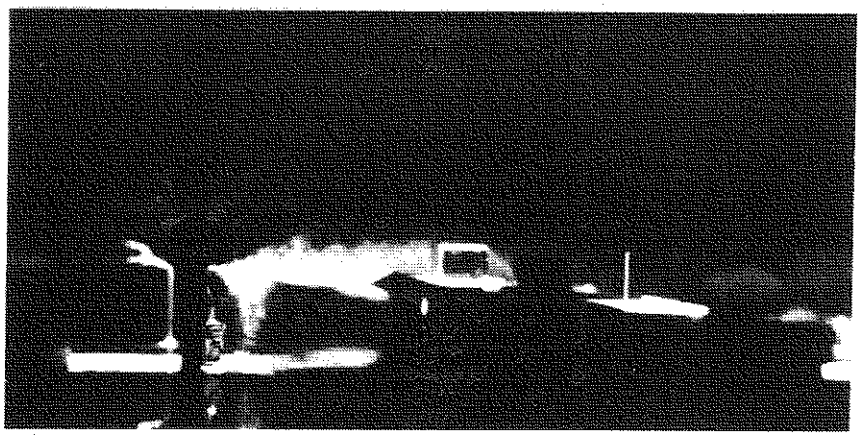

Outlet VII

Figure A5m. Smoke flow tests. Wind from east (90°). Light section through test house II

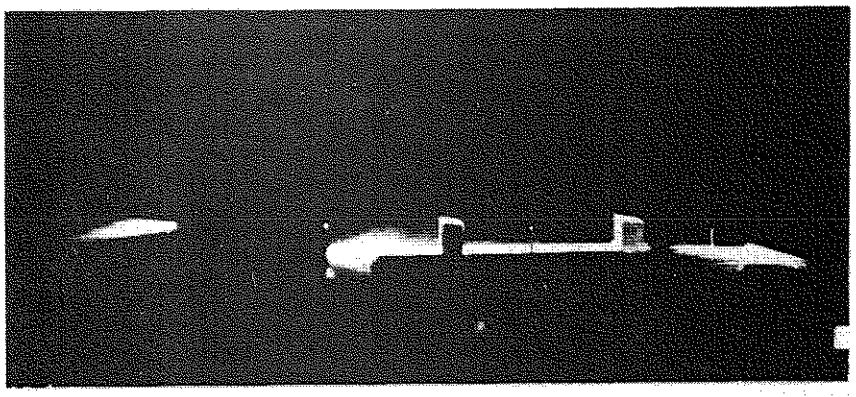

Outlet VIII

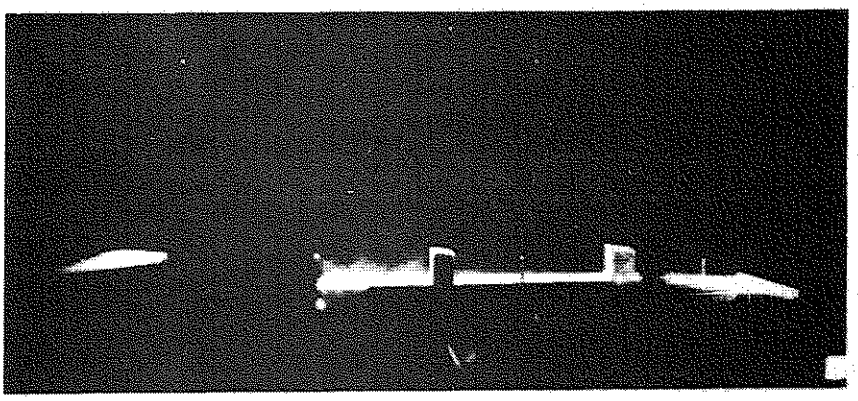

Outlet IV

Wind from south (180°)

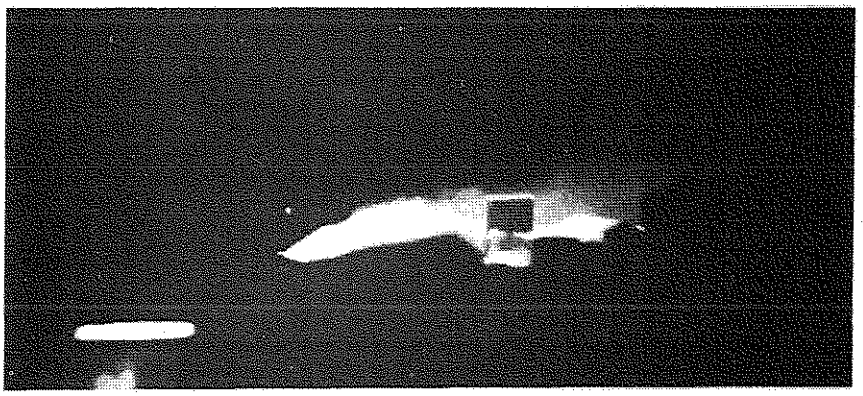

Outlet X

Wind from WSW (255°), perpendicular to the central laboratory building. Light section between the test houses

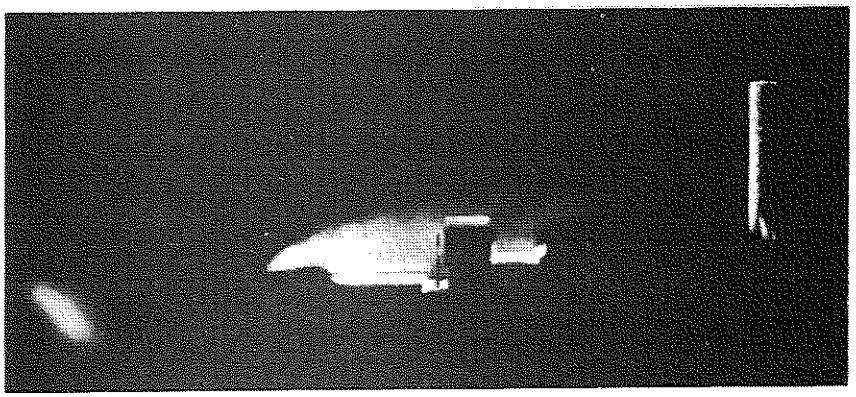

Outlet X

Wind from west (270°). Light section through test house II

Figure A5n. Smoke flow tests

A6. SURVEY OF REPORTED TESTS

Test method	Wind direction	Fig.no	Remarks
Naphtalene evaporation tests		A5a	Model sprayed with naphtalene, before wind exposure
"	N (0°)	A5b	
"	E (90°)	A5c	
"	S (180°)	A5d	
"	W (270°)	A5e	
"	NNW (345°)	A5f	Parallel to base laboratory building
Oil-flow tests	N (0°)	A5g	
"	E (90°)	A5h	
"	S (180°)	A5i	
"	W (270°)	A5j	
"	NNW (345°)	A5k	Parallel to base laboratory building
Smoke flow tests	N (0°); E (90°)	A5ℓ	Light section through test house I
"	E (90°)	A5m	Light section through test house II
"	S (180°); WSW (255°); W (270°)	A5n	WSW (255°), wind perpendicular to the base laboratory building

A7. SUMMARY

Three types of model scale tests, viz. evaporation tests, oil-flow tests and smoke flow tests, have been carried out in the FFA building aerodynamics-tunnel in order to give a rough understanding of the wind flow characteristics around two test houses, built on the roof of the Central Laboratory building of Höganäs AB for a long-range study of the behaviour of multilayer, external walls when exposed simultaneously to a long-term loading and a fluctuating exterior climate. The model was in scale 1:250 and the wind velocity, applied in the tunnel tests about 20 m/s. For a simulation of the atmosphere boundary layer, a generator consisting of triangular wedges was used together with a distributed ground roughness consisting of small-sized stones glued on a sheet-metal, placed immediately downstream the boundary layer generator. The purpose of the investigation was:

for the evaporation tests - to locate areas with high or low flow velocity nearest to the wall surfaces

for the oil-flow tests - to visualize the flow directions over the test house surfaces

for the smoke flow tests - to study the vertical extent of the separated flow regions over the base laboratory building on which the test houses are located.

The results are reported in the form of photos giving the flow pattern characteristics. The results are discussed summarily and conclusions are drawn with regard to the requirements on anemometer measurements in the long-range full scale investigation in Höganäs.

REFERENCES

[1] COUNIHAN, J., An Improved Method of Simulating an Atmospheric Boundary Layer in a Wind Tunnel. Central Electricity Research Laboratories, England. Atmospheric Environment, Vol 3, No 2, pp 197-214, 1969.

Observations at a full scale test concerning the wind flow characteristics around the test houses at the Central Laboratory building of Höganäs AB[1)]

By Tommy Lovén
The Aeronautical Research Institute of Sweden (FFA), Stockholm

During the autumn 1972, FFA participated in a full scale experiment comprising a visualization by using smoke of the flow conditions around the two test houses, built on the roof of the Central Laboratory building of Höganäs AB. The purpose of the test was to control some of the results, obtained in a model scale investigation, carried out previously in the building aerodynamics-tunnel at FFA and described in FFA-Report AU-348, cf. Fig. A5ℓ-n in this appendix.

Unfortunately, a mutual misunderstanding caused that suitable smoke-torches were not available at the test. Consequently, the test had to be made by using a smoke production unit, developed and manufactured by FFA for aerodynamics-tunnel tests. The produced smoke quantity then was found to be barely enough, especially at documenting the flow patterns by photographing. At the test, there was an approximately west wind with some inclination towards south. The wind velocity was about 5-7 m/s - the gusts ranging up to 10 m/s - which was estimated as acceptable with respect to the requirements of a neglectable influence of the thermal motion of the smoke.

Due to the limited quantity of produced smoke, it was not possible - as in the wind tunnel tests - to study the extent of the whole flow separation region above the roof of the laboratory building at one and the same occasion, but the study had to be limited to a smaller part of the flow pattern at a time. In doing so, it was found to be most essential to investigate the character of the flow separation region nearest to the roof edge barrier and then particularly the angle formed by the separation region to the roof. This angle is important to the height of the flow separation region further downstream. It is also of interest to get an idea of the flow character immediately up-stream the test houses.

---

1) Translation of Report FFAP-A-337, The Aeronautical Research Institute of Sweden, Stockholm, 1975.

Fig. Aa shows how the flow separates at the west edge of the roof of the laboratory building, to be compared with the flow conditions according to Fig. A5n for the corresponding wind tunnel test at wind from WSW. In Fig. Ab, the conditions of the model scale case are reproduced, reflected in relation to Fig. A5n and with the contour of the laboratory building marked in order to give an improved interpretation of the separation flow angle, since the west edge of the laboratory roof was shadowed of one of the adjacent buildings at the model test. A comparison between Fig. Aa and Ab indicates an acceptable agreement.

Fig. Ac-e illustrate a smoke outlet in three different points windward of the test house II. The figures demonstrate a fluctuating wind direction which is characteristic of the turbulent flow within a separated flow region. Fig. Ae, which refers to a smoke outlet close to the upper part of one of the test house walls, also shows how the test house instantaneously can give rise to an own separated flow region above the test house roof.

The relatively few smoke flow tests, carried out in full scale at an approximately west wind, seem to verify the flow conditions obtained in the model scale wind tunnel tests. This increases the confidence in the results received in the wind tunnel tests also at other wind directions.

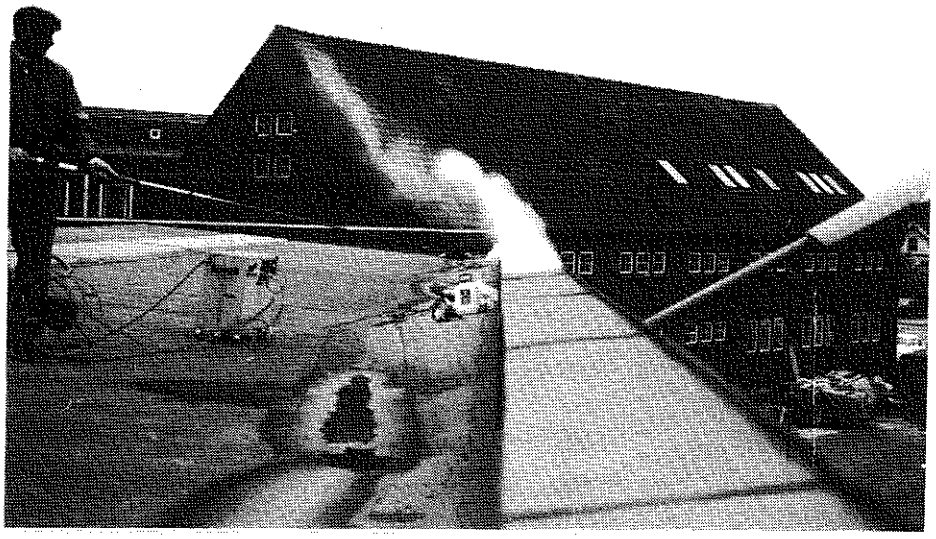

Figure Aa. The boundary of the separated flow region at a wind from W-WSW. Smoke outlet immediately down-stream the west roof edge barrier of the laboratory building

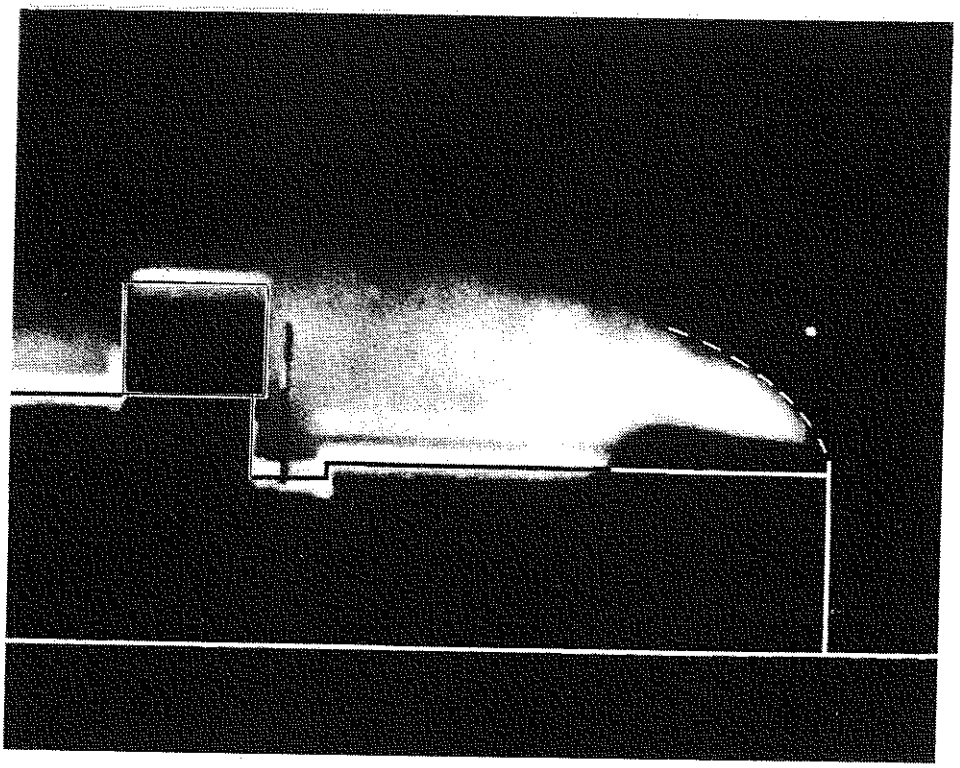

Figure Ab. The extent of the separated flow region, obtained in a model scale wind tunnel test at a wind from WSW. From Fig. A5n - the figure reflected and the contour of the laboratory building marked in order to give an improved interpretation of the separation flow angle

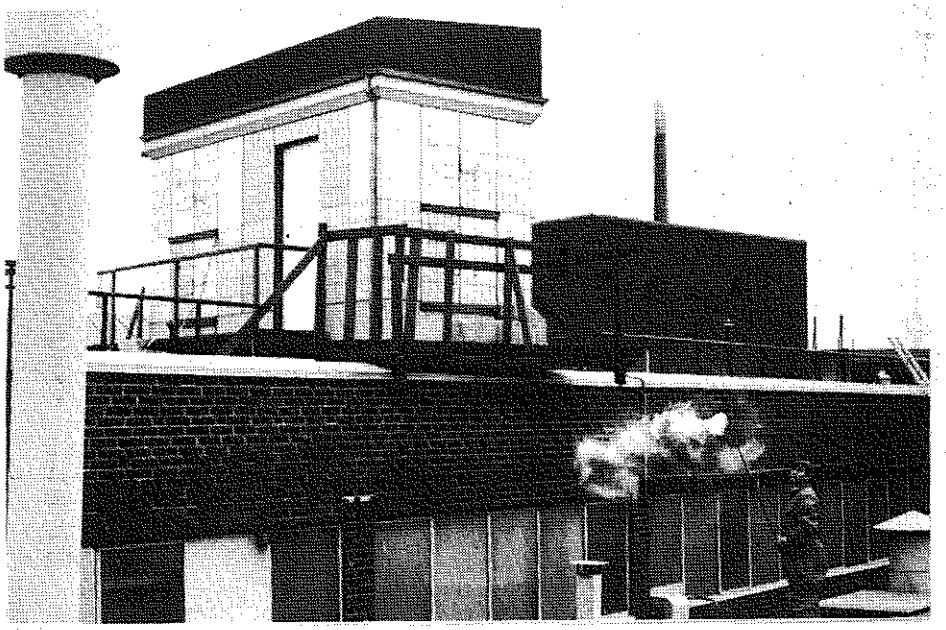

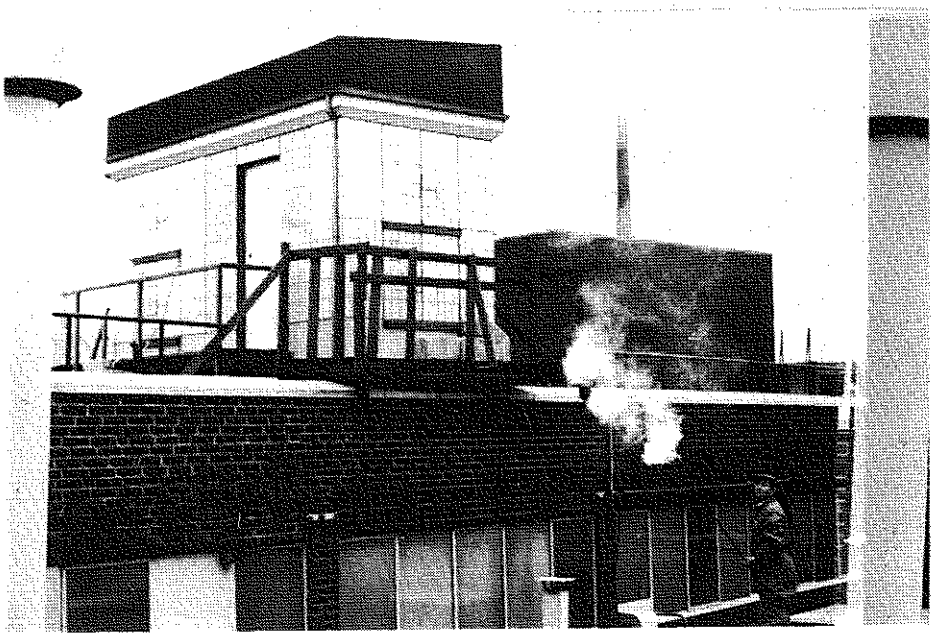

Figure Ac. Smoke outlet immediately below test house II. The smoke is spread in varying directions due to the turbulence within the separated flow region above the laboratory roof

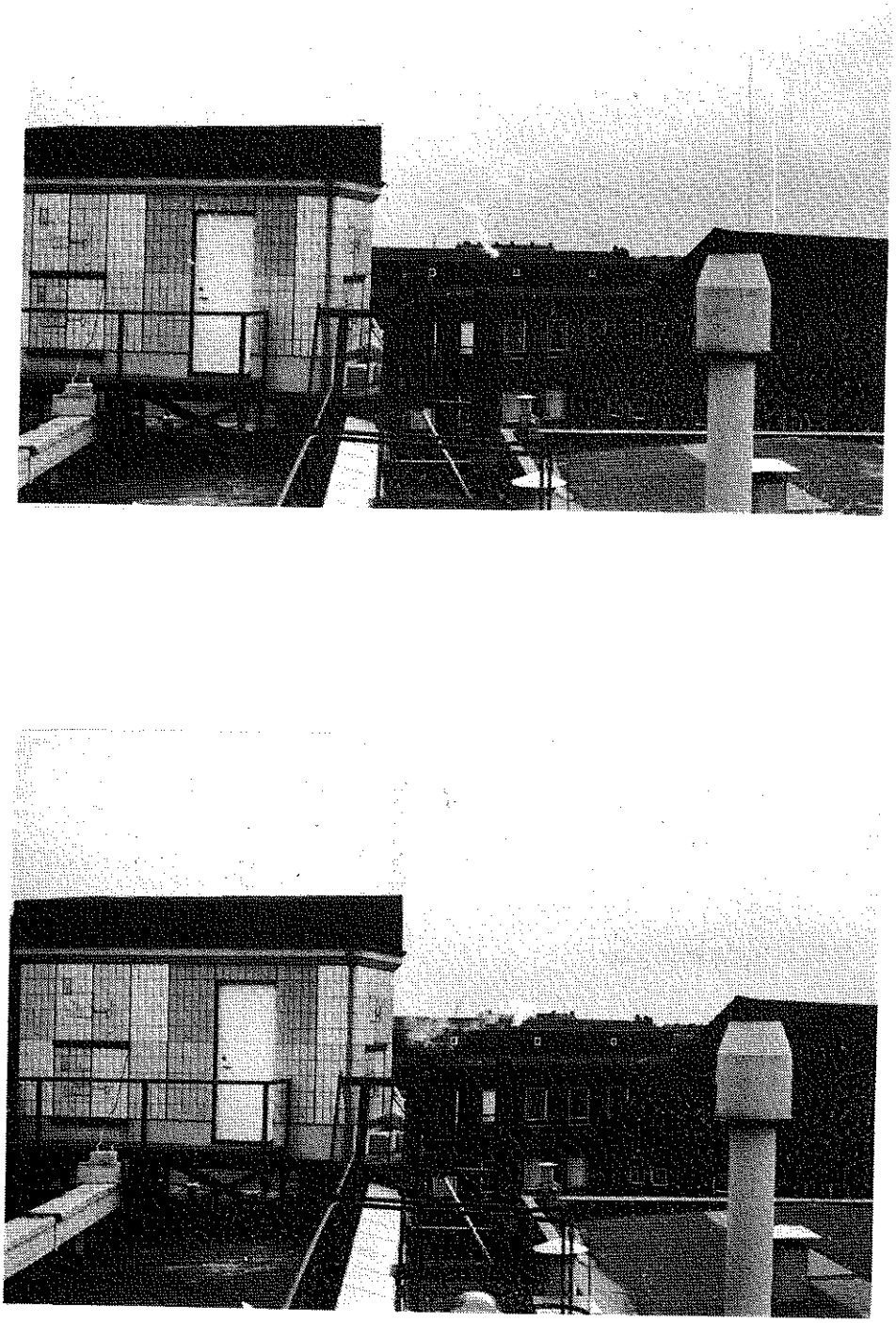

Figure Ad. Smoke outlet in windward in front of test house II, illustrating a fluctuating flow direction due to a turbulent flow

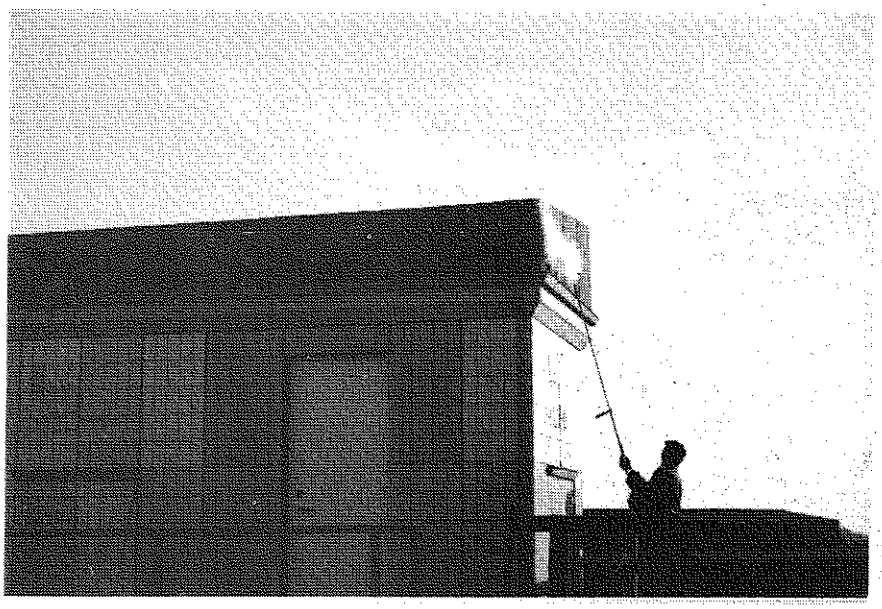

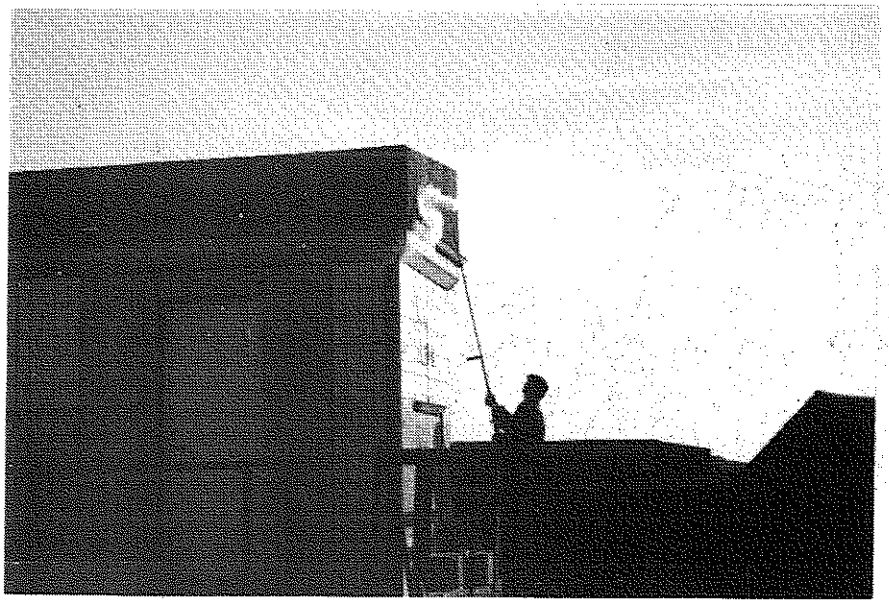

Figure Ae. Smoke outlet immediately in front of the upper part of test house II, showing no definite flow direction. In the upper figure, it can be seen how the test house instantaneously gives rise to an own separated flow region

Meteorological journal Week no. Year

Date	Hr	Clouds		Air temp			Precip		Wind		Remarks	Barom
		1.low 2.medium 3.high	quant 0-10	dry	wet	rel. hum.	type	mm	dir.	m/s	1.fog 5.frost 2.haze^{m} 6.ice int. 3.haze^{s} 7.thunder 4.dew 8.others	mbar
Sun	04											
	07											
	10											
	13											
	16											
/	19											
	22										max min	
Mon	04											
	07											
	10											
	13											
/	16											
	19											
	22										max min	
Tue	04											
	07											
	10											
	13											
/	16											
	19											
	22										max min	
Wed	04											
	07											
	10											
	13											
/	16											
	19											
	22										max min	
Thur	04											
	07											
	10											
	13											
/	16											
	19											
	22										max min	
Fri	04											
	07											
	10											
	13											
/	16											
	19											
	22										max min	
Sat	04											
	07											
	10											
	13											
/	16											
	19											
	22										max min	

Haze^{m} = haze at mist

Haze^{s} = haze at sun

Corrections of electrical signals from test house II due to variation in cable temperature

The heat insulated, 20 m long cable drum from House II to the data collector in House I was from start on designed to be fed by conditioned air (22°C) from the test houses by a suction outlet at the middle of the drum.

Air leakages along the drum resulting in fluctuating drum temperature were observed round test week no. 25 (end of 1969), why design was changed to an overpressure feeding from test week no. 32 on giving the required temperature stability of the drum air and of the cables.

In order to get cable corrections for the period week no. 5 to 32 and check the period week no. 33 to 135, signals from reference bodies in House II were analysed. This correction procedure is exemplified and illustrated in Fig. 1, giving the time variation during the period week no. 5 to 135 of

(1) the strain of the measuring points 444 (reference element of aerated concrete, placed inside House II), 445 (the concrete back of a reference wall element of the type N, placed inside House II), and 456 (the concrete back of the non loaded wall element 11, type N, of House I) - cf section 1.4.5

(2) the air temperature outside the cable drum

(3) the air temperature inside House II, and

(4) the relative humidity inside House II.

To the exemplified time curves, the following comment can be made:

(1) The reference element of aerated concrete, measuring point 444, shows a strong correlation to the variations of the relative humidity inside House II

(2) From test week no. 33 on, the longitudinal shrinkage of the reference wall element, measuring point 445, is very near that of the non loaded wall element 11 of House I, measuring point 456

(3) The small deviations between the measuring points 445 and 456, observed in test weeks no. 50 to 70 and no. 100 to 120 is considered mainly to depend on a moisture movement for the reference wall element, placed inside House II and not on any increased temperature of the cables in the drum - cf also the very small influence on the recorded values of measuring point 445 of the variations in the outside air temperature between the 07 and 13 o'clock observations

(4) The increase of the signal of measuring point 445 in the weeks no. 20 to 30 of about 160 μ-strain is in good agreement with the corresponding decrease of about 12°C of the air temperature outside the drum for the same period.

Computations and estimations on the basis of recordings of the type exemplified have led to corrections of the μ-strain values from House II according to the following table, to be applied to the 07 o'clock observations for the weeks no. 5 to 32, as concerns the week average values.

Corrections of μ-strain values from House II for weeks no. 5 to 32

to be used for the 07 o'clock observations, as concerns the week average values

Week no.	Tile strain gauges	Strain gauges on concrete
5	1 -	2 -
6	5 -	10 -
7	14 +	27 +
8	21 +	42 +
9	27 +	54 +
10	20 +	39 +
11	5 +	9 +
12	10 +	19 +
13	6 -	11 -
14	5 +	10 +
15	6 +	11 +
16	0	0
17	2 -	3 -
18	25 -	50 -
19	9 -	17 -
20	17 -	34 -
21	19 -	38 -
22	27 -	54 -
23	42 -	84 -
24	35 -	70 -
25	42 -	84 -
26	64 -	128 -
27	70 -	140 -
28	59 -	118 -
29	53 -	106 -
30	69 -	138 -

Week no.	Tile strain gauges	Strain gauges on concrete
31	39 -	77 -
32	17 -	34 -

Notice: The signals from the resistance thermometers normally do not need any correction for the cable drum temperature

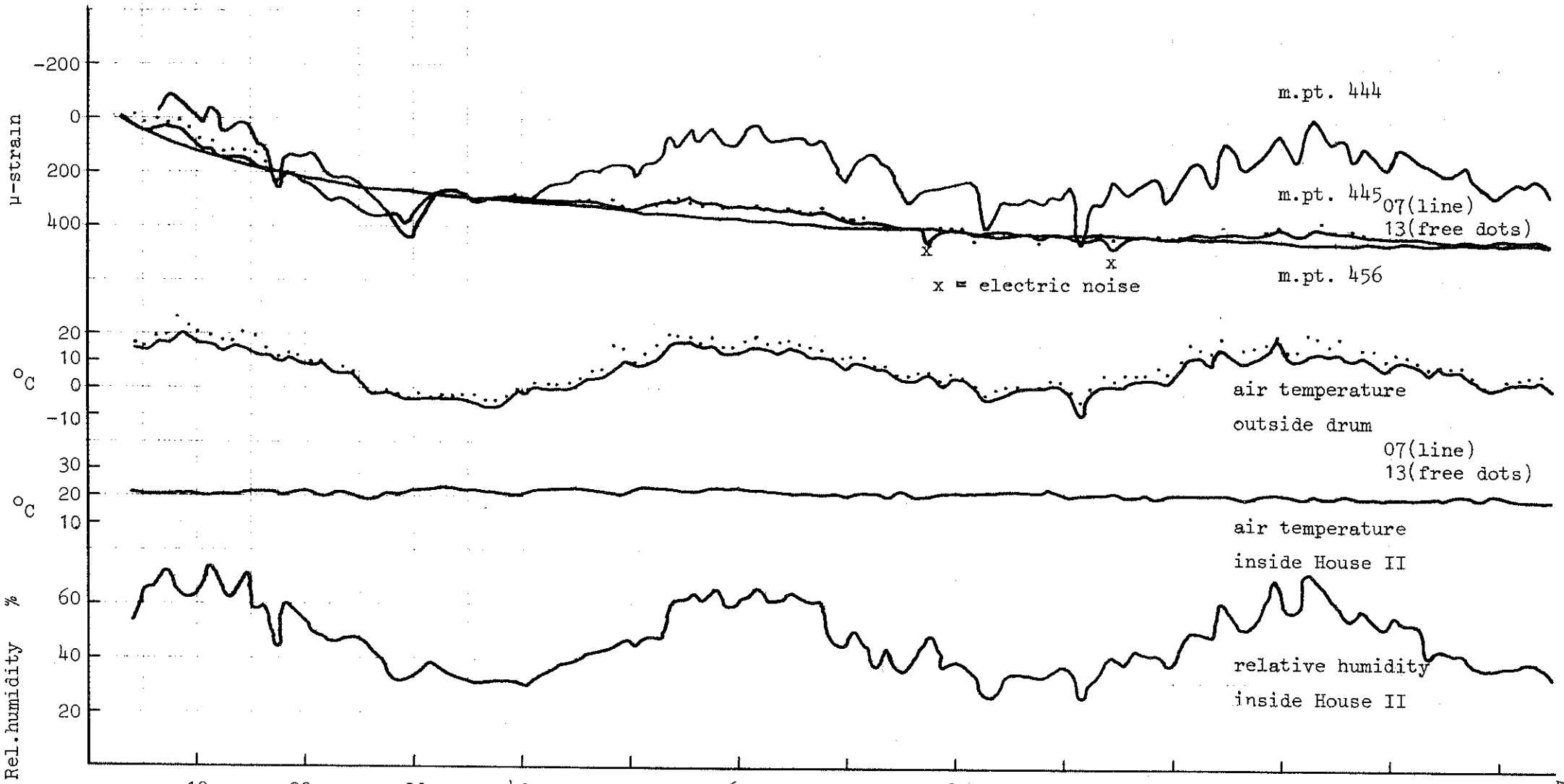

Figure Aa. Time variations of the strain of measuring points 444, 445 and 456, the air temperature outside the cable drum and inside House II, and the relative humidity inside House II

Paper 40

LONG-TERM STRAIN-GAUGE MEASUREMENTS IN OUTDOOR ENVIRONMENT ON CERAMIC TILES

MESURES DE LONGUE DUREE AVEC DES JAUGES A RESISTANCE ELECTRIQUE ATTACHEES A DES TUILES CERAMIQUES EXPOSEES AUX INTEMPERIES

LANGZEITVERSUCHE MIT DMS AUF KERAMISCHEN, DEM EINFLUSS DES WETTERS AUSGESETZTEN ZIEGELN

Gösta E. Scherling*

Materials exposed to outdoor environment are subjected to various damaging kinds of stress. In ceramic tiles on surfaces of buildings, damage may be caused by various weather conditions. It has been assumed that the main reasons for the occurrence of mechanical stresses are the influence of temperature variations and the combined action of humidity and frost. This may be verified by strain measurements with bonded resistive strain gauges, a method described in this paper. Some results from the preliminary runs and from the main tests are included. A large number of tiles instrumented with gauges have been attached to outside walls of the test building.

Les matériaux exposés aux intempéries subissent divers types d'efforts, qui les endommagent. Par exemple, dans les tuiles céramiques utilisées pour couvrir les façades des bâtiments, des dégats sont souvent causés par différentes conditions météorologiques. Il est probable que des gradients de température et l'influence combinée de l'humidité et du gel sont des causes primaires d'efforts mécaniques. À ce propos, des mesures avec des jauges à résistance électrique collées devraient fournir des renseignements intéressants. La communication décrit cette méthode de mesure, et donne quelques résultats pour les essais préliminaires ainsi que pour les essais principaux effectués. Un grand nombre de tuiles munies de jauges ont été maçonnées à l'extérieur du bâtiment d'essais.

In Werkstoffen, welche dem Einfluss des Wetters ausgesetzt sind treten verschiedene Arten mechanischer Spannungen auf, welche mit der Zeit zu Schäden führen können. Zu Schäden Anlass geben Witterungseinflüsse z.B. in keramischen Ziegeln, welche zur Aussenbekleidung von Gebäuden verwendet werden. Die Hauptgründe für das Auftreten mechanischer Spannungen sind hier wahrscheinlich Temperaturschwankungen sowie der kombinierte Einfluss von Feuchtigkeit und Frost. Eine Möglichkeit zur Ueberprüfung dieser Hypothese besteht in der Durchführung von Dehnungsmessungen mit aufgeklebten Dehnungsmesstreifen, welche aufschlussreiche Unterlagen über die Art der auftretenden Belastungen liefern sollte. Die verwendeten Messmethoden sowie die Ergebnisse von Vorversuchen werden beschrieben und einige Resultate der Dehnungsmessungen an einem Gebäude erwähnt. Bei diesen Versuchen wurde eine grosse Zahl der später zur Fassadenbekleidung des Testgebäudes verwendeten Ziegel mit Dehnungsmesstreifen versehen.

INTRODUCTION

THIS PAPER reports experiences with strain-gauge measurements on ceramic tiles for outside wall facing. The project is part of a large investigation that will include measurements during 2–3 years on two test houses located at an industrial site on the coast of southern Sweden.

The Aeronautical Research Institute of Sweden (FFA) was consulted for the installation of strain gauges in this project by the National Swedish Council for Building Research with co-operation of the Royal University of Lund and the Höganäs Co, manufacturer of tiles.

The part of the project assigned to FFA included choice of material and components, development of application methods and protective arrangements for bonded resistive strain gauges. Using the experience from initial tests, 372 strain gauges have been applied to tiles, which have then been walled on two test houses. In addition to strain measurements, temperature and moisture measurements as well as comprehensive weather observations are now being made.

* *The Aeronautical Research Institute of Sweden (FFA), P.O. Box 11021, S-161 11 Bromma 11, Sweden.*

PURPOSE AND SCOPE OF MEASUREMENTS

Many materials, particularly those used in construction of buildings (e.g. ceramic tiles) are liable to be affected by weather changes, radiation and air pollution. Under certain circumstances, physical damage will result. The glaze may crack or peel or the tiles may come loose from the wall. Ceramics absorb humidity, and this may cause deformations at very low temperatures and under rapid changes in temperature.

Such deformations may occur as movements, initially very small, and it may be possible to map these deformations in terms of strains. Therefore, a comprehensive investigation has been initiated for ceramic materials subjected to long-term load and weather stresses. Investigations and measurements are at present being carried out on two newly erected test houses, where strain, temperature and humidity conditions of the tiles are continuously recorded (Fig. 40.1). The strains are measured by a large number of resistance foil strain gauges cemented directly on the tiles attached to the wall.

Stability and reliability of strain gauges and recorders cannot be set too high, because the measurements are to be carried on for probably 2–3 years under unfavourable environmental conditions.

A total of 372 strain gauges were applied on 218 separate tiles. On most of these, the gauges were cemented on both the glazed and the ceramic side at places accurately opposite each other, either at the centre of the tile or near one of the short edges (Fig. 40.2).

The signals from the strain gauges and from temperature sensors are fed to a digital data acquisition system at predetermined time intervals; the humidity is measured manually.

THE ENVIRONMENT

The glaze side is mainly affected by the weather, while the ceramic side is influenced by the mortar and by humidity penetration. The tiles may be exposed to conditions of both positive and negative gradients of temperature and humidity, owing to the combined influence of weather, humidity absorption and thermal inertia of the wall.

Mechanical stresses generally occur as a consequence of displacements in the load-carrying structure of the house, and these are caused by, among other things, local displacements in the foundations, vibrations and wind pressures.

It is, of course, impossible to predict weather conditions of the test place for long periods. However, the most important annual weather factors are:

(1) Ambient temperature (−25 to +30°C).
(2) Solar radiation (heat, UV radiation).
(3) Humidity (rain, mist, dew).
(4) Snow, hail, frost, freezing rain.
(5) Wind velocity (0 to 30 m/s).

The industrial environment may add to these:

(6) Mechanical load changes.
(7) Electrostatic and electrodynamic disturbances.
(8) Air pollution (factory smoke, salt).
(9) Bird droppings, mould, etc.

On the inner side of the tiles, the environment is better known and also more inert. The chemical components of the mortar can affect, for example, the electric insulation of

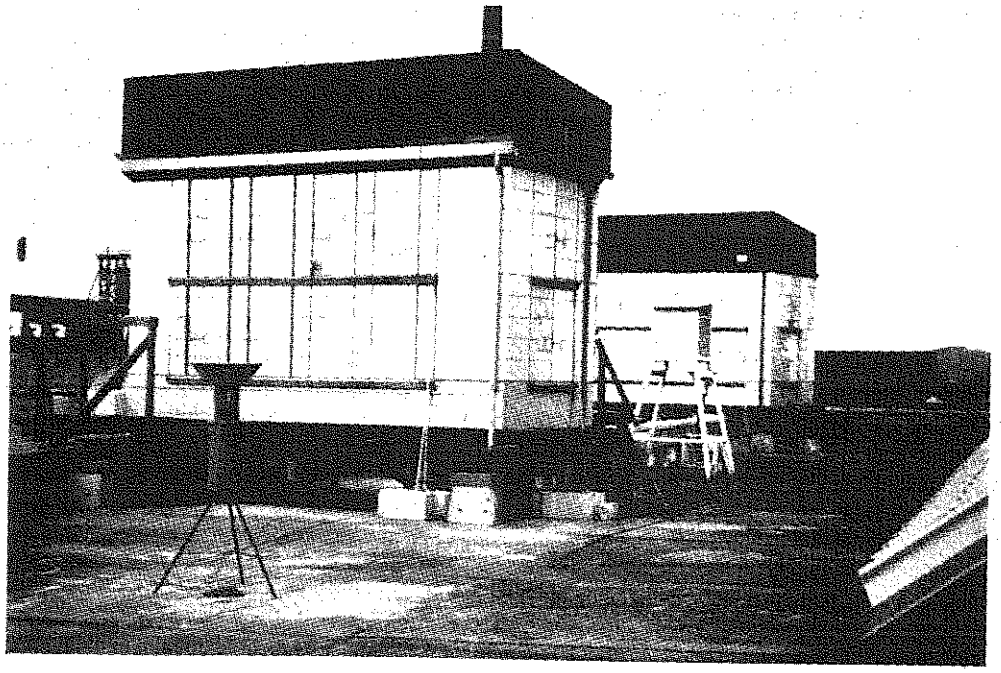

Fig. 40.1. Test houses complete with strain-gauged tiles

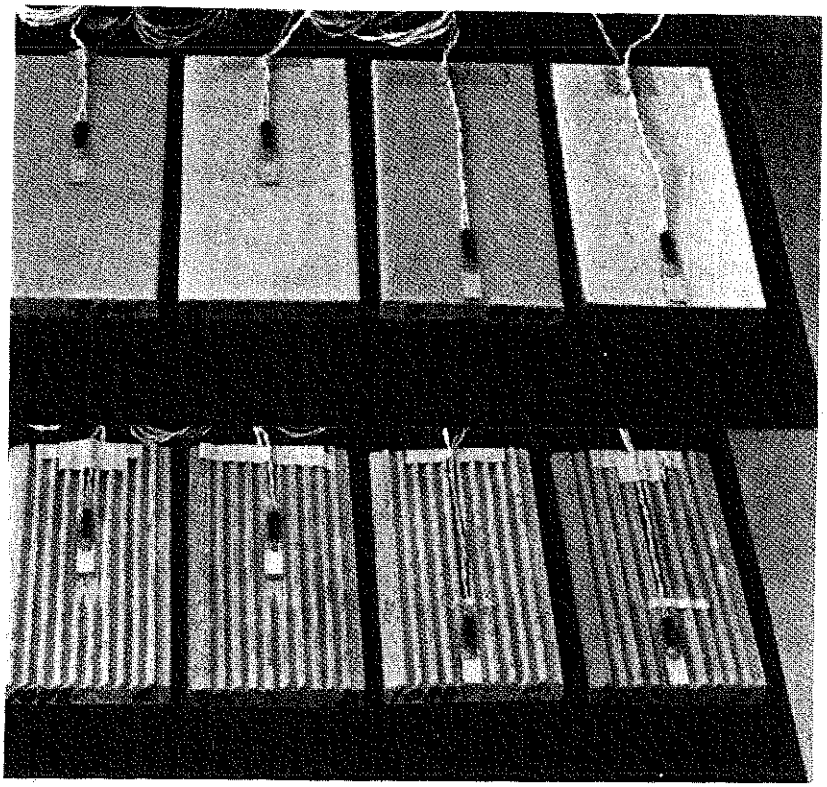

Fig. 40.2. Examples of strain gauges mounted on tiles

the gauge or the quality of its bond to the tile, in an unpredictable manner.

The digitial data acquisition equipment is placed in a room of the test house and thus subjected to a stable room environment.

CHOICE OF STRAIN GAUGES

The determining factors in the choice of a strain gauge for a specified purpose are environment, accuracy and cost. At places where only very small strains are expected, semiconductor gauges are preferable, but high cost, bad matching to the linear temperature expansion coefficient and plain mechanical fragility exclude their use. Hence the conventional type with a nominal gauge factor of about 2·0 has been chosen. Desirable data and qualities of the gauge are:

(1) resistance of 600 $\Omega \pm 0{\cdot}5$ per cent (for impedance matching to the data-acquisition system);
(2) temperature compensation matching that of molybdenum ($5{\cdot}5 \times 10^{-6}$/C° or 3×10^{-6}/°F) which closely corresponds to that of ceramic material (Fig. 40.3);
(3) encapsulated design (humidity protection);
(4) welded gauge leads;
(5) materials insensitive to humidity (low humidity absorption);
(6) suitability for heat-curing cement, max. 180°C;
(7) easy soldering with tin;
(8) low sensitivity to changes in Young's modulus and in temperature;
(9) physical and chemical stability;
(10) supply of all gauges from the same batch so as to reduce scatter in gauge factor, resistance and apparent strain.

APPLICATION TECHNIQUE AND CEMENT

Room-temperature hardening or curing cement is cheaper to use but cements cured at elevated temperatures, e.g. epoxy cement curing at 150–180°C, show better bonds and

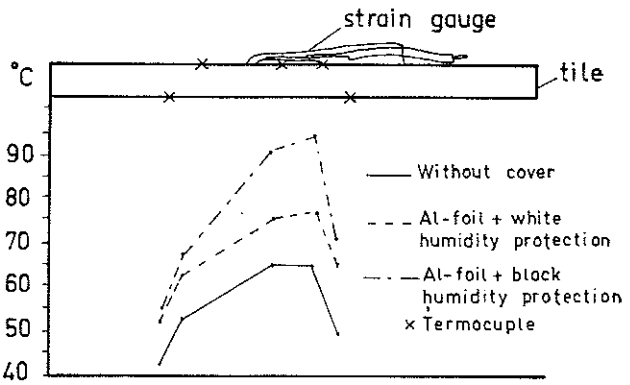

Fig. 40.3. Temperature distribution in tile and underneath gauge for various modes of protection

higher long-term stability. The bond to the glazed surface is improved by slight blasting with a special kind of fine grain steel sand called 'Mull'. The gauge positions on the ceramic side of the tile were ground flat to allow for evenly distributed application pressure and for an evenly thick cement layer between surface and gauge.

On porous materials like unglazed ceramics, several adhesive precoats must be applied and cured consecutively. If only one such layer is applied, it will be absorbed by the pores at elevated temperature during curing and thus jeopardize the adhesion of the gauge. (An advantage of the pre-coats is that the viscosity of the cement can be chosen suitably.)

To apply the gauges on the actual tiles, the FFA V cement was used. Its main ingredient is Shell 'Epikote' (1).* The V cement has been used and evaluated for many years at FFA. It has good bond quality and stability, and its viscosity can be varied to suit special conditions.

During application, cleanliness was of prime importance. All tiles were treated by (*a*) visual inspection, (*b*) washing with slightly alkaline water (soap solution) and (*c*) drying for 24 h at 120°C. All auxiliary equipment was cleaned and degreased.

Three persons carried out the various application phases; one did all the pre-work, another did the cementing, and a third connected the leads and put on the insulation. Two persons then inspected the installation on all the tiles, measured and recorded the insulation resistance and the resistance of the gauge-lead combinations, and finally tested the functioning of the whole installation. The necessary auxiliary equipment had been manufactured previously, e.g. jigs and loading devices for suitable application pressure during curing. The cementing required (*a*) pre-coating three times, with a final cure at 180°C; (*b*) curing of the gauges at approximately 80–90°C for 3 h in an oven evacuated down to 610 mmHg, under an application pressure of about 1 kp/cm^2 (14·4 lb/in^2); and (*c*) final cure at 180°C for 1 h. All the gauge resistances proved to be about 2 Ω above nominal value during the cementing phase.

LEAD WIRES AND CONNECTIONS

The gauge lead wire was connected to a p.v.c.-insulated cable with copper conductors of 0·25 mm^2 cross-section (2). Stringent requirements were put on the insulation, which would have to endure outdoor environment for several years without deterioration (3). At the joint between gauge and lead wire, the moisture protection must adhere to the lead insulation so that the joint is moisture proof.

For an investigation of the lead insulation, one 165 ft (50 m) untwisted double lead wire and two 1·5 ft (0·5 m) twisted leads were tested immersed in water. After 67 days, the insulation resistances were 2·5 MΩ between the 165-ft single wires and the surrounding water, but 1000 MΩ between the two 20-ft twisted wires as well as between the 20-ft twisted wires and water and between the 20-ft twisted wires and the 165-ft single wires.

The soldering of the lead joints is especially important for long-term measurements. Corrosion and other metallurgical changes may cause considerable resistance changes in the soldered joints and thus jeopardize the validity of measurements (4). The joints have been soldered with lead/tin alloy solder (supplied by Budd, 0·8 mm diameter, melting point approximately 185°C).

PROTECTION OF GAUGE INSTALLATIONS

It is difficult to achieve reliable weather protection of strain-gauge installations where a complete metallic enclosure is not possible. Moreover, the complete installation for the tests was required to occupy the least space possible in order to avoid shadowing the test object underneath and thus changing the ambient conditions and causing erroneous thermal stresses.

Temperature measurements were carried out on shadowed and non-shadowed areas of tiles during laboratory radiation tests. Thermal effects greater than the normal solar radiation were introduced to disclose tendencies and orders of magnitude of the gradients, and the measurements were carried out on a free tile as indicated in Fig. 40.3.

Covering the gauge with an aluminium foil provides a simple but adequate protection, with little extra space. The main difficulty is getting the leads through the moisture proofing layer without reducing its effectiveness.

During strain-gauge work it proved difficult to obtain a value for the insulation resistance because the tile material was not electrically conductive. However, in the dry state of the tile, the insulation resistance could be measured between aluminium foil and tile. Only in two cases out of 372 did the insulation resistance show such unacceptable values as 1000 MΩ. It is possible that moisture can squeeze through the tile to the back of the gauge, because there is no aluminium foil between carrier and ceramic body. After 15 days immersion in fresh water, the insulation resistance between gauge and water was not less than 150 MΩ for gauges on the back of the tile and not less than 1000 MΩ for gauges on its glazed side.

The insulation resistance was also measured between leads of a cemented gauge and a bare wire embedded in the mortar covering the gauge on a tile exposed to outdoor environment. The ambient temperature fluctuated between +5 and −16 C. Insulation resistance was measured once a week and, after 58 days, amounted to 1000 MΩ. This installation had been moisture proofed as shown in Fig. 40.4.

Poor insulation can also appear between lead wires as a shunt resistance, which can be measured only if the circuit is open at the gauge, but the tests do not include any special arrangement to evaluate deterioration of shunt resistance. Since the leads have two insulation layers between each other and only one layer is between them and the surrounding media, the chances of an error reading due to shunting will be small as long as resistance to the surrounding media is satisfactory. After prolonged exposure, penetration of salt mist from the sea, as well as externally accumulated layers of salt on gauges and leads, may cause the insulation quality to deteriorate appreciably. This may result in shunting of

* *References are given in Appendix 40.1.*

LONG-TERM STRAIN-GAUGE MEASUREMENTS IN OUTDOOR ENVIRONMENT ON CERAMIC TILES

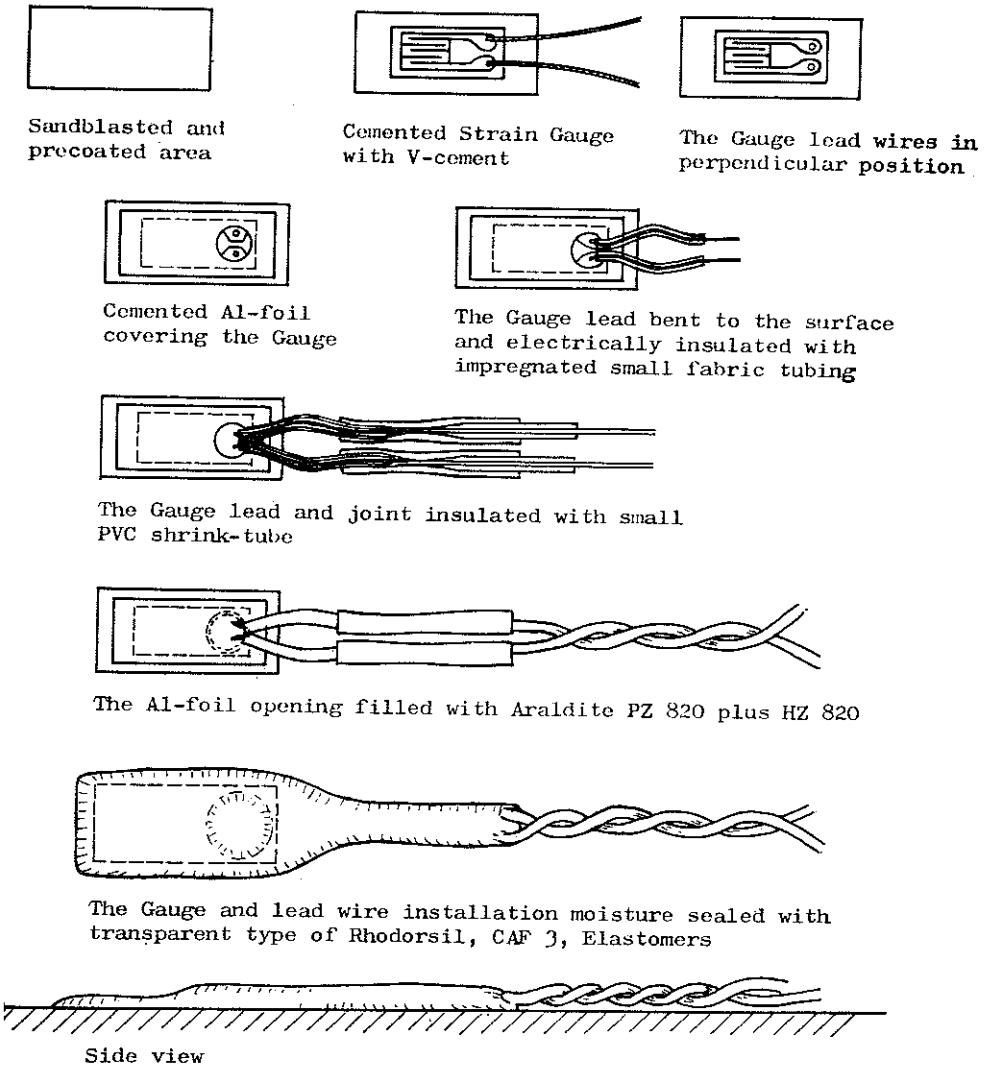

Fig. 40.4. Illustration of strain-gauge installation procedure, including lead wire attachment and moisture proofing, for long-term measurements

the gauges and in erroneous strain readings. Shunting with a 100 MΩ resistance corresponds to an error in the recorded strain of approximately 5×10^{-6} (5)–(7).

INSTALLATION PROCEDURE

After the gauges had been applied to the tile, the remaining installation procedure, protection and checking operations were completed in the following sequence (Fig. 40.4):

(1) Covering the gauge with V cement.
(2) Applying the aluminium foil over the gauge.
(3) Covering the aluminium foil with V cement.
(4) Mounting a spaghetti tubing on the gauge wire.
(5) Anchoring the gauge wire and the spaghetti with Araldite (PZ 820 plus HZ 820) at the hole of the aluminium foil.
(6) Mounting a shrinkable tubing over spaghetti and lead.
(7) Soldering the joint between gauge wire and connecting lead.
(8) Shrinking a larger tube over the joint.
(9) Filling the foil opening with PZ 820 mixed with aluminium scales.
(10) Checking the total resistance of gauge and lead.
(11) Checking the resistance through the insulation to the aluminium foil.
(12) Testing the functioning of the gauge by manually bending the tile and recording the strain.
(13) Applying a moisture protection consisting of Rhône-Poulenc, Rhodorsil, CAF 3, elastomers (transparent).

The tile was then installed on the wall and the checks were repeated. In order to prevent adhesion of mortar, the moisture proofing was covered with a layer of paraffin immediately before fastening of the tile to the wall. After mounting

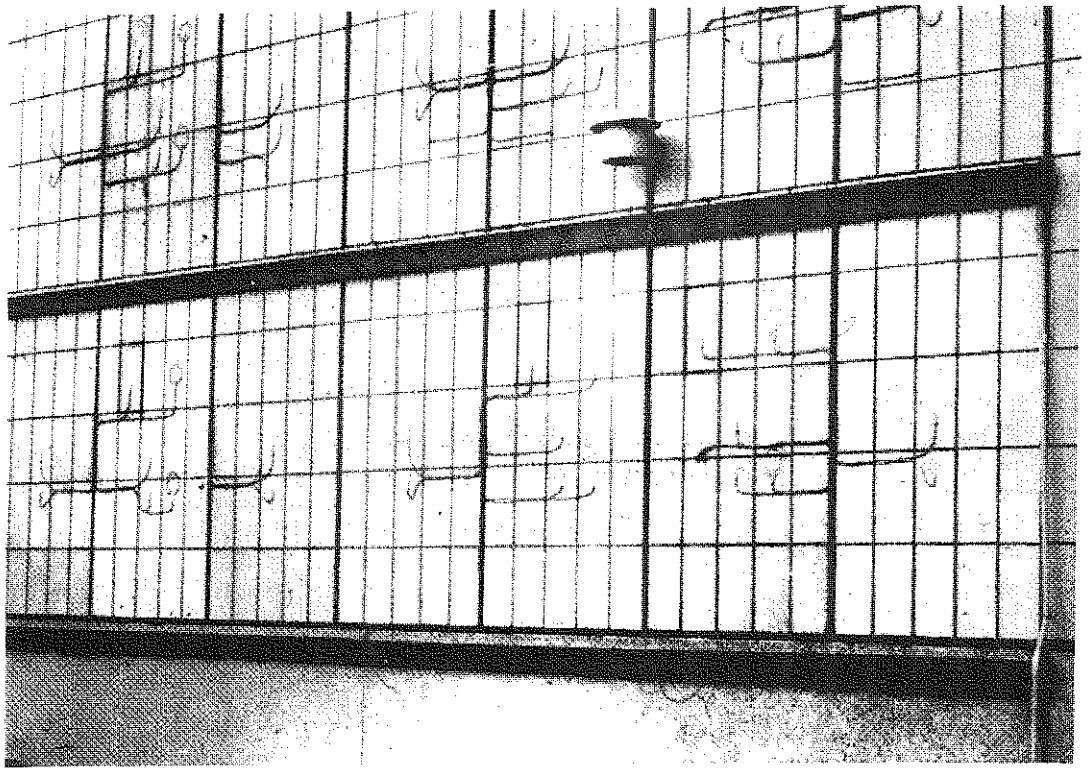

Fig. 40.5. Completed wall with strain-gauged tiles and cables

on the wall, the installation was painted on the outside with plastic paint of the same colour as the tile. This paint, together with the aluminium foil, serves as a protection against UV radiation.

The connecting leads, about 5 ft long, are twisted along their whole length, anchored to the humidity protection layer and connected to the digital data acquisition system inside the house by means of shielded cables (Fig. 40.5).

INVESTIGATION OF THE STRAIN-GAUGE BOND UNDER VARIOUS CONDITIONS

Tests to study the bonding quality of the cement layer between test object and gauge included visual inspection of the cement layer and strain measurements during loading both before and after artificial aging of the test specimens.

The prepared gauge areas on five tiles were coated three times with V cement. On one of the tiles, an encapsulated foil gauge was cemented. This tile was aged together with three others precoated with the V cement. The fourth precoated tile was not aged but was used exclusively as a reference specimen.

Table 40.1. Cycling procedure

Cycling	Drying	Inspection, min	Water immersion, h	Freezing, h
1–9	120°C for 2 h	10	1–2	20
10–41	60°C for 2 h	5	1–2	20

The aging procedure, 'cycling', included a specified programme of separate water immersion, freezing and heating phases. Approximately 40 cycles were used (Table 40.1).

Visual inspection at close intervals did not reveal any damage to the cement layers. After the cycling test, the insulation resistance between gauge and water was found to be greater than 1000 MΩ. The reliability of the gauge bond to the test specimen was checked also by loading the tile several times and by measuring the strain simultaneously after application of a certain number of cycles under various physical conditions (Table 40.2).

The investigation described is considered incomplete because the zero position could not be recorded during the difference test phases. An unnecessary spread of results was also obtained because the tile had reacted to the load by bending, the influence of which could probably have been separated from the results by means of back-to-back gauges.

INVESTIGATION OF STRAIN-GAUGE CHARACTERISTICS

At the planning stage, a certain amount of component testing had been considered essential, and various types of strain gauges were investigated for gauge factor, temperature matching and humidity endurance.

Gauge factor

To investigate the gauge factor, an encapsulated foil gauge, temperature matched for steel, was chosen. The gauge was

Table 40.2. Instrument deflections, strain values and zero differences taken from one tile under various circumstances

Test no.	Condition	Measurements taken	Deflection or Strain	Load							Zero difference	
				O	P	O	2P	O	4P	O	$\times 10^{-6}$	%
1	Dry	At room temperature	D	4810	4730	4818	4662	4818	4530	4820	1–1	3·5
			S	0	80	8	156	8	288	10	10	
2	Dry	After 16 h in water	D	4796	4706	4790	4625	4793	4470	4790	1–2	6·0
			S	0	90	−6	165	−3	323	−6	−20	
3	Dry	After drying 4 h at 20°C and reduced pressure	D	4810	4734	4812	4648	4810	4488	4806	1–3	1·2
			S	0	76	2	164	±0	322	−4	−4	
4	Dry	After 77 h in water	D	4818	4734	4820	4665	4820	4510	4818	1–4	2·9
			S	0	84	2	155	2	310	±0	8	
5	Frozen	After 77 h in water, frozen to −25°C. Tested at −20°C	D	4696	4575	4652	4502	4660	4355	4672	1–5	45
			S	0	71	−44	150	−36	305	−24	−138	
6	Dry	After drying 4 h at 55°C. Tested at 50°C	D	4832	4760	4832	4688	4829	4544	4828	1–6	2·6
			S	0	72	±0	144	−3	285	−4	+18	
7	Dry	After drying 2 h at 90°C. Tested at 75°C	D	4820	4738	4820	4660	4818	4508	4818	1–7	1·1
			S	0	82	±0	160	−2	310	−2	8	
8	Dry	After drying 2 h at 90°C. Tested at 75°C	D	4815	4738	4815	4645	4813	4500	4818	1–8	1·3
			S	0	77	±0	170	−2	313	+3	+6	
9	Dry	After 17 cycles. Tested at room temperature	D	7317	7227	7314	7149	7314	7015	7312	9–9	9–9
			S	0	90	−3	165	−3	298	−5	−5	1·7
10	Dry	After 40 cycles. Tested at room temperature	D	7540	7453	7540	7437	7540	7192	7532	10–10	10–10
			S	0	87	±0	190	±0	340	−8	−8	2·3
11	Dry	After drying 30 days at room temp. Tested at room temp.	D	7060	6917	—	6810	—	6652	7058	11–11	11–11
			S	0	143		250		408	−2	−2	0·49
12	Dry	After outdoor condition for 8 months. Tested at room temp.	D	6450	6370	—	6295	—	6150	6449	13–13	13–13
			S	0	80		155		300	−1	−1	0·33

cemented with V cement to a steel bar, which was loaded in bending for comparison of measured and theoretical strain. The results are given in Table 40.3.

Table 40.3. Results of gauge factor investigation

Amount of strain, per cent	Percentage deviation from nominal gauge factor value	
	Gauge I	Gauge II
E = 0·0487 . . .	−0·24	+0·6
E = 0·1664 . . .	−0·18	+0·6

Apparent strain

To investigate the temperature matching of the gauge for the ceramic test specimen, an encapsulated foil gauge temperature matched for molybdenum was selected. The gauge was applied in the conventional manner and recordings were taken within the actual temperature region. The temperature matching to the ceramic material was slightly better than that to molybdenum (Fig. 40.6).

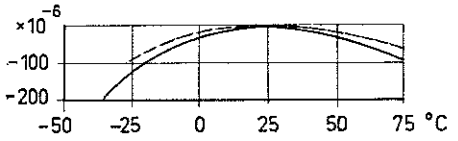

Fig. 40.6. Apparent strain indicated by strain gauge on molybdenum (full line) and on ceramic tile (dotted line)

Humidity endurance

To investigate humidity endurance, another encapsulated foil gauge was immersed in tap water to two-thirds of its length. The insulation resistance between gauge and water was measured (Table 40.4).

Table 40.4. Humidity endurance test

Gauge A		Gauge B	
Number of days in water	MΩ	Number of days in water	MΩ
77	>1000	22	1000
78	7	35	6
91	1·4	48	6

THE MAIN TESTS

The walls of the test house face north, east, south and west, and this orientation influence the exposure conditions of the gauge installations. Other parameters are: type of wall design, tile quality, techniques and material for brick laying and nature of mechanical loading. A certain number of tiles are used as references on unattached bricks or by mechanical relief of the gauge area by cutting a circular slot around it. Unattached tiles may be dismounted for control calibration. Some tiles with applied strain gauges are also placed inside the test house for observation and measurements under a stable environment.

It is evident that the initial zero strain before attachment of the tiles to the wall cannot be checked afterwards owing to the impossibility of unloading the specimens. Aging, creep or other indications that cannot be referred to the behaviour of the base material are evaluated by comparison with unloaded reference tiles or by measurements made after taking down the tiles.

The signals from strain gauges and thermocouples are displayed by a printer in digital form and on punched paper tape for automatic data processing.

At present, records are normally taken four times every 24 h and more frequently during exceptional weather conditions.

SOME OBSERVATIONS FROM THE MEASUREMENTS ON THE TEST HOUSES

Strain measurements have now been in progress since June 1969. The period June–September 1969 has seen an exceptionally large number of sunny hours during June, July and August. In September, on the other hand, an unusually large number of stormy days have occurred with rain, with hail, and with wind speeds approaching 30 m/s. The storms have caused damage to the lead anchoring, which had to be repaired and strengthened. Of the 372 strain gauges applied, only one gauge has shown abnormal values. The experience of the four-month period can be summarized as follows:

(1) For 24 unloaded reference tiles, data collected during a 10-week period show a spread in the strain readings of $\pm 2 \times 10^{-6}$ for tiles of type A and of $\pm 20 \times 10^{-6}$ for tiles of type B. The difference is considered to be significant and is interpreted as a clear indication of differences between the tile materials.

(2) Strains now indicated by tiles attached to the wall are interpreted as caused by temperature changes. During 24 h, the temperatures have varied between +7 and +36°C on a single wall, and the corresponding strain variations have been 36×10^{-6}.

(3) A relationship between storm gusts and strain deflections has been noted. A dynamic strain change of $\pm 2 \times 10^{-6}$ has been observed at such times.

(4) The temperature during the period has fluctuated between +4 and +39°C.

CONCLUDING REMARKS

The number of test points is large and the information abundant. A certain portion of the information is, intentionally, redundant so that a number of gauges failures need not cause loss of results. So far, after four months of testing, only one single gauge seems to have failed. If extrapolation is allowed at this stage, about 10 gauges will be out of action after 36 months, provided the deterioration does not accelerate.

When the tests were initiated, it was considered uncertain whether the expected small strains could be measured under ambient conditions for so long a time. The measuring period (four months) that has now elapsed is too short to predict future development and results. Besides, this period does not include the harsh seasons, winter and spring. The measured results from the laboratory and the test houses, however, give cause for optimism.

Some of the results obtained between the press date of the pre-prints and that of the final proceedings of this Conference will be found following the author's closure of the written discussion of this paper.

ACKNOWLEDGEMENTS

The author would like to thank the National Swedish Council for Building Research, the Royal University of Lund and the Höganäs Co. for permission to publish this paper and for their co-operation during preparations, and also to express his appreciation to the members of the FFA Instrumentation Dept for their valuable assistance.

APPENDIX 40.1

REFERENCES

(1) *Shell 'Epikote' Resins* 62:6.

(2) BAYLE, H. B. 'Waterproofing of electric resistance strain gauges', *Strain* 1968 **4** (No. 1, January).

(3) DRYBURGH, R. B., PETER, B. G. W. and PLEWES, W. G. 'Waterproofing strain gauges on reinforcing bars in concrete exposed to the sea', *Mater. Res. Stand.* 1965 (July).

(4) BUDD. 'Long-term, static outside or subterranean strain gauge testing', Applicating Data Sheet E-01-22, E-01-23.

(5) DOLLY, J. W. and RILEY, W. F. *Experimental stress analysis* (McGraw-Hill).

(6) MCKILLERS, R. R., BRADING, K. F. and WILLIAMS, A. 'Measurement of internal strain in concrete'.

(7) WEIR, R. M. 'The effects of earth leakage on electrical resistance strain gauges', *Strain* 1969 **5** (No. 2, April).

Determination of ultimate compressive strength of ceramic tiles at balanced deformation

Determinations of the compressive strength of hard and brittle materials, such as ceramic tiles, normally show a high standard deviation. This is partly due to the tested material itself but, as a rule, also to a scatter in the conditions around the load application in the test.

In the light of these facts, a particular study was carried out within the main project in order to develop a test procedure, reducing the influence of the scatter in the testing conditions as far as possible.

An introductory test of 6 carefully prepared test specimens of the tile type F, size 11 x 17 x 28 mm, all surfaces being precision ground, showed a mean value $\bar{x}$ = 290 MPa and a standard deviation s = 60 MPa, which later figure was considered not true for the material tested.

New test series of the tiles, type N and F, then were performed and after some further pre-tests, not reported here, the following conditions were considered important and should be used in the principal tests:

(1) The test body should have large load surfaces, with the load applied along the tile

(2) The pad material between the test specimen and the load surfaces of the testing machine should be selected through further investigations

(3) The load distribution over the cross section of the test specimen should be observed by means of strain-gauges and trimmed to a position, as centric as possible.

The final test specimens used were obtained by cutting not split pairs of tiles in three approximately equal parts with an indi-

vidual size and form according to Fig. Aa. Of these, one end piece of each pair of tiles was selected for testing. The end surfaces were smoothed (plane-parallel ± 0.02 mm) by means of diamond tools. The test specimens were dried at 120°C during 24 hours and provided with strain-gauges. Dimensions of the prepared test specimen and the strain-gauge positions are shown in Fig. Aa.

The following pad materials were pre-tested:

(1) Different rubber materials, with and without fabric reinforcement
(2) Soft and hard types of wood fibre boards
(3) Lead
(4) Aluminium and
(5) Polished steel.

A soft wood fibre board, "Treetex" 13 mm, gave the smallest deviation and was chosen as pad material.

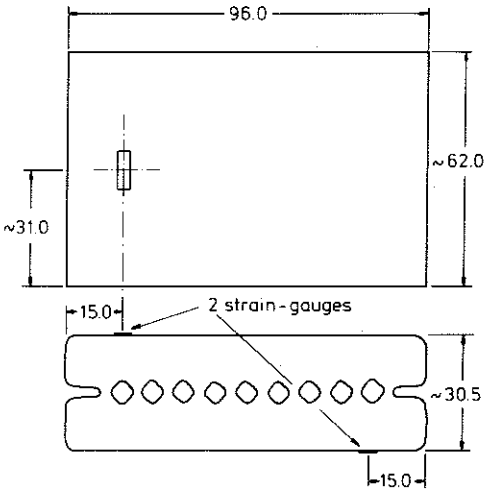

Figure Aa. Dimensions and strain-gauge positions of a prepared test specimen

Test procedure

By use of a first pressure of up to 20 MPa - about 1/10 of the pressure, giving compression failure of the test specimen - adjustments

were made to minimize the difference between the two strain-gauge signals. A maximum strain difference of $20 \cdot 10^{-6}$ was accepted which is less than 10% of the total strain at this pressure. The pressure was then increased at the rate of 20 MPa/min. The total strain and the strain difference at further increased pressure were observed at a compressive stress of 150 MPa. The final crushing of the test specimens occurred in the tests, summarily reported in the table below, within the compressive stress range 233 to 287 MPa.

Separate measuring bridges were used to obtain the strain difference between the two gauges and the total strain of one of the gauges.

Test results

Test no.	N-tiles			F-tiles		
	Strain, 10^{-6}, at 150 MPa		MPa at crush.	Strain, 10^{-6}, at 150 MPa		MPa at crush.
	total	diff.		total	diff.	
1	2600	170	236	2500	200	276
2	2800	200	233	2400	10	263
3	3100	46	254	2500	110	270
4	2700	200	234	2500	185	160
5	-	-	236	2300	20	264
6	3200	85	251	2400	4	287
$\bar{x}$	-	-	241	-	-	270
s	-	-	9.3	-	-	10.1

Remark: An average value of the area of cross section was used in the calculation of the compressive stress. N-tile : 2700 mm^2 and F-tile : 2620 mm^2.

The results show the importance of a precise definition of the conditions and a connected careful preparation around the load application in compressive strength tests of ceramic materials and products.

Tensile strength of ceramic tiles, determined by splitting tension test

Several mechanical tests methods are in use for the determination of the tensile strength of brittle ceramics. A survey of the different test procedures is given in [1]. Among the indirect tests, the diametrical compression test or the splitting tension test has several advantages; a relatively simple testing arrangement, the fact that the test has for a long time been used extensively for other types of brittle material, particularly concrete. The test specifications are given by ASTM Method C496. Although ASTM C496 calls for the testing to be done on cylinders, its validity on cubical or parallelepipedal specimens is equally verified [2]. The main drawback is that the test only gives a measure of the fracture strength in tension and does not permit an evaluation of the stress-strain characteristics in tension.

A1. THEORETICAL BACKGROUND

The test is performed by loading the tile, according to Fig. Ala, in compression on the two opposite longer sides, causing the specimen to fail in tension in the plane of the load application.

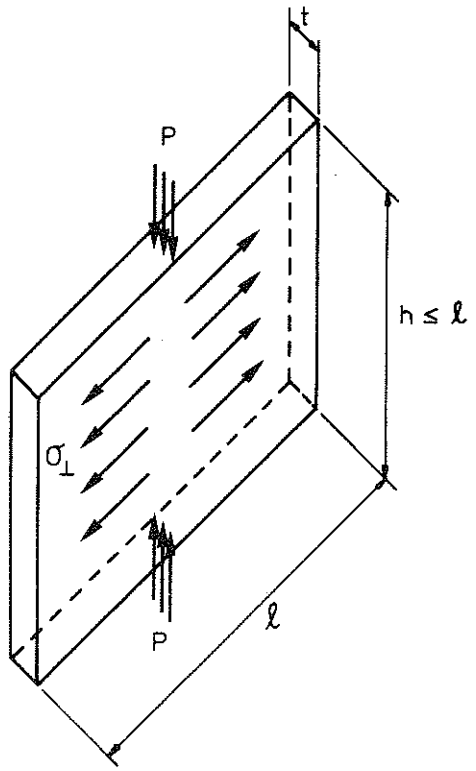

Figure Ala. Principle of splitting tension test

Assuming a concentrated line load P and a linearly elastic, isotropic and homogeneous material, a relatively uniformly distributed tension stress arises over the main part of the splitting section. The maximum value of this tension stress $\sigma_\perp$ is given by the formula [3] - notations according to Fig. Ala

$$\sigma_\perp = \frac{2P}{\pi ht} \qquad \text{(Ala)}$$

In theory, the formula for $\sigma_\perp$ may be used for materials having an ultimate compressive strength greater than three times the ultimate tensile strength. Experimental evidence suggests that to give reliable results, the ratio of the ultimate strengths should be higher, preferably ≈ 10 [2], [4].

To prevent failure by local crushing, the loads P have to be distributed over a finite distance s in the length direction of the tile [2].

As long as the ratio s/h is kept small compared with unity, the influence of different ratios on the tension stress value $\sigma_\perp$ is comparatively insignificant. In the present tests, the s/h-ratio = 0.15 was chosen. For this value of s/h the maximum tensile stress $\sigma_\perp$ is [5]

$$\sigma_\perp = 0.97 \frac{2P}{\pi ht} \qquad \text{(A1b)}$$

A2. TESTING PROCEDURE

All specimens were tested in a hydraulic, universal testing machine with a stress application at a rate of about 5 MPa/min. A photo of the loading frame, that had to be developed and manufactured for this purpose, is shown in Fig. A2a.

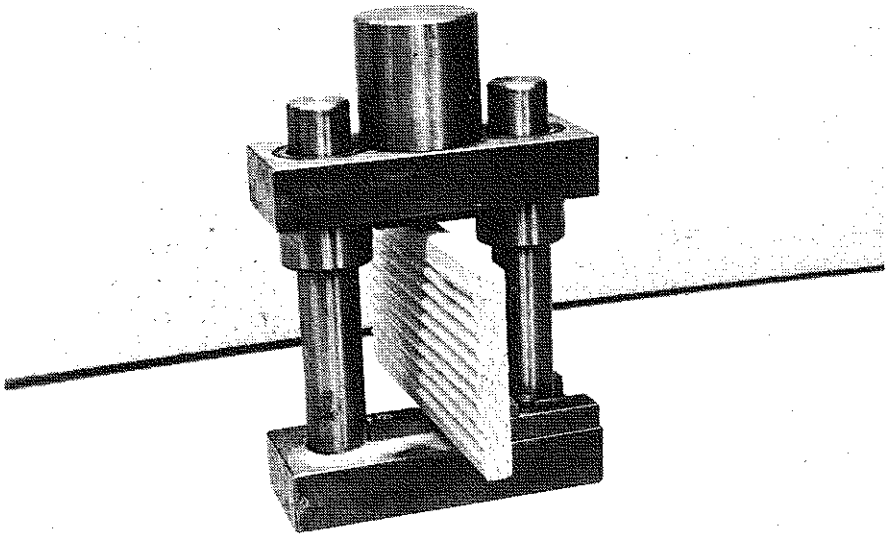

Figure A2a. Testing equipment - loading frame - for splitting tension test of ceramic tiles

Alignement of the test specimen and the loading strips was achieved by providing the frame with a retractable side arm which supported the tile before the load was applied and which facilitated the placing of the packing strips and the centering of the specimen with respect to the loading heads of the testing machine.

As in other tests of this type, the selection of the dimensions and material of the packing strip proved to be critical. The combination of the elastic properties of the specimen and the loading surfaces determines the area over which loading is applied. If the strip is too hard the load application will approach line contact due to the unavoidable surface irregularities and fracture may initiate in compression or shear rather than in tension. A too soft packing strip means that the loading area has to be increased,

which means a larger s/h-ratio and a resulting possibility of shear failure.

The ASTM Test for Splitting Tensile Strength of Molded Concrete Cylinders, 496-66, requires the packing strip to be made of plywood, 1 in. wide by 1/8 in. thick. The influence on the computed tensile strength of concrete of strip material and strip dimension has been reported, e.g. in [4]. No similar investigations have been found concerning the ceramic material tested here. As a consequence, the selection of the proper packing strip material was done experimentally. Strips of moulded rubber, with a thickness = 3 mm and a width s = 14.4 mm, corresponding to a s/h-value of 0.15, proved to produce consistent tensile failures, a well formed and consistent rupture along the vertical plane of load application. Due to the loading characteristics of the testing machine, this primary failure was as a rule followed by some local crushing in the loading region. The rupture was accompanied by a considerable energy release, with the two halves of the test specimen in some cases tending to fly out of the loading frame at high speed. After each test, the pieces of the specimen were put together again to check that the failure had been of true tensile character. Examples of tested specimens are shown in Fig. A2b.

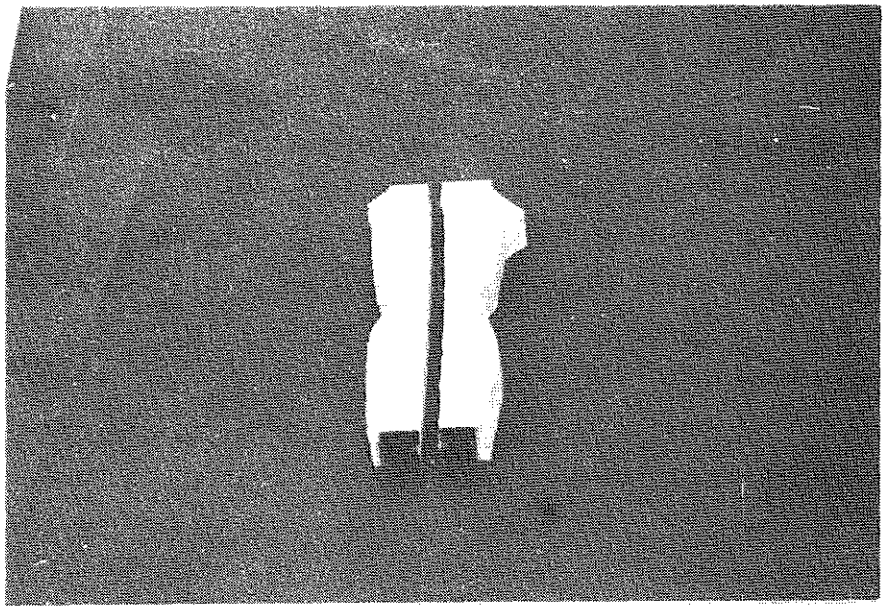

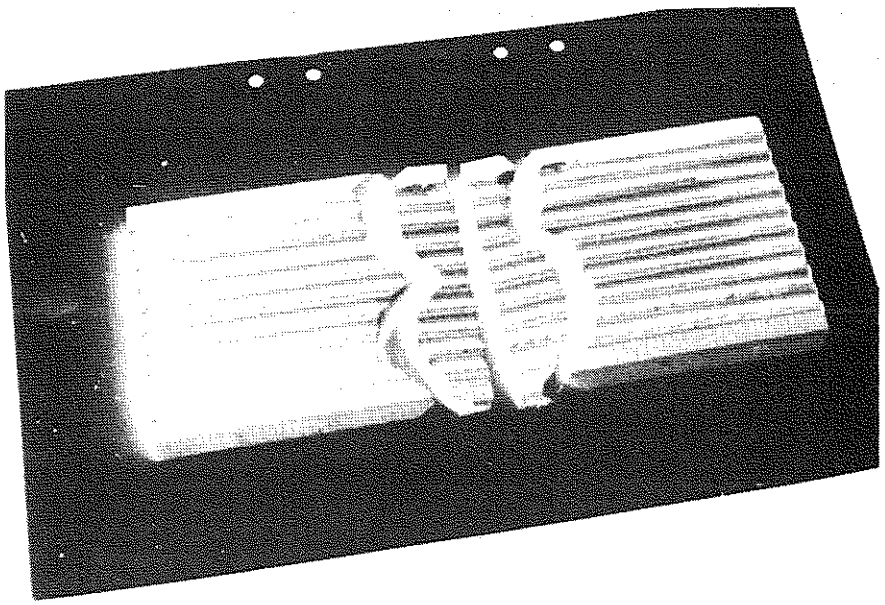

Figure A2b. Representative examples of failure character of split ceramic tiles

A3. TEST RESULTS

In all, 82 specimens were tested. All tiles derived from the original material selection made in 1967, cf. section 1.2.3. 11 tiles were taken down from the test-houses and subjected to the splitting tension test. The others were taken from twin tiles, stored in a climate of approximately 20°C and a 40 per cent relative humidity. The tested material can be divided into the following groups.

1. Tiles, stored in room climate

Mean value and standard deviation of $\sigma_{\perp}$ are given in the table below.

	N-tiles	F-tiles
Number	27	23
Mean value (MPa)	9.82	9.98
Std dev. (MPa)	0.58	0.66

2. Tiles with 1 to 4 years' service

	N-tiles	F-tiles
Number	6	5
Mean value (MPa)	10.14	11.05
Std dev. (MPa)	0.37	0.37

3. Twin tiles to the tiles of type N in group 2 - stored for 6 years in room climate

Number	6
Mean value (MPa)	10.13
Std dev. (MPa)	0.42

4. Tiles without rills (quality N)

Number	5
Mean value (MPa)	11.56
Std dev. (MPa)	0.37

5. Tiles without rills and glaze

	N-tiles	F-tiles
Number	5	5
Mean value (MPa)	17.16	17.56
Std dev. (MPa)	0.91	0.96

A4. DISCUSSION OF TEST RESULTS

Some of the conclusions that may be drawn from the test results are:

(1) Removing the rills and keeping the glaze of the tiles does not to any essential degree change the value of $\sigma_{\perp}$, valid for the composite tile

(2) Removing both rills and glaze, i.e. testing a carefully ground and polished body of pure ceramic material, increases the tensile strength with about 70%. It is clear that the presence of a glaze coating initiates local cracking or crushing during testing process

(3) If the test results from group 5 are compared with the values of the ultimate compressive strength $\sigma_{\shortparallel}$, see section 1.5.1, p 1.5.1-5, the ratio $\sigma_{\shortparallel}/\sigma_{\perp} \approx 7.6$ for the material constituting the body of the N-tiles and ≈ 10.0 for the same material in the F-tiles, justifying use of the testing procedure

(4) A long-time normal working environment exposure does not seem to have any significant influence on the tensile strength of the composite tile.

REFERENCES

[1] Mechanical and Thermal Properties of Ceramics. Proceedings of a Symposium, April 1-2, 1969, NBS, Special Publication 303.

[2] BONZEL, J., Über die Spaltzugfestigkeit des Betons. Betontechnische Berichte 1964. Beton-Verlag GmbH, Düsseldorf, 1965.

[3] FROCHT, M. M., Photoelasticity, Vol II. John Wiley & Sons, New York, 1948.

[4] MITCHELL, N. B., Jr., The Indirect Tension Test for Concrete. Material Research and Standard, Vol. 1, No. 10, October 1961, pp 780-788.

[5] TIMOSHENKO, S. - GOODIER, J. N., Theory of Elasticity. Mc Graw-Hill, New York - Toronto - London, 1951.

Determination of critical moisture contents at freezing of two types of glazed ceramic tiles

By Göran Fagerlund, Dr. Techn.
Swedish Cement and Concrete Research Institute, Stockholm

A1. AIM OF THE INVESTIGATION

The investigation was performed at the Department of Building Materials at the Lund Institute of Technology by directions of Höganäs AB.

The aim was to determine the critical moisture contents in connection with freezing of two types of ceramic tiles which are glazed on one side.

By comparison between the eventual critical moisture contents, measured during practical conditions or at capillary water uptake experiments, it is possible to get an estimation of the frost susceptibility of the materials. The principle is shown in Eq. (A1a)

$$F = S_{cr} - S_{act} = \frac{U_{cr} - U_{act}}{U_o} \qquad \text{(A1a)}$$

where

F = the frost susceptibility,
S = the degree of saturation defined according to Eq. (A1b), and
U = the moisture ratio according to Eq. (A1c).

The indici "cr" and "act" indicate the critical moisture contents, determined by freezing experiments, and the actual moisture contents, measured during practical conditions or by water absorption experiments, respectively. U_o is the moisture content, valid at full saturation. The degree of saturation S and the moisture ratio U are given by the formulas

$$S = \frac{V_W}{V_{Po}} \qquad \text{(A1b)}$$

$$U = \frac{Q_W}{Q_{dry}} \cdot 100\% \qquad \text{(A1c)}$$

where

V_W = the volume of water in the specimen,
V_{Po} = the volume of open pores,
Q_W = the weight of water in the specimen, and
Q_{dry} = the dry weight of the specimen.

A2. MATERIALS TESTED

Two types of tiles were tested, viz. type N and F. Both types are glazed on one side. The open porosities and densities, according to Table A2a, were measured before freezing. The closed porosities - inaccessible for water - are calculated on the assumption that the true densities are 2665 kg/m^3 for type N and 2565 kg/m^3 for type F.

Table A2a. Porosities and densities before freezing (the values are based on 17 specimens of type N and 8 specimens of type F)

type of tile	density kg/m^3	open porosity P_o	σ 1)	closed porosity P_s	U_o %
N	2214	0.145	0.007	0.024	6.59
F	2332	0.010	0.002	0.081	0.44

1) σ = standard deviation

The values of the porosity P_o and P_s and the moisture content U_o are based on specimens with two days of water storage after vacuum-treatment at a residual pressure of 2 torr. The open porosity increases somewhat at the expense of the closed, when the time of water storage is prolonged. This is the case especially for type F, cf. section A5.1 below. Fig. A2a shows this increasing water absorption of specimens which are vacuum-treated. The starting point in the figure is the specimen-weight after two days of water uptake, i.e. the weight, giving the values in Table A2a.

These time-dependent absorptions of tiles type F are small in comparison with the specimen volume ($\simeq$ 260 cm^3) but large in comparison with the total open pore-volume. It is, however, not completely sure that the total weight increase registered is assigned solely to the absorption in the pores. It might also be caused by a chemical reaction between water and the pore-wall.

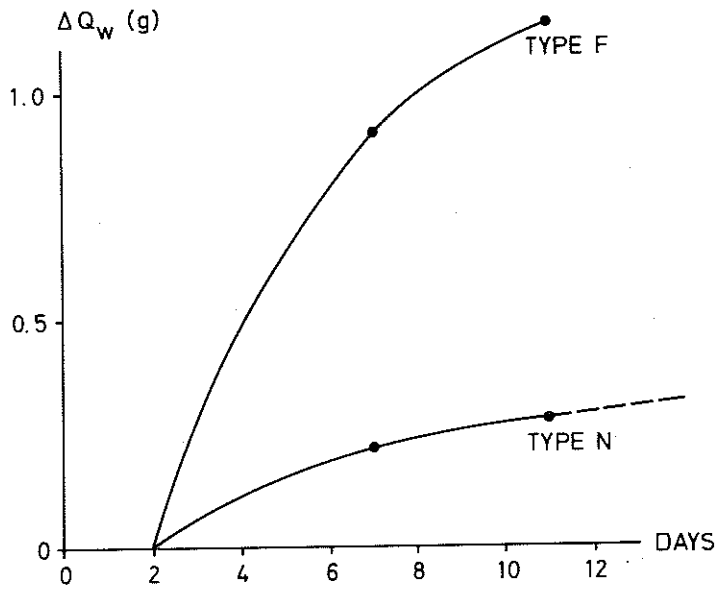

Figure A2a. Water absorption ΔQ_w of tiles type N and F after vacuum-treatment in relation to the specimen weight after two days of water uptake

A3. SPECIMENS

The specimens were partly used for freezing experiments - "freezing specimens" - and partly for water uptake experiments - "suction specimens". The following number of specimens were used:
for freezing: 17 of type N and 8 of type F,
for water uptake: 6 of type N and 2 of type F.

A4. SCOPE

A graphical time-table for the experiments is shown in Fig. A4a.

The same freezing-specimens were used for two (type F) or three (type N) different freezing-rounds. The reason for this was that the specimens showed much less damage after the first freezing-round than was expected, especially then at the highest moisture contents.

The only explanation for this is that ice is escaping from the unglazed surfaces without causing damage and/or that some of the formerly closed pores are opened during ice-formation without causing any considerable or measurable damage. The second and third freezing-rounds were performed in order to study the significance of the latter mechanism.

It must then be noticed that all specimens are sealed during a whole freezing-round so that pores which are eventually opened cannot be filled with water during one and the same freezing-round. However, at the subsequent freezing-round a certain, sufficiently high, degree of saturation which at the preceding freezing-round signified that the just opened pores were empty, will now signify that the same pores are partly water-filled. The damage, therefore, ought to be more severe.

It also must be noticed that only the first freezing-round is performed with specimens that are never dried at +105^{o}C, cf. Fig. A4a.

Two "special freezings" were performed, too. "Special freezing 1" comprises one single freezing-and-thawing cycle with one completely water-saturated specimen of each type. The freezing was somewhat more rapid than normally since only these two specimens were present in the freezing-chamber. This freezing therefore gives a certain indication of the influence of the freezing-rate.

"Special freezing 2" is a freezing-round with specimens which are provided with an epoxy-layer on the unglazed flat surface. 7 specimens of type N and 1 of type F were used. The specimens had earlier been used for the water uptake experiment and therefore been exposed to a drying at +105^{o}C.

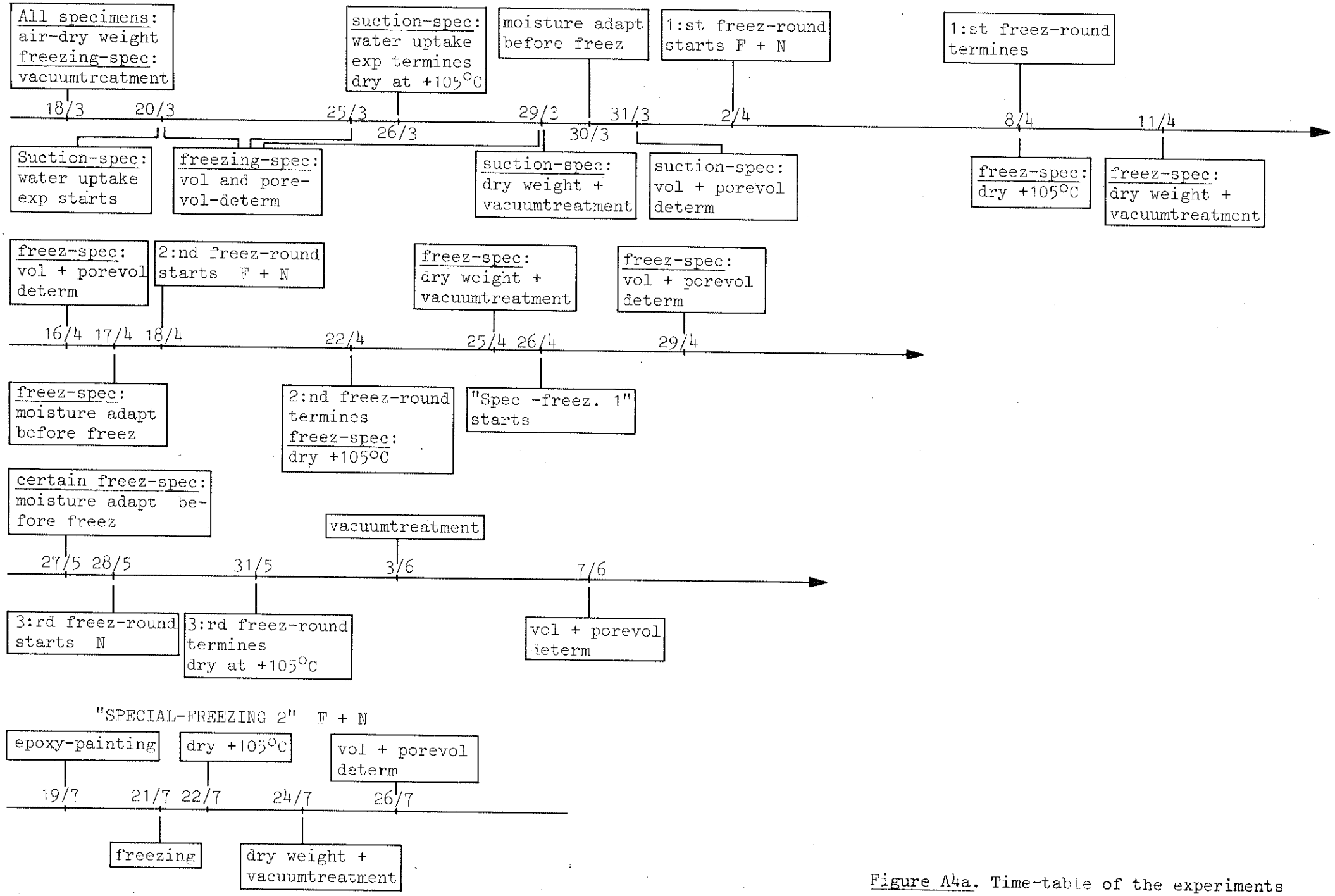

Figure A4a. Time-table of the experiments

A5. DETERMINATION OF CRITICAL MOISTURE CONTENTS - METHOD AND RESULTS

A5.1. Determination of degree of saturation before freezing

A calculation of the degree of saturation S according to Eq. (A1b) demands that the amount of water and the amount of open pores are known.

The amount of water is obtained by knowledge of the specimen weight before freezing (inclusive of water) and the dry weight. The latter weight is defined as the weight after drying for three days at +105°C. The specimens are undried before the first freezing. The dry weight is then based on the air-dried weight reduced by the hygroscopic moisture which was determined to 0.10 g on "dummies".

The open pore-volume is, as mentioned above, dependent on the time of water storage after the vacuum-treatment at 2 torr residual pressure, see Fig. A2a. In the following, all open pore-volumes are defined on the basis of 11 days of absorption. Fig. A4a shows that the pore-volume determination was done only 2 to 5 days after the vacuum-treatment. In order to obtain the "proper" open pore-volume it is, therefore, necessary to add the values of water absorption from Fig. A2a to the measured values. The justification of this has been confirmed since the values in Fig. A2a have been almost completely reproduced at the pore-volume determination after the second freezing-round.

The degree of saturation at a freezing is always defined as the value before freezing as the first freezing causes the most severe damage.

The degree of saturation before freezing is then

$$S_i = \frac{V_W}{V_{Po_i}^{11}} \qquad \text{(A5.1a)}$$

where $V_{Po_i}^{11}$ indicates the pore-volume determined after 11 days of water storage after vacuum-treatment. Index i = 1,2,3 indicates freezing-round 1,2 and 3, respectively, i.e.

$$\left.\begin{aligned} V^{11}_{Po_2} &= V^{11}_{Po_1} + \Delta V_{Po_1} \\ V^{11}_{Po_3} &= V^{11}_{Po_2} + \Delta V_{Po_2} \end{aligned}\right\} \qquad \text{(A5.1b)}$$

where ΔV_{Po_1} is caused by the freezings in round 1 and ΔV_{Po_2} by the freezings in round 2 etc. Hence, at a new freezing-round the specimens are considered as a "virgin material".

The principles behind the definition of the open pore-volumes before freezing and the increase of the open pore-volume caused by freezing is shown in Fig. A5.1a.

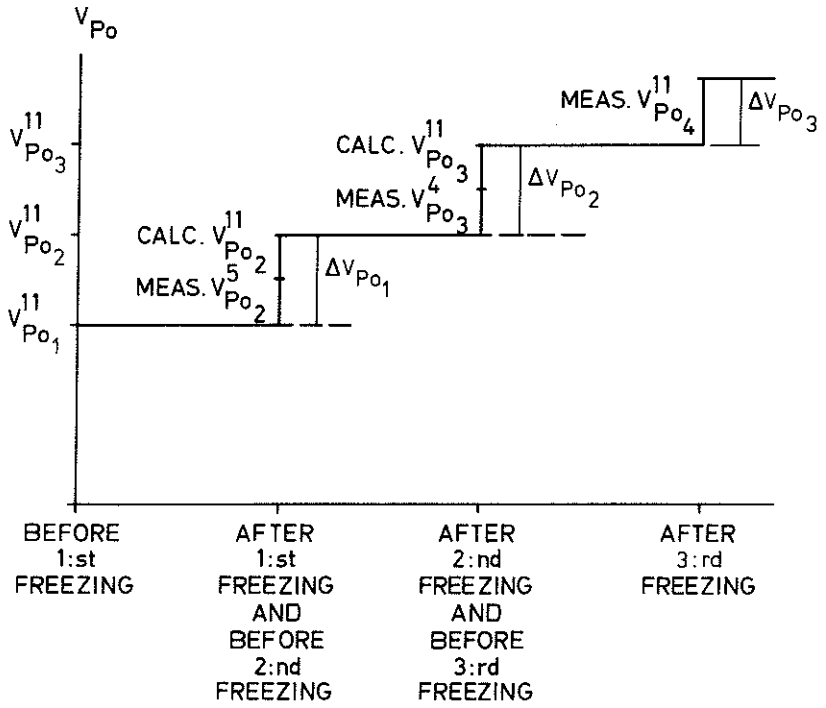

Figure A5.1a. Principle of definition of open pore-volume

A5.2. Moisture adaptation before freezing

By knowledge of the open pore-volume and the dry weight, it is possible to calculate the specimen-weight which corresponds to a certain degree of saturation. The specimens were at first filled with water after which

they were dried to correct weight at +50°C. They were then sealed in plastic bags in order to prevent moisture losses.

A5.3. Measurements

The dynamic E-modulus, determined at a transverse vibration, was used for the indication of damage.

Damage could also be indicated by the increase in the total volume, the increase in the open pore-volume and by a visual inspection.

A5.4. Freezing method

The tiles were mounted on slowly rotating wheels placed in an ordinary deep-freezer. They were sealed during all cycles in one and the same freezing-round.

The number of freezing cycles was
9 in round 1,
8 in round 2,
5 in round 3,
5 in special freezing 1, and
2 in special freezing 2.

Other characteristics of the freezings are described in [1].

The freezing rate during special freezing 1 was probably somewhat higher than at the other freezings. The total weight of specimens was only 1.2 kg in special freezing 1 in relation to 15 kg in the normal case. Earlier investigations have shown that, in the rapid case with a regulated cycle, the air temperature in the box is lowered from 0°C to -5°C in 1/2 h and from 0°C to -10°C in 2.5 h, whilst at a large amount of specimens, i.e. at a partly unregulated experiment, the same temperature lowering takes 3/4 and 3.5 h, respectively.

A5.5. Results

A5.5.1. Type N

1:st freezing-round: See Fig. A5.5.1a-c. The E-modulus decreases some-

what with increasing degree of saturation S. Any directly critical value of S can, however, not be discerned.

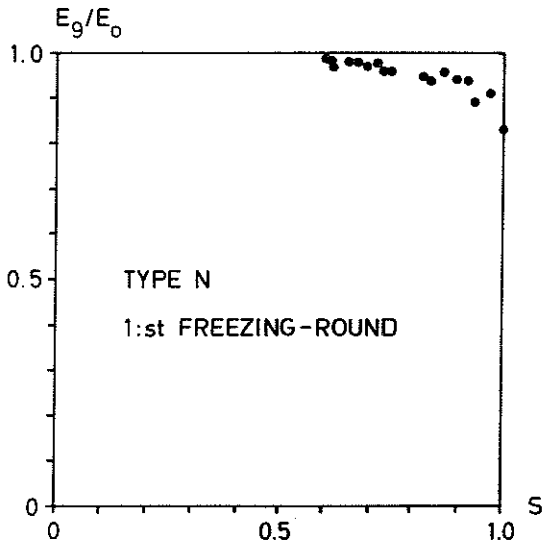

Figure A5.5.1a. Decrease in E-modulus with increasing degree of saturation S. Tiles type N, 1:st freezing-round

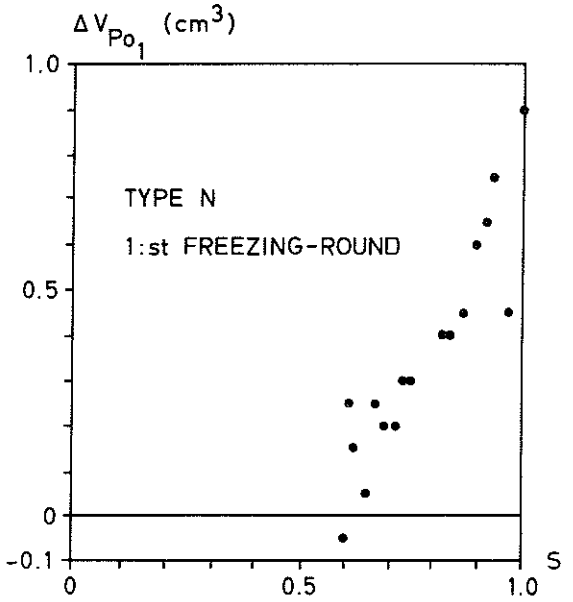

Figure A5.5.1b. Increase in open pore-volume ΔV_{Po_1} with increasing degree of saturation S. Tiles type N, 1:st freezing-round

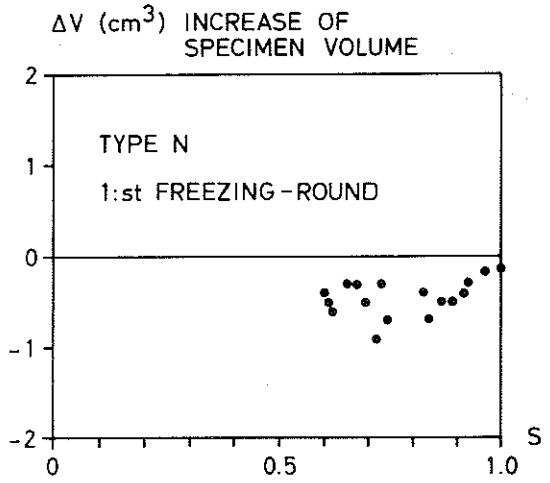

Figure A5.5.1c. Increase of specimen volume ΔV with increasing degree of saturation S. Tiles type N, 1:st freezing-round

The open porosity increases with increasing S, despite the specimen volume in all cases is smaller after freezing than before. The closed pore-volume must therefore be reduced with about 25%. The open pore-volume increase is, however, too small to influence the degree of saturation in the specimen.

The reason for the reductions in specimen volume is not quite clear. It is, however, a well-known fact that many materials containing water shrink when drying. They do also expand during re-wetting but a part of the shrinkage is often not reversible. The permanent shrinkage is by far largest during the first shrinkage-swelling cycle. The mechanism behind this feature is often considered to be a formation of new chemical bonds between such parts of the pore-walls that come in contact during the initial shrinkage. In the actual case, the irreversible shrinkage must have occcured during the + 105°C-drying after the first freezing-round. Moisture induced shrinkages and swellings have also been noticed for ceramics; see for example /3/.

2:nd freezing-round: See Fig. A5.5.1d-f. Also at the second freezing-round, it is impossible to see any signs of any drastical decrease in E-modulus or increase in volume, when a certain critical value of S is transgressed. Even now, however, a certain increase in the open pore-volume occurs. This increase is about the same as the increase in the specimen volume, why the closed pore-volume must be almost unchanged.

No damage could be observed visually.

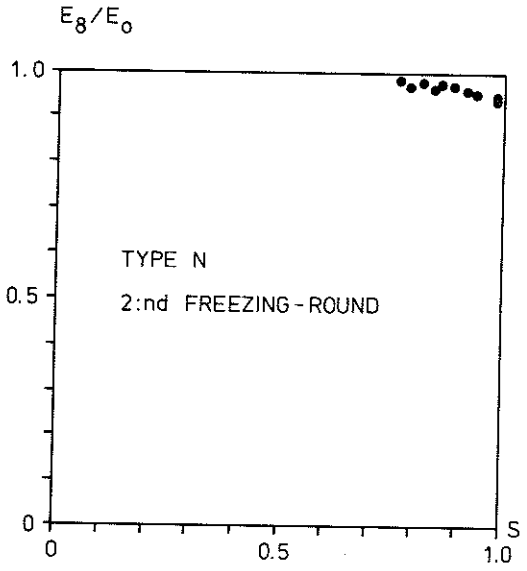

Figure A5.5.1d. Decrease in E-modulus with increasing degree of saturation S. Tiles type N, 2:nd freezing-round

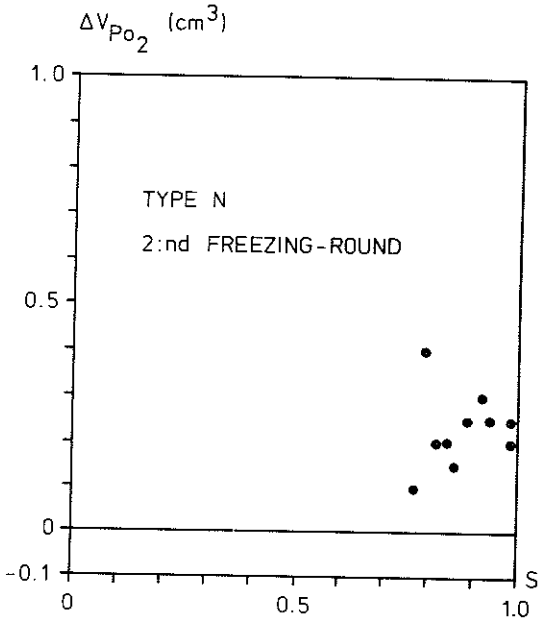

Figure A5.5.1e. Increase in open pore-volume ΔV_{Po_2} with increasing degree of saturation S. Tiles type N, 2:nd freezing-round

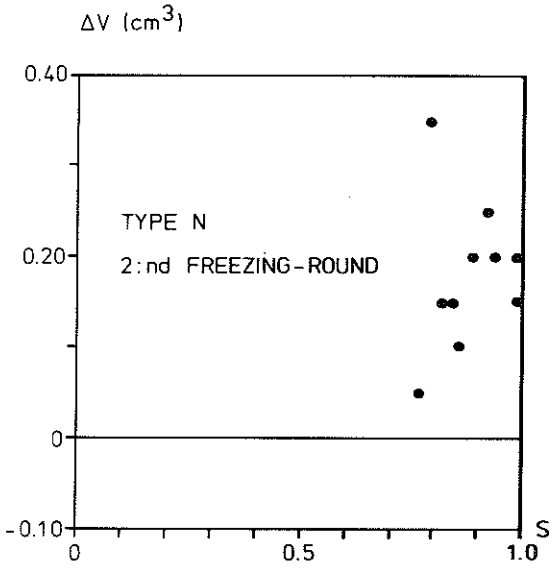

Figure A5.5.1f. Increase of specimen volume ΔV with increasing degree of saturation S. Tiles type N, 2:nd freezing-round

3:rd freezing-round: See Fig. A5.5.1g and h. At the third freezing-round, damage of the glazing occurs at degrees of saturation greater than 0.94. This damage is, however, not indicated by the E-modulus measurement,

which therefore seems to be unsensitive to these types of damage.

The volume changes have not been measured at this freezing-round. However, since a considerable amount of closed porosity was transformed to open already at the first freezing-round, the volume changes ought to be approximately the same as the increase in the open pore-volume as was the case in freezing-round 2.

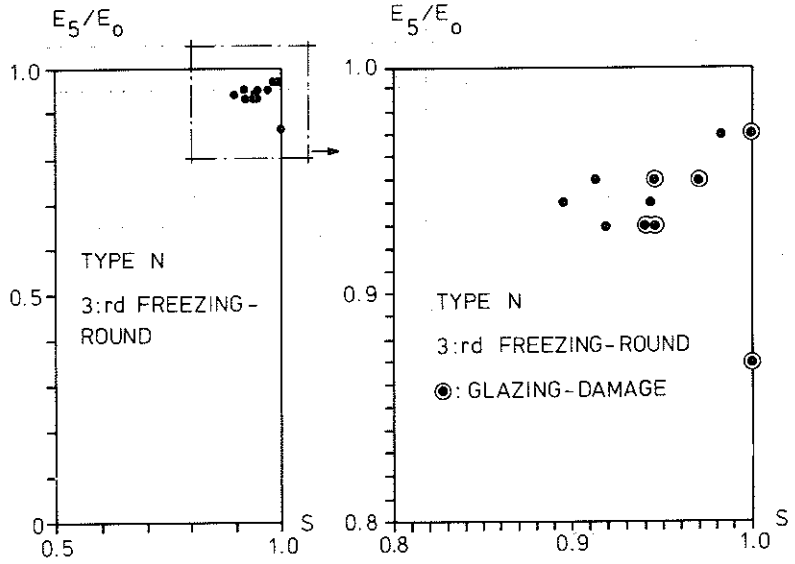

Figure A5.5.1g. Decrease in E-modulus with increasing degree of saturation S. Tiles type N, 3:rd freezing-round

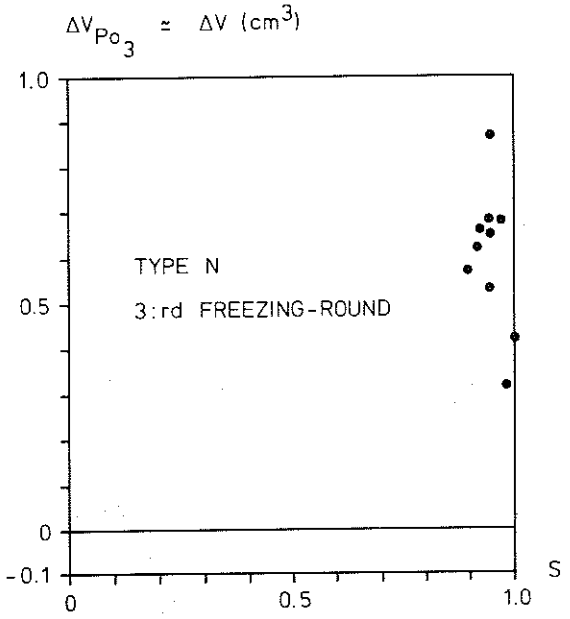

Figure A5.5.1h. Increase in open pore-volume ΔV_{Po_3} with increasing degree of saturation S. Tiles type N, 3:rd freezing-wound

Special freezing 1: The completely water-saturated specimen, which was unfrozen in advance, was strongly damaged by spalling of the glazing already at the first freezing cycle. The E-modulus did, however, decrease as little as 13%. The result of this freezing should be compared with freezing-round 1, at which the specimen with S=1 was undamaged after 9 cycles.

Special freezing 2: See, Fig. A5.5.1i. The specimens were filled to different moisture contents after vacuum-treatment to different residual pressures. This explains the big differences in water contents.

The damage is now very extensive at S=1, despite only 2 cycles were used and specimens were unfrozen before the test. This indicates that a hindered ice-extrusion through the unglazed surface increases the tension stresses inside the material very strongly. The epoxy did in some cases spall off. The increases in the open pore-volume of the two damaged specimens were 1.26 and 1.46 cm^3, respectively.

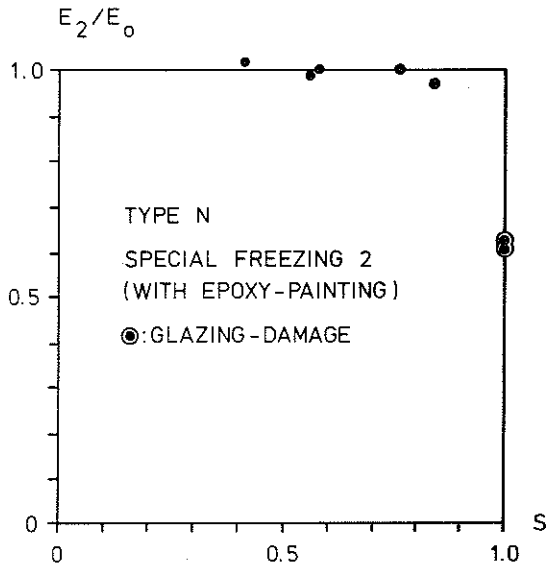

Figure A5.5.1i. Decrease in E-modulus with increasing degree of saturation S. Tiles type N, special freezing 2

A5.5.2. Type F

1:st freezing-round: See Fig. A5.5.2a-c. The E-modulus is apparently almost unchanged even at high degrees of saturation. The increase in

the open pore-volume must occur on the expense of the closed pore-volume since the specimen-volume has decreased. The decrease in the closed pore-volume is, however, only 7.3% of this. As is shown in Fig. A5.5.2d, this small increase in the open pore-volume does reduce the effective degree of saturation in the specimen considerably. Any damage could not be observed.

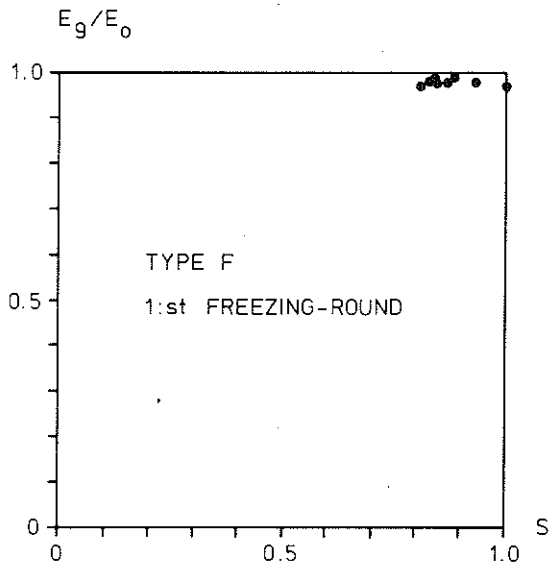

Figure A5.5.2a. Decrease in E-modulus with increasing degree of saturation S. Tiles type F, 1:st freezing-round

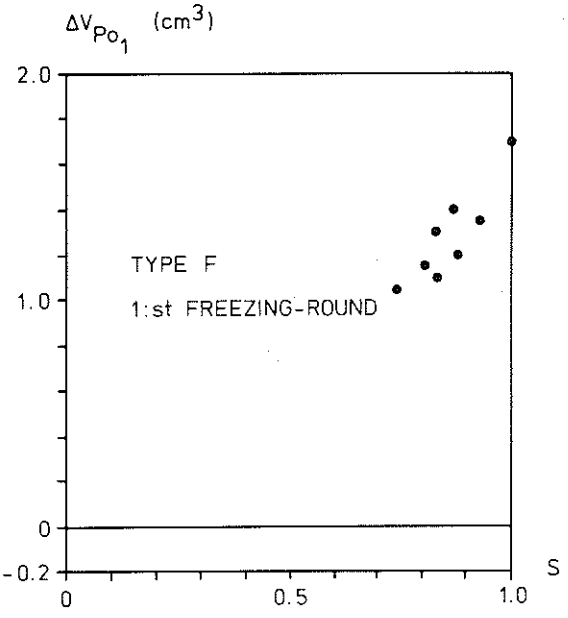

Figure A5.5.2b. Increase in open pore-volume ΔV_{Po_1} with increasing degree of saturation S. Tiles type F, 1:st freezing-round

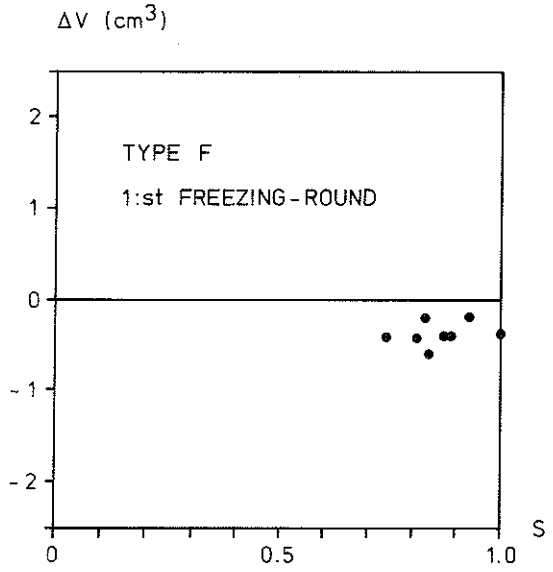

Figure A5.5.2c. Increase of specimen volume ΔV with increasing degree of saturation S. Tiles type F, 1:st freezing-round

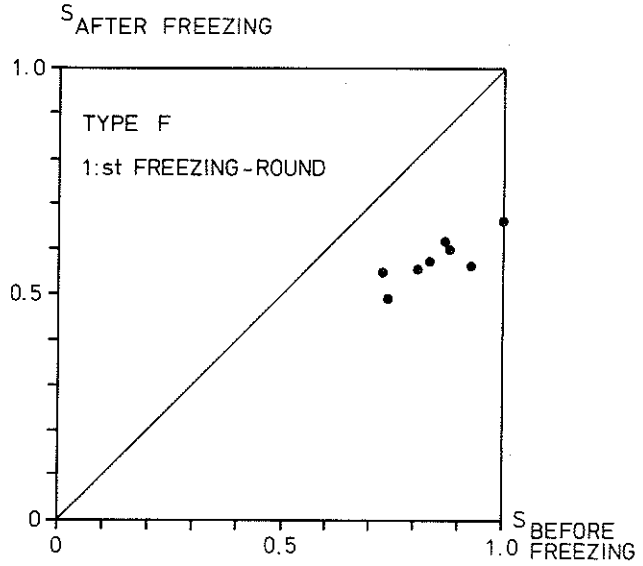

Figure A5.5.2d. Relationship between degree of saturation after and before freezing. Tiles type F, 1:st freezing-round

2:nd freezing-round: See Fig. A5.5.2e and f. The effective degrees of saturation are rather low due to a certain drying-out before the start of freezing. Despite this, the open pore-volume increases to the same extent as earlier.

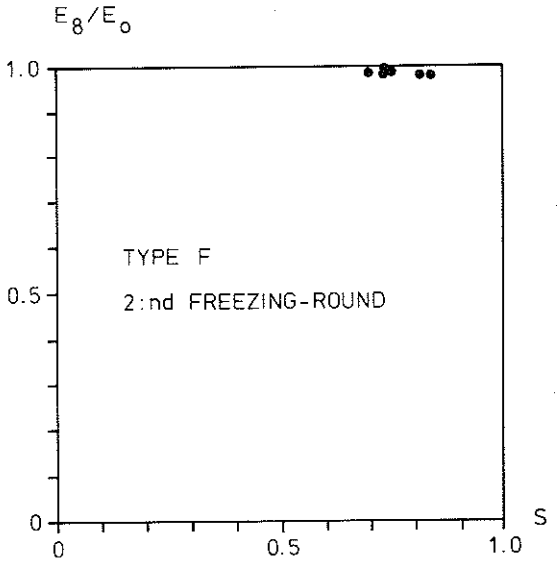

Figure A5.5.2e. Decrease in E-modulus with increasing degree of saturation S. Tiles type F, 2:nd freezing-round

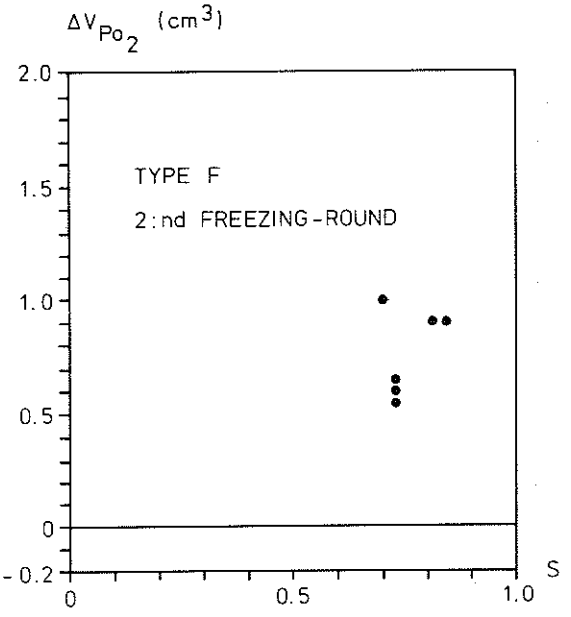

Figure A5.5.2f. Increase in open pore-volume ΔV_{Po_2} with increasing degree of saturation S. Tiles type F, 2:nd freezing-round

Special freezing 1: No damage could be discerned at the rapid freezing.

Special freezing 2: No damage could be discerned at the freezing of specimen with impermeable surfaces.

A5.6. Discussion of results

A5.6.1. Type N

Internal damage does always occur, when a specimen is exposed to its first freezing. The damage consists in a transformation of closed pores into open pores, cf. Fig. A5.5.1b. Outer damage in the form of a spalling of the glazing seems to occur only when the freezing rate is sufficiently high - special freezing 1 - or when the unglazed surface is made dense, cf. Fig. A5.5.1i.

These observations indicate that pressure relief at freezing of a single tile is occuring by ice beeing forced out of the tile, viz. at a complete saturation, the freezable water content in the tile is approximately 35 cm^3. This water swells with 3.2 cm^3 at freezing. The increase in the open pore-volume is approximately 0.9 cm^3 (Fig. A5.5.1b). The ductility of the tile is at maximum 0.3‰ which gives a maximum allowable volume-swelling of ≈ 0.3 cm^3 of a tile. Consequently, 2 cm^3 of water must go out of the specimen. This water should create an ice-crust of only 0.1 mm on the unglazed surface of the tile.

Permanent volume-increases of about 1.4 cm^3 occurred for the two completely water-saturated specimens, that were tightened. This indicates that, in this case, the ice must to a greater extent be formed inside the tile which causes an extensive damage.

Previous results have shown that the so called critical thickness of well-burned clay brick is about 14 mm at a rapid freezing [2].

The transport distance of unfrozen water is about 12 mm in the actual tiles, when they are saturated. This means that, if the critical thickness of the tile at the freezing rate used is more than 24 mm, damage cannot occur even at S=1. The value 24 mm is not unrealistic at a relatively slow freezing of a coarse-porous ceramic material. However, when the unglazed surface is tightened, the distance of water transport needed is increased to 50 mm which is the half-width of the tile. The critical thickness is thereby exceeded and damage is occurring at the glaze as well as at the epoxy-painting.

After a couple of freezings with full saturation, the open porosity can probably not be increased any more but a larger fraction of water must be forced out of the tile. This could be the explanation why glazing-damage occurs at freezing-round 3 but not at freezing-round 1.

At practical conditions, the tile is to a certain extent tightened on the bottom-surface by the mortar. In reality, the tile therefore freezes more or less as a closed container. Because of the reasoning just carried through, one can assume with a large degree of probability that damage cannot occur when $S < 0.91$ because in this case water can be redistributed within the tile without occurence of any considerable stresses. The critical degree of saturation is therefore

$$S_{cr} = 0.91$$

The critical moisture condition is

$$U_{cr} = 6.0\%$$

A5.6.2. Type F

No damage whatever was observed on specimens of type F even when they were completely water-saturated and tightened on the unglazed side.

Fig. A5.5.2b and f show, however, that considerable increases of the open pore-volume occur at each freezing-round. This increase is even greater than the increase in the water-volume at freezing. From a theoretical point of view, it is therefore possible that if the tile is filled up to a complete water-saturation a great number of times with freezings in between, damage might occur at some instant. Not even for this tile in a state of aging, according to the mechanism described above, does it seem probable that damage could occur when $S < 0.91$. The critical degree of saturation is therefore

$$S_{cr} = 0.91$$

The critical moisture ratio is undefined since the value depends on the fraction of originally closed pores that are opened due to previous freezings.

A6. DETERMINATION OF WATER UPTAKE - METHOD AND RESULTS

A6.1. Method

The air-dry specimens were placed with their unglazed flat surfaces a couple of millimeters below the water surface in a vessel which was then covered with a PMMA-slab. The specimens were taken up, dried against a wet sponge and weighed at certain time-intervals. The experiment lasted for 5 days after which the dry weights and the pore-volumes were determined.

A6.2. Results

The result for tiles type N is shown in Fig. A6.2.a. The time-axis is in square-root of time. The moisture is expressed in the degree of saturation in order to be comparable with the results of the freezings.

The absorption after the so called knick-point absorption is very small. An extrapolation shows that the critical moisture content is not reached even after a very long time of water absorption.

The absorption for tiles type F is very low, ≈ 0.7g. The correspondent degree of saturation is 0.34, i.e. much less than the critical value.

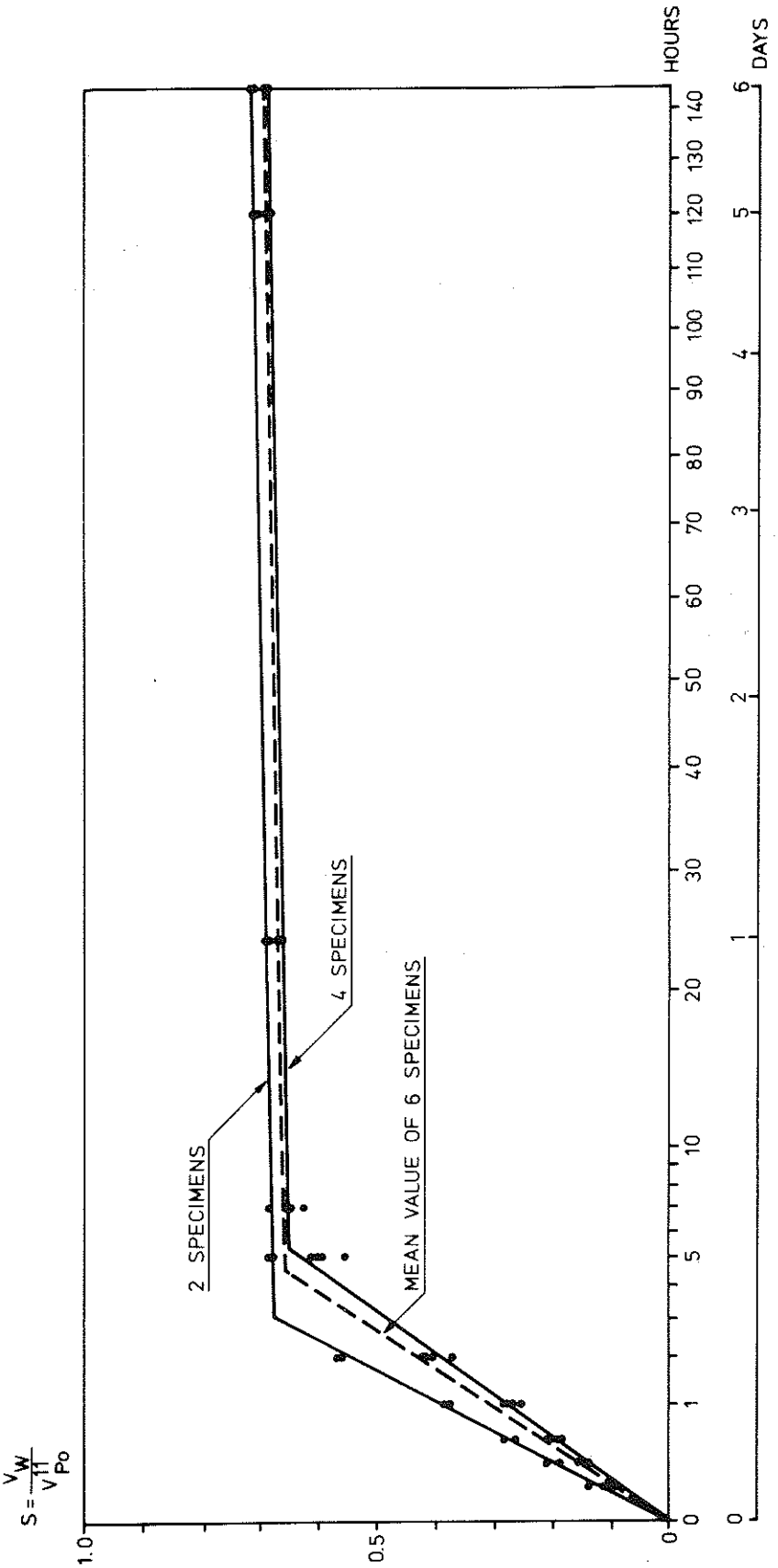

Figure A6.2a. Water absorption, expressed in degree of saturation S, versus time. Tiles type N

A7. SUMMARY

(1) A freezing of completely water-saturated tiles of type N causes serious damage only if
- the freezing rate is high, or
- the unglazed flat side of the tile is tightened.

From this, the conclusion can be drawn that tiles will not be damaged at a practical use when the degree of saturation is less than 0.91.

(2) A tile of type F is not damaged at a freezing even when it is completely saturated and the unglazed surface is tightened. Instead, internal damage occurs in the form of cracks opening the closed pores. At very long sight and during very unfavourable conditions, the frost-resistance of the tile must therefore be somewhat lower. A minimum value of the critical degree of saturation is also for this tile 0.91 for the "aged" tile. For the new tile it is 1.0.

(3) None of the tiles can fill themselves to a dangerous level only by a capillary water uptake.

REFERENCES

[1] FAGERLUND, G., Critical Degrees of Saturation at Freezing of Porous and Brittle Materials. Report 34, Division of Building Technology, Lund Institute of Technology, Lund, 1972 (In Swedish).

[2] FAGERLUND, G., Significance of Critical Degrees of Saturation at Freezing of Porous and Brittle Materials. Report 40, Division of Building Technology, Lund Institute of Technology, Lund, 1973.

[3] NORRIS, A W,. VAUGHAN, F., HARRISON, R., SEABRIDGE, K C J., Size changes of porous ceramics caused by water and soluble salts. Proc. 6th Int Ceramic Congr. Wiesbaden 1958, p 63.